The Role of the Prion Protein in the Immune System

Dissertation

zur

Erlangung der naturwissenschaftlichen Doktorwürde
(Dr. sc. nat.)

vorgelegt der

Mathematisch-naturwissenschaftlichen Fakultät
der

Universität Zürich

von

Veronika Kana

von

Chur GR

Promotionskomitee

Prof. Dr. Adriano Aguzzi (Vorsitz)
Prof. Dr. Cornelia Halin Winter
Prof. Dr. Christian Grimm
Prof. Dr. Christian Münz

Zürich, 2013

TABLE OF CONTENTS

1 SUMMARY 3

2 ZUSAMMENFASSUNG 6

3 ABBREVIATIONS 9

4 THE ROLE OF THE PRION PROTEIN IN THE IMMUNE SYSTEM 11

4.1 INTRODUCTION 12

4.1.1 Prion diseases – the inglorious reason for the prion protein's fame 12

4.1.2 A function for PrP^C in the immune system 16

4.1.3 The *Prnp* knockout mouse and the flanking gene problem 22

4.1.4 Scientific aims 25

4.2 RESULTS 26

4.2.1 Higher phagocytic activity in congenic – but not in coisogenic – *Prnp* knockout mice 26

4.2.2 RNA sequencing identifies candidate confounder genes linked to *Prnp* on mouse Chr2 33

4.2.3 Analysis of candidate confounder genes *Sirpa*, *Mertk*, *Tyro3* and *Thbs1* 41

4.2.4 $Sirpa^{129}$ is linked to $Prnp^{-/-}$ allele in all analysed *Prnp* knockout strains 44

4.2.5 $Sirpa^{129}$ enhances phagocytosis in the absence of *Prnp* 46

4.2.6 *Sirpa* regulates phagocytosis irrespective of *Prnp* status 49

4.2.7 $Sirpa^{129}$ exacerbates mouse EAE in the absence of *Prnp* 59

4.2.8 EAE development in congenic B6.129 mice with different combinations of *Prnp* (wt and ZrchI) and *Sirpa* (B6 and 129) alleles 67

4.3 DISCUSSION 71

4.3.1 Mouse genetics excludes PrP^C as inhibitor of phagocytosis 71

4.3.2 Modulation of EAE development by *Prnp* and its polymorphic flanking genes – a blurry picture 73

4.3.3 Concluding remarks 75

4.4 MICE, MATERIAL AND METHODS 78

4.4.1 Mice 78

4.4.2 RNA-Seq 79

4.4.3 RFLP and sequencing analysis of candidate genes 80

4.4.4 Genome-wide and Chr2 STR analysis 82

4.4.5 High-resolution microsatellite genotyping on Chr2 82

4.4.6 Phagocytosis assay with pMΦ 83

4.4.7 Phagocytosis assay with BMDM 84

4.4.8 Flow cytometric analysis 84

4.4.9 Immunofluorescence 85

4.4.10 Induction of EAE and clinical evaluation 85

4.4.11 Histology and immunohistochemistry 85

4.4.12 Statistical analysis 86

4.5 SUPPLEMENTARY TABLES 87

4.5.1 Supplementary Table 1. List of differentially expressed genes in pMΦ of B6.129-*Prnp*$^{Zrchl/Zrchl}$ vs. B6.129-*Prnp*$^{wt/wt}$ identified by RNA-Seq. 87
4.5.2 Supplementary Table 2. Genes containing non-synonymous SNPs between B6.129-*Prnp*$^{Zrchl/Zrchl}$ vs. B6.129-*Prnp*$^{wt/wt}$ 96
5 TRANSPLANTED STROMAL-VASCULAR PDGFRβ^{+} CELLS DEVELOP INTO FUNCTIONAL FOLLICULAR DENDRITIC CELLS 101
5.1 INTRODUCTION 102
5.1.1 The stromal compartment of lymphoid tissues 102
5.1.2 FDC in physiological and pathological conditions 107
5.1.3 Scientific aims 109
5.2 RESULTS 111
5.2.1 FDC are derived from PDGFRβ^{+} precursors 111
5.2.2 Characterization of isolated stromal-vascular PDGFRβ^{+} cells 115
5.2.3 Transplanted PDGFRβ^{+} stromal-vascular cells develop into mature FDC 121
5.2.4 FDC derived from transplanted PDGFRβ^{+} stromal-vascular cells trap IC 126
5.2.5 Factors influencing outcome of stromal-derived PDGFRβ^{+} cells transplantations 130
5.3 DISCUSSION 132
5.3.1 PDGFRβ as a marker for FDC precursors 132
5.3.2 Recapitulation of FDC development in a collagen sponge 134
5.3.3 A role for FDC precursors in prion diseases? 136
5.4 MICE, MATERIAL AND METHODS 139
5.4.1 Mice 139
5.4.2 Isolation of perigonadal white adipose stromal-vascular cell fraction 139
5.4.3 Quantitative RT PCR 140
5.4.4 Subcapsular renal transplantation of PDGFRβ^{+} stromal-vascular cells 141
5.4.5 *In vitro* IC trapping 141
5.4.6 In vivo IC trapping 142
5.4.7 Immunohistochemistry and immunofluorescence 142
5.4.8 Quantification of Mfge8 staining on *Pdgfrb*-Cre^{+} x CAG-tdTomato (Ai14) spleen sections 143
6 ACKNOWLEDGMENTS 144
7 CURRICULUM VITAE AND PUBLICATIONS 147
8 BIBLIOGRAPHY 149

1 SUMMARY

The cellular prion protein termed PrP^C is an extracellular GPI-linked protein expressed by cells in many organs, including those of the nervous and immune system. It has attracted broad scientific interest due to its crucial role in the pathogenesis of prion diseases, which are transmissible and fatal neurodegenerative conditions occurring in humans and animals. Overwhelming evidence indicates that the infectious prion agent consists solely of a misfolded and aggregated isoform of PrP^C, as formulated in the protein-only hypothesis. One of the main pillars of this hypothesis is that mice lacking PrP^C fail to succumb to prion diseases. These *Prnp*$^{-/-}$ mice have been the subject of extensive investigations to search for the physiological role of PrP^C, which to date remains enigmatic. Various subtle phenotypes have been reported in *Prnp*$^{-/-}$ mice, many of which are not reproducible in different laboratories, suggesting the influence of confounding genetic elements. Most of these studies with discordant results were conducted using knockout animals on a specific genetic background that contained residual ESC-derived genetic material surrounding *Prnp*. These flanking regions may contain polymorphic genes that may be responsible for misinterpretation of phenotypes attributed to the ablated gene. The goal of the first project described in this thesis was to identify any potential confounding genes in *Prnp*$^{-/-}$ mice and to revisit two immune phenotypes attributed to PrP^C based on observations in *Prnp*$^{-/-}$ mice that lacked mechanistic explanation: modulation of phagocytosis of apoptotic cells and regulation of neuroinflammation. Applying formal genetics with genomic and transcriptomic approaches as well as functional studies, we provide evidence that the polymorphic immunoregulatory signal regulatory protein alpha (SIRPα), and not PrP^C, regulate the uptake of apoptotic cells, thus disproving the proposed function of PrP^C as an inhibitor of phagocytosis. However, the development of the experimentally induced neuroinflammation seems to be regulated neither by SIRPα polymorphisms nor by PrP^C.

Hence, these results conflict with previously published findings that the absence of PrP^C exacerbates neuroinflammation, and also suggest that other polymorphic genes flanking *Prnp* exert a stronger effect on the EAE disease course than *Prnp* and/or *Sirpa*. In conclusion, our study not only questions many previously reported phenotypes attributed to the prion protein, but also provides an approach to identify possibly confounding genes in knockout mice.

In the second part of my thesis, I describe the experiments that enabled us to prove that FDC derive from perivascular PDGFRβ^+ precursors. FDC are stromal cells located in SLO, where they provide a crucial scaffold for lymphoid follicles and facilitate the encounter between immune cells and antigens to generate high-affinity antibodies. In chronic inflammatory states such as rheumatoid arthritis and persistent infections, ectopic lymphoid structures containing FDC can arise almost anywhere in the body, suggesting that radiation-resistant stromal FDC precursors must develop *in situ* from unknown local precursors. Previous work in our lab identified perivascular PDGFRβ^+ cells as the earliest cells co-expressing the FDC marker Mfge8. We lineage-traced FDC and confirmed that mature PDGFRβ^- FDC expressed PDGFRβ during their development. When isolated from the stromal-vascular fraction of perigonadal fat, pure PDGFRβ^+ cells fractions respond to FDC maturation factors by expressing FDC differentiation markers *in vitro*. To test their identity as *bona fide* FDC precursors, we soaked collagen sponges with purified stromal-vascular PDGFRβ^+ cells and transplanted them under the renal capsule of FDC-deficient *Ltbr*$^{-/-}$ hosts. After four weeks we detected networks of cells expressing mature FDC markers and capable of trapping IC and recruiting B cells. Because *Ltbr*$^{-/-}$ animals cannot generate FDC, these experiments demonstrate that stromal-vascular PDGFRβ^+ cells can give rise to mature and functional FDC. The identification of the perivascular origin of FDC explains their ability to arise rapidly in almost every region of the body under conditions of continuous inflammatory stimulation and may contribute to understanding the pathogenesis of autoimmune and other chronic

inflammatory disorders. Also, mature FDC are used as Trojan horses by various pathogens, such as HIV, and participate in the accumulation and replication of prions. Our findings provide the basis for future experiments to assess whether FDC precursors can participate in these destructive processes.

2 ZUSAMMENFASSUNG

Das zelluläre Prion Protein, genannt PrP^C, ist ein extrazelluläres Protein, welches durch einen GPI-Anker mit der Zellmembran verbunden ist. Viele Zellen exprimieren PrP^C, darunter auch Zellen des Nervensystems und des Immunsystems. Dieses Protein hat grosse Aufmerksamkeit der Forschung auf sich gezogen, da es entscheidend an der Entstehung von Prionenerkrankungen beteiligt ist. Diese Gruppe von übertragbaren und unheilbaren neurodegenerativen Erkrankungen findet sich sowohl beim Menschen als auch beim Tier. Gemäss der sogenannten „Prionhypothese“ besteht das infektiöse Agens nur aus PrP^{Sc} Protein, welches einer falsch gefalteten und aggregierten Isoform von PrP^C entspricht. Einer der wichtigsten Grundpfeiler dieser Hypothese ist die Tatsache, dass genetisch manipulierte Mäuse, welche kein PrP^C herstellen, resistent für Prionenerkrankungen sind. Diese *Prnp*$^{-/-}$ Tiere wurden auch in zahlreichen Studien untersucht, die sich der Ergründung der physiologischen Funktion des Prion Proteins widmeten. Bis heute gibt es jedoch keine mechanistisch geklärte Funktion, die man dem Prion Protein zuschreiben kann. *Prnp*$^{-/-}$ Mäuse weisen verschiedene sehr subtile Auffälligkeiten auf, die Hinweise auf die Funktion von PrP^C geben könnten. Viele dieser Auffälligkeiten konnten jedoch von verschiedenen Forschergruppen nicht bestätigt werden, was auf möglicherweise vorhandene genetische Störfaktoren hinweist. Die meisten dieser kontroversen Studien wurden mit auf einen bestimmten genetischen Hintergrund gekreuzten Knockout-Mäusen durchgeführt, die jedoch residuelles genetisches Material rund um den manipulierten *Prnp*-Locus enthalten, welches von der genetisch manipulierten embryonalen Stammzelle stammt. Diese benachbarten genetischen Anteile können Gene mit Polymorphismen enthalten, die beim Zuschreiben eines beobachteten Phänotyps zum manipulierten Gen zu falschen Interpretationen führen können. Das Ziel des Projektes, welches ich im ersten Teil meiner Dissertation beschreibe, war einerseits die Identifikation solcher möglicherweise vorhandenen Gene

um den *Prnp*-Locus. Andererseits wollten wir zwei Immunfunktionen reevaluieren, welche dem Prion Protein basierend auf Studien in *Prnp*$^{-/-}$ Mäusen zugeschrieben wurden: Modulation der Phagozytose von apoptotischen Zellen und Regulierung der Entstehung von Neuroinflammation. Mit Hilfe von genetischen, genomischen und transkriptomischen Untersuchungen, sowie mit funktionellen Studien konnten wir zeigen, dass das polymorphe immunregulierende Protein SIRPα, und nicht PrP^{C}, die Phagozytose von apoptotischen Zellen reguliert. Bei der Untersuchung von experimenteller autoimmunen Enzephalomyelitis (EAE) sahen wir jedoch, dass weder SIRPα Polymorphismen, noch PrP^{C} deren Entstehung beeinflussten. Diese Resultate widersprechen demnach publizierten Studien, in denen *Prnp*$^{-/-}$ Mäusen einen schlimmeren Verlauf der Entzündung aufwiesen, und weisen auch darauf hin, dass zusätzliche polymorphe Gene, die *Prnp* benachbart sind, den EAE Verlauf stärker als *Prnp* und/oder *Sirpa* beeinflussen könnten. Unsere Studie stellt deshalb nicht nur zahlreiche vorgeschlagene Funktionen des Prion Proteins in Frage, sondern kann als Beispiel dienen, wie Gene, die dem manipulierten Locus benachbart sind und möglicherweise als Störfaktoren fungieren, untersucht werden können.

Im zweiten Teil meiner Arbeit beschreibe ich die Experimente, mit denen wir zeigen konnten, dass follikuläre dendritische Zellen (FDC) von perivaskulären PDGFRβ^{+} Vorläuferzellen abstammen. FDC sind stromale Zellen, welche in sekundären lymphoiden Organen entscheidend am Aufbau von Lymphfollikeln und an der Interaktion zwischen Immunzellen und Antigenen beteiligt sind. Während chronischer Entzündungen, wie zum Beispiel der Rheumatoiden Arthritis, oder bei chronischen Infektionen, können ektope Entzündungsherde mit FDC fast überall im Körper neu entstehen. Dies weist darauf hin, dass die strahlenresistenten und stromalen FDC Vorläufer lokal von dort ansässigen, bisher unbekannten Vorläuferzellen abstammen müssen. Frühere in unserem Institut durchgeführte Arbeiten haben perivaskuläre PDGFRβ^{+} Zellen mit Hilfe des FDC Markermoleküls Mfge8 als früheste FDC

Vorläuferzellen identifiziert. Wir führten weitere Experimente durch, welche zeigen, dass reife FDC, bei denen PDGFRβ nicht nachweisbar ist, dieses Molekül während ihrer Entwicklung exprimiert haben. Wir isolierten stromal-vaskuläre PDGFRβ$^+$ Zellen aus perigonadalem Fettgewebe und sahen, dass diese Zellen *in vitro* auf Gabe von FDC Differenzierungsfaktoren mit der Expression von FDC-Molekülen reagierten. Um zu ergründen, ob diese Zellen wirkliche FDC Vorläufer sind, transplantierten wir einen Schwamm mit reinen stromal-vaskulären PDGFRβ$^+$ Zellen unter die Nierenkapsel von FDC-freien *Ltbr*$^{-/-}$ Mäusen. Nach vier Wochen fanden wir in diesen Transplantaten Zellnetzwerke, die reife FDC Marker aufwiesen und fähig waren Immunkomplexe zurückzuhalten und B Zellen zu rekrutieren. Da sich in *Ltbr*$^{-/-}$ Mäusen keine reifen FDC entwickeln können, konnten diese neu entstandenen reifen FDC nur von den transplantierten stromal-vaskulären PDGFRβ$^+$ Zellen abstammen. Die Erkenntnis, dass FDC von perivaskulären Zellen abstammen, erklärt die rasche und fast ubiquitäre Entstehung von FDC unter chronischen Entzündungszuständen. Diese Resultate werden hoffentlich dazu beitragen, neue Erkenntnisse über die Pathogenese von Autoimmunkrankheiten und anderen chronisch entzündlichen Erkrankungen zu erlangen. Auch werden reife FDC von verschiedenen Erregern, wie dem HIV, als Versteck, oder von Prionen als Akkumulations-, und Replikationsorte missbraucht. Die Identifizierung von FDC Vorläuferzellen wird es ermöglichen die Frage zu beantworten ob diese auch schon an solch heimtückischen Prozessen beteiligt sind.

3 ABBREVIATIONS

129	129 mouse strain (including substrains, e.g. 129/Sv)
AA	amino acid
α-SMA	smooth muscle alpha-actin
B6	C57BL/6 mouse strain
BEC	blood endothelial cell
BMDM	bone-marrow derived macrophages
C	BALB/c mouse strains
CD	cluster of differentiation
cDNA	complementary desoxyribonucleic acid
CFA	complete Freund's adjuvant
Chr2	chromosome 2 of the laboratory mouse
CJD	Creutzfeldt–Jakob disease
CNS	central nervous system
CR	complement receptor
CXCL	CXC-chemokine ligand
DNA	desoxyribonucleic acid
EAE	experimental autoimmune encephalomyelitis
ESC	embryonic stem cell
FDC	follicular dendritic cell
FGCZ	functional genomic center Zürich
FRC	fibroblastic reticular cell
GC	germinal center
gDNA	genomic DNA
GPI	glycosyl phosphatidyl inositol
HEV	high endothelial venule
IAP	integrin alpha 7 expressing pericyte
IC	immune complex
ICAM	intercellular adhesion molecule
Ig	immunoglobulin
i.p.	intraperitoneal
HE	hematoxylin and eosin
LEC	lymphatic endothelial cell
LN	lymph node
LT	lymphotoxin
LTβR	lymphotoxin β receptor
LTi	lymphoid tissue inducer cell
LTo	lymphoid tissue organizer cell
Madcam	mucosal vascular addressin cell adhesion molecule
MALT	mucosa-associated lymphoid tissue
Mertk	gene encoding c-mer proto-oncogene tyrosine kinase MER
Mfge8	milk fat globule-EGF factor 8 protein
MGG	May-Grünwald-Giemsa
MRC	marginal reticular cell

MS	multiple sclerosis
M:T	macrophage : thymocytes (ratio)
NGS	next generation sequencing
ORF	open reading frame
PAP	peroxidase-anti-peroxidase
PCR	polymerase chain reaction
PDGFRβ	platelet-derived growth factor receptor beta
PE	phycoerythrin
p.i.	post immunization
pMΦ	peritoneal macrophages
Prnp	gene encoding the prion protein
PrP	prion protein
PrP^{C}	normal cellular isoform of the prion protein
PrP^{Sc}	pathological misfolded (scrapie) isoform of the prion protein
qPCR	quantitative PCR
RFLP	restriction fragment length polymorphism
ROI	region of interest
RNA	ribonucleic acid
RNAi	RNA interference
RNA-Seq	RNA sequencing
RT-PCR	reverse transcription PCR
s.c.	subcutaneous
SD	standard deviation
SEM	standard error of the mean
Sirpa	gene encoding signal regulatory protein alpha
SIRPα	signal regulatory protein alpha
SLO	secondary lymphoid organs
SNP	single nucleotide polymorphism
SPF	specific pathogen free
sRBC	sheep red blood cells
STR	short tandem repeat
TBM	tingible body macrophage
Thbs1	gene encoding thrombospondin 1 protein
TLO	tertiary lymphoid organs
TNF	tumor necrosis factor
TNFR	tumor necrosis factor receptor
TSE	transmissible spongiform encephalopathies
TSP-1	thrombospondin 1 protein
Tyro3	gene encoding tyrosine-protein kinase receptor 3
VCAM	vascular cell adhesion molecule
vSMC	vascular smooth muscle cell
WAT	white adipose tissue

4 THE ROLE OF THE PRION PROTEIN IN THE IMMUNE SYSTEM

Parts of this chapter of my thesis are reproduced or adapted from the following manuscript in preparation:

The SIRPα receptor, but not the prion protein, controls phagocytosis of apoptotic cells

Mario Nuvolone[1,2+], Veronika Kana[1,+], Gregor Hutter[1,+], Daiji Sakata[1], Steven M. Mortin-Toth[3], Giancarlo Russo[4], Jayne S. Danska[3,#] and Adriano Aguzzi[1, #]

[1] Institute of Neuropathology, University Hospital of Zurich, Zurich, Switzerland
[2] Amyloidosis Research and Treatment Centre, Foundation IRCCS San Matteo Hospital and Department of Molecular Medicine, University of Pavia, Institute for Advanced Studies, Pavia
[3] Hospital for Sick Children, Programme in Genetics and Genome Biology, University of Toronto, Faculty of Medicine, Departments of Immunology and Medical Biophysics MaRS East Tower 14-313, 101 College Street, Toronto, ON, Canada M5G 1L7
[4] Functional Genomic Center Zurich, University of Zurich, Zurich, Switzerland
[+] Equal contribution

[#] Correspondence:
Adriano Aguzzi, Institute of Neuropathology, University Hospital of Zurich, Schmelzbergstrasse 12, CH-8091 Zurich, Switzerland, Phone: +41 (44) 255-2107, Fax: +41 (44) 255-4402, email: adriano.aguzzi@usz.ch

Jayne S. Danska, Hospital for Sick Children, Programme in Genetics and Genome Biology, MaRS East Tower 14-313, 101 College Street, Toronto, ON, Canada M5G 1L7, Phone: +1 416 813 8810, Fax: +1 416 813 8823, email: jayne.danska@sickkids.ca

Parts of the introduction of this chapter of my thesis are reproduced or adapted with the permission from John Wiley and Sons, Rightslink license number: 3127170502680, from the following book chapter:

Aguzzi, A. and Kana, V. (2011) Introduction to Prion Disorders, in Neurodegeneration: The Molecular Pathology of Dementia and Movement Disorders, Second Edition (eds D. W. Dickson and R. O. Weller), Wiley-Blackwell, Oxford, UK. doi: 10.1002/9781444341256.ch31

4.1 INTRODUCTION

4.1.1 Prion diseases – the inglorious reason for the prion protein's fame

Prion diseases, also called TSE, are deadly neurodegenerative diseases occurring in humans and animals (Aguzzi and Calella, 2009). A defining trait of TSE is their infectious nature. The infectious agent causing TSE, the prion, consists solely of ordered aggregates of PrP^{Sc}, the abnormally folded, protease-resistant, beta-sheet rich isoform of the normal PrP^{C}, the main statement of the "protein-only"-hypothesis (Fig. 1) (Aguzzi and Polymenidou, 2004). The provocative concept, that protein alone, without genetic material, could act as an infectious agent was proposed by Griffith (Griffith, 1967), who found that the unknown infectious material in brains from Scrapie-affected sheep was resistant to ultraviolet irradiation, high temperatures and various aggressive chemicals, hence devoid of nucleic acids. Later, Prusiner purified and characterized PrP^{Sc} (Bolton et al., 1982), and called this infectious protein "prion", a portmanteau word fusing *Pr*oteinaceous *I*nfectious particle with viri*on*. More specifically, he defined prion as "a small proteinaceous infectious particle that is resistant to inactivation by most procedures that modify nucleic acids" (Prusiner, 1982). Since then, the "protein-only"-hypothesis was endorsed by many findings, among them the crucial identification of the *Prnp* gene, which encodes PrP^{Sc} and also the normal cellular prion protein PrP^{C} (Chesebro et al., 1985; Oesch et al., 1985), followed by the generation of *Prnp* knockout mice lacking PrP^{C} (Büeler et al., 1992). The striking resistance of these mice to prion infectivity provided strong evidence for the protein-only hypothesis (Büeler et al., 1993). The generation of de novo infectivity from defined compounds would ultimately prove that PrP^{Sc} is the sole infectious agent (Colby and Prusiner, 2011). Yet, prions produced by genetically engineered bacteria and converted into aggregates that contained recombinant PrP^{C} alone, yielded only low infectivity (Kim et al., 2010; Legname et al.,

2004; Makarava et al., 2010). Interestingly, by adding “cofactors” such as lipids or RNA, the de-novo generated prions reached equal infectivity similar to brain homogenates from terminally ill prion infected mice (Deleault et al., 2007; Supattapone, 2010; Wang et al., 2010). The role of these cofactors is not well defined. While the association of these cofactors with misfolded PrP^{Sc} is a possible explanation for the prion strain phenomenon (Aguzzi et al., 2007; Li et al., 2010), their precise role in the promotion of prion replication and generation of infectivity is unclear (Colby and Prusiner, 2011).

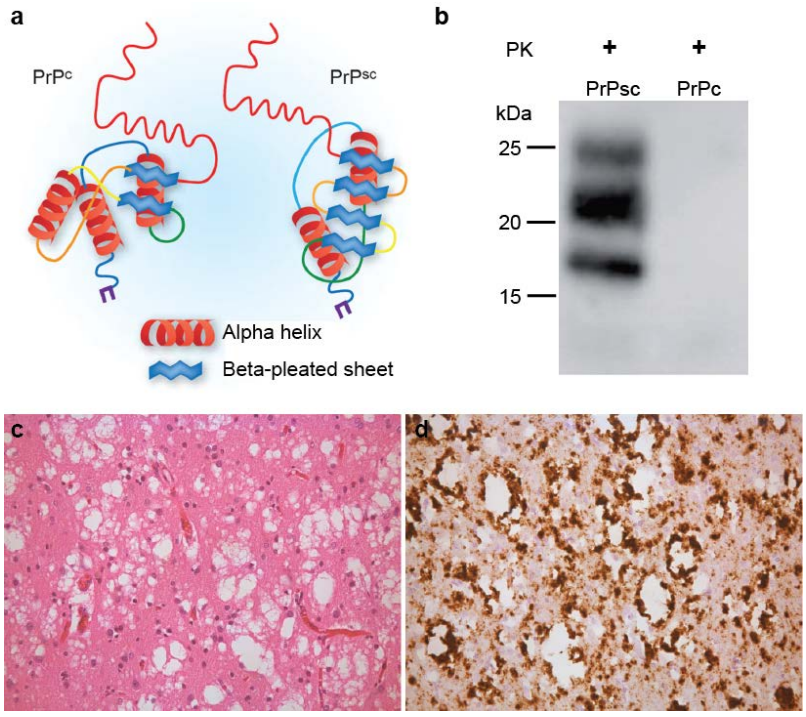

Figure 1. Characteristics of prion diseases. (a) Schematic representation of normal (PrP^{C}) and disease-associated (PrP^{Sc}) isoforms of the prion protein, which have identical amino-acid sequences, but differ in their secondary structure. The high amount of beta-sheets in PrP^{Sc} increases its propensity to form higher ordered aggregates and elongate into fibrils (Goldschmidt et al., 2010). (b) PrP^{Sc} aggregates are partially resistant to proteinase K (PK) digestion as shown in a PrP^{C}-immunoblot of brain homogenates from prion-infected (left) and uninfected (right) mice. (c) Formation of large vacuoles in the cerebral cortex of a patient affected by sCJD. This observed “*status spongiosus*” is a pathological hallmark of TSE, along with extensive neuronal cell loss and astrogliosis. (d) Another cardinal feature of prion diseases is the widespread deposition of amyloid plaques or amorphous PrP aggregates (Glatzel et al., 2005). The cortex of a sCJD patient stained with PrP-specific antibodies shows accumulation of insoluble PrP^{Sc} deposits. Panel (a) reused and adapted from (Wilson and Nixon, 2009), and panels (b-d) reused and adapted from (Aguzzi and O'Connor, 2010), with the permission of Nature Publishing Group, Rightslink license numbers: 3127540974267 and 3127541294550.

In humans, prion diseases present with rapidly progressive dementia, akinetic mutism, myoclonus, ataxia, visual and cerebellar impairments. Based on clinical, neuropathological and genetic findings, human prion diseases are classified as sporadic, inherited, or infectious (Glatzel et al., 2005). In most cases, patients are affected with the sporadic form of CJD (sCJD), whose cause is unknown. Less than 10% of reported human prion cases are familial forms such as familial CJD, Gerstmann–Sträussler–Scheinker syndrome or fatal familial insomnia, where mutations in the human *PRNP* gene have been identified as the causative primary pathogenic event (Glatzel et al., 2005; Hsiao and Prusiner, 1990). Yet the best-known, most threatening forms of prion diseases are those caused by transmission between individuals due to iatrogenic infection (Brown et al., 2012), or even from animals to humans, as seen in the bovine spongiform encephalopathy (BSE) crisis in the late 20th century, where the ingestion of contaminated animal products is believed to have led the outbreak of variant CJD (Ironside, 2012).

How do peripherally acquired prions reach the CNS? The immune system has been shown to be the major player in this process called neuroinvasion, since the peripheral immune system is indispensable for extraneural prion replication and subsequent spread of the infectious agent to the CNS (Fig. 2) (Aguzzi and Heikenwalder, 2006). Experiments in mice lacking various components of the immune system have pointed to the crucial role of FDC in the process of prion accumulation and replication. FDC depend on signaling through LTβR, thus interfering with this pathway at various levels inhibits peripheral prion replication (Klein et al., 1997; Mabbott et al., 2000; Montrasio et al., 2000; Prinz et al., 2003; Prinz et al., 2002). However, ectopic inflammatory foci without mature FDC and mice, whose FDC differentiation is stopped at a premature level, still show prion replication competence, suggesting that stromal cells other than mature FDC, possibly FDC precursors, can participate in prion propagation (Heikenwalder et al., 2008; Krautler et al., 2012; Oldstone et al., 2002; Prinz et al., 2002). Accordingly, generic

stimulation of the immune system and induction of chronic inflammatory conditions, which favor the generation of tertiary lymphoid organs (TLO), enhance the susceptibility to prion infection and lead to an increased peripheral prion deposition – even in organs previously deemed prion free – and accelerate the disease process (Bremer et al., 2009; Heikenwalder et al., 2005; Klein et al., 2001; Ligios et al., 2005; Seeger et al., 2005). Since replication-competent cells of the secondary lymphoid organs have been shown to be in direct contact with dendrites from peripheral neurons, the spread via axons of peripheral nerves might explain how prions finally find their way into the CNS (Glatzel et al., 2001; Heikenwalder et al., 2007).

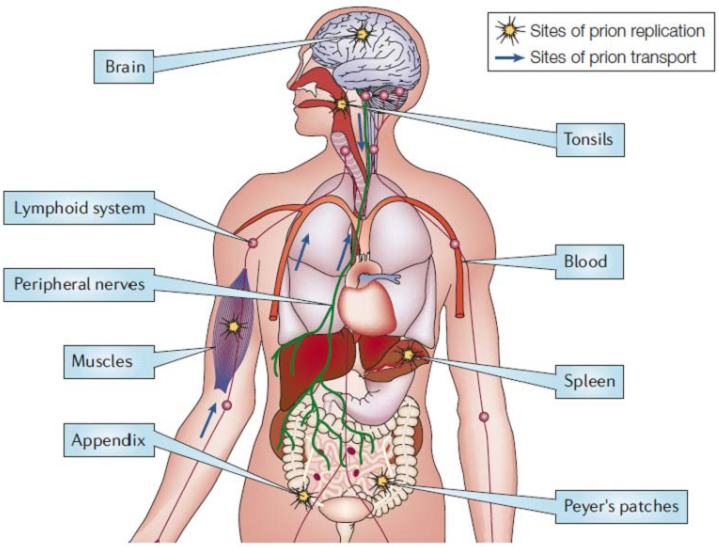

Figure 2. Propagation of prions in the organism. Orally acquired prions are taken up by M cells in the intestine (Donaldson et al., 2012) and reach SLO either directly or via blood and lymphoid fluids. After peripheral replication in SLO, prions are transported to the brain primarily by peripheral nerves. Apart from SLO, prions can be detected in other extraneural tissues, such as skeletal muscle (Glatzel et al., 2003). Figure reprinted from (Aguzzi and Heikenwalder, 2006) with permission from Nature Publishing Group; Rightslink license number: 3127721289952.

The role of the immune system in CNS prion propagation is less clear. Mice whose peripheral immune system was genetically or pharmacologically modulated show equal susceptibility to prion diseases after intracerebral inoculation. On the other hand, prion diseases lead to a dramatic activation of CNS-resident microglia, which can phagocytose PrP^{Sc} *in vitro*, and – less efficiently – *in vivo* (Aguzzi et al., 2013). Moreover, experiments with organotypic tissue slice cultures show that the removal of microglia leads to a 15-

fold increase of prion titers, suggesting that microglia play an important role in the clearance of PrP^{Sc} (Falsig and Aguzzi, 2008; Heppner et al., 2005), even though they eventually lose the battle against the rapidly replicating infectious agent.

4.1.2 A function for PrP^{C} in the immune system

The cellular isoform of the prion protein, PrP^{C}, is a GPI-anchored extracellular protein containing two N-terminal glycosylation sites and is associated to lipid rafts (Taylor and Hooper, 2006). NMR studies of mouse prion protein (Hornemann et al., 1997; Riek et al., 1996; Riek et al., 1997) have revealed a long, flexible, unstructured amino-terminal part (AA 23–120) with several octapeptide repeats (termed OR) and two charged clusters (CC_1: AA 23-37; CC_2: AA 95-110) and a structured carboxy-terminal globular domain (AA 121-231) containing three α-helices, and two β-sheets. The carboxy-terminal globular domain and the amino-terminal flexible part are connected by a hydrophobic part (AA 111-134, termed hydrophobic core (HC)). The prion protein is highly conserved across species, suggesting a broad and important function (Aguzzi et al., 2008). This notion is strengthened by its virtually ubiquitous expression: PrP^{C} is not only highly expressed in the developing and adult CNS, but is also found in the peripheral nervous system, kidney, heart, skeletal muscle, in various hematopoietic cells (monocytes, dendritic cells, megakaryocytes, lymphocytes, hematopoietic progenitors), pericytes, and in secondary lymphoid organs, particularly in FDC (Aguzzi and Heikenwalder, 2006; Ford et al., 2002; Linden et al., 2008).

The dramatic phenotype of prion diseases, the threatening BSE crisis and the fascinating, yet highly controversial protein-only hypothesis has led to an enormous scientific interest in prion biology and the normal function of the cellular prion protein. Although among the most studied proteins, the function of PrP^{C} has not been explained at a mechanistic level to date (Aguzzi et al., 2008). Most searches for the physiological

role of PrP^C are based on experiments in *Prnp* knockout mice. These mice have a clear and irrefutable phenotype characterized by resistance to the infectivity of the prion agent (Büeler et al., 1993; Büeler et al., 1992). In addition, studies in *Prnp* knockout mice have revealed numerous subtle phenotypes, which affect a large variety of physiological functions of an organism. These include neuronal signal transduction, various behavioral, metabolic and immunological functions, myelin maintenance, copper binding, amyloid capture, and both pro- and anti-apoptotic functions (Aguzzi et al., 2008; Biasini et al., 2012; Bremer et al., 2010; Calella et al., 2010; Laurén et al., 2009; Linden et al., 2008; Steele et al., 2007). Some of these proposed functions have been confirmed, but equally many have been refuted by subsequent studies from other laboratories, questioning their validity. In the following paragraphs, I will introduce two functions, which were attributed to PrP^C: and include the inhibition of phagocytosis and modulation of neuroinflammation.

PrP^C as an inhibitor of phagocytosis of apoptotic cells

Phagocytosis of apoptotic cells is a basic process of the organism crucial for development, tissue homeostasis, innate and adaptive immunity. Defects in its function or regulation can lead to autoimmunity, developmental defects, organ dysfunction and cancer (Gregory and Devitt, 2004; Lemke and Rothlin, 2008; Ravichandran and Lorenz, 2007). Removal of apoptotic cells is carried out by special, so-called “professional” mononuclear phagocytes, which are dendritic cells, and include circulating monocytes in the blood and tissue-resident macrophages (Kindt et al., 2007). But also “non-professional” phagocytes, such as retinal pigment epithelial cells, kidney mesangial cells, or Sertoli cells in the testis, take up dying cells and their debris, and thereby contribute to the function of their resident organ (Gregory and Devitt, 2004). In contrast to the phagocytic uptake of pathogens, where pathogens recognition patterns lead to the direct recognition of the target and opsonization activates Fc receptor-mediated uptake (Poon

et al., 2010), the removal of apoptotic cells involves a multistep signal exchange between the dying cell and the phagocyte. After having sent out “find-me” signals, which help the phagocyte to sense the dying cell, the engulfment process itself is initiated by “eat-me” signals, which are displayed by the dying cell and recognized by various engulfment receptors on the phagocyte (Fig. 3) (Lauber et al., 2012; Nagata et al., 2010). The process of apoptosis involves also the downregulation of “don’t-eat-me” signals, which are expressed on cells to avoid phagocytosis and thereby regulate and balance the phagocytic uptake of cognate cells (Fig. 3) (Lauber et al., 2012). One of the best-described molecule pairs mediating a “don’t eat me” signal are the ubiquitously expressed CD47 and SIRPα found on the phagocyte. The ligation of CD47 on the target cell and SIRPα on the phagocyte negatively regulates the phagocytic process and hence the CD47 expressing cell evades engulfment (Matozaki et al., 2009). Accordingly, cells from CD47 deficient mice are rapidly cleared from wild type phagocytes (Oldenborg et al., 2000).

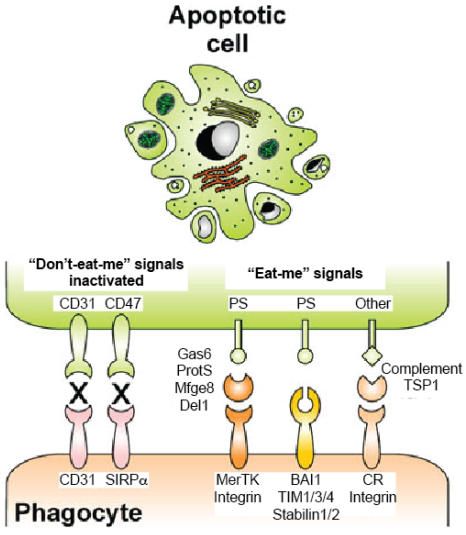

Figure 3. Phagocytosis of apoptotic cells: examples of "eat-me" and “don’t-eat-me” signals”. Apoptotic cells downregulate “don’t-eat-me” signals, such as CD31 and CD47, hence the inhibitory signal of CD31 and SIRPα on phagocytes is abolished. The exposure of PS, normally found inside the plasma membrane, is the major “eat-me” signal. PS alone or in combination with attached molecules (e.g. Gas6, Mfge8) is recognized by engulfment receptors on the phagocyte (Ravichandran and Lorenz, 2007). Other eat me signals bind complement or TSP1, and mediate binding to SR, CR and integrins. BAI-1, brain angiogenesis inhibitor 1; PS, phosphatidylserine; TIM, T cell Ig and mucin; SR, scavenger

receptor. Figure adapted from (Lauber et al., 2012), © 2012 Lauber, Ernst, Orth, Herrmann and Belka, Creative Commons Attribution License.

PrP^C was reported to be an additional phagocyte receptor that would sense and mediate "don't-eat-me" signals, and hence act as an inhibitor of phagocytosis (de Almeida and Linden, 2005). Peritoneal macrophages and retinal Müller glial cells from *Prnp*$^{-/-}$ mice were shown to be more active in engulfing apoptotic cells than phagocytes expressing wildtype PrP^C (de Almeida et al., 2005). The molecular mechanisms by which PrP^C could act as inhibitor of phagocytosis are unclear. It was proposed that the GPI-anchored PrP^C might influence the ligand-binding of other engulfment receptors or regulate their relocation to lipid rafts (de Almeida et al., 2005; de Almeida and Linden, 2005; Peyron et al., 2000).

PrP^C as a modulator of neuroinflammation

While expression of PrP^C in mature quiescent T cells was shown to be low (Liu et al., 2001), T cell activation leads to PrP^C upregulation (Cashman et al., 1990; Isaacs et al., 2006). In addition, PrP^C was found to be part of the immunological synapse (Ballerini et al., 2006; Paar et al., 2007) and to co-precipitate with the TCR (Mattei et al., 2004), suggesting that PrP^C might actively modulate T cell activation and function.

This hypothesis can be tested in an *in vivo* model of $CD4^+$ T cell-mediated autoimmune disease, EAE, which is widely used to study neuroinflammation and has led to the elucidation of important aspects of MS pathogenesis (Baxter, 2007; Schreiner et al., 2009). EAE is characterized by perivascular inflammation, primary demyelination and subsequent axonal damage leading to ascending paralysis. These events are induced by peripheral immunization with CNS tissue or an emulsion of myelin peptide, such as myelin basic protein or proteolipid protein in complete Freud's adjuvants, together with pertussis toxin (Miller et al., 2010). This leads to the peripheral priming of myelin-specific

$CD4^+$ T cells, which transmigrate through the choroid plexus and enter the subarachnoid space, where they are re-stimulated by local antigen-presenting cells to finally enter the brain parenchyma (Greter et al., 2005). Activated T cells produce chemokines and cytokines, which activate local microglia, further, disrupt the blood-brain barrier and induce a massive influx of effector T cells and monocytes (Ajami et al., 2011; Ransohoff and Engelhardt, 2012). The demyelination of axonal tracts is a result of inflammatory and cytotoxic effector molecules released by activated T and mononuclear cells, and the subsequent phagocytosis by activated microglia and monocytes (Miller et al., 2010).

Several groups have studied the effect of removal of the *Prnp* gene (henceforth termed *Prnp*$^{-/-}$) on the development of mouse EAE (Table 1). In the first study, the authors Tsuitsui et al reported that the lack of PrP^C led to an earlier onset and a more severe EAE disease course during the chronic phase (Tsutsui et al., 2008). This was accompanied by increased infiltration of inflammatory cells and higher activity of myelin-primed T cells, suggesting a T-cell dependent attenuation of neuroinflammation (Tsutsui et al., 2008). A subsequent study reported a slight exacerbation of EAE during the onset of disease with increased T cell infiltrates in the brain, yet lower amounts of IL-17 responses, again suggesting an involvement of PrP^C in T cell activation (Ingram et al., 2009). In another study, *Prnp*$^{-/-}$ mice and mice treated with small interfering RNA (siRNA) blocking *Prnp* developed a more severe EAE and a higher antigen-specific T cell activation (Hu et al., 2010). In addition, PrP^C-overexpressing *tga20* mice (Fischer et al., 1996) showed only mild EAE symptoms, suggesting a PrP^C-dependent rescue of EAE exacerbation (Hu et al., 2010). In contrast, PrP^C-overexpressing *tga35* mice (Fischer et al., 1996) showed a similar exacerbation as *Prnp*$^{-/-}$ mice, both in the development of EAE and optic neuritis, yet PrP^C-overexpression had a neuroprotective effect on retinal ganglion cells in *tga35* mice as compared to *Prnp*$^{-/-}$ and the respective wild type mice (Williams et al., 2011). The authors of this study point to the reported insertional artifact reported in *tga20* mice, which perturbs T cell development (Zabel et al., 2008), and might

explain less sever EAE in *tga20* versus *tga35* mice. However, they do not comment on the exacerbation of EAE in presence of 4-5 times more PrP^C, which was comparable to the disease seen in *Prnp*$^{-/-}$ animals. Finally, a recent report again confirmed the exacerbation of EAE in mice lacking *Prnp*, but reciprocal bone-marrow reconstitution experiments demonstrated that the effect was caused by the lack of PrP^C function in the central nervous system, rather than the result of altered T cell function in *Prnp*$^{-/-}$ mice (Gourdain et al., 2012). Taken together, these studies consistently report a worsening of the EAE development in the absence of PrP^C – with considerable variation in the onset and severity of the effect. This might be the result of different immunization protocols, the heterogeneity of the mouse strains, or reflect the intrinsic variability of the EAE model (Gold et al., 2006; Gourdain et al., 2012). Yet the studies in PrP^C-overexpressing mouse strains yielded conflicting results and there are unresolved discrepancies concerning the underlying mechanisms of the observed phenotype.

***Prnp*$^{-/-}$ strain**	***Prnp*$^{+/+}$ strain**	***Prnp*$^{-/-}$ phenotype**	**Rescue/other experiments**	**Reference**
FVB129-*Prnp*$^{Zrchl/Zrchl}$ littermates (F1) B6129-*Prnp*$^{Zrchl/Zrchl}$ backcrossed for 7-8 generations	FVB129-*Prnp*$^{+/+}$ littermates (F1) C57BL/6 wild type	Exacerbation of EAE, at onset and during chronic phase	T-cell mediated	(Tsutsui et al., 2008)
FVB/N.129-*Prnp*$^{Zrchl/Zrchl}$ backcrossed for 10 generations	FVB/N wild type	Exacerbation of EAE, at onset	T-cell mediated	(Ingram et al., 2009)
Sv129/Ola-*Prnp*$^{Edbg/Edbg}$	Sv129/Ola-*Prnp*$^{wt/wt}$	Exacerbation of EAE, at onset	-*Prnp*-siRNA -*tga20*: EAE suppression -T cell mediated	(Hu et al., 2010)
B6129-*Prnp*$^{Zrchl/Zrchl}$	C57BL/6 wild type	Exacerbation of EAE, optic neuritis	*tga35*: EAE exacerbation	(Williams et al., 2011)
B6.129-*Prnp*$^{Zrchl/Zrchl}$ backcrossed for > 12 generations	C57BL/6 wild type	Exacerbation of EAE, during chronic phase	-non T-cell mediated -dependent on PrP^C in CNS	(Gourdain et al., 2012)

Table 1. Studies investigating the role of PrP^C in EAE development.

4.1.3 The *Prnp* knockout mouse and the flanking gene problem

Since the generation of the first Zürich I-*Prnp*$^{-/-}$ line (*Prnp*$^{ZrchI/ZrchI}$) (Büeler et al., 1992), a remarkable number of other laboratories have engineered independent *Prnp*$^{-/-}$ mouse strains using homologous recombination. Similarly to the Zürich I line, the genetic modification in Edinburgh-*Prnp*$^{-/-}$ (*Prnp*$^{Edbg/Edbg}$) (Manson et al., 1994) is restricted to the open reading frame of exon 3 in the mouse *Prnp* gene. These two mouse lines showed normal development and no severe pathologies in adulthood. Yet they have been fundamental in supporting the protein-only hypothesis, since these mice were resistant to prion infection (Büeler et al., 1993; Weissmann and Flechsig, 2003). In contrast to the normal development of these two lines, the subsequently generated Nagasaki-*Prnp*$^{-/-}$ line (*Prnp*$^{Ngsk/Ngsk}$) (Sakaguchi et al., 1995), as well as the Rcm0-*Prnp*$^{-/-}$ line (*Prnp*$^{Rcm0/Rcm0}$) (Moore et al., 1995), and the Zürich II-*Prnp*$^{-/-}$ line (*Prnp*$^{ZrchII/ZrchII}$) (Rossi et al., 2001) developed severe neurological abnormalities with ataxia and Purkinje cell loss (Fig. 4).

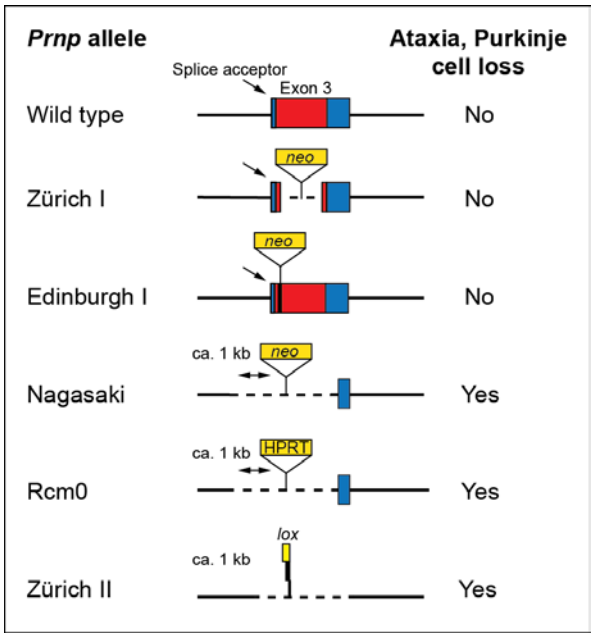

Figure 4. Mouse lines with disrupted *Prnp* locus. Different strategies used to knock out *Prnp*. Dotted line: segment of deleted *Prnp* DNA. Yellow, inserted sequence; red, open reading frame; blue, noncoding region; neo, neomycin phosphotransferase; HPRT, hypoxanthine phosphoribosyltransferase; lox, a 34-bp recombination site from phage P1. Figure adapted from (Weissmann and Aguzzi, 1999) with the permission of Science.

Since the reintroduction of a *Prnp* transgene reversed the, this effect was originally thought to relate to *Prnp* deletion (Nishida et al., 1999). However, the lack of phenotype observed in the Zürich I and Edinburgh lines did not support this hypothesis. These

divergent results could only be resolved when a new gene, *Prnd*, located 16 kb downstream of *Prnp* and coding for the Doppel (Dpl) protein, was discovered. A careful examination of the *Prnp* deletion strategies revealed that the deletion in Nagasaki, Rcm0, and Zürich II-lines involved also a splice acceptor site for *Prnp* exon 3. As a result, *Prnd* was expressed under the control of the *Prnp* promoter, which led to the formation of chimeric RNA and a Dpl-overexpression in the brain, causing ataxia and Purkinje cell loss (Moore et al., 1999; Weissmann and Aguzzi, 1999).

All available *Prnp*$^{-/-}$ lines were generated using ESC derived from the inbred 129 strain of the laboratory mouse (Silver, 2008; Wade and Daly, 2005). The Edinburgh-*Prnp*$^{-/-}$ and the Rcm0 lines represent the only lines that were generated and maintained on the same genetic background, thus representing coisogenic mouse strains (Fig. 5; Manson et al., 1994; personal communication D. Melton). Coisogenic knockout and wild type animals are genetically identical, with the exception of the targeted locus, which in this example is *Prnp*. Furthermore, they represent the most clean genetic experimental setting when searching for a knockout phenotype (Silver, 2008).

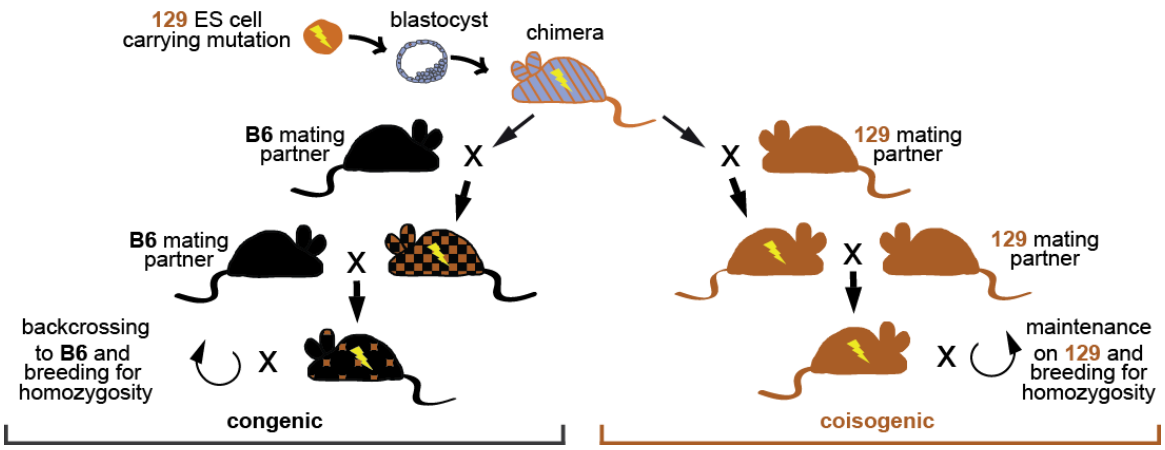

Figure 5. Main steps in the generation of coisogenic and B6.129 congenic mouse strains. 129-derived ESC carrying the targeted mutation are injected into blastocysts from variable strains (most frequently B6, C, FVB), which are injected in pseudopregnant females (not shown). To generate a coisogenic strain (right), chimeric mice are bred with mating partners form the same strain as the ESC, thereby creating coisogenic 129-knockout mice, which differ only in the targeted locus from their wild type counterparts. To generate a congenic mouse strain (left), the chimeric mice are bred with mating partners from another strain, here B6. Backcrossing to B6 for

at least 10 generations creates a congenic B6.129 knockout strain. In B6.129 congenic mice, residual 129 genomic material derived from the ESC (in brown) is present, particularly in the region flanking the targeted locus.

However, the 129 mouse strain has certain disadvantages, such as poor breeding performance, and behavioral and immunological abnormalities, and therefore researches traditionally preferred to backcross the knockout lines to more robust strains, such as the B6 strain (Fig. 5) (Seong et al., 2004). Hence, in all other *Prnp*$^{-/-}$ lines, the chimeric *Prnp*$^{wt/-}$ mice were crossed with wild type mice of a strain other than 129, most frequently the B6 strain. The resulting mice carrying the targeted allele were then maintained either on a mixed background (mainly B6 and 129, B6.129) or repeatedly backcrossed for a minimum of 10 generation to a specific inbred strain to create a so-called congenic strain (Fig. 5) (Silver, 2008). Every backcrossing event progressively reduces the 129-derived genetic material. However, despite extensive backcrossing to a non-129 strain, a significant fragment of 129-derived genomic material will cosegregate with the *Prnp* locus (Sparkes et al., 1986), due to the low probability of recombination between closely linked genes. Thus, any polymorphism located within these flanking fragments will contaminate all congenic *Prnp*$^{-/-}$ strains. As a result of this, in most of the studies comparing *Prnp*$^{wt/wt}$ and *Prnp*$^{-/-}$ mice, the two experimental groups differed not only at the targeted locus, *Prnp*, but also for an undetermined number of polymorphic loci between the 129 and the non-129 strain used for backcrossing.

This phenomenon, which is commonly observed in knock out animal studies, is referred to as the “flanking gene problem” (Eisener-Dorman et al., 2009; Gerlai, 1996; Smithies and Maeda, 1995). It creates a fundamental confounder when attributing specific functions to a gene based on observations made in knockout animals. This observation also holds true for the functions reported for PrP^{C}, since most of the subtle phenotypes reported in *Prnp*$^{-/-}$ mice were studied in congenic animals (Steele et al., 2007). In order to

validate subtle phenotypes as seen in *Prnp*$^{-/-}$ mice, it becomes crucial to exclude the contribution of linked polymorphic genes cosegregating with *Prnp*.

4.1.4 Scientific aims

Prnp$^{-/-}$ mice are resistant to prion diseases (Büeler et al., 1993; Büeler et al., 1992) and show many subtle phenotypes, which however have not been reproduced in different laboratories (Steele et al., 2007), suggesting the presence of interfering genetic confounders. All currently available *Prnp*$^{-/-}$ mice have been generated using 129-derived ESC, and with two exceptions, were kept in a mixed background, or backcrossed for > 10 generations, thereby creating congenic mice (Crusio et al., 2009). Whilst this approach progressively reduces the content of the 129-derived genomic material, 129-derived regions flanking *Prnp* co-segregate with it and persist. These regions may contain many polymorphic genes, which may confound the attribution of phenotypes to PrP^{C} based on studies in *Prnp*$^{-/-}$ mice (Steele et al., 2007; Wolfer et al., 2002).

We have selected two phenotypes, which were previously reported in *Prnp*$^{-/-}$ mice and lack mechanistic explanation - first, a simple, cell-autonomous function, modulation of phagocytosis (de Almeida et al., 2005), and second, a complex phenotype involving the interplay of many different immune cells, the regulation of EAE development (Gourdain et al., 2012; Ingram et al., 2009; Tsutsui et al., 2008).

Here I will describe the genetic, genomic and transcriptomic approaches we used to validate the influence of *Prnp* and its linked genes on phagocytosis of apoptotic cells and EAE development.

4.2 RESULTS

4.2.1 Higher phagocytic activity in congenic – but not in coisogenic – *Prnp* knockout mice

To determine the potential contribution of PrP^C in regulating phagocytosis of apoptotic cells, we compared the phagocytic activity of primary macrophages isolated from *Prnp*$^{wt/wt}$ and three independent strains of *Prnp*$^{-/-}$ mice. As assessed by a microscopy-based *in vitro* phagocytosis assay (Fig. 6a), pMΦ from congenic B6.129-*Prnp*$^{Zrchl/Zrchl}$ mice (Büeler et al., 1992) phagocytosed more apoptotic thymocytes than macrophages from heterozygous B6.129-*Prnp*$^{wt/Zrchl}$ and wildtype congenic B6.129-*Prnp*$^{wt/wl}$ littermates (Fig. 5, Fig. 6b, Fig. 7), in agreement with the previously reported hyperphagocytic phenotype of B6.129-*Prnp*$^{Zrchl/Zrchl}$ mice (de Almeida et al., 2005). We observed the same hyperphagocytosis also seen in BMDM of B6.129-*Prnp*$^{Zrchl/Zrchl}$ mice, as well as in BMDM of another *Prnp*$^{-/-}$ mouse strain, the congenic B6.129-*Prnp*$^{Ngsk/Ngsk}$ mice (Sakaguchi et al., 1995) (Fig. 8). However, when assessing the phagocytosis activity of pMΦ isolated from coisogenic 129-*Prnp*$^{Edbg/Edbg}$ mice (Manson et al., 1994), we could not detect any significant difference compared to 129-*Prnp*$^{wt/wt}$ littermate pMΦ (Fig. 9). 129-*Prnp*$^{Edbg/Edbg}$ mice were generated from 129 ESC and kept as a strictly coisogenic line (Fig. 5). Therefore, coisogenic 129-*Prnp*$^{Edbg/Edbg}$ and 129-*Prnp*$^{wt/wt}$ are thought to differ only in their *Prnp* status, and are considered free of potentially confounding polymorphic flanking genes. Thus, the lack of increased phagocytic activity in 129-*Prnp*$^{Edbg/Edbg}$ macrophages indicated that ablation of *Prnp* was insufficient to drive hyperphagocytosis, and suggested the presence and influence of additional non-identical genetic elements in the congenic Zrchl-, and Ngsk-lines.

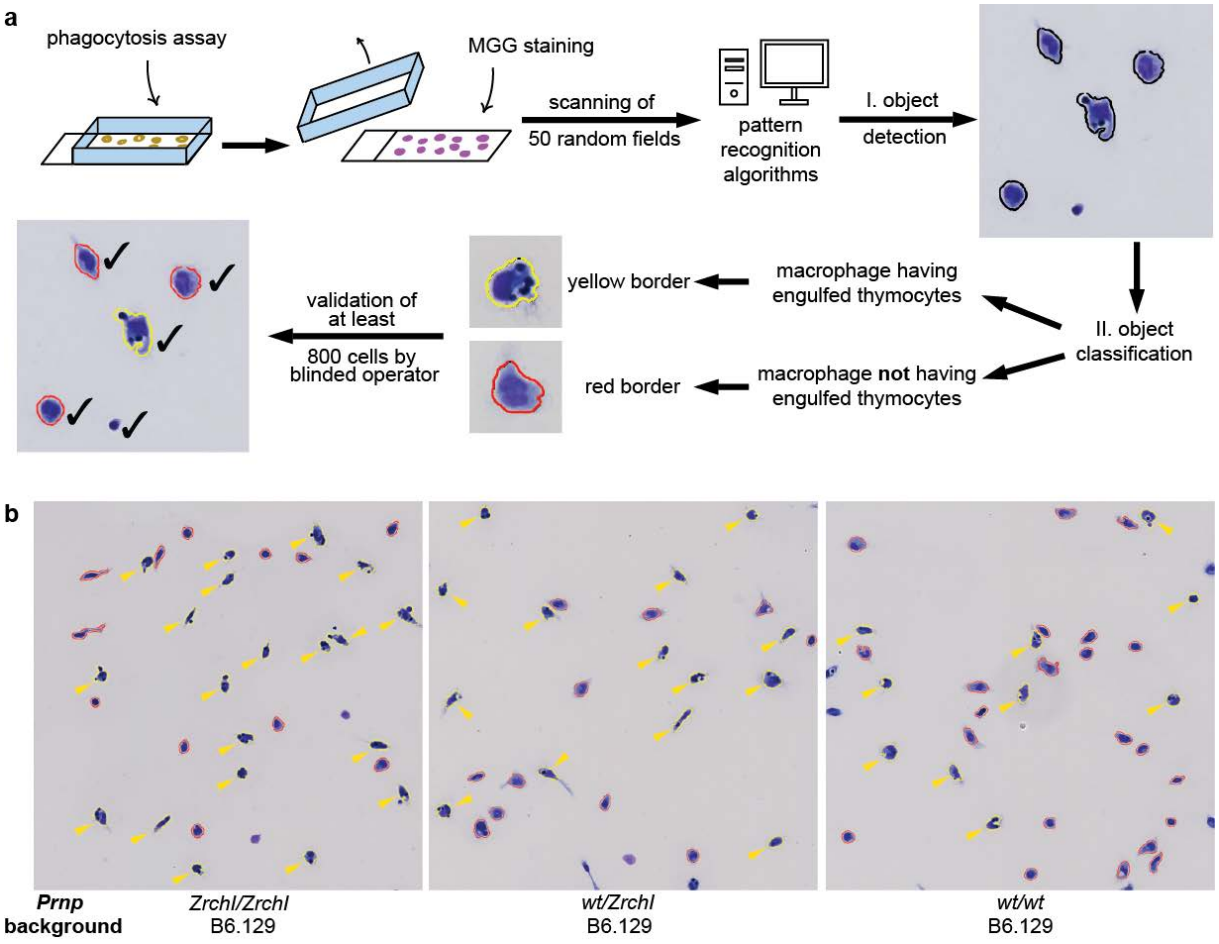

Figure 6. Microscopy-based phagocytosis assay. (a) Workflow for assessing phagocytic activity of pMΦ using microscopy and software-based image analysis. After interaction of cultured pMΦ with apoptotic thymocytes, the wall of the one-well chamber slide was removed and the slide was stained with MGG. 50 randomly selected fields were scanned using an automated slide-scanning device. The obtained images were then analyzed by software developed by Monika Bieri and Norbert Wey for an automated detection and classification of cells. The software was trained to recognize macrophages according to their shape and size using a classification algorithm. An additional algorithm is applied to classify the detected cells into macrophages having engulfed thymycytes (yellow border) and macrophages not having engulfed thymocytes (red border). The analyzed images are then sent to a blinded operator, who validates at least 800 cells. **(b)** Representative light microscopy images of B6.129-*Prnp*$^{Zrchl/Zrchl}$, B6.129-*Prnp*$^{wt/Zrchl}$ and B6.129-*Prnp*$^{wt/wt}$ pMΦ. Yellow arrows indicate pMΦ having engulfed apoptotic thymocytes.

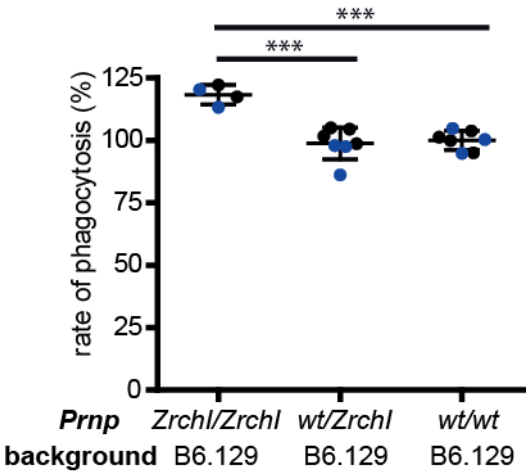

Figure 7. Phagocytic activity of pMΦ from congenic B6.129-*Prnp*$^{ZrchI/ZrchI}$, B6.129-*Prnp*$^{wt/ZrchI}$ and B6.129-*Prnp*$^{wt/wt}$ mice. pMΦ from congenic B6.129-*Prnp*$^{ZrchI/ZrchI}$ mice showed higher phagocytic activity that those of B6.129-*Prnp*$^{wt/ZrchI}$ and B6.129-*Prnp*$^{wt/wt}$ mice. Two independent experiments (shown as blue and black dots) were performed; mean phagocytic activities of B6.129-*Prnp*$^{wt/wt}$ (44.4% and 33.0% respectively) were set as 100%.

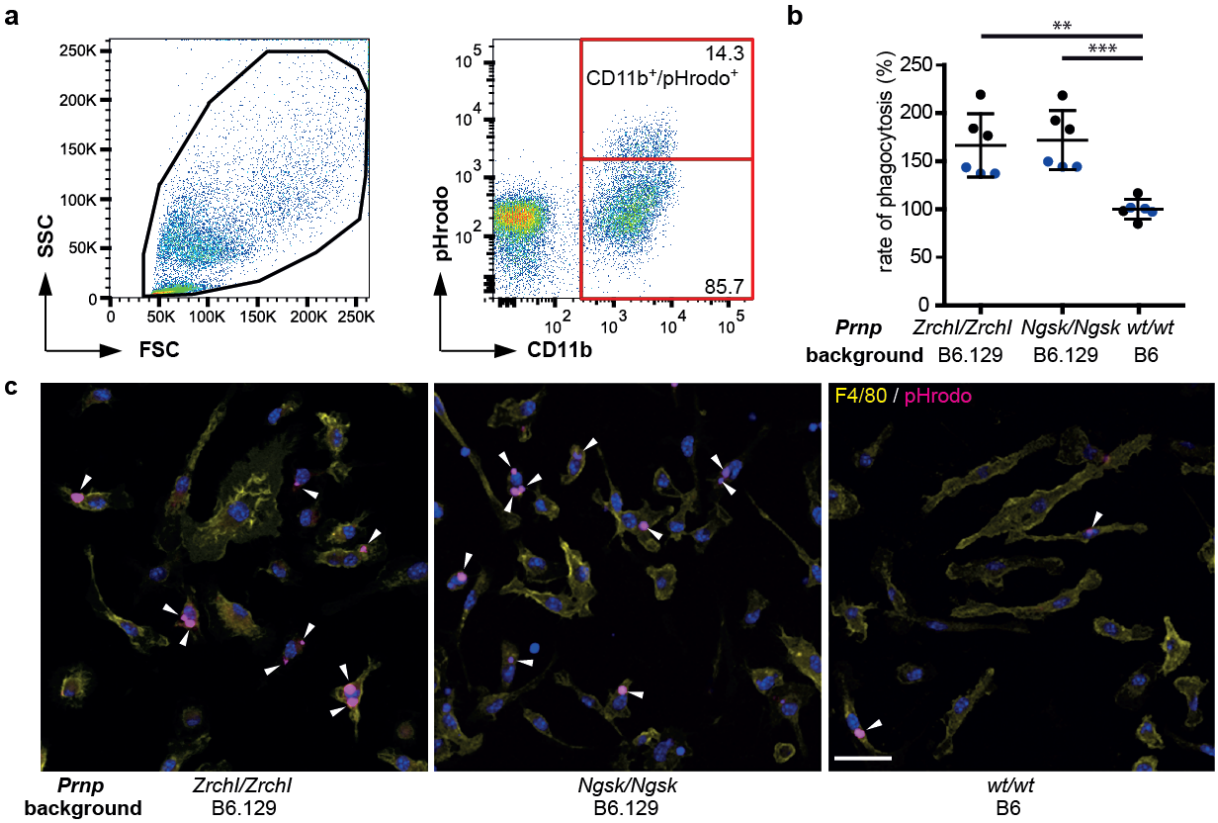

Figure 8. Phagocytic activity of BMDM from congenic B6.129-*Prnp*$^{ZrchI/ZrchI}$, congenic B6.129-*Prnp*$^{Ngsk/Ngsk}$ and B6-*Prnp*$^{wt/wt}$ mice. (a) Flow cytometry gating strategy for assessing phagocytic activity of BMDM. Gating of live nucleated cells (left panel) and quantification of CD11b+ pHrodo+ cells (macrophages having engulfed pHrodo-labelled apoptotic thymocytes, right panel). (b) BMDM from congenic B6.129-*Prnp*$^{ZrchI/ZrchI}$ and congenic B6.129-*Prnp*$^{Ngsk/Ngsk}$ show higher phagocytic activity than B6-*Prnp*$^{wt/wt}$ BMDM. Two independent experiments were performed (shown as blue and black dots); mean phagocytic activites of B6-*Prnp*$^{wt/wt}$ BMDM (11.9% and 18.4% respectively) were set as 100%

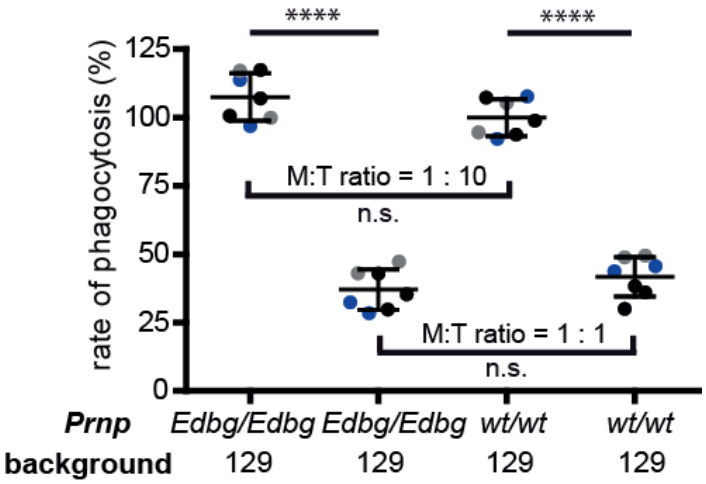

Figure 9. Phagocytic activity of coisogenic 129-*Prnp*$^{Edbg/Edbg}$ and 129-*Prnp*$^{wt/wt}$ pMΦ. The phagocytic activity of 129-*Prnp*$^{Edbg/Edbg}$ and 129-*Prnp*$^{wt/wt}$ macrophages was similar, both at higher (1:10) and lower (1:1) M:T ratios. Data are from three individual experiments (shown as blue, grey and black dots) and mean phagocytic activities of 129-*Prnp*$^{wt/wt}$ pMΦ at 1:10 (31.3%, 26.7% and 19.4% respectively) were set as 100%.

Having determined that *Prnp*$^{-/-}$ mice generated and maintained on the same genetic background as their *Prnp*$^{wt/wt}$ counterparts did not display the reported phagocytic phenotype, we hypothesized that the phenotype observed in backcrossed, congenic *Prnp*$^{-/-}$ mouse lines might be due to polymorphic flanking genes derived from the original ESC 129-strain (Fig. 5).

To control the genetic background of the three investigated *Prnp*$^{-/-}$ lines and to investigate the extend of the 129-derived region flanking the targeted *Prnp* locus that possibly contained polymorphic flanking genes, we performed low density microsatellite-assisted analysis of the whole genome (Fig. 10) and a medium density microsatellite analysis of the region on Chr2 containing the *Prnp* locus (Fig. 11). Whole-genome STR analysis confirmed that congenic B6.129-*Prnp*$^{ZrchI/ZrchI}$ and B6.129-*Prnp*$^{Ngsk/Ngsk}$ mice contained mostly B6 strain-specific STRs, comparable to the B6-reference (Fig. 10). On the other hand, 129-*Prnp*$^{Edbg/Edbg}$ mice and their 129-*Prnp*$^{wt/wt}$ littermates contained a homogeneous 129 strain genetic background (Fig. 10). As expected, the 129-*Prnp*$^{Edbg/Edbg}$ and 129-*Prnp*$^{wt/wt}$ strains also showed no differences in Chr2 around *Prnp* as assessed by a more dense STR analysis (Fig. 11), documenting their coisogenic generation.

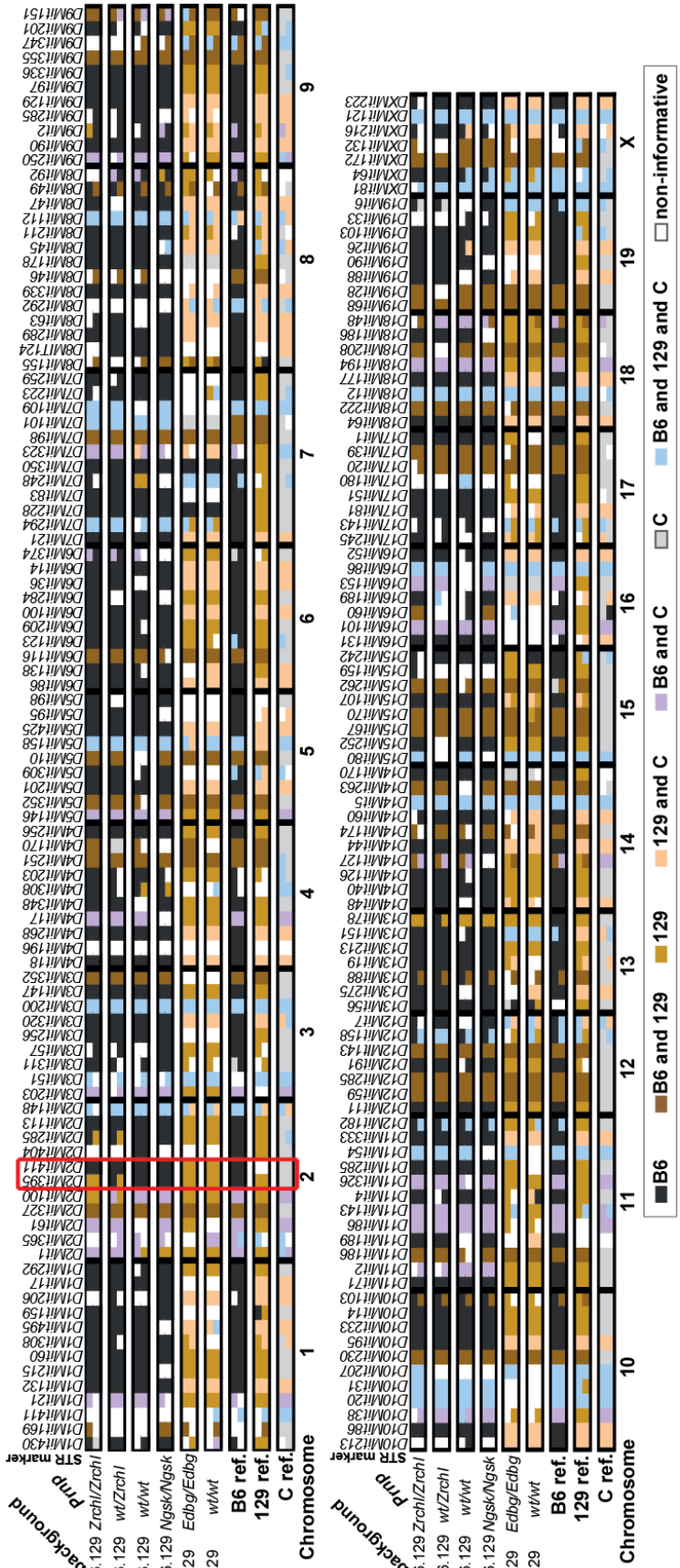

Figure 10. Whole genome STR analysis of B6.129-*Prnp*$^{Zrchl/Zrchl}$, B6.129-*Prnp*$^{Ngsk/Ngsk}$, 129-*Prnp*$^{Edbg/Edbg}$ and 129-*Prnp*$^{wt/wt}$ littermates. The red box denotes the region on Chr2 containing Prnp. Each line represents one mouse of a strain designated on the left. For heterozygous markers, the strain-defining color is arbitrary and does not represent a specific haplotype.

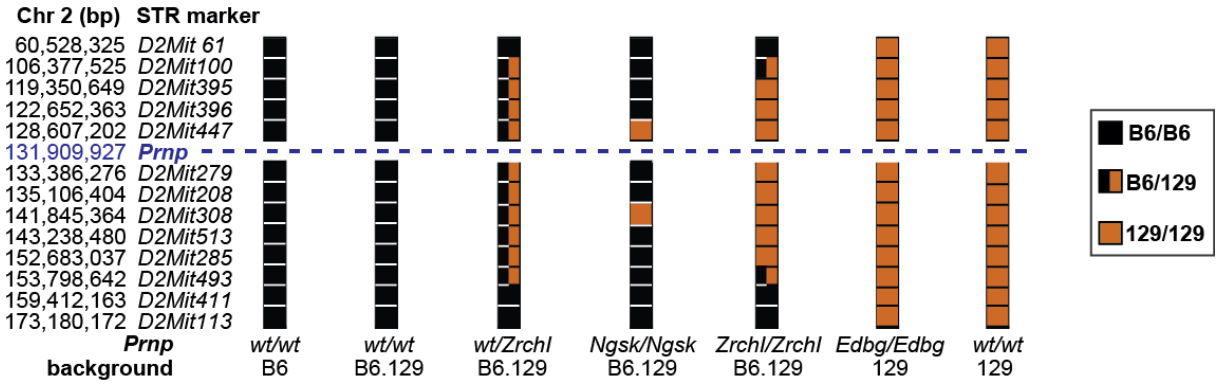

Figure 11. STR analysis of Chr2 of B6.129-*Prnp*$^{ZrchI/ZrchI}$, B6.129-*Prnp*$^{Ngsk/Ngsk}$, 129-*Prnp*$^{Edbg/Edbg}$ and 129-*Prnp*$^{wt/wt}$ mice. For each STR marker (colored box), name and position on Chr2 are indicated on the left. Blue dashed line indicates the position of *Prnp*. B6.129-*Prnp*$^{ZrchI/ZrchI}$, B6.129-*Prnp*$^{Ngsk/Ngsk}$ contain 129-derived genetic material flanking the *Prnp* locus. Conversely, the markers flanking the *Prnp* locus in129-*Prnp*$^{Edbg/Edbg}$ were identical to 129-*Prnp*$^{wt/wt}$ mice.

In congenic B6.129-*Prnp*$^{Ngsk/Ngsk}$ mice most markers were B6-derived, except the two markers *D2Mit308* and *D2Mit447*, which were homozygous for 129. *D2Mit447* is located 3.3 Mbp upstream of *Prnp* (Fig. 11), suggesting that the recombination breakpoint might be located between Chr2:128,607,202-131,909,927 bp in B6.129-*Prnp*$^{Ngsk/Ngsk}$ mice. However, when analyzing Chr2 of congenic B6.129-*Prnp*$^{ZrchI/ZrchI}$ mice, we found that these mice harbored 129-derived genomic material in a region of ≥ 47 Mbp flanking *Prnp* on Chr2, despite having been backcrossed for >12 generations (Fig. 11). This region was delimited by the microsatellite markers *D2Mit100* (Chr2:106,537,368-106,537,479 bp) and *D2Mit493* (Chr2:153,972,906-153,973,015 bp, MGI database) and contained 689 genes derived from the 129 genome (NCBI map viewer resource, mouse genome build 37.2). In order to narrow down the list of potential candidate genes explaining the observed phagocytic phenotype of B6.129-*Prnp*$^{ZrchI/ZrchI}$ macrophages, we systematically interrogated public databases for genes that were in linkage disequilibrium with the *Prnp* locus. We applied the following restrictions: a. mapped between Chr2: 106,537,479-153,972,906 bp; b. expressed in macrophages (MGI gene expression database); c.

involved in phagocytosis (if retrievable records on pubmed.gov using the search terms: “gene xy phagocytosis”, and/or associated terms on geneontology.org, using unfiltered search parameters and considering all recorded species); d. polymorphic between B6 and 129 strains (containing coding-non-synonymous SNPs, using MGI Strains, SNPs & Polymorphisms database). Out of the 698 genes mapped in this region, we found 8 genes that fulfilled all the criteria (Table 2), and thereby qualified as candidate confounder genes in studies comparing congenic *Prnp*$^{-/-}$ mice vs. *Prnp*$^{wt/wt}$ mice.

Region on Chr2 (bp)	Gene name	Protein
117,937,658-117,952,869	*Thbs1*	thrombospondin 1
119,625,250-119,643,840	*Tyro3*	TYRO3 protein tyrosine kinase 3
128,524,733-128,627,923	*Mertk*	c-mer proto-oncogene tyrosine kinase
129,418,575-129,457,964	*Sirpa*	signal-regulatory protein alpha
131,735,664- 131,764,167	***Prnp***	**prion protein**
148,262,387-148,269,271	*Cd93*	CD93 antigen
150,506,438-150,514,873	*Vsx1*	visual system homeobox 1 homolog
152,934,204-152,977,177	*Hck*	hemopoietic cell kinase
152,987,037-153,036,199	*Tm9sf4*	transmembrane 9 superfamily protein member 4

Table 2. Public database search identifies candidate confounder genes in the B6.129-*Prnp*$^{Zrchl/Zrchl}$ mouse on Chr2 in the *Prnp* flanking region delimited by D2Mit 100 and D2Mit493. All genes were shown to be expressed in macrophages and to be involved in phagocytosis and contain coding-non-synonymous SNPs between B6 and 129. In blue is the location of *Prnp*.

4.2.2 RNA sequencing identifies candidate confounder genes linked to *Prnp* on mouse Chr2

We were able to identify possible confounder genes using STR-markers and database searches (Table 2). To determine the allelic status of these eight candidates and to possibly identify other candidate confounder genes in our mice, we applied a NGS technology, RNA-Seq (Majewski and Pastinen, 2011; Wang et al., 2009). In order to find genes that are linked to *Prnp*, polymorphic between B6 and 129, and expressed only in macrophages, we performed RNA-Seq on B6.129-*Prnp*$^{Zrchl/Zrchl}$ and B6.129-*Prnp*$^{wt/wt}$ pMΦ (n = 3 per group) at the FGCZ. The use of RNA-Seq permitted us to a) find genes differentially expressed between B6.129-*Prnp*$^{Zrchl/Zrchl}$ and B6.129-*Prnp*$^{wt/wt}$ pMΦ, and b) to analyze the gene-coding sequences for the presence of single nucleotide variants between B6.129-*Prnp*$^{Zrchl/Zrchl}$ and B6.129-*Prnp*$^{wt/wt}$ pMΦ. Technical quality parameters of the RNA-Seq experiment are indicated in Table 3.

Mouse	Total number of reads	Mapped reads	Average coverage
WT 1	58,838,924	56,801,099 (96.5%)	58.604
WT 2	56,971,575	55,447,441 (97.3%)	60.104
WT 3	77,632,102	75,325,378 (97.0%)	67.430
KO 1	71,507,393	69,906,771 (97.8%)	64.637
KO 2	70,456,814	68,728,168 (97.6%)	62.745
KO 3	75,295,650	73,039,778 (97.0%)	65.377

Table 3 Technical quality parameters RNA-Seq: sequencing depth, mapping of reads, average coverage. WT: B6.129-*Prnp*$^{wt/wt}$; KO: B6.129-*Prnp*$^{Zrchl/Zrchl}$.

Detection of differentially expressed genes

Out of 11,586 transcribed genes, 304 were differentially expressed between the two groups (Fig. 12). The full list of genes is shown in Supplementary Table 1. 55 of the 304 differentially regulated genes were located on Chr2, significantly more than on any other

chromosome (p based on z-score (z > 44) = 0.0011, corrected for chromosome size). This clustering was even more pronounced, when considering the highly differentially expressed genes (absolute Log_2-fold change > 1) and correcting for chromosome size (p based on z-score (z > 29) = 0.00039).

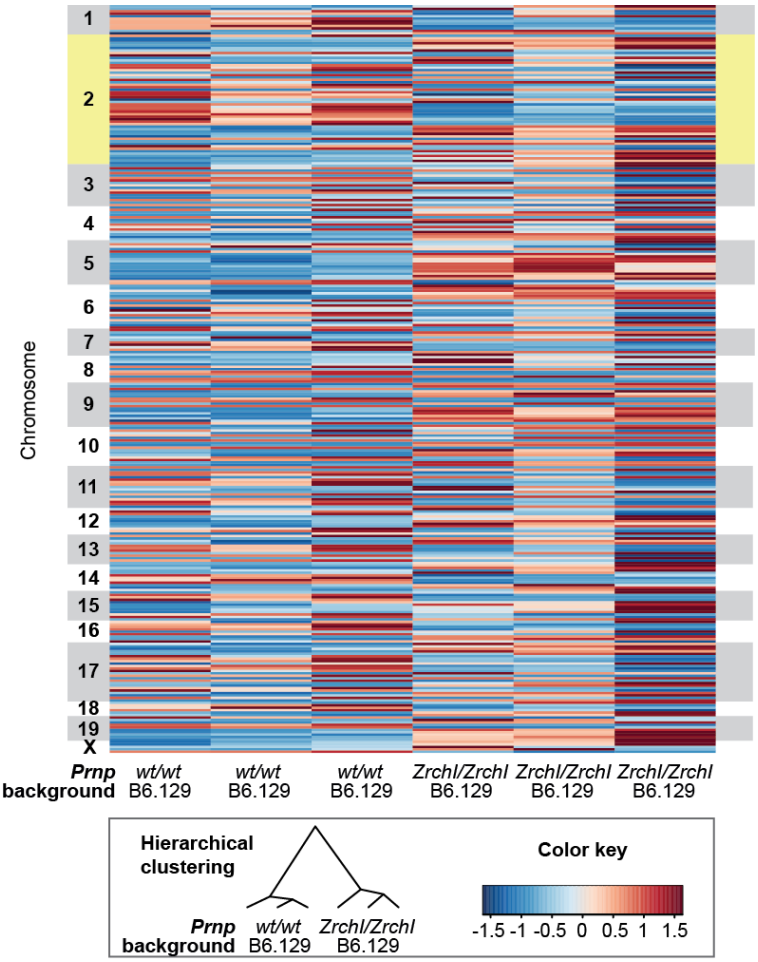

Figure 12. Heatmap of mRNA of 304 differentially expressed genes between B6.129-*Prnp*$^{ZrchI/ZrchI}$ and B6.129-*Prnp*$^{wt/wt}$ pMΦ. Genes are listed according to their chromosomal location. Columns represent data of individual mice, sorted by hierarchical clustering, as indicated by the dendrogram in the legend. Yellow: Chr2. All genes are listed in Supplementary Table 2.

Detection of single nucleotide variants

The reads were then analyzed for the presence of variants from the B6 transcriptome. Compared to B6 reference, B6.129-*Prnp*$^{ZrchI/ZrchI}$ pMΦ RNA contained more overall numbers of SNPs and more insertion/deletion mutations (indels) than did B6.129-

Prnp$^{wt/wt}$ pMΦ RNA (Table 4). To determine the distribution of variants among the transcriptome, we plotted the density of sequence variation of genes expressed in B6.129-*Prnp*$^{Zrchl/Zrchl}$ pMΦ against the chromosomal map and detected the highest SNP density on Chr2 (Fig. 13), located around *Prnp* at 128-156 Mbp (Fig. 14).

Mouse	# SNPs	# Het. SNPs	# Hom. SNPs	# Indels	# Nonsyn. variants	# Nonsyn. variants genes
WT 1	102,465	14,249	88,216	6,860	2,902	284
WT 2	102,756	12,591	90,165	7,451	2,874	280
WT 3	117,354	15,501	101,853	8,356	3,360	329
common for all WT	84,205	9,535	74,670	5,644	2,277	197
KO 1	117,979	15,146	102,833	8,164	3,517	365
KO 2	114,906	14,943	99,963	8,185	3,391	367
KO 3	117,592	15,539	102,053	8,405	3,515	379
common for all KO	92,176	9,569	82,607	6,397	2,682	264

Table 4 Summary of variants of the B6.129-*Prnp*$^{wt/wt}$ and B6.129-*Prnp*$^{Zrchl/Zrchl}$ transcriptomes as detected by RNA-Seq. WT: B6.129-*Prnp*$^{wt/wt}$; KO: B6.129-*Prnp*$^{Zrchl/Zrchl}$; #, number; SNPs: single nucleotide polymorphisms; Het.: heterozygous; Hom.: homozygous; Nonsyn.: nonsynonymous; Indels: insertions/deletions.

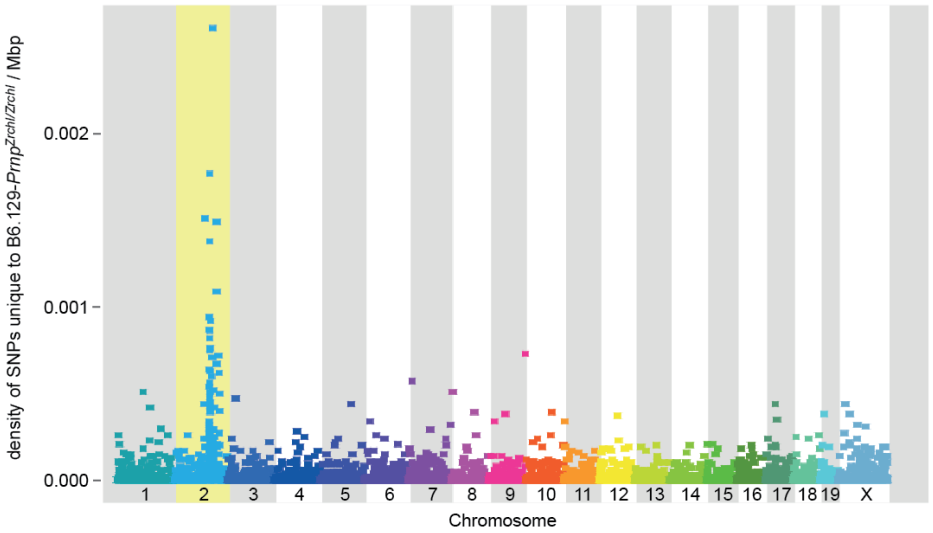

Figure 13. Manhattan plot showing the chromosomal distribution of SNPs found in the transcriptome of B6.129-*Prnp*$^{Zrchl/Zrchl}$, but not of B6.129-*Prnp*$^{wt/wt}$, pMΦ by RNA-Seq. Variants unique to B6.129-*Prnp*$^{Zrchl/Zrchl}$ pMΦ clustered on Chr 2 (in yellow, t-test, two tailed, p=0.019).

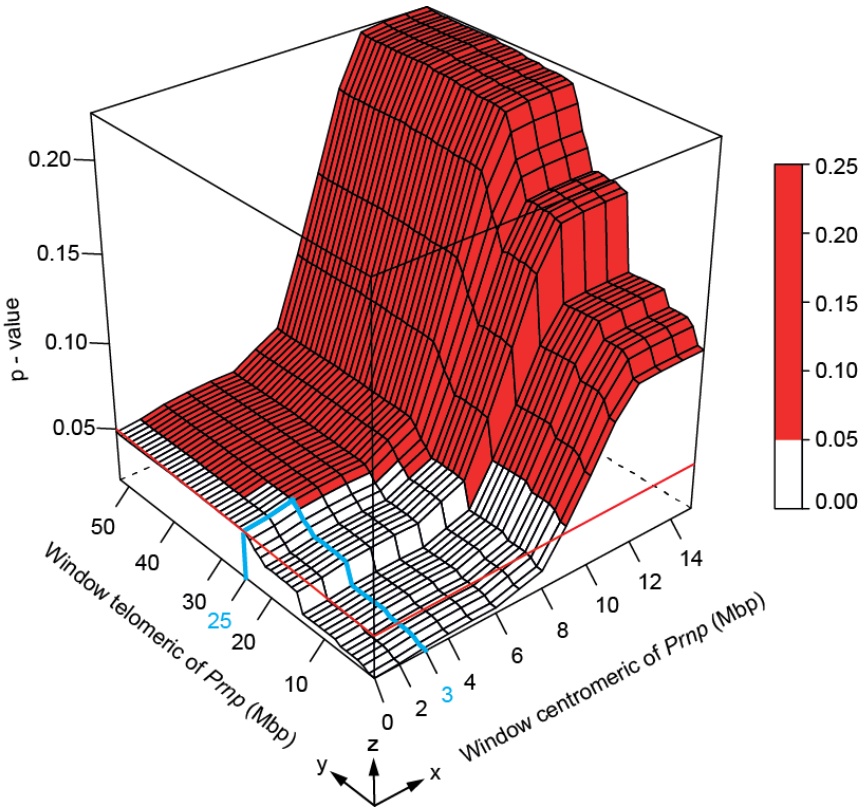

Figure 14. Clustering of SNPs on Chr2 around *Prnp* in B6.129-*Prnp*$^{Zrchl/Zrchl}$ vs. B6.129-*Prnp*$^{wt/wt}$. To identify the minimal region containing excess SNPs in the B6.129-*Prnp*$^{Zrchl/Zrchl}$ vs. B6.129-*Prnp*$^{wt/wt}$ peritoneal macrophage transcriptome, we determined the *p* value of SNP density comparison between these two groups when different regions of Chr 2 comprising *Prnp* where excluded from the analysis. In detail, we calculated p-values (two tailed t-test, z-axis) for every possible window spanning 2-100 Mbp around *Prnp* (set to position Chr 2: 130 Mbp) in steps of 1 Mbp. We compared the average SNP density between the two groups in the region 129-131 Mbp, then moved telomerically (y axis) or centromerically (x-axis) in 1-Mbp steps. Red area: $p \geq 0.05$. Blue line: boundaries of the minimal significantly SNP-enriched region comprising *Prnp* between B6.129-*Prnp*$^{Zrchl/Zrchl}$ and B6.129-*Prnp*$^{wt/wt}$ peritoneal macrophages, located at 128-156 Mbp on Chr 2.

Both differentially expressed genes and genes with high SNP density cluster on Chr2

Studies analyzing the effect of regulatory SNPs on gene expression have reported robust allele-specific differences in gene expression among different inbred mouse strains (Cowles et al., 2002). Consequently, when comparing congenic B6.129-*Prnp*$^{Zrchl/Zrchl}$ pMΦ vs. B6.129-*Prnp*$^{wt/wt}$ pMΦ RNA, where we found the largest density of SNPs around *Prnp*, we expected to find the majority of differentially expressed genes in

the same region, suggesting a 129-mouse strain-specific expression pattern. Indeed, we observed that genes that contained a high SNP density and were also differentially expressed, clustered on Chr2 around *Prnp* (Table 5). Apart from 1 gene (*Chd3)*, all genes that were polymorphic between B6 and 129 and also differentially expressed between the two groups are located on Chr2. Thereof, 8 genes are located < 12 Mbp from *Prnp*.

Gene	Locus	Log_2 - fold change	q-value
Dnm1	chr2:32308470-32353304	0.814	3.927e-02
Eif2ak4	chr2:118388616-118475234	-0.864	8.504e-05
Plcb2	chr2:118707516-118728438	0.790	1.755e-04
Zfyve19	chr2:119172499-119217050	-0.941	8.040e-04
Chac1	chr2:119351241-119354327	0.995	7.664e-04
Exd1	chr2:119519403-119547627	3.252	8.384e-06
Mtap1a	chr2:121289601-121351013	1.443	9.860e-03
Spg11	chr2:122053526-122118386	-1.104	4.966e-06
Slc28a2	chr2:122426476-122461130	0.735	2.236e-02
Chd3	chr11:69344350-69369391	-0.505	1.848e-02

Table 5. Genes containing a high density of SNPs and being differentially regulated in B6.129-*Prnp*$^{Zrchl/Zrchl}$ vs. B6.129-*Prnp*$^{wt/wt}$ mice. Display of top 10 genes according to their absolute log_2-fold change. 9 of 10 genes are located on chromosome 2.

Identification of candidate confounder genes linked to Prnp *controlling phagocytosis in* Prnp$^{Zrchl/Zrchl}$ *vs.* Prnp$^{wt/wt}$ *mice*

To identify genes that possibly act as a confounder in the phagocytic phenotype in congenic *Prnp*$^{-/-}$ mouse strains, we introduced a filtering strategy to narrow down the list of candidates (Fig. 15). We analyzed all 22,981 SNPs not shared between B6.129-*Prnp*$^{wt/wt}$ and B6.129-*Prnp*$^{Zrchl/Zrchl}$ pMΦ for the presence of variants affecting the amino acid sequence of the transcribed protein (non-synonymous coding SNPs). We found 132 transcribed genes harboring non-synonymous coding variants between B6.129-*Prnp*$^{wt/wt}$

and B6.129-*Prnp*$^{Zrchl/Zrchl}$ pMΦ (Supplementary Table 2). Of these, 62 genes mapped on Chr2 (47%) between 34,943,257 and 175,061,548 bp, and 56 of these were located in the region previously identified using STR analysis as being 129-derived in congenic B6.129-*Prnp*$^{Zrchl/Zrchl}$ vs. B6.129-*Prnp*$^{wt/wt}$ mice (delimited by the microsatellite markers *D2Mit100* (Chr2:106,537,368-106,537,479 bp) and *D2Mit493* (Chr2:153,972,906-153,973,015 bp), Fig. 11). We then searched public databases for prior evidence demonstrating an involvement in phagocytosis (Fig. 15). Four of the 62 genes located on chromosome 2 matched this criterion: *Sirpa*, *Mertk*, *Tyro3* and *Thbs* (Box 1) and therefore qualified as potential confounder genes when comparing the phagocytic activity of macrophages isolated from congenic *Prnp*$^{-/-}$ vs. *Prnp*$^{+/+}$ mice

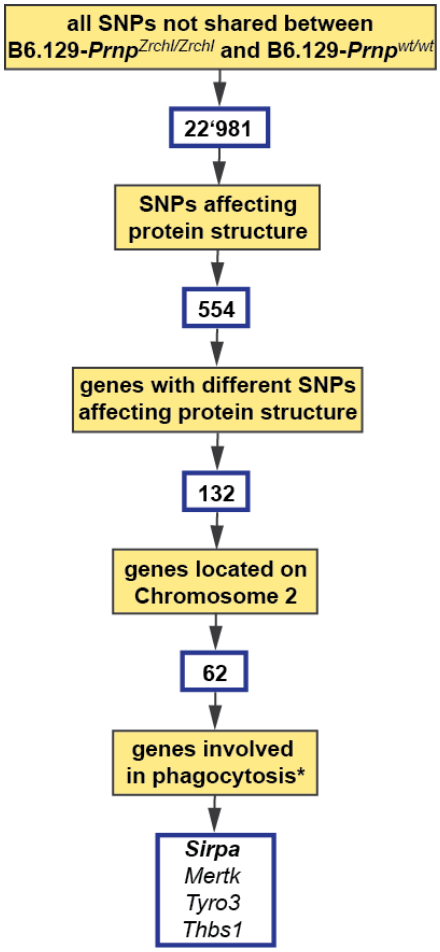

Figure 15. Filtering strategy to prioritize genes controlling phagocytosis in *Prnp*$^{Zrchl/Zrchl}$ vs. *Prnp*$^{wt/wt}$ mice. Single nucleotide polymorphisms (SNPs), including insertions/deletions (or genes with SNPs) not shared between the transcriptomes of B6.129-*Prnp*$^{Zrchl/Zrchl}$ and B6.129-*Prnp*$^{wt/wt}$ peritoneal macrophages were subjected to sequential filters (yellow boxes). SNPs affecting protein structure refers to non-synonymous SNPs or insertions/deletions. * based on Gene Ontology annotations and PubMed search. § based on PubMed search. *Sirpa*, *Mertk*, *Thbs1* and *Tyro3* have non-synonymous SNPs between B6.129-*Prnp*$^{Zrchl/Zrchl}$ and B6.129-*Prnp*$^{wt/wt}$ mice, reside on chromosome 2 and are involved in phagocytosis. Of these genes, we prioritized *Sirpa*, since only *Sirpa* polymorphisms have been shown to modulate phagocytosis (Takenaka et al., 2007; Yamauchi et al., 2013)

Sirpa

The transmembrane glycoprotein SIRPα encoded by *Sirpa* belongs to the group of SIRP receptors, which are part of the immunoglobulin (Ig) superfamily (Barclay and Brown, 2006). It consists of an extracellular region with three highly variable Ig-like loops and a cytoplasmatic tail containing two tyrosine phosphorylation sites and mostly expressed in neurons and myeloid cells, especially on macrophages, dendritic cells and neutrophils (Matozaki et al., 2009). SIRPα is mostly known as a negative regulator of phagocytosis (Okazawa et al., 2005; Tada et al., 2003) Via binding of its main binding partner, the ubiquitously expressed CD47 on cognate cells, SIRPα transmits "don't eat me" signals that protect the targets from phagocytosis. In contrast, downregulation of CD47 leads to phagocytosis (Oldenborg et al., 2000; Tada et al., 2003). As a consequence, tumor cells upregulate CD47 expression to evade phagocytosis (Jaiswal et al., 2009) and molecules targeting CD47 are considered promising immunotherapeutics (Chao et al., 2012). SIRPα was also shown to be part of the immunological synapse between dendritic cells and T cells (Brooke et al., 2004), and is required for T and NK cell homeostasis (Legrand et al., 2011b). *Sirpa* is highly polymorphic in mice (Nakaishi et al., 2008) and humans (Barclay, 2009; Hatherley et al., 2007) and its polymorphisms have been shown to have a profound impact on its function (Takenaka et al., 2007; Yamauchi et al., 2013)

Mertk and Tyro3

Mertk and *Tyro3* encode two of the three members of the TAM receptor protein tyrosine kinases, which are TYRO3, AXL and MER. MER and TYRO3 largely share their expression patterns with differences in the abundance of expression. Both receptors are found in monocytes/macrophages and other immune cells, platelets, ovary, testis, lung, retina and nervous system (Linger et al., 2008). TAM receptors and their ligands Gas6 and Protein S are crucial in the process of recognition and engulfment of apoptotic cells and membranes (Halliday, 1997; Scott et al., 2001), they regulate innate immunity, and are fundamental for tissue homeostatis in organs with a high cellular turnover, such as the retina and reproductive system (Lemke and Rothlin, 2008; Rothlin and Lemke, 2010). Consequently, alterations in expression and function of TAM receptors are implicated in a variety of dysfunctions, such as autoimmune diseases (Rothlin and Lemke, 2010), malignancies (Linger et al., 2008; Verma et al., 2011) and mutations in *Mertk* can cause retinopathies (Gal et al., 2000; Ksantini et al., 2012; Li et al., 2011).

Thbs1

Thbs1 encodes the large secreted matricellular glycoprotein TPS-1, which is expressed in most adult tissues, especially in fibroblasts and endothelial cells (Adams and Lawler, 2004; Carlson et al., 2008a). It binds to a multitude of adhesion-molecules (Roberts and Lau, 2011), among others CD47 (Gao et al., 1996) and is involved in the regulation of various cellular processes, such as angiogenesis, cell motility, platelet activation and immunomodulation (Adams and Lawler, 2004). Interestingly, TSP-1 and CD47-SIRPα interact in erythrophagocytosis: CD47 on aged

erythrocytes seems to undergo conformational changes, thereby exposing a TSP-1 binding site, which inhibits CD47- SIRPα binding, thereby permitting the phagocytosis of the aged erythrocyte (Burger et al., 2012). TSP-1 has been implicated in various cancers, where its downregulation leads to cancer progression and metastasis (Chong et al., 2012). *Thbs1* is highly polymorphic and several functional polymorphisms have been reported, for instance the human N700S *Thbs1* polymorphism, which alters the function of the protein and is associated with premature coronary heart disease (Carlson et al., 2008b).

Box 1. Characteristics of the four candidate confounder genes *Sirpa*, *Mertk*, *Tyro3* and *Thbs1*.

4.2.3 Analysis of candidate confounder genes *Sirpa*, *Mertk*, *Tyro3* and *Thbs1*

We determined the allelotypes of the four candidate confounder genes in *Prnp*$^{-/-}$ mouse lines previously used for assessing the phagocytic activity of pMΦ and BMDM (Fig. 7, Fig. 8, Fig. 9). Coisogenic 129-*Prnp*$^{Edbg/Edbg}$ were *Sirpa*$^{129/129}$ *Mertk*$^{129/129}$ *Tyro3*$^{129/129}$ *Thbs1*$^{129/129}$, reflecting their generation using 129-derived ESC and their coisogenic maintenance (Table 6). Also congenic B6.129-*Prnp*$^{ZrchI/ZrchI}$ were *Sirpa*$^{129/129}$ *Mertk*$^{129/129}$ *Tyro3*$^{129/129}$ *Thbs1*$^{129/129}$, despite having been backcrossed to B6 for 12 generations (Table 6). Therefore, in experiments comparing congenic B6.129-*Prnp*$^{ZrchI/ZrchI}$ and B6.129-*Prnp*$^{wt/wt}$ mice, all four genes (*Sirpa*, *Mertk*, *Tyro3* and *Thbs1*) can act as genetic confounder. On the other hand, congenic B6.129-*Prnp*$^{Ngsk/Ngsk}$ mice were *Sirpa*$^{129/129}$ *Mertk*$^{129/129}$ *Tyro3*$^{B6/B6}$ *Thbs1*$^{B6/B6}$ (Table 6), most likely reflecting a recombination event between *Prnp-Sirpa-Mertk* and *Tyro3-Thbs1* during backcrossing to B6 and in accordance to the results obtained by microsatellite analysis, where B6.129-*Prnp*$^{Ngsk/Ngsk}$ mice had less 129-derived material (Fig. 11). Since congenic B6.129-*Prnp*$^{Ngsk/Ngsk}$ mice had retained the hyperphagocytic phenotype (Fig. 8), allelic variation in *Tyro3* or *Thbs1* is not necessary to explain the different phagocytic activity of *Prnp*$^{wt/wt}$ and *Prnp*$^{-/-}$ mice. As a consequence, we excluded *Tyro3* and *Thbs1* (but not *Sirpa* and *Mertk*) as candidate genes.

	Prnp	***Sirpa***	***Mertk***	***Tyro3***	***Thbs1***
	chr2:131,909,927 -131,938,431	chr2:129,592,838 -129,632,228	chr2:128,698,996 -128,802,188	chr2:119,799,513 -119,818,103	chr2:118,111,921 -118,127,133
***Prnp*$^{Edbg/Edbg}$**	*-/-*	*129/129*	*129/129*	*129/129*	*129/129*
***Prnp*$^{ZrchI/ZrchI}$**	*-/-*	*129/129*	*129/129*	*129/129*	*129/129*
***Prnp*$^{Ngsk/Ngsk}$**	*-/-*	*129/129*	*129/129*	*B6/B6*	*B6/B6*

Table 6 Allelotypes of the four candidate genes on chromosome 2 linked to *Prnp* (*Sirpa, Mertk, Tyro3, Thbs1*) in the three *Prnp*$^{-/-}$ mouse lines used for assessing phagocytic activity of pMΦ and BMDM. Second row designates the location on Chr2**.**

Having *Sirpa* and *Mertk* as remaining two candidate genes, we searched the databases for reports on functional polymorphisms, i.e., polymorphisms altering the function of a gene (Albert, 2011). *Sirpa* (Box 1) is highly polymorphic in laboratory mice (Sano et al., 1999) and polymorphisms of the immunoglobulin-like variable domain of SIRPα affect the binding to CD47, thereby modulating phagocytosis (Takenaka et al., 2007; Theocharides et al., 2012; Yamauchi et al., 2013). Therefore, we considered *Sirpa* as a plausible candidate in our paradigm.

Functional polymorphisms have also been reported for *Mertk* (Box 1) For instance, sequence variations in *Mertk* have been identified in patients suffering from autosomal retinitis pigmentosa (Gal et al., 2000). Some of these polymorphisms in *Mertk* were predicted to lead to truncated protein lacking the intracellular region and thereby possibly altering the phagocytic capacity of the retinal pigment epithelial cells (McHenry et al., 2004).

In our mice, RNA-Seq identified only a single non-synonymous SNP in $Mertk^{129}$ vs. $Mertk^{B6}$ alleles (chr2:128776396, Att/Gtt), which has been reported in the CD-1 strain (Dowds et al., 1996) and predicted to result in a isoleucine to valine substitution (I516V). Both AA have side chains with similar properties, and therefore, this AA substitution is considered conservative. We used the SIFT algorithm to predict the impact of this non-synonymous SNP on *Mertk* function (Kumar et al., 2009; Ng and Henikoff, 2001). Applying default parameter settings (Kumar et al., 2009), the SIFT algorithm predicted the I516V AA substitution to be tolerated and not impacting on *Mertk* function. Also, since this conservative AA substitution was located within the transmembrane region of the protein, we reasoned that it was unlikely to significantly impact the function of the protein. One natural non-disease-causing variant in the transmembrane region has been reported in humans (I518V) (Gal et al., 2000; Li et al., 2011), which corresponds to the (I516V) variant in our mice. Moreover, all disease-causing *MERTK* mutations identified so far in patients suffering from retinitis pigmentosa (Gal et al., 2000), Leber congenital

amaurosis (Li et al., 2011), or cancer (Greenman et al., 2007) were located in the extracellular or cytoplasmic, but not in the transmembrane region, again suggesting that the variant identified in our mice is unlikely to impact *Mertk* function. For these reasons, we excluded *Mertk* as a plausible candidate in our paradigm and we prioritized *Sirpa* over *Mertk* as the candidate confounder gene for the phagocytic phenotype described in B6.129-*Prnp*$^{Zrchl/Zrchl}$ vs. B6.129-*Prnp*$^{wt/wt}$ mice.

4.2.4 *Sirpa*^{129} is linked to *Prnp*$^{-/-}$ allele in all analysed *Prnp* knockout strains

Using RNA-Seq and a subsequent filtering strategy, we had identified the highly polymorphic macrophage-expressed gene *Sirpa* as potentially controlling phagocytosis in *Prnp*$^{ZrchI/ZrchI}$ vs. *Prnp*$^{wt/wt}$ mice. Despite extensive backcrossing, congenic B6.129-*Prnp*$^{ZrchI/ZrchI}$ and B6.129-*Prnp*$^{Ngsk/Ngsk}$ mice still carried two *Sirpa*^{129} alleles (Table 6). We analyzed additional five *Prnp*$^{-/-}$ strains: two congenic, one coisogenic and one on a mixed B6129 background. Table 7 summarizes the parental and congenic strains of all analyzed *Prnp*$^{-/-}$ animals and Fig. 16 shows the whole genome STR analysis of the additionally analyzed *Prnp*$^{-/-}$ strains.

Mouse line	ESC	Origin of ESC	Strain of partner of chimeric mouse	Reference
Prnp$^{ZrchI/ZrchI}$	AB1	129S7/SvEvBrd	C57BL/6	(Büeler et al., 1992)
Prnp$^{Ngsk/Ngsk}$	J1	129S4/SvJae	C57BL/6	(Sakaguchi et al., 1995)
Prnp$^{Edbg/Edbg}$	E14	129/Ola	129/Ola	(Manson et al., 1994)
Prnp$^{GFP/GFP}$	HM-1	129/Ola	C57BL/6	(Heikenwalder et al., 2008)
Prnp$^{Rkn/Rkn}$	E14	129P2/OlaHsd	C57BL/6	(Yokoyama et al., 2001)
Prnp$^{ZrchII/ZrchII}$	E14.1	129/OlaHsd	C57BL/6	(Rossi et al., 2001)
Prnp$^{Rcm0/Rcm0}$	HM-1	129/Ola	129/Ola	(Moore et al., 1995)

Table 7. Parental and congenic strains of analyzed *Prnp*$^{-/-}$ mice.

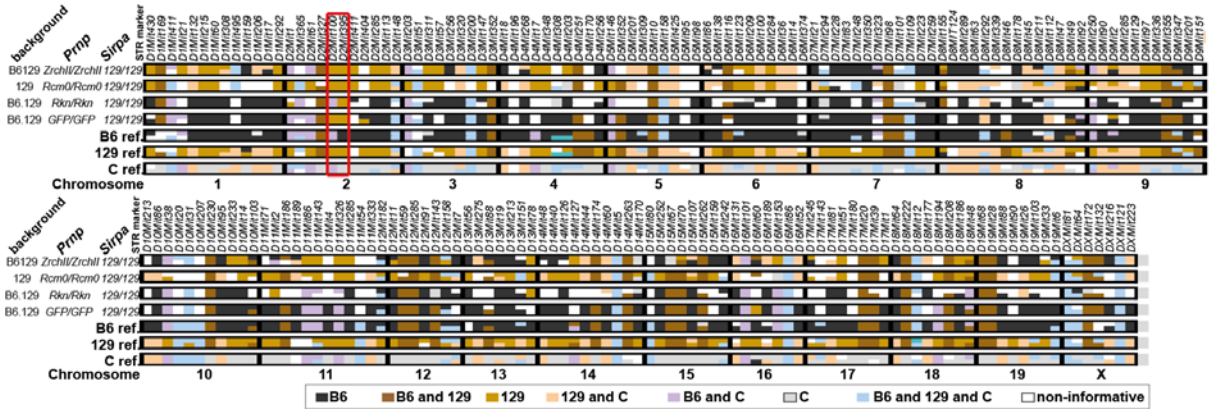

Figure 16. Whole genome STR analysis of additional 5 *Prnp*$^{-/-}$ strains. The red boarder marks the region on Chr2 containing *Prnp* and *Sirpa*. For each line a representative mouse is shown. For heterozygous markers, the strain-defining color is arbitrary and does not define a specific

haplotype. Reference B6, 129 and C samples are the same as in all shown whole genome STR analyses.

We found that in all seven analyzed independently generated *Prnp*$^{-/-}$ strains the *Prnp*$^{-}$ allele segregated with the 129-allele of *Sirpa* (Fig. 17).

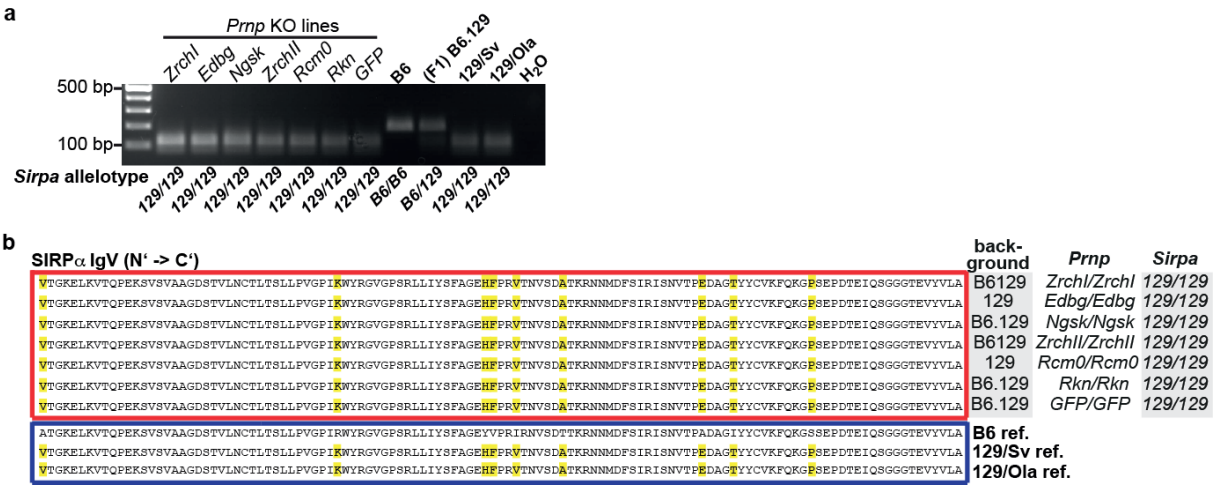

Figure 17. *Sirpa*^{129} segregates with *Prnp*$^{-}$. (a) RFLP analysis of *Sirpa* allelotypes. The *Sirpa*^{129} allele segregates with *Prnp*$^{-}$ allele in *Prnp*$^{-/-}$ mouse lines from 7 independent targeting events (**Table 7**). Sample names in bold font are reference strain DNA. (b) Red box: protein sequence alignment of mouse SIRPα immunoglobulin-like variable domain (IgV) confirming the 129 *Sirpa* allelotype in all of the 7 *Prnp*$^{-/-}$ lines showing in panel (a). Blue box: SIRPα protein reference sequences for the B6, 129/Sv, and 129/Ola strains. Polymorphisms are highlighted in yellow.

4.2.5 *Sirpa*^{129} enhances phagocytosis in the absence of *Prnp*

PrP^{C}-overexpressing *tga20* transgenic mice had been generated by introducing a transgene encoding wild type murine PrP into *Prnp*$^{Zrchl/Zrchl}$ blastocysts on a mixed B6129 background (Fischer et al., 1996), and are therefore expected to carry two *Sirpa*^{129} alleles. However, we incidentally observed that some animals in our PrP^{C}-overexpressing *tga20* colony segregated *Sirpa*^{B6} and *Sirpa*^{129} alleles, perhaps due to an unintentional cross with B6-*Prnp*$^{wt/wt}$ breeders in the early days of this colony (M. Fischer, personal communication). We took advantage of this serendipitous discovery to generate B6129-*Prnp*$^{Zrchl/Zrchl}$ littermates with all three combinations of *Sirpa*^{B6} and *Sirpa*^{129} alleles. We backcrossed B6129-*Prnp*$^{Zrchl/Zrchl}$ *Sirpa*$^{B6/B6}$ *tga20*$^{tg/tg}$ mice to B6129-*Prnp*$^{Zrchl/Zrchl}$ *Sirpa*$^{129/129}$ mice (Fig. 18, Fig. 19) and tested the phagocytic activity of their pMΦ.

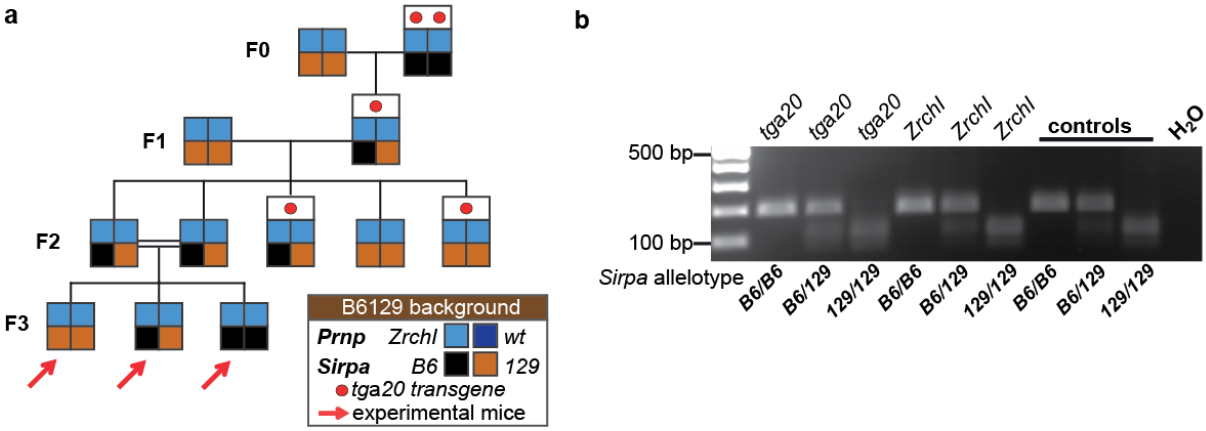

Figure 18. Generation of B6129-*Prnp*$^{Zrchl/Zrchl}$ mice with all three combinations of *Sirpa* B6-, and 129-alleles. (a) Breeding scheme applied to generate B6129-*Prnp*$^{Zrchl/Zrchl}$ mice containing *Sirpa*^{B6} and *Sirpa*^{129} alleles. B6129-*Prnp*$^{Zrchl/Zrchl}$ *Sirpa*$^{B6/B6}$ *tga20*$^{tg/tg}$ mice (F0) were backcrossed to B6129-*Prnp*$^{Zrchl/Zrchl}$ *Sirpa*$^{129/129}$ mice for two generations to produce B6129-*Prnp*$^{Zrchl/Zrchl}$ littermates with all three combinations of *Sirpa*^{B6} and *Sirpa*^{129} alleles (F3, indicated with red arrows and used to assess the phagocytic activity of pMΦ as in **Fig. 20**. (b) RFLP analysis of *Sirpa* allelotypes (B6 vs 129). *tga20* mice (lanes 1-3) contained combinations of *Sirpa*^{B6} and *Sirpa*^{129} allelotypes. Lanes 4-6 represent B6129-*Prnp*$^{Zrchl/Zrchl}$ mice indicated with red arrows in panel b. Controls: reference DNA.

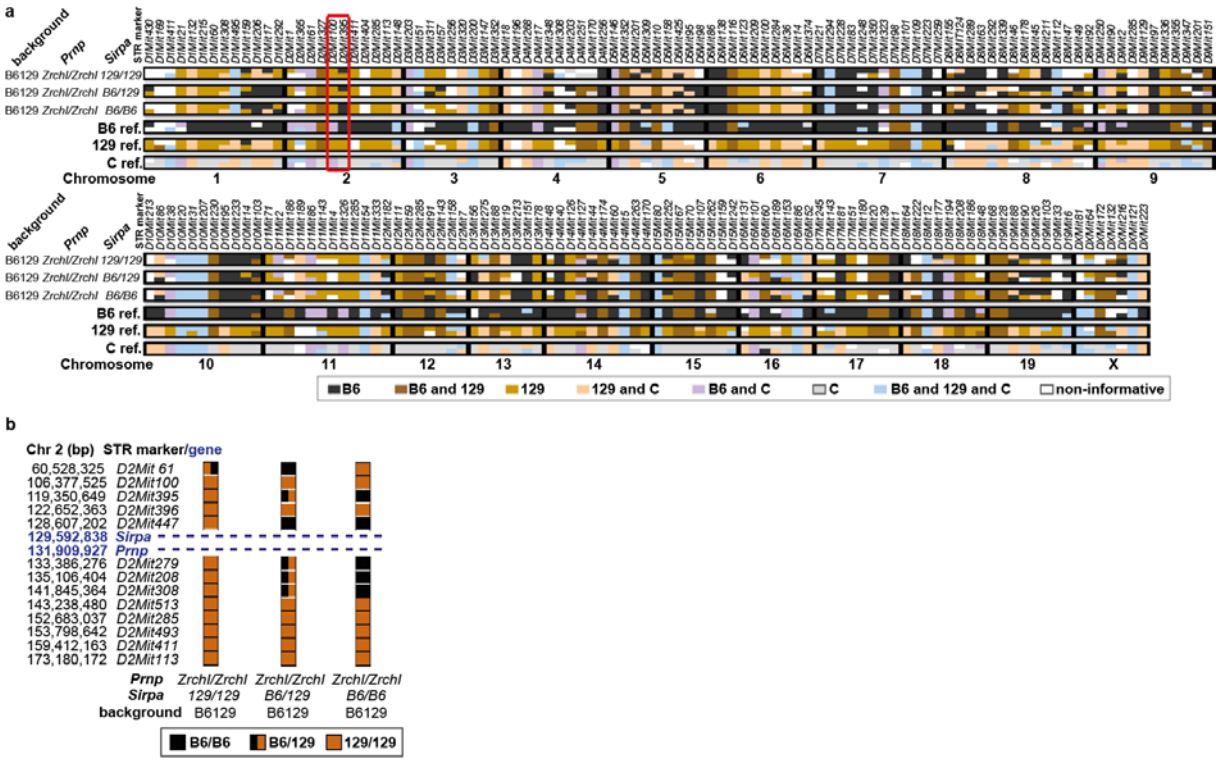

Figure 19. Genetic background of B6129-*Prnp*$^{Zrchl/Zrchl}$ mice with different combinations of *Sirpa* B6/129. (a) Whole-genome STR analysis of B6129-*Prnp*$^{Zrchl/Zrchl}$ with different combinations of *Sirpa* alleles (B6 vs. 129). The red border marks the region on Chr2 containing *Prnp* and *Sirpa*. For each line, a representative mouse is shown. For heterozygous markers, the strain-defining color is arbitrary and not intended to designate a specific haplotype. Reference B6, 129 and C samples are the same as in all shown whole genome STR analyses. (b) STR analysis documenting the boundaries of B6 vs. 129-derived genome in Chr 2 of B6129-*Prnp*$^{Zrchl/Zrchl}$ with different combinations of *Sirpa* alleles (B6 vs. 129). Blue dashed line indicates the location of *Prnp* and *Sirpa*. For each STR marker (colored box) name and position on Chr 2 are indicated on the left.

pMΦ from B6129-*Prnp*$^{Zrchl/Zrchl}$ *Sirpa*$^{129/129}$ mice showed higher rates of phagocytosis than B6129-*Prnp*$^{Zrchl/Zrchl}$ *Sirpa*$^{B6/129}$ and B6129-*Prnp*$^{Zrchl/Zrchl}$ *Sirpa*$^{B6/B6}$ pMΦ (Fig. 20). Hence, compared to *Sirpa*$^{129/129}$, a single *Sirpa*^{B6} allele reduced phagocytosis in the absence of *Prnp*. These results supported the hypothesis that homozygosity for *Sirpa*^{129}, rather than *Prnp* deficiency was responsible for the hyperphagocytic phenotype of *Prnp*$^{Zrchl/Zrchl}$ mice.

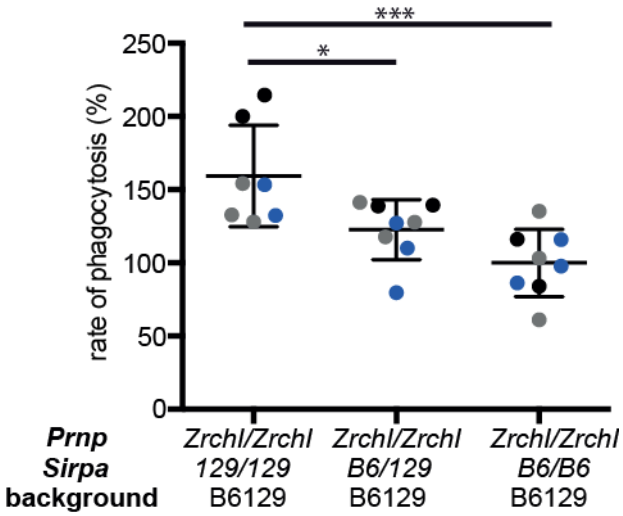

Figure 20. *Sirpa*^{B6} allele segregates with enhanced inhibition of phagocytosis in the absence of *Prnp*. Phagocytic hyperactivity of B6129-*Prnp*$^{Zrchl/Zrchl}$ pMΦ was associated with the *Sirpa*$^{129/129}$ allelotype. Data are from three independent experiments (in blue, black and grey), mean B6129-*Prnp*$^{Zrchl/Zrchl}$ *Sirpa*$^{B6/B6}$ phagocytic rates at 1:5 (23.6%, 44.4% and 35,0%, respectively) were set as 100%. One-way ANOVA, Bonferroni's multiple comparisons test: *p<0.05; ***p<0.001, error bars: s.d.

4.2.6 *Sirpa* regulates phagocytosis irrespective of *Prnp* status

In mice lacking *Prnp*, we observed that the *Sirpa* B6/129 polymorphism was associated with modulation of the phagocytic activity of pMΦ (Fig. 20). Alternatively, we reasoned that *Prnp* might influence phagocytosis independently of *Sirpa*. To study whether different *Sirpa* alleles could modify phagocytosis also in $Prnp^{wt/wt}$ mice, we generated mice with recombination between *Prnp* and *Sirpa* in two different backgrounds (B6 and C). The genetic distance between *Sirpa* (chr2:129,592,838-129,632,228) and *Prnp* (chr2:131,909,927-131,938,431) is approximately 2.4 Mbp, corresponding to approximately 2 cM and an estimated recombination frequency of 2%.

On the B6 background, we screened 103 pups from B6.129-$Prnp^{wt/ZrchI}$ $Sirpa^{B6/129}$ intercrosses for meiotic transallelic recombination between *Prnp* and *Sirpa* and observed two events producing a $Prnp^{wt}$-$Sirpa^{129}$ and a $Prnp^{ZrchI}$-$Sirpa^{B6}$ haplotype (recombination frequency 1.9%) (Fig. 21). Mice carrying the original and novel recombinant haplotypes were bred to generate congenic mice with the following *Prnp*-*Sirpa* haplotypes (Fig. 21): B6.129-$Prnp^{ZrchI/ZrchI}$ $Sirpa^{129/129}$ (original), B6.129-$Prnp^{wt/wt}$ $Sirpa^{B6/B6}$ (recombinant), B6.129-$Prnp^{wt/wt}$ $Sirpa^{B6/B6}$ (original), and B6.129-$Prnp^{wt/wt}$ $Sirpa^{129/129}$ (recombinant). Mice form the four groups exhibited a highly similar genetic background (Fig. 22), apart from the region flanking *Prnp* on Chr2. In collaboration with Prof. J. Danska and S. Mortin-Toth (Hospital for Sick Children, University of Toronto), we performed high density STR analysis of the region flanking *Sirpa* and *Prnp*, and documented the recombination breakpoint between *Sirpa* and *Prnp* in B6.129-$Prnp^{wt/wt}$ $Sirpa^{B6/B6}$ mice between the markers D2Ngul1888 (Chr2:129,913,603-129,914,407) and D2Ngul1937 (Chr2: 130,287,604-130,288,020). Sequencing of the *Sirpa* ORF confirmed the presence of the four different *Sirpa*-*Prnp* haplotypes (Fig. 22)

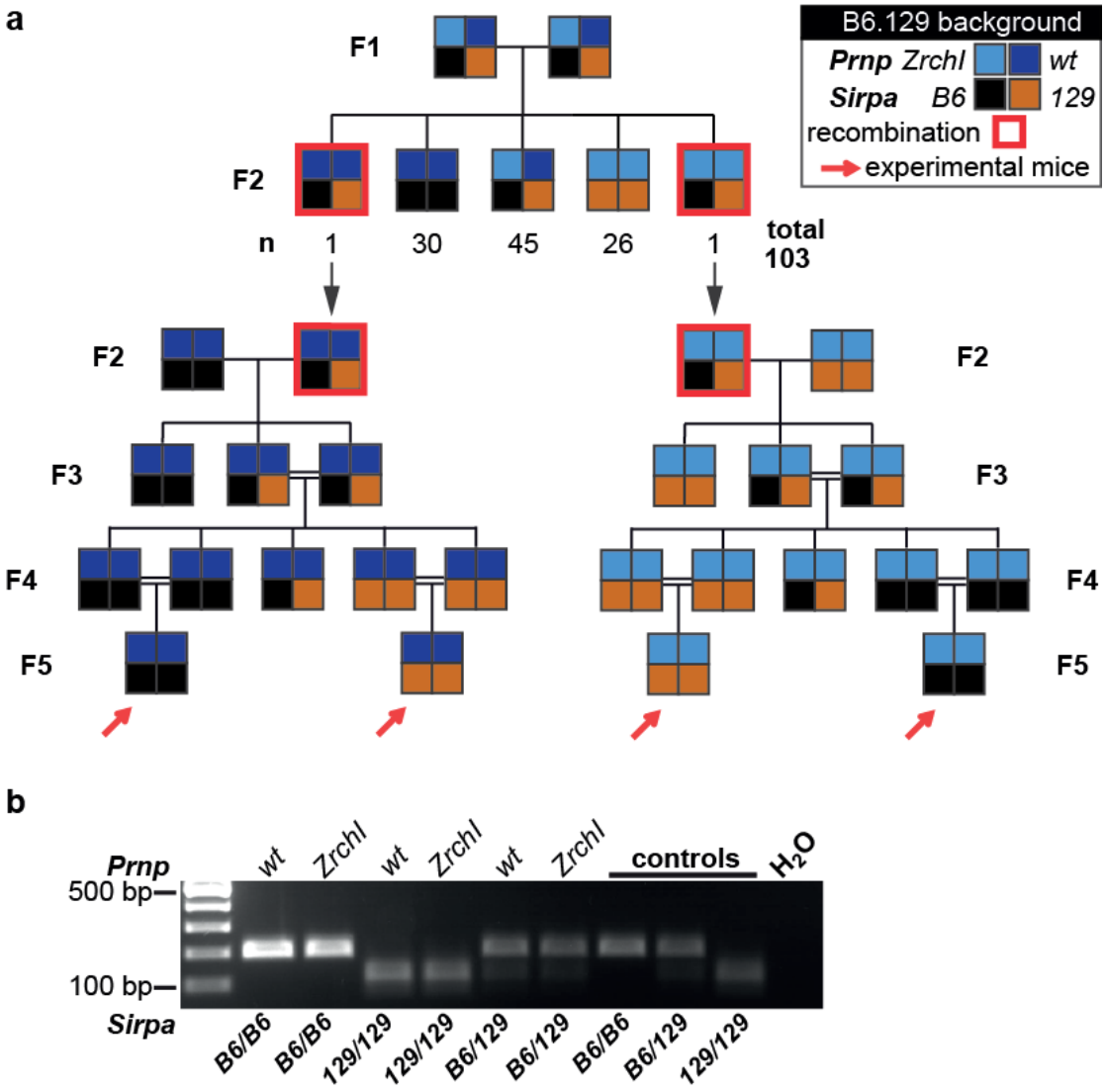

Figure 21. Recombinant congenic B6.129 mice with different combinations of *Prnp* (wt and Zrchl) and *Sirpa* (B6 and 129) alleles. (a) Breeding scheme to generate recombinant congenic B6.129 mice with different combinations of *Prnp* (wt and ZrchI) and *Sirpa* (B6 and 129) alleles. B6.129-*Prnp*$^{wt/ZrchI}$ mice (F1) were intercrossed and the occurrence of meiotic recombination between *Prnp* and *Sirpa* was assessed in the F2-offspring. 103 F2 mice with different combinations of *Prnp* genotypes and *Sirpa* allelotypes were obtained. Two mice (red frame) were obligate carriers for a recombinant haplotype, *Prnp*^{wt}-*Sirpa*^{129} and *Prnp*^{ZrchI}-*Sirpa*^{B6}, respectively. Obligate carriers of the recombinant *Prnp-Sirpa* haplotype were interbred to generate B6.129-*Prnp*$^{ZrchI/ZrchI}$ and B6.129-*Prnp*$^{wt/wt}$ mice homozygous for *Sirpa*^{B6} or *Sirpa*^{129} alleles. (b) RFLP analysis to discriminate *Sirpa*^{129} from *Sirpa*^{B6}. B6.129-*Prnp*$^{wt/wt}$ (lanes 1, 3 and 5) and B6.129-*Prnp*$^{ZrchI/ZrchI}$ (lanes 2, 4 and 6) mice with different combinations of *Sirpa*^{129} and *Sirpa*^{B6} alleles. Controls are reference DNA. Mice in lanes 1 to 4 were used to assess the phagocytic activity of pMΦ.

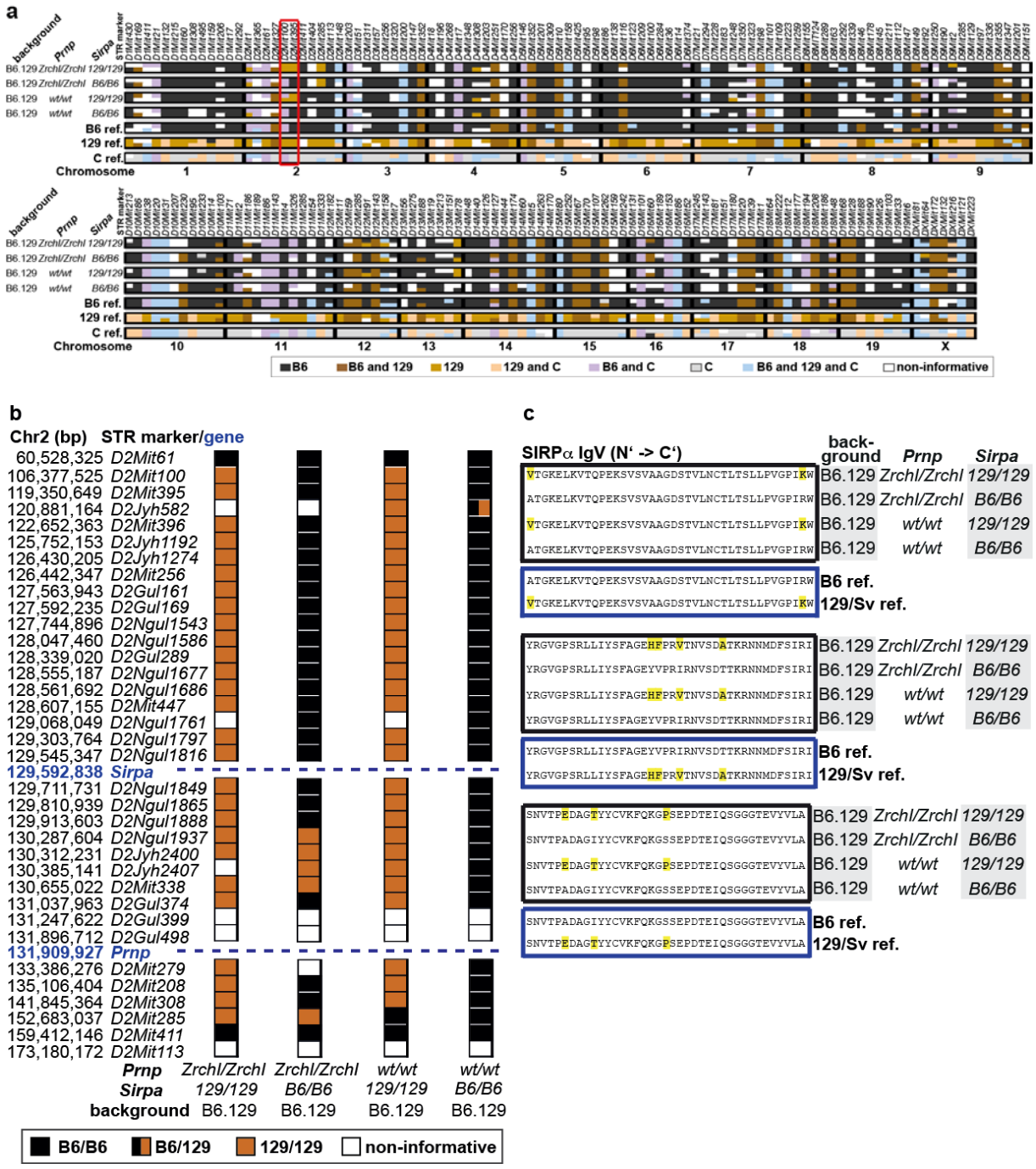

Figure 22. STR analysis and SIRPα alleles of recombinant congenic B6.129 mice with different combinations of *Prnp* (wt and Zrchl) and *Sirpa* (B6 and 129) alleles. (a) Whole-genome STR analysis of congenic B6.129 mice with different combinations of *Sirpa-Prnp* haplotypes. The red border marks the region on Chr2 containing *Prnp* and *Sirpa*. For each line, a representative mouse is shown. For heterozygous markers, the strain-defining color is arbitrary and not intended to designate a specific haplotype. Reference B6, 129 and C samples are the same as in all shown whole genome STR analyses. (b) STR analysis documents the result of transallelic meiotic recombination between *Prnp* and *Sirpa*. Blue dashed line indicates the location

of *Prnp* and *Sirpa*. For each STR marker (colored box) name and position on Chr2 are indicated on the left. (c) Protein sequence variants (yellow) in SIRPα immunoglobulin-like variable domain (IgV). Homozygous recombinant congenic B6.129 mice displayed four combinations of *Prnp*-*Sirpa* haplotypes (black boxes). Blue boxes: SIRPα sequence of reference B6 and 129/Sv strains.

Next we wanted to exclude that different *Sirpa*-*Prnp* haplytypes could influence the abundance of pMΦ in these different strains, or that different *Sirpa*-*Prnp* haplytypes could mutually influence its protein expression. We did not observe any effect of the *Prnp*-*Sirpa* haplotype on the prevalence of F4/80$^+$ cells in peritoneal lavages (Fig. 23a-b).

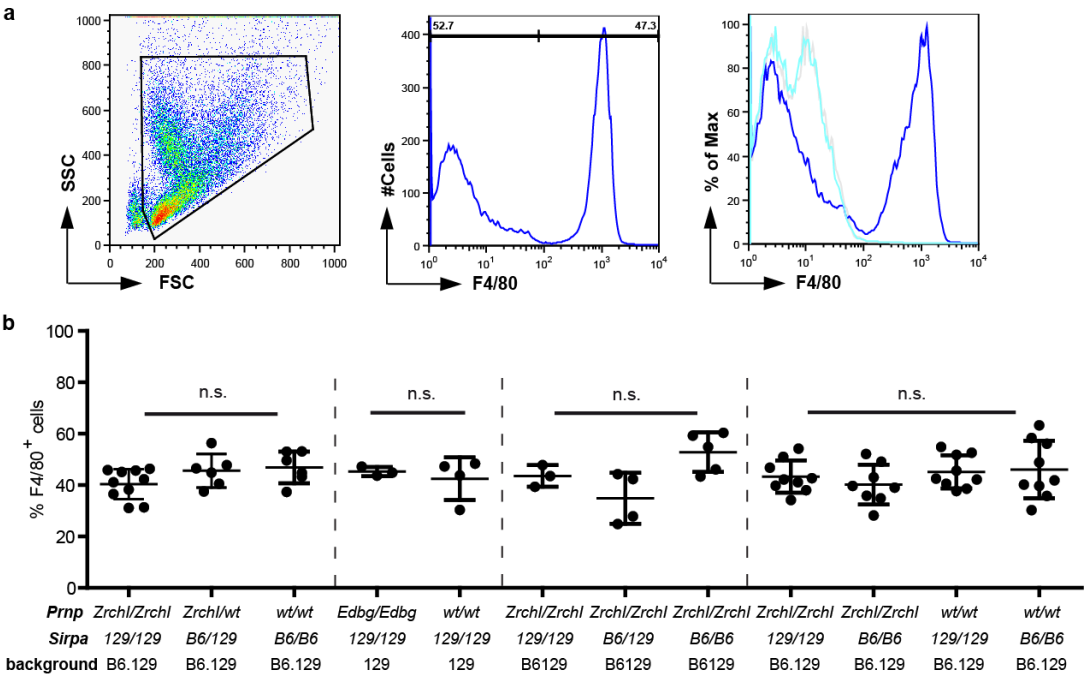

Figure 23. *Sirpa* allelotype does not influence peritoneal macrophage abundance. (a) Peritoneal lavages were gated for nucleated cells (left panel), and the percentage of F4/80$^+$ cells was assessed (middle panel, right peak). Right panel: overlay of histograms of F4/80 (dark blue), isotype antibody (light blue) and unstained peritoneal cells (grey) confirming the specificity of the staining. (b) Percentage of F4/80$^+$ macrophages in peritoneal lavage cells of experimental mice. The dotted lines delimit individual experiments in which groups of mice (n=3-10 for each haplotype) were analyzed.

Also, *Sirpa* allelotype did not impact on PrP^C expression (Fig. 24a). RNA-Seq showed no differences in *Sirpa* mRNA levels between pMΦ from B6.129-*Prnp*$^{Zrchl/Zrchl}$ and B6.129-*Prnp*$^{wt/wt}$ mice (375.60 vs 356.34 fragments per kilobase of transcript per million mapped reads, FPKM, respectively, p=0.73), and immunoblotting of pMΦ lysates failed to detect different SIRPα protein levels in congenic mice with different *Prnp*-*Sirpa* haplotypes (Fig. 24b). This excluded a mutual influence of *Prnp* and *Sirpa*, which could complicate the interpretation of phagocytic activity in mice with different *Prnp*-*Sirpa* haplotypes.

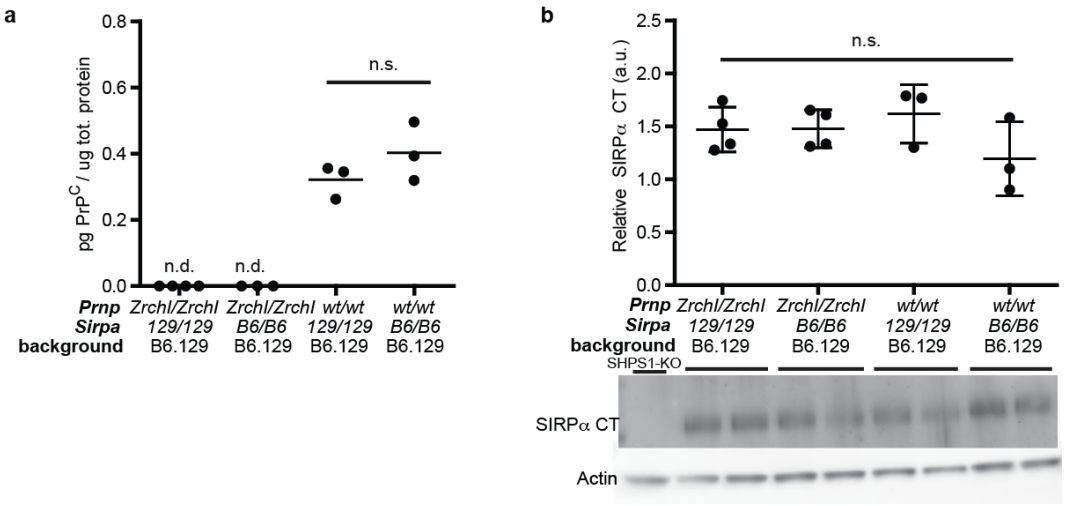

Figure 24. *Sirpa* allelotype does not influence PrP^C and SIRPα expression. (a) PrP^C ELISA analysis of pMΦ lysates showed no difference (n.s.) in PrP^C levels between B6.129-*Prnp*$^{wt/wt}$ mice with different *Sirpa* allelotypes. Two-tailed unpaired t-test, p=0.241, n=3. N.d. not detectable. (b) Unchanged expression of the SIRPα cytoplasmic tail (CT) in cultured pMΦ lysates as quantified to actin levels. SHPS-1 KO macrophage lysates lacking the cytosolic tail of SIRPα were used as negative control. One-way ANOVA, n.s.: not significant, p=0.27, n=3-4.

Next, we tested the phagocytic activity of pMΦ isolated from congenic B6.129 mice with different combinations of *Prnp* (wt and ZrchI) and *Sirpa* (B6 and 129) alleles using apoptotic thymocytes as prey. As with B6129-*Prnp*$^{Zrchl/Zrchl}$ pMΦ, where *Sirpa*-129 homozygosity led to a higher rate of phagocytosis (Fig. 20), we observed that B6.129-*Prnp*$^{Zrchl/Zrchl}$ *Sirpa*$^{129/129}$ pMΦ phagocytosed more apoptotic thymocytes than B6.129-

Prnp$^{ZrchI/ZrchI}$ *Sirpa*$^{B6/B6}$ pMΦ. Importantly, this effect held true also in the presence of PrP^{C}: pMΦ from congenic B6.129-*Prnp*$^{wt/wt}$ *Sirpa*$^{129/129}$ mice showed a higher phagocytic activity than B6.129-*Prnp*$^{wt/wt}$ *Sirpa*$^{B6/B6}$ pMΦ. In summary, in congenic B6.129 mice with different combinations of *Prnp* and *Sirpa* alleles (wt and ZrchI, B6 and 129, respectively), hyperphagocytosis segregated with *Sirpa*$^{129/129}$ irrespective of the *Prnp* status (Fig. 25).

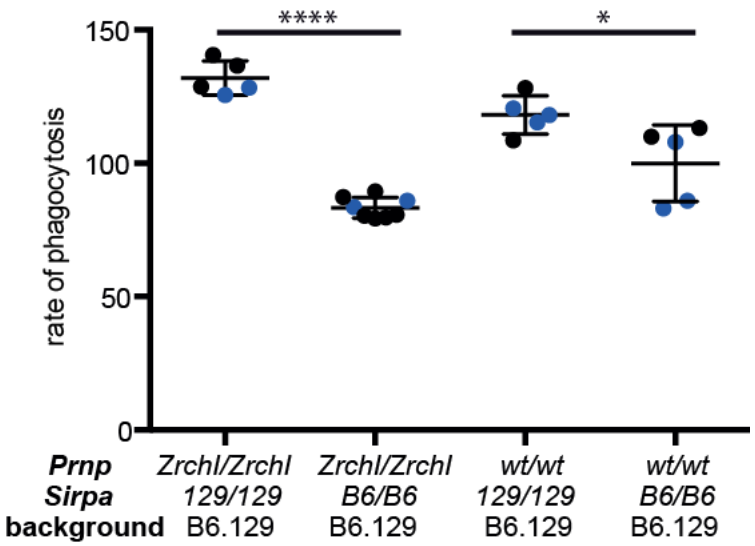

Figure 25. *Sirpa*$^{129/129}$, but not *Prnp*$^{-/-}$, was associated with hyperphagocytosis in congenic B6.129 mice. Data show two independent experiments (in blue and black), mean phagocytosis rates of B6.129 *Prnp*$^{wt/wt}$ *Sirpa*$^{B6/B6}$ were set as 100%. One-way ANOVA, Bonferroni's multiple comparisons post-test: *p<0.05; ****p<0.0001.

In the next step, we asked whether homozygosity for *Sirpa*^{129} - and not the presence or absence of *Prnp* - could also modulate the phagocytic activity of macrophages on a strain background other than B6. We therefore crossed congenic C.129-*Prnp*$^{ZrchI/ZrchI}$ mice backcrossed for > 18 generations with C-*Prnp*$^{wt/wt}$ mice. We intercrossed the resulting C.129-*Prnp*$^{wt/ZrchI}$ mice (F1) and screened their F2-offspring for the occurrence of a meiotic recombination event between *Sirpa* and *Prnp* (Fig. 26a). Out of 243 pups, we found four animals, where a recombination between *Sirpa* and *Prnp* had occurred (recombination frequency 1.65%): one animal with a *Prnp*$^{wt/ZrchI}$ *Sirpa*$^{C/C}$ haplotype, a

single animal carrying a *Prnp*$^{wt/wt}$ *Sirpa*$^{C/129}$ haplotype, and two animals with a *Prnp*$^{ZrchI/ZrchI}$ *Sirpa*$^{C/129}$ haplotype (Fig. 26a). Following the analogous breeding strategy as on the B6-background (Fig. 21), we bred the mice carrying the original and the novel recombinant haplotypes to generate congenic mice with the following *Prnp*-*Sirpa* haplotypes: C.129-*Prnp*$^{ZrchI/ZrchI}$ *Sirpa*$^{129/129}$ (original), C.129-*Prnp*$^{ZrchI/ZrchI}$ *Sirpa*$^{C/C}$ (recombinant), C.129-*Prnp*$^{wt/wt}$ *Sirpa*$^{C/C}$ (original), and C.129-*Prnp*$^{wt/wt}$ *Sirpa*$^{129/129}$ (recombinant) (Fig. 26a-b). Again, we performed a whole genome low density STR analysis of representative animals of all four groups and found a highly similar genetic background (Fig. 27a), with the exception of the region on Chr2 flanking *Prnp* (Fig. 27b), where mice carrying *Prnp*$^{ZrchI/ZrchI}$ alleles contained 129-derived chromosomal material, as assessed by a high density STR analysis of the region flanking *Sirpa* and *Prnp*. Again, sequencing of the *Sirpa* ORF confirmed the presence of the four different *Sirpa*-*Prnp* haplotypes (Fig. 27c).

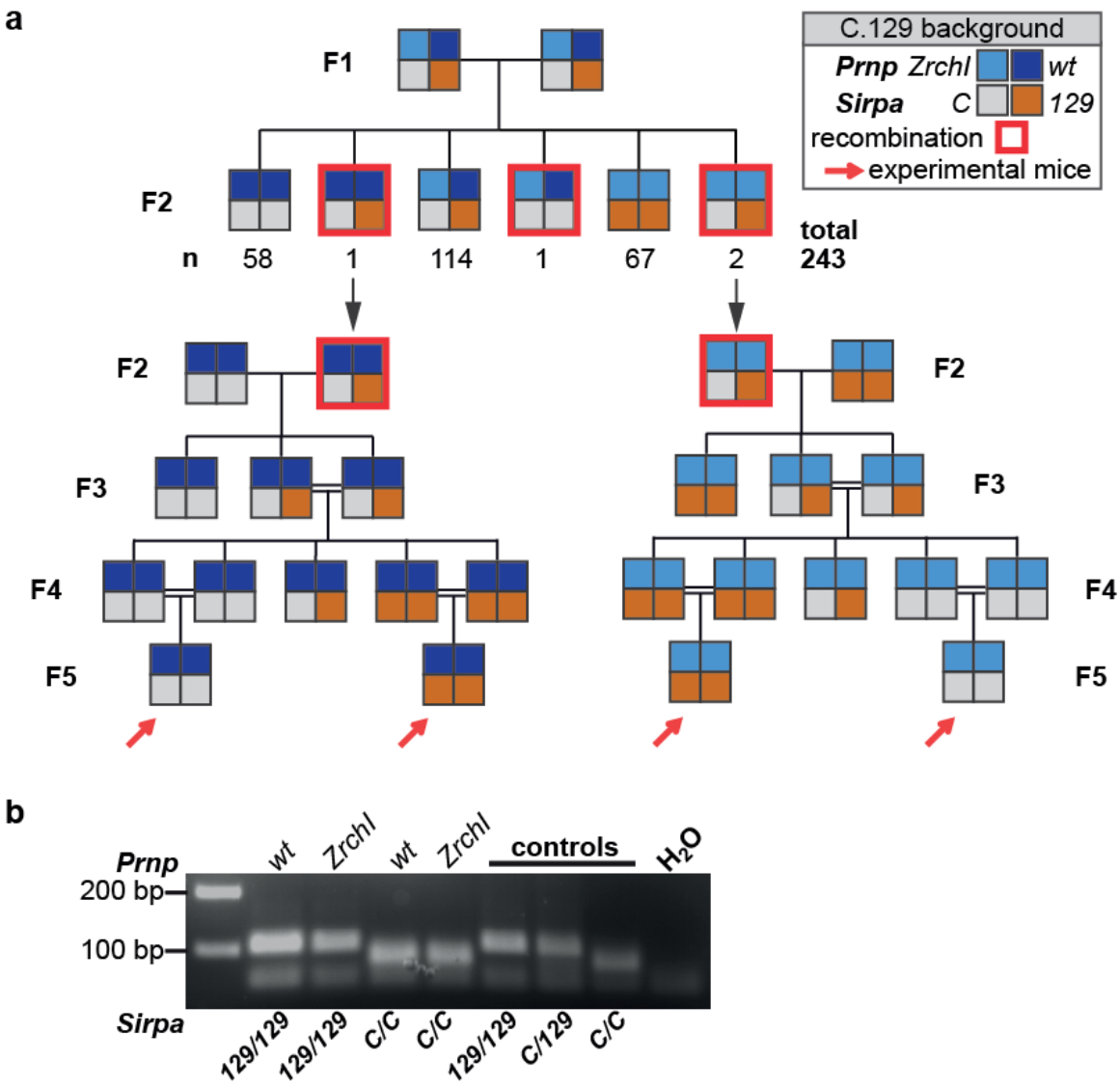

Figure 26. Recombinant congenic C.129 mice with different combinations of *Prnp* (wt and Zrchl) and *Sirpa* (C and 129) alleles. (a) Breeding scheme to generate recombinant congenic C.129 mice with different combination of *Prnp* (wt and Zrchl) and *Sirpa* (C and 129) alleles. C.129-*Prnp*$^{wt/Zrchl}$ mice (F1) were intercrossed and the occurrence of meiotic recombination between *Prnp* and *Sirpa* was assessed in the F2-offspring. 243 F2 mice with different combinations of *Prnp* genotypes and *Sirpa* allelotypes were obtained. Three mice (red frame) were obligate carriers for a recombinant haplotype. Obligate carriers were bred to generate C.129-*Prnp*$^{Zrchl/Zrchl}$ and C.129-*Prnp*$^{wt/wt}$ mice homozygous for *Sirpa*^{C} or *Sirpa*^{129} alleles.

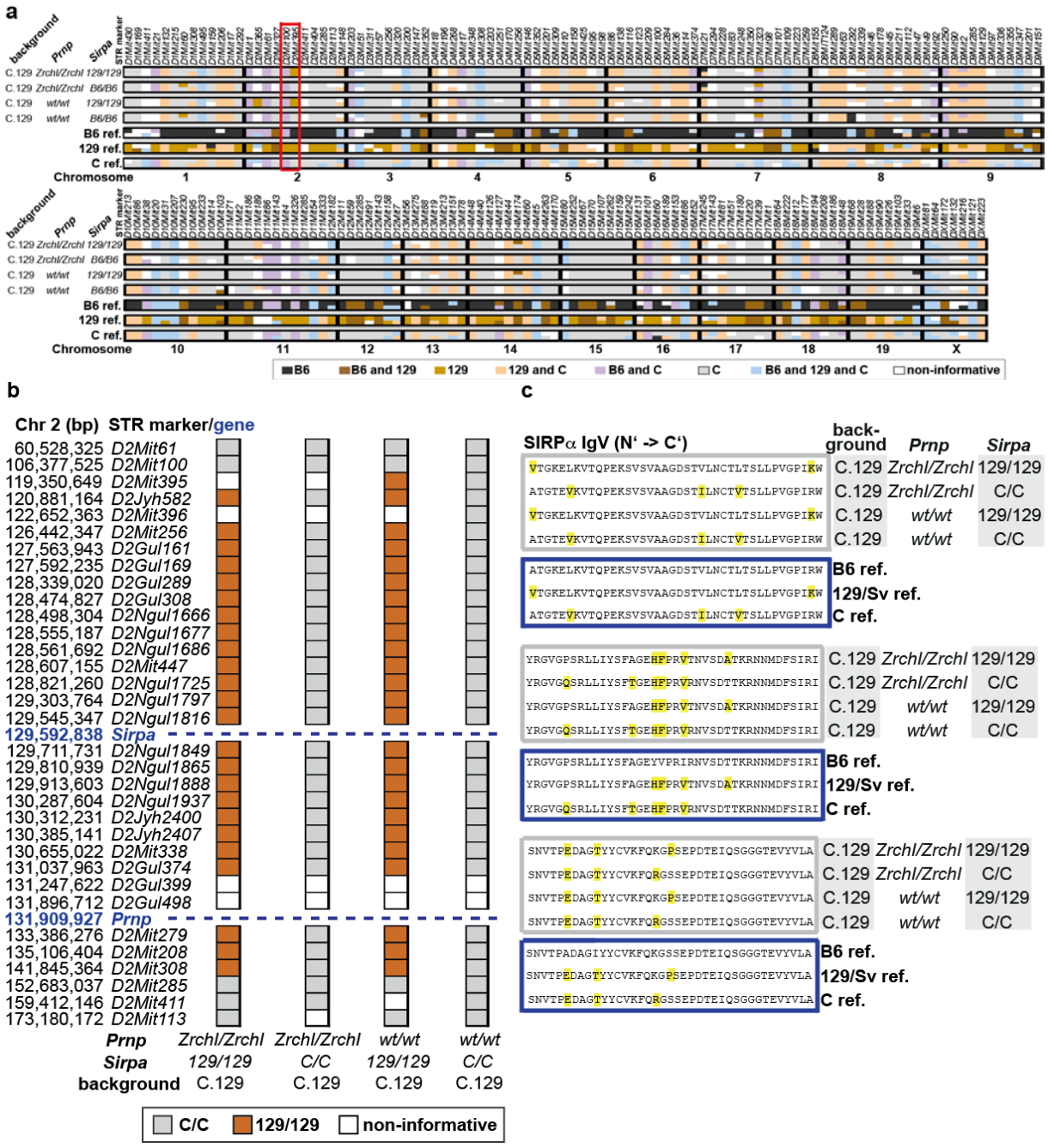

Figure 27. STR analysis and SIRPα alleles of recombinant congenic C.129 mice with different combinations of *Prnp* (wt and Zrchl) and *Sirpa* (C and 129) alleles. (a) Whole-genome STR analysis of congenic B6.129 mice with different combinations of *Sirpa-Prnp* haplotypes. The red border marks the region on Chr2 containing *Prnp* and *Sirpa*. For each line, a representative mouse is shown. For heterozygous markers, the strain-defining color is arbitrary and not intended to designate a specific haplotype. Reference B6, 129 and C samples are the same as in all shown whole genome STR analyses. (b) Short tandem repeat (STR) analysis documents the result of transallelic meiotic recombination between *Prnp* and *Sirpa* Blue dashed line indicates the location of *Prnp* and *Sirpa*. For each STR marker (colored box) name and position on Chr 2 are indicated on the left. (c) Protein sequence alignment of mouse SIRPα

immunoglobulin-like variable domain (IgV) illustrates recombinant congenic C.129 mice with different combination of *Prnp* and $Sirpa^{129}$ vs. $Sirpa^{C}$ (grey border). Blue box: SIRPα protein reference sequences for the B6, 129/Sv, and C strains (yellow: polymorphisms).

To assess the influence of *Prnp* and the *Sirpa* C/129 polymorphism on the modulation of phagocytic activity, we isolated BMDMs from congenic C.129-$Prnp^{ZrchI/ZrchI}$ mice with different combinations of *Prnp* and *Sirpa* alleles (Fig. 26Fig. 27) and performed phagocytosis assays using apoptotic thymocytes as prey (Fig. 8a). Again, we observed that a higher phagocytosis rate correlated with $Sirpa^{129/129}$, independently of the presence or absence of *Prnp* (Fig. 28). The comparison of BMDM derived from C.129-$Prnp^{ZrchI/ZrchI}$ $Sirpa^{129/129}$ vs. C.129-$Prnp^{ZrchI/ZrchI}$ $Sirpa^{C/C}$ mice yielded only a borderline significance (p = 0.075), most likely due to the high variability in the C.129-$Prnp^{ZrchI/ZrchI}$ $Sirpa^{129/129}$ group.

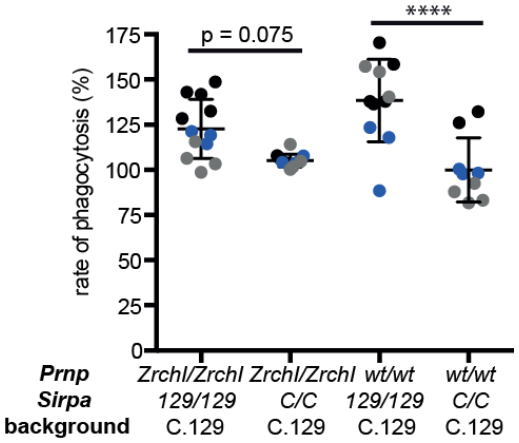

Figure 28. $Sirpa^{129/129}$ allelotype, but not the absence of *Prnp*, was associated with hyperphagocytosis of BMDMs in congenic C.129 mice. Data are from three independent experiments (blue, black and grey). Average phagocytosis rates of C.129 $Prnp^{ZrchI/ZrchI}$ $Sirpa^{B6/B6}$ were set as 100%. One-way ANOVA, Bonferroni's multiple comparison post-test,****p<0.0001.

Together, these results eliminate a role for PrP^{C} as an inhibitor of phagocytosis and instead support *Sirpa* polymorphisms as major regulators of phagocytosis in mouse strains carrying both wildtype and deleted *Prnp* alleles.

4.2.7 *Sirpa*^{129} exacerbates mouse EAE in the absence of *Prnp*

We have determined that a function previously ascribed to PrP^C on the basis of studies in congenic *Prnp*$^{-/-}$ mice, regulation of phagocytosis, was not influenced by *Prnp* gene expression. Instead, our results suggest that the polymorphic *Sirpa* gene, which flanks *Prnp*, regulates this cell-autonomous phenotype. The process of phagocytosis does also play a role in a complex model of neuroinflammation, EAE (Baxter, 2007; Schreiner et al., 2009). Both CNS-resident phagocytes (microglia) as well as infiltrating phagocytic cells (monocytes) contribute to the development and progression of EAE, both by inducing neurotoxicity and exerting a protective role by the clearance of apoptotic bodies (Aguzzi et al., 2013; Ajami et al., 2011; Napoli and Neumann, 2010). Several studies have reported that *Prnp* removal leads to exacerbation of the EAE phenotype at various time points of EAE induction and/or progression (Gourdain et al., 2012; Ingram et al., 2009; Tsutsui et al., 2008), using not only congenic *Prnp*$^{-/-}$ mice, but also coisogenic *Prnp*$^{-/-}$ mice and gene silencing approaches, such as RNAi (Hu et al., 2010). On the other hand, mice carrying a dominant-negative knock-in for *Sirpa* were shown to be resistant to EAE development (Tomizawa et al., 2007), suggesting that SIRPα is needed for EAE development. In light of these studies and our findings, we asked whether we could reproduce the reported effect of *Prnp* gene on EAE development and whether the B6/129 *Sirpa* polymorphism would additionally influence/modify the clinical course of EAE development.

All EAE experiments were performed in collaboration with Sabine Spath (laboratory of Prof. Burkhard Becher, Institute of Experimental Immunology, University of Zurich). We MOG_{35-55}-immunized B6129-*Prnp*$^{Zrchl/Zrchl}$ mice carrying *Sirpa*$^{B6/B6}$, *Sirpa*$^{B6/129}$ or *Sirpa*$^{129/129}$ alleles (Fig. 18, Fig. 19), and used B6 (henceforth termed B6-*Prnp*$^{wt/wt}$ *Sirpa*$^{B6/B6}$) and B6x129 (F1; henceforth termed B6129-*Prnp*$^{wt/wt}$ *Sirpa*$^{B6/129}$) mice as wild type controls. In two independent experiments, we scored the mice for 93 days and 79

days, respectively. Fig. 29 and Table 8 summarize the EAE clinical course and the detailed clinical development of all five experimental groups.

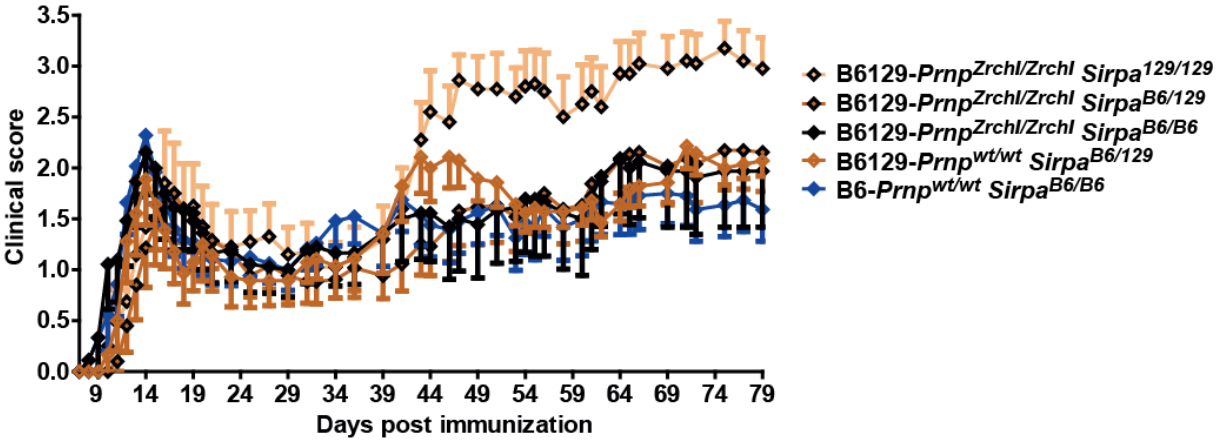

Figure 29. Overview of EAE development in B6129-*Prnp*$^{Zrchl/Zrchl}$ mice with all three combinations of *Sirpa* B6-, and 129-alleles and *Prnp*$^{wt/wt}$ controls on a B6-, or B6129-background. Data are pooled from two independent experiments. Here and henceforth, graphs present mean disease scores, error bars are SEM. Detailed EAE disease course is summarized in **Table 8**.

Mice	Number of mice	Incidence° (%)	Mortality* (%)	Mean day of onset (±SD)	Mean maximal disease score (±SD)	Mean cumulative disease score (±SD)
B6129-*Prnp*$^{Zrchl/Zrchl}$ *Sirpa*$^{129/129}$	16	10/16 (62.5)	4/16 (25)	16.70±10.14	3.5±0.5	96.0±40.7
B6129-*Prnp*$^{Zrchl/Zrchl}$ *Sirpa*$^{B6/129}$	16	13/16 (81.25)	3/16 (18.75)	20.31±16.41	3.1±1.0	70.0±41.7
B6129-*Prnp*$^{Zrchl/Zrchl}$ *Sirpa*$^{B6/B6}$	16	13/16 (81.25)	4/16 (25)	26.38±29.43	3.2±0.8	89.0±61.1
B6129-*Prnp*$^{wt/wt}$ *Sirpa*$^{B6/129}$	10	9/10 (90)	0/10 (0)	16.89±10.52	3.0±0.4	67.0±8.7
B6-*Prnp*$^{wt/wt}$ *Sirpa*$^{B6/B6}$	16	12/16 (75)	1/16 (6.25)	12.75±5.85	2.9±0.7	70.0±36.9

Table 8. Detailed clinical EAE development in B6129-*Prnp*$^{Zrchl/Zrchl}$ mice with all three combinations of *Sirpa* B6-, and 129-alleles, B6129-*Prnp*$^{wt/wt}$ *Sirpa*$^{B6/129}$ and B6- *Prnp*$^{wt/wt}$ *Sirpa*$^{B6/B6}$ mice. Data are from two pooled experiments. B6129-*Prnp*$^{wt/wt}$ *Sirpa*$^{B6/B6}$ mice were included only in one experiment. The five groups did not significantly differ in mean day of onset (Kruskal-Wallis test, p=0.0695), mean maximal disease score (Kruskal-Wallis test, p=0.1268), or the mean cumulative disease score (Kruskal-Wallis test, p=0.5494). ° represents mice with a clinical score of at least one. * represents mice that died or were euthanized due to termination criteria.

We first assessed the effect of different *Sirpa* alleles (B6 vs. 129) on the clinical development of EAE in the absence of *Prnp*. We did not observe a difference in disease onset or disease severity between the 3 groups in the acute (day 11-22 p.i.), or remission phase (day 22-42 p.i.; Fig. 30). At day 14 p.i. (peak disease), all 3 groups showed comparable amounts of inflammatory infiltrates (CD3-positive T-cells and Iba-1-positive microglia or monocyte-derived Iba-1-positive macrophages) in spinal cord (Fig. 31) and brain sections.

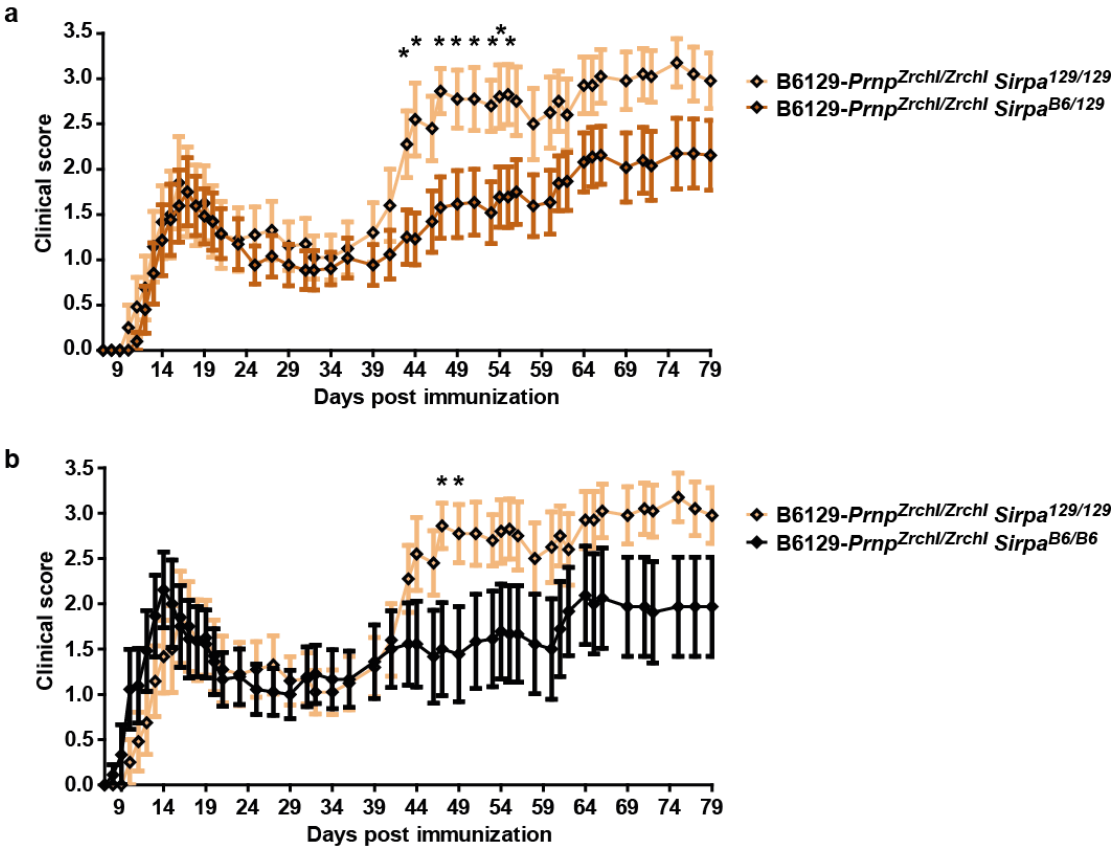

Figure 30. In the absence of *Prnp*, the B6/129 *Sirpa* polymorphism modulates the clinical severity of MOG-induced EAE. B6129-*Prnp*$^{ZrchI/ZrchI}$ *Sirpa*$^{129/129}$ mice show a more severe relapse phase than B6129-*Prnp*$^{ZrchI/ZrchI}$ *Sirpa*$^{B6/129}$ mice (a) and than B6129-*Prnp*$^{ZrchI/ZrchI}$ *Sirpa*$^{B6/B6}$ mice (b). Data are pooled from two independent experiments (n=16 for each group); see Fig. 29 for overview of all five experimental groups and Table 8 for detailed clinical development. *, $p<0.05$, two-tailed unpaired Student's t-test.

However, after day 43 p.i., B6129-*Prnp*$^{ZrchI/ZrchI}$ homozygous for *Sirpa*^{129} had a significantly stronger relapse than B6129-*Prnp*$^{ZrchI/ZrchI}$ *Sirpa*$^{B6/129}$ (Fig. 30a) and B6129-*Prnp*$^{ZrchI/ZrchI}$ *Sirpa*$^{B6/B6}$ (Fig. 30b) mice. In representative spinal cord sections at 92 day

p.i. (Fig. 32) B6129-*Prnp*$^{Zrchl/Zrchl}$ *Sirpa*$^{129/129}$ and B6129-*Prnp*$^{Zrchl/Zrchl}$ *Sirpa*$^{B6/129}$ mice showed predominantly acute inflammatory infiltrates containing CD3-positive lymphocytes and Iba1-positive phagocytes, whereas B6129-*Prnp*$^{Zrchl/Zrchl}$ *Sirpa*$^{B6/B6}$ mainly showed chronic, non-florid lesions with a more pronounced loss of myelin (LN) and larger NF-negative areas (Fig. 32).

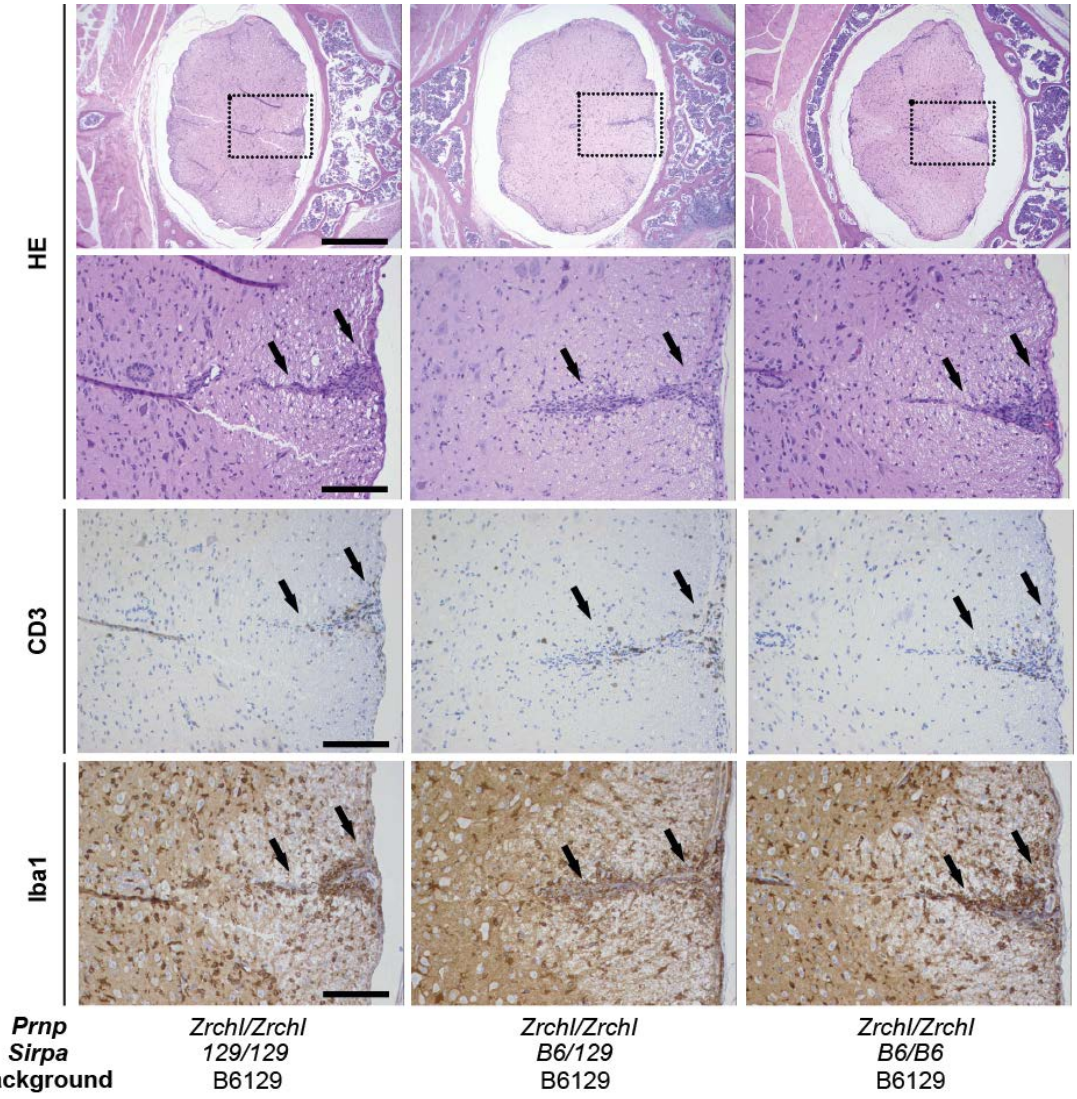

Figure 31. Similar amount of inflammatory infiltrates in B6129-*Prnp*$^{Zrchl/Zrchl}$ mice with all three combinations of *Sirpa* B6-, and 129-alleles at day 14 post MOG-immunization (peak disease). Representative spinal cord sections of mice with disease score 3.0 (complete bilateral hind limb paralysis) - 3.25 (complete bilateral hind limb paralysis and unilateral partial fore limb paralysis). All three mice show a comparable amount of inflammatory cells mainly located in the spinal cord perivascular space (HE), consisting mostly of CD3-positive T cells and Iba1-positive

activated resident microglia or differentiated monocyte-derived Iba-1-positive macrophages. Scale bar 100 μm, except for upper panel: 500 μm.

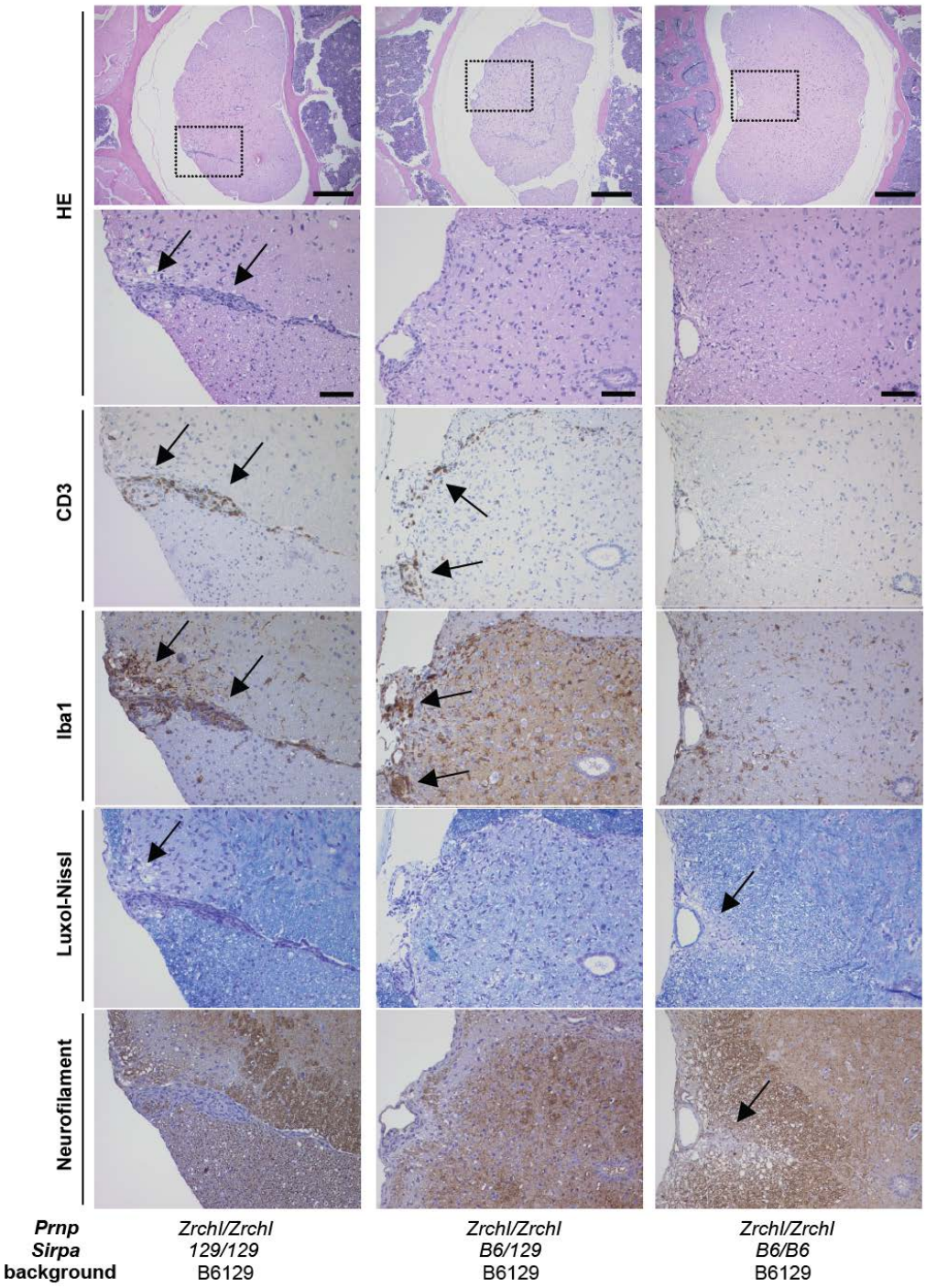

Figure 32. *Sirpa*^{129} promotes acute inflammatory lesions in B6129-*Prnp*$^{Zrchl/Zrchl}$ mice. Representative spinal cords 92 days p.i.. B6129-*Prnp*$^{Zrchl/Zrchl}$ *Sirpa*$^{129/129}$ and *Sirpa*$^{B6/129}$ mice predominantly show acute inflammatory infiltrates. B6129-*Prnp*$^{Zrchl/Zrchl}$ *Sirpa*$^{B6/B6}$ mice show mainly chronic, non-florid lesions with evidence of demyelination and concomitant axonal loss. Scale bar 100 μm, except for upper panel: 500 μm.

In summary, when inducing EAE in B6129-*Prnp*$^{Zrchl/Zrchl}$ mice carrying different *Sirpa* allelotypes, homozygosity for *Sirpa*^{129} was associated with a more severe clinical disease course corresponding to a strong relapse phase associated with florid inflammatory lesions in the spinal cord. These data suggest that different *Sirpa* allelotypes (B6 and 129) modulate the disease course of EAE in a B6129-*Prnp*$^{-/-}$ background.

Next, we compared the EAE development of B6129-*Prnp*$^{Zrchl/Zrchl}$ mice with different *Sirpa*-B6/129 alleles with the two *Prnp*$^{wt/wt}$ groups (B6-*Prnp*$^{wt/wt}$ *Sirpa*$^{B6/B6}$ and B6129-*Prnp*$^{wt/wt}$ *Sirpa*$^{B6/129}$). Notably, B6129-*Prnp*$^{Zrchl/Zrchl}$ *Sirpa*$^{129/129}$ animals showed significantly higher disease score during the relapse phase than B6-*Prnp*$^{wt/wt}$ *Sirpa*$^{B6/B6}$ animals (Fig. 33a). The presence of one or two *Sirpa*^{B6} alleles abolished this difference: the clinical course of B6129-*Prnp*$^{Zrchl/Zrchl}$ *Sirpa*$^{B6/129}$ and B6129-*Prnp*$^{Zrchl/Zrchl}$ *Sirpa*$^{B6/B6}$ animals largely overlapped with the one of B6 wt animals (Fig. 33b). This finding suggests that the presence of at least one *Sirpa*^{B6} allele can rescue the B6129-*Prnp*$^{-/-}$ phenotype.

However, since the B6129-*Prnp*$^{Zrchl/Zrchl}$ animals used in these experiments were on a mixed B6129 background (Fig. 19), we considered B6-*Prnp*$^{wt/wt}$ *Sirpa*$^{B6/B6}$ mice as a suboptimal control group. We therefore induced EAE also in F1-offsprings of a B6x129 cross. To compare their genetic background to B6129-*Prnp*$^{Zrchl/Zrchl}$ mice, we performed whole genome STR analysis. As expected, the genetic background of the B6x129 (F1) offsprings was similar but not identical to the B6129-*Prnp*$^{Zrchl/Zrchl}$ mice (Fig. 34). We then compared the EAE development of B6129-*Prnp*$^{wt/wt}$ *Sirpa*$^{B6/129}$ and B6129-*Prnp*$^{Zrchl/Zrchl}$ *Sirpa*$^{B6/129}$. Again, B6129-*Prnp*$^{Zrchl/Zrchl}$ *Sirpa*$^{B6/129}$ mice showed a similar disease course as B6129-*Prnp*$^{wt/wt}$ *Sirpa*$^{B6/129}$ on a comparable mixed background (Fig. 35). These findings confirmed the observation that the lack of *Prnp* is not sufficient to aggravate the EAE disease course, when the mice do not differ in their *Sirpa* allelotypes.

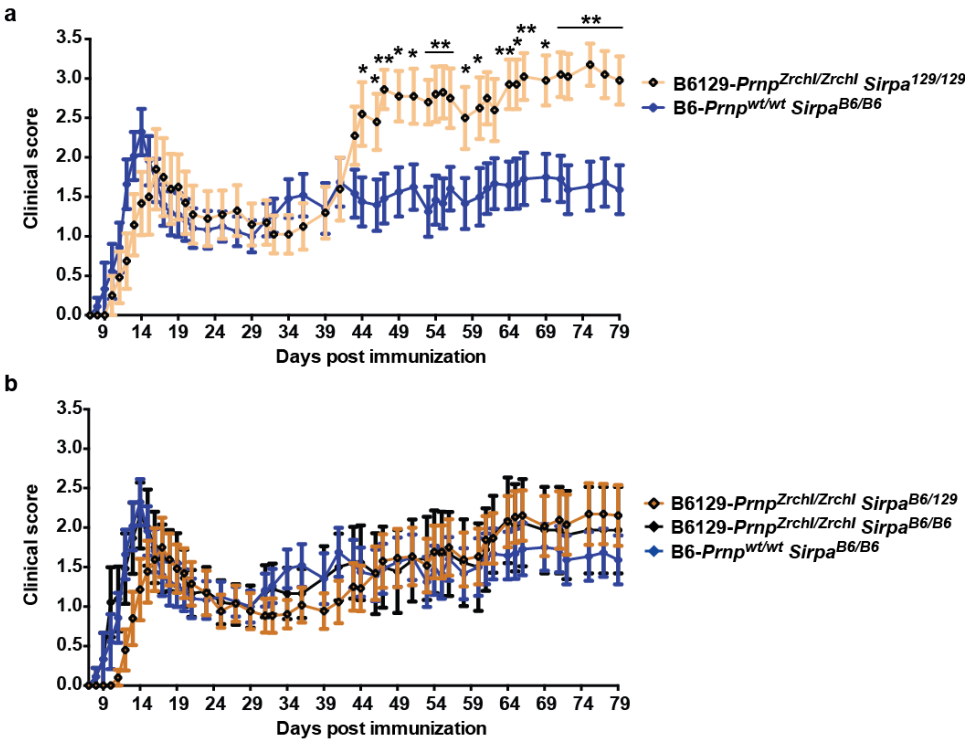

Figure 33. EAE development in B6129-*Prnp*$^{Zrchl/Zrchl}$ mice with *Sirpa*$^{129/129}$, *Sirpa*$^{B6/129}$ or *Sirpa*$^{B6/B6}$ compared to B6-*Prnp*$^{wt/wt}$ *Sirpa*$^{B6/B6}$ mice. (a) B6129-*Prnp*$^{Zrchl/Zrchl}$ *Sirpa*$^{129/129}$ animal show a strong and continuous relapse phase after day 42 p.i., whereas disease scores B6-*Prnp*$^{wt/wt}$ *Sirpa*$^{B6/B6}$ remain stable. (b) EAE disease scores of B6129-*Prnp*$^{Zrchl/Zrchl}$ with *Sirpa*$^{B6/129}$ or *Sirpa*$^{B6/B6}$ and of B6-*Prnp*$^{wt/wt}$ *Sirpa*$^{B6/B6}$ overlap. The exacerbation during the relapse phase in B6129-*Prnp*$^{Zrchl/Zrchl}$ mice is rescued by the presence of one or two *Sirpa*^{B6} alleles. Data are pooled from two independent experiments (n=16 per group); see Fig. 29 for overview of all five experimental groups and Table 8 for detailed clinical development. * p<0.05, ** p<0.01, two-tailed unpaired Student's t-test.

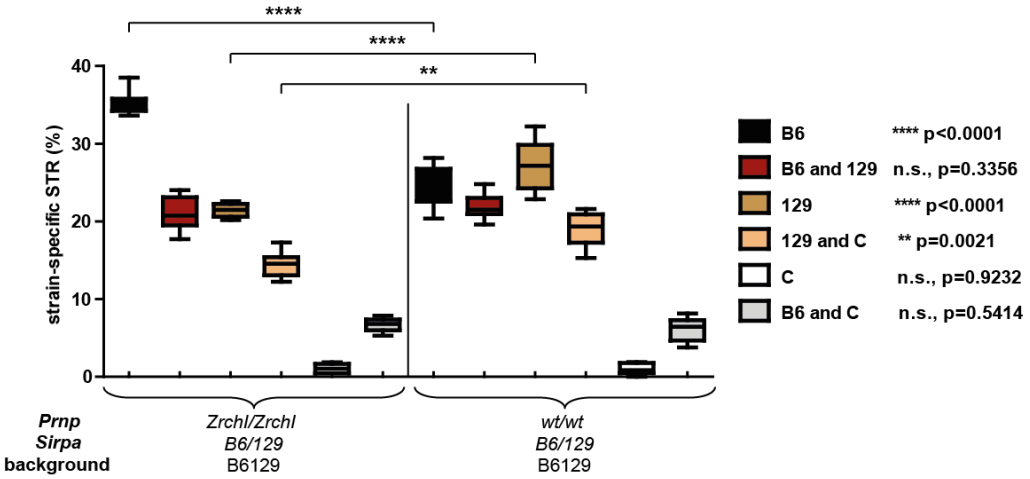

Figure 34. Genetic background of B6129-*Prnp*$^{Zrchl/Zrchl}$ *Sirpa*$^{B6/129}$ vs. B6129-*Prnp*$^{wt/wt}$ *Sirpa*$^{B6/129}$ is similar, but not equal. Box plots show percentages of 192 polymorphic STR

markers distributed across the whole genome in B6129-*Prnp*$^{Zrchl/Zrchl}$ *Sirpa*$^{B6/129}$ (n=9) vs. B6129-*Prnp*$^{wt/wt}$ *Sirpa*$^{B6/129}$ (n=8) mice. B6129-*Prnp*$^{wt/wt}$ *Sirpa*$^{B6/129}$ mice are F1-offsprings from a B6x129 cross. Two-tailed Mann Whitney test (alpha level 0.05) revealed significant differences in the amount of B6 markers (****, p<0.0001), 129 markers (****, p<0.0001) and 129/C markers (**, p=0.0021). No difference was found for B6/129, C and B6/C markers.

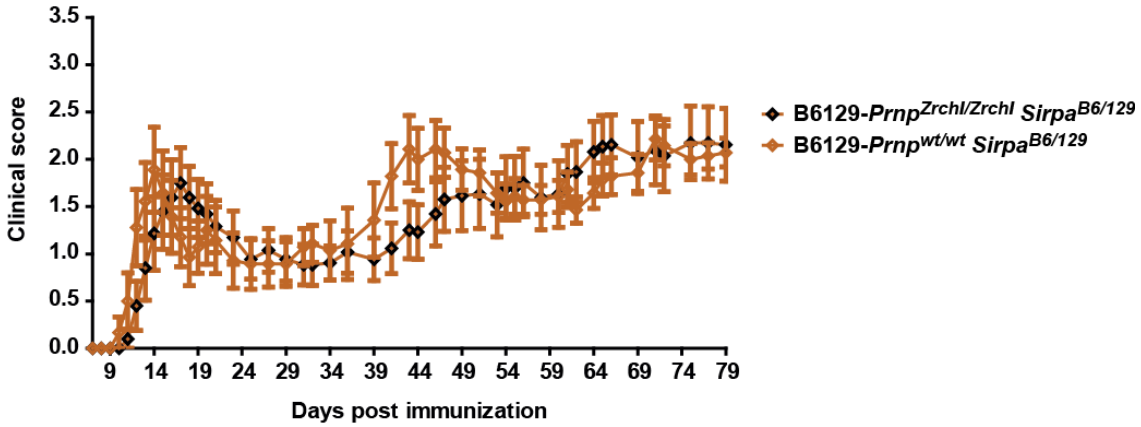

Figure 35. No difference of EAE development between *Sirpa*$^{B6/129}$ mice on a mixed B6129-background differing in their *Prnp* (wt vs. Zrchl) status. Data are pooled from two independent experiments (n=16 for B6129-*Prnp*$^{Zrchl/Zrchl}$ *Sirpa*$^{B6/129}$ and n=10 for B6129-*Prnp*$^{wt/wt}$ *Sirpa*$^{B6/129}$); see Fig. 29 for overview of all five experimental groups and Table 8 for detailed clinical development. Two-tailed unpaired Student's t-test revealed no significant difference between the two groups.

So far, we have found that i) in absence of *Prnp*, the B6/129 *Sirpa* polymorphism is sufficient to modulate EAE disease course, and ii) when comparing mice with and without *Prnp* on a similar (but not equal) mixed genetic background and having the same *Sirpa* allelotype, lack of *Prnp* did not lead to exacerbation of EAE. These results suggest that homozygosity for *Sirpa*^{129}, rather than *Prnp* deficiency is responsible for the exacerbation of EAE in *Prnp*$^{Zrchl/Zrchl}$ mice.

4.2.8 EAE development in congenic B6.129 mice with different combinations of *Prnp* (wt and ZrchI) and *Sirpa* (B6 and 129) alleles

Our studies in mice with a mixed background suggested that the B6/129 *Sirpa* polymorphism can modulate EAE disease course in the absence of *Prnp*, and that absence of *Prnp* is not sufficient for EAE exacerbation in groups of mice with a comparable genetic background and the same *Sirpa* allelotype. So far we could not exclude that the differences in background (Fig. 34) could complicate the interpretation of these results. In addition, we wanted to test whether the B6/129-*Sirpa* polymorphism could modulate EAE disease course also in the presence of *Prnp*. We therefore used congenic B6.129-*Prnp*$^{ZrchI/ZrchI}$ and B6.129-*Prnp*$^{wt/wt}$ mice, where we had screened for transallelic meiotic recombinations between the *Prnp* and *Sirpa* loci, thereby having created recombinant congenic B6.129 mice with different combinations of *Prnp* (wt and ZrchI) and *Sirpa* (B6 and 129) alleles on a highly homogeneous genetic background (Fig. 21 and Fig. 22). We used these mice in experiments testing the reported inhibitory function of PrP on phagocytosis of apoptotic cells (de Almeida et al., 2005), and could show that not the lack of *Prnp*, but homozygosity for *Sirpa*^{129} leads to hyperphagocytosis of apoptotic cells.

We MOG_{35-55}-immunized four groups of congenic B6.129 mice with different combinations of *Prnp* (wt and ZrchI) and *Sirpa* (B6 and 129) in two independent experiments and followed the clinical score for 52 and 61 days, respectively. Fig. 36 and Table 9 summarize the EAE clinical course and the detailed clinical development of all four experimental groups. In contrast to the results obtained in B6129-*Prnp*$^{ZrchI/ZrchI}$ mice, the *Sirpa* B6/129-polymorphism did not modulate EAE disease course in B6.129-*Prnp*$^{ZrchI/ZrchI}$ with different *Sirpa* allelotypes: B6.129-*Prnp*$^{ZrchI/ZrchI}$ *Sirpa*$^{129/129}$ and B6.129-*Prnp*$^{ZrchI/ZrchI}$ *Sirpa*$^{B6/B6}$ showed overlapping disease scores (Fig. 36). We observed a different picture in the presence of *Prnp*: here, the *Sirpa* B6/129 polymorphism seemed

to influence EAE disease progression. But unexpectedly, and in contrast to the results obtained in B6129-*Prnp*$^{Zrchl/Zrchl}$ animals, mice homozygous for *Sirpa*^{B6} showed a more severe disease course than *Sirpa*$^{129/129}$ animals (Fig. 36).

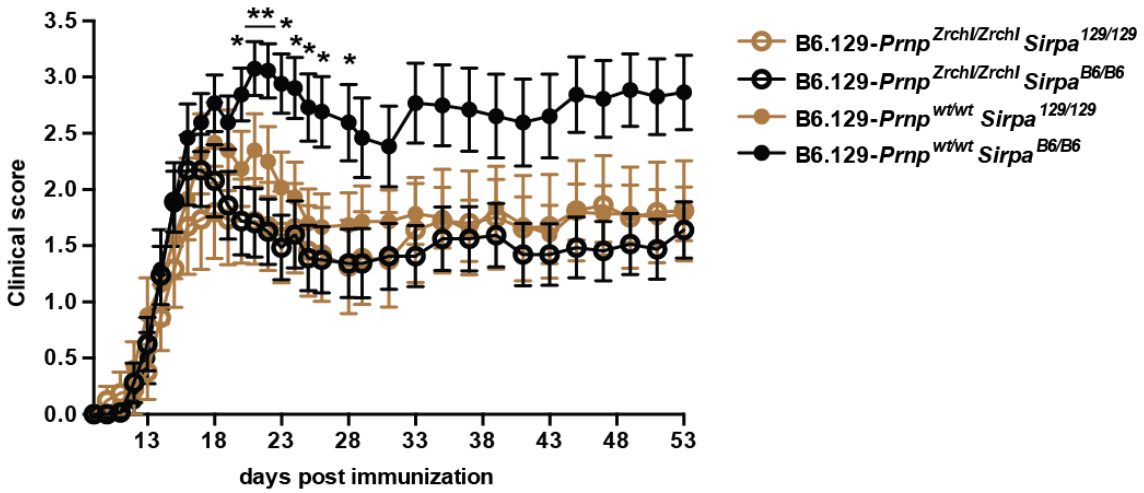

Figure 36. EAE development in recombinant congenic B6.129 mice with different combinations of *Prnp* (wt and Zrchl) and *Sirpa* (B6 and 129) alleles. Overview of the clinical evolution of the four experimental groups (n=16 per group, pooled two independent experiments). B6.129-*Prnp*$^{wt/wt}$ *Sirpa*$^{B6/B6}$ mice show a more severe clinical development than B6.129-*Prnp*$^{wt/wt}$ *Sirpa*$^{129/129}$, B6.129-*Prnp*$^{Zrchl/Zrchl}$ *Sirpa*$^{129/129}$ and B6.129-*Prnp*$^{Zrchl/Zrchl}$ *Sirpa*$^{B6/B6}$ mice. * p<0.05, ** p<0.01, two-tailed unpaired Student's t-test.

Mice	Number of mice	Incidence° (%)	Mortality* (%)	Mean day of onset (±SD)	Mean maximal disease score (±SD)	Mean cumulative disease score (±SD)
B6.129-*Prnp*$^{Zrchl/Zrchl}$ *Sirpa*$^{129/129}$	16	12/16 (75)	3/16 (18.8)	14.3±2.6	3.0±1.1	68.5±45.5
B6.129-*Prnp*$^{Zrchl/Zrchl}$ *Sirpa*$^{B6/B6}$	16	13/16 (81.3)	1/16 (6.3)	13.2±1.2	3.1±0.5	62.3±23.6
B6.129-*Prnp*$^{wt/wt}$ *Sirpa*$^{129/129}$	16	14/16 (87.5)	1/16 (6.25)	15.2±4.4	3.0±0.7	63.0±29.3
B6.129-*Prnp*$^{wt/wt}$ *Sirpa*$^{B6/B6}$	13	13/13 (100)	5/13 (38.5)	14.5±2.1	3.6±0.6	83.3±27.1

Table 9. Detailed clinical EAE development in recombinant congenic B6.129 mice with different combinations of *Prnp* (wt and Zrchl) and *Sirpa* (B6 and 129) alleles. Data are from two pooled experiments. The four groups did not significantly differ in mean day of onset (Kruskal-Wallis test, p=0.4314), mean maximal disease score (Kruskal-Wallis test, p=0.2417), or mean cumulative disease score (Kruskal-Wallis test, p=0.3272). ° mice with a clinical score of at least one. * mice that died or were euthanized due to termination criteria.

We wondered, whether we could still observe different EAE disease scores between the groups when ignoring either the *Prnp* status or the *Sirpa* allelotype. When mice were pooled according to their *Prnp* genotype and irrespective of their *Sirpa* allelotype, B6.129-*Prnp*$^{wt/wt}$ mice showed a more severe disease course than B6.129-*Prnp*$^{ZrchI/ZrchI}$ mice (Fig. 37a). In contrast, when pooling the groups according to *Sirpa* allelotype and irrespective of their *Prnp* genotype, the difference between the groups was abolished (Fig. 37b), suggesting that the *Sirpa* B6/129 polymorphism does not modulate EAE development.

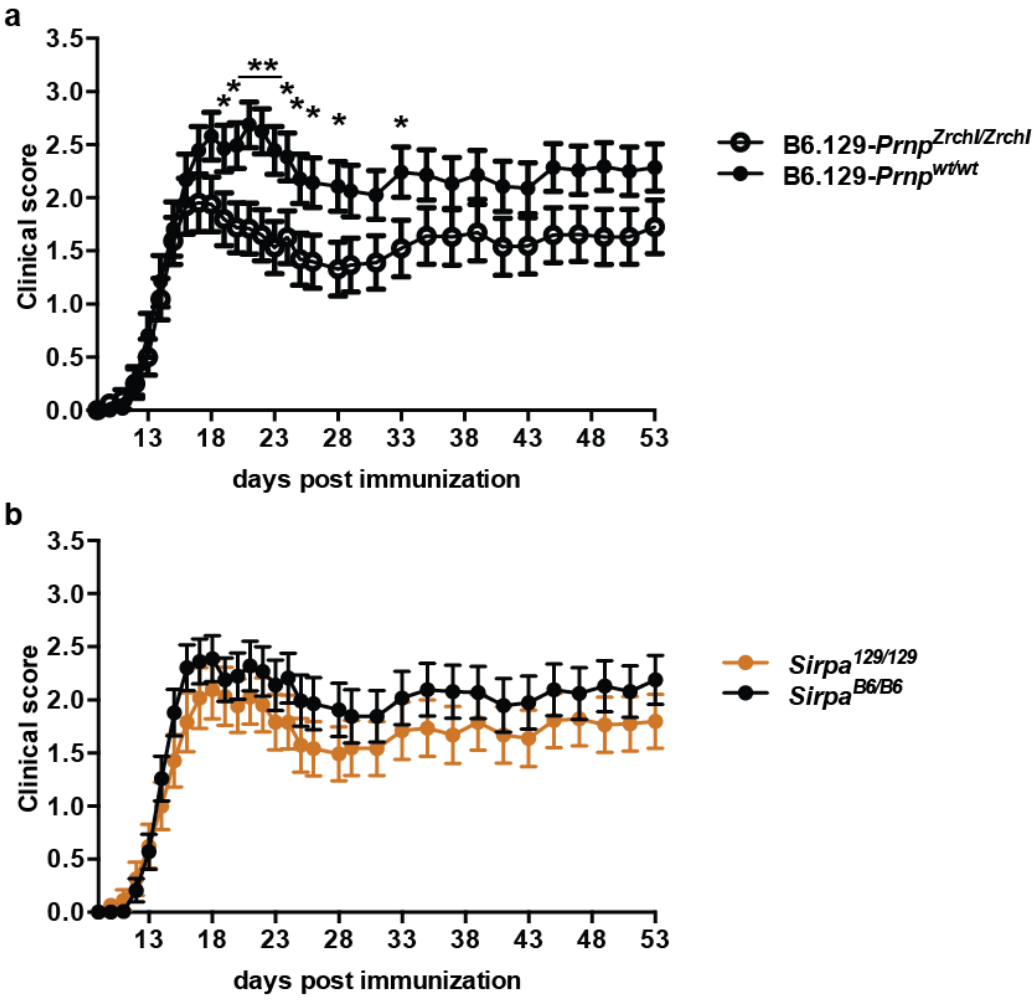

Figure 37. Exacerbated EAE development in B6.129-*Prnp*$^{wt/wt}$ mice and no influence of the *Sirpa* B6/129 polymorphism. (a). Pooling of groups shown in **Fig. 36** according to their *Prnp* genotype and irrespective of the *Sirpa* polymorphism (n=32 per group, two independent experiments). (c) Pooling of groups shown in **Fig. 36** according to their *Sirpa* allelotype and

irrespective of the *Prnp* genotype (n=32 per group, two independent experiments). The B6/129 polymorphism did not significantly influence EAE disease course. * $p<0.05$, ** $p<0.01$, two-tailed unpaired Student's t-test.

Taken together, these results do not support the hypothesis that *Sirpa* polymorphisms – rather than *Prnp* deficiency – modulate EAE disease course. On the other hand, we could not reproduce previously reported findings that the lack of *Prnp* exacerbates EAE (Gourdain et al., 2012; Hu et al., 2010; Ingram et al., 2009; Tsutsui et al., 2008; Williams et al., 2011). In contrary, in our hands, B6.129-$Prnp^{wt/wt}$ showed a more severe EAE development than B6.129-$Prnp^{Zrchl/Zrchl}$ mice. These results suggest the influence of other polymorphic genes flanking *Prnp* and *Sirpa*, which exert a stronger effect on EAE disease course than *Prnp* and/or *Sirpa*.

4.3 DISCUSSION

4.3.1 Mouse genetics excludes PrP^C as inhibitor of phagocytosis

One of the various functions attributed to PrP^C based on studies in *Prnp*$^{-/-}$ mice kept on a mixed or congenic background is the inhibition of phagocytosis of apoptotic cells (de Almeida et al., 2005). Since studies using knockout animals generated as chimeras with different strains are subject to the confounding effect of polymorphic genes flanking the targeted locus, we sought to revisit the impact of PrP^C gene dosage on phagocytosis of apoptotic cells. When using coisogenic *Prnp*$^{-/-}$ mice, which differ from their wild type counterpart only at the mutated site, but are otherwise are genetically identical, the inhibitory effect of PrP^C on phagocytosis was no longer present. In addition, we analyzed the regions flanking *Prnp* in B6129-*Prnp*$^{Zrchl/Zrchl}$, and found a 129-derived segment, which, when homozygous, correlated with higher rate of phagocytosis independent of *Prnp*. Taken together, these data showed that *Prnp* does not impact phagocytosis, and suggests that the conclusion of previous studies resulted from unrecognized effects of polymorphic flanking genes, which were the in truth responsible for the observed effect. A detailed genomic, transcriptomic and functional analysis of candidate genes in the 129-derived region flanking *Prnp* supports a focus on the well-characterized inhibitor of phagocytosis *Sirpa*, whose polymorphisms alter this phenotype (Legrand et al., 2011a; Strowig et al., 2011; Takenaka et al., 2007). Indeed, *Sirpa*^{129}, rather than *Prnp*$^{-}$, segregates with increased phagocytosis.

The search for polymorphic candidate confounder genes was based on the detection of genetic variants in the transcriptome of pMΦ isolated from B6.129-*Prnp*$^{Zrchl/Zrchl}$ and B6.129-*Prnp*$^{wt/wt}$ mice using RNA-Seq. We chose this approach because it permitted us to focus on (i) genes expressed only in our cells of interest, macrophages, and (ii) genetic variants only in protein-coding regions of genes possibly relevant for the function

of the protein in the execution of phagocytosis (Chepelev et al., 2009). Yet we have to consider several technical and conceptual limitations of the use of RNA-Seq and our subsequent filtering strategy to identify candidate confounding genes involved in phagocytosis (Fig. 15). For instance, it is highly unlikely, but not formally excluded that genes silent in macrophages – and therefore missed by RNA-Seq – could indirectly affect isolated, cultured macrophages, and ultimately account for the observed differences in phagocytic activity. Also, by using RNA-Seq, we did not consider variations in noncoding regions, which might potentially alter functional cis-regulatory elements that control transcription and possibly alter abundance of the transcripts. Furtehrmore, we did not include differentially expressed genes into our candidate gene search strategy - yet differentially expressed genes could also influence the phagocytic phenotype. Interestingly, we found a significant proportion of differentially expressed genes mapping on Chr2. This finding could reflect the presence of DNA polymorphisms that regulate gene expression (cis-acting regulatory SNPs) in this region (Noyes et al., 2010). Also, 50 of the 304 differentially expressed genes were found to be associated with phagocytosis, possibly influencing phagocytosis of apoptotic cells. To further examine whether the expression of these genes is influenced by *Prnp*, and to exclude the influence of different genetic backgounds on gene expression (Cowles et al., 2002), we will analyze the transcriptome of pMΦ derived from coisogenic 129-*Prnp*$^{Edbg/Edbg}$ and 129-*Prnp*$^{wt/wt}$ mice.

In addition to *Sirpa*, B6.129-*Prnp*$^{ZrchI/ZrchI}$ and B6.129-*Prnp*$^{wt/wt}$ macrophages harbored sequence variations of several other genes of interest. In particular, we found that *Mertk*, *Tyro3* and *Thbs1,* genes also implicated in phagocytosis, are linked to *Prnp* on Chr2, and polymorphic between the two strains. The segregation pattern of the B6 and 129 alleles of *Tyro3* and *Thbs1* in various hyperphagocytic *Prnp*$^{-/-}$ lines allowed us to dismiss these two genes as candidates. This was not possible for *Mertk*, since the allelotypes always followed the *Sirpa* allelotypes in all our experimental mice. The only non-synonymous coding SNP found between B6.129-*Prnp*$^{ZrchI/ZrchI}$ and B6.129-*Prnp*$^{wt/wt}$ codes for a

conservative AA substitution within the transmembrane region of MER (I516V), and is predicted not to alter the function of this protein. The corresponding AA substitution is also present in humans and was classified as a non-disease causing normal variant. For these reasons, we excluded *Mertk* as a candidate gene. Yet we have to take into consideration that *Mertk* encodes a receptor protein tyrosine kinase (PTK), whose activation involves receptor dimerization (Lemke and Rothlin, 2008). Therefore, the transmembrane regions of these proteins are considered an important part of the signaling process and pathogenic mutations involving the transmembrane region of PTK have been identified in different cancers (Li and Hristova, 2010). To discriminate the effect of polymorphisms of *Sirpa* and *Mertk*, we would need to screen mouse breedings for the occurrence of transallelic meiotic recombination between *Sirpa* and *Mertk*, or alternatively, perform phagocytosis assays testing different *Sirpa* polymorphisms using compounds blocking MER signaling.

Finally, we cannot rule out that additional polymorphic genes not yet implicated in phagocytosis, and thereby missed by our filtering strategy, may contribute to the phagocytic phenotype. Irrespective of potential contributions by these other genes, our data exclude a role for PrP^{C} in the modulation of phagocytosis and strongly suggest polymorphisms of *Sirpa* as the cause of the previously reported phagocytic phenotype of *Prnp* knockout mice.

4.3.2 Modulation of EAE development by *Prnp* and its polymorphic flanking genes – a blurry picture

Encouraged by our findings that polymorphic flanking genes and not *Prnp* status, in particular *Sirpa* polymorphisms, explained the reported role of PrP^{C} in phagocytosis, we strived to determine the influence of different *Sirpa* polymorphisms in combination with presence or absence of *Prnp* in the development of mouse EAE. When inducing EAE in $Prnp^{Zrchl/Zrchl}$ mice on a B6129 background with all possible combinations of $Sirpa^{129}$ and

Sirpa^{B6} alleles, we found that B6129-*Prnp*$^{Zrchl/Zrchl}$*Sirpa*$^{129/129}$ mice showed a more severe disease course, whereas *Sirpa*$^{B6/B6}$ homozygosity rescued the *Prnp*$^{-/-}$ phenotype, suggesting a role of the *Sirpa* B6/129 polymorphism in EAE development. The influence of *Prnp* was not detectable when comparing B6129-*Prnp*$^{Zrchl/Zrchl}$ *Sirpa*$^{B6/129}$ with mice derived from a B6x129 crossing (B6129-*Prnp*$^{wt/wt}$ *Sirpa*$^{B6/129}$). As assessed by STR-analysis, the background of each of the two groups was not well matched, since the F1 wild type animals were heterozygous for all genes and the *Prnp* knockout group contained more B6-derived homozygous genes. Hence the lack of EAE exacerbation in *Prnp*$^{-/-}$ could be attributed to genetic background differences. Finally, we tested the effect of *Sirpa* polymorphisms and *Prnp* gene dosage using congenic *Prnp*$^{-/-}$ mice with all *Prnp*/*Sirpa* combinations. These experiments revealed the lack of influence of the *Sirpa* B6/129 polymorphism; however, a more severe EAE disease course in *Prnp* wild type mice was observed, in contrast to previously published findings. In summary, we found a potential influence of *Sirpa* and/or flanking genes in the absence of *Prnp*, and could not reproduce previous findings showing a protective role of PrP^{C} in neuroinflammation (Gourdain et al., 2012; Hu et al., 2010; Ingram et al., 2009; Tsutsui et al., 2008; Williams et al., 2011). These findings raise the question whether one or several additional genes flanking *Prnp* and *Sirpa* might exert a stronger effect on disease course, and play a role in the outcomes observed in our experiments (Fig. 38).

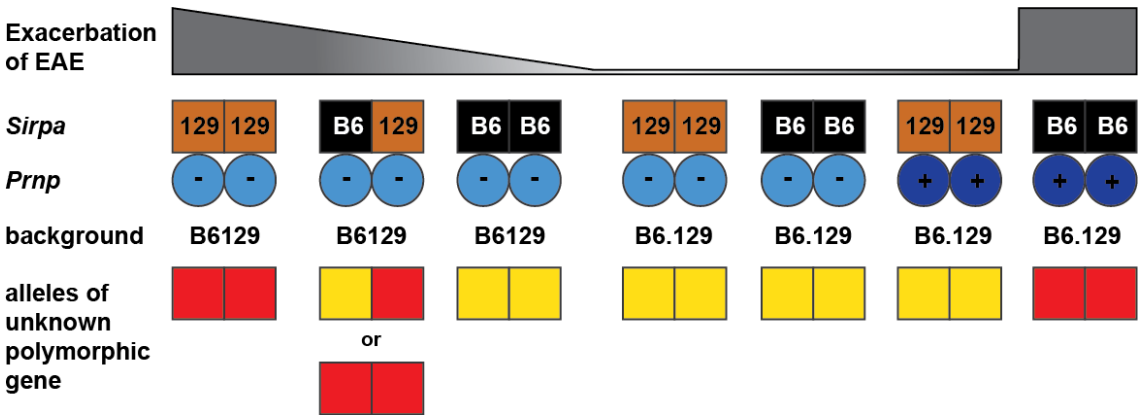

Figure 38. A polymorphic gene other than *Prnp* and *Sirpa* might influence EAE disease course. EAE severity was not influenced by *Prnp*, nor by the B6/129 polymorphism of *Sirpa*. Red and yellow boxes depict alleles of an unknown polymorphic flanking gene, which might be responsible for the observed differences in EAE disease course.

Are there any indications for the effect of such confounding effects in the previously published studies? In contrast to the phagocytosis phenotype found in congenic *Prnp* mice carrying confounding ESC-derived flanking genes, exacerbation of EAE also occurred in coisogenic *Prnp* mice, where knockout and wildtype mice differed only in *Prnp*. In this study, the use of siRNA to block *Prnp* provided additional support for a role of *Prnp* in EAE development. However, in comparison to studies performed in congenic *Prnp*$^{-/-}$ mice, the effect of *Prnp* ablation seemed rather low. In addition, EAE studies using of PrP^C overexpression yielded inconsistent results, along with discrepant findings about a causative *Prnp*-dependent alteration in T cell activation. Possible explanations for these findings are variations in protocols and the use of mice with different genetic backgrounds. EAE is a highly complex model, and the susceptibility to EAE is known to be influenced by many genes, pathways and induction protocols (Baxter, 2007; Constantinescu et al., 2011; Gold et al., 2006). Another possible explanation might be the influence of another flanking locus that could alter EAE susceptibility to a greater extent than *Prnp* alone (Fig. 38), or in combination with *Prnp*.

A similar complex situation was recently described in a model of kainate-induced seizures. Using congenic and coisogenic *Prnp*$^{-/-}$ strains, in combination with genetic complementation studies with a *Prnp* transgenic line, the authors disproved a previously attributed role of PrP^C in alteration of synaptic and electrophysiological activities, and attributed this effect to unknown 129-derived flanking genes (Striebel et al., 2013). Hence, careful examination of the role of polymorphic genes flanking *Prnp* and their interactions is necessary to clarify their impact in such complex models as EAE or kainate-induced seizures.

4.3.3 Concluding remarks

The linkage of *Sirpa*^{129} to *Prnp*$^{-}$ in all analyzed *Prnp*$^{-/-}$ lines may contribute to processes beyond the control of phagocytosis. The *Sirpa* sequence of mouse strains typically

employed for backcrossing of *Prnp*$^{-/-}$ mice (e.g. C57BL/6, BALB/c, and FVB) differs from that of 129 mice (Sano et al., 1999; Takenaka et al., 2007), hence rendering *Sirpa* a potential confounder in most studies of *Prnp*$^{-/-}$ mice. The expression pattern of *Sirpa* mirrors that of *Prnp*, and includes myeloid cells, hematopoietic stem cells, neurons and pancreatic β cells (Linden et al., 2008; Matozaki et al., 2009). Also, PrP^{C}-deficient mice share numerous subtle phenotypes with mice lacking functional *Sirpa*, including behavioral (Gadotti et al., 2012; Nico et al., 2005; Ohnishi et al., 2010) and metabolic phenotypes (Kobayashi et al., 2008; Strom et al., 2011). These observations suggest that additional and also non-immunological phenotypes attributed to *Prnp* may reflect the effects of polymorphic *Sirpa*.

The confounding effects of ESC-derived genes flanking the targeted locus are known (Gerlai, 1996; Smithies and Maeda, 1995), and there are recommendations regarding breeding schemes and genetic quality control of mouse colonies (Crusio et al., 2009; Ridgway et al., 2007; Wolfer et al., 2002) – but they are rarely implemented (Holmdahl and Malissen, 2012). Consequently, reports of flanking gene problems are rare and mostly rely on the observation that a certain phenotype of knockout mouse can be rescued via extensive backcrossing to a specific background after reduction of the 129-derived region flanking the targeted locus (de Ledesma et al., 2006; Eisener-Dorman et al., 2010; Kanagawa et al., 2000; Schalkwyk et al., 2007), and rarely demonstrate the effect of flanking genes using a coisogenic line (Striebel et al., 2013). Accordingly, a solution to this problem is the use of coisogenic knockout animals, such as the Edinburgh-*Prnp*$^{-/-}$ line in the prion field – yet they are rarely available. Today's possibility to use B6-derived ESC for the generation of knockout animals (Pettitt et al., 2009; Seong et al., 2004), and new efficient genome editing technologies (Horvath and Barrangou, 2013; Joung and Sander, 2013) will hopefully advance the generation of coisogenic knockout lines. However, it is important to keep in mind that also these lines are subject to spontaneous mutations and must therefore be regularly screened for genetic stability.

Finally, these new tools may also help to resolve unanswered questions regarding the function of the prion protein - in the immune system and beyond.

4.4 MICE, MATERIAL AND METHODS

4.4.1 Mice

The following mice were analysed: *Prnp*$^{Zrchl/Zrchl}$ mice (Büeler et al., 1992), on a mixed B6129 background or backcrossed to B6 for >12 generations or to C for >17 generations and congenic wild-type B6 and C mice purchased from Harlan or Charles River or bred in house; *Prnp*$^{Ngsk/Ngsk}$ (Sakaguchi et al., 1995) extensively backcrossed to B6; *Prnp*$^{Edbg/Edbg}$ mice on a pure 129/Ola background (Manson et al., 1994) and coisogenic wild-type 129/Ola mice; *Prnp*$^{ZrchII/ZrchII}$ mice (Rossi et al., 2001) on a mixed B6129 background; *Prnp*$^{GFP/GFP}$ mice (Heikenwalder et al., 2008) backcrossed to B6 for 10 generations; *tga20* mice (Fischer et al., 1996) on a mixed B6129 *Prnp*$^{Zrchl/Zrchl}$ background; SHPS-1 (Inagaki et al., 2000) backcrossed to B6 for >5 generations. Mice were genotyped as indicated in the original description of each line. To introduce *Sirpa*^{B6} into B6129-*Prnp*$^{Zrchl/Zrchl}$ mice, B6129-*Prnp*$^{Zrchl/Zrchl}$ *Sirpa*$^{B6/B6}$ *tga20*$^{tg/tg}$ mice were crossed with B6129-*Prnp*$^{Zrchl/Zrchl}$ *Sirpa*$^{129/129}$ mice (Fig. 18). To generate congenic B6.129-*Prnp*$^{Zrchl/Zrchl}$ and *Prnp*$^{wt/wt}$ mice with all possible combinations of *Sirpa*^{B6} and *Sirpa*^{129} alleles, B6.129-*Prnp*$^{wt/Zrchl}$ *Sirpa*$^{B6/129}$ mice were intercrossed and meiotic recombination events between *Prnp* and *Sirpa* were identified by *Prnp* genotyping and RFLP analysis of *Sirpa* exon 2 in the offspring (Fig. 21). Mice with a recombinant haplotype (referred to as obligate carriers) were further crossed as shown in Fig. 21. The same approach was followed to generate congenic C.129-*Prnp*$^{Zrchl/Zrchl}$ and *Prnp*$^{wt/wt}$ mice with all possible combinations of *Sirpa*^{C} and *Sirpa*^{129} alleles (Fig. 26). All animal experiments were performed in compliance with the Swiss Animal Protection Law, with the approval of the Veterinary office of the Canton Zurich.

4.4.2 RNA-Seq

All steps of RNA-Seq were performed at the FGCZ. All bioinformatics analyses were performed by Giancarlo Russo, FGCZ.

Library preparation

Total RNA was isolated from cultured pMΦ using the RNeasy mini Kit (QIAGEN), snap frozen and kept at -80°C until further analysis. RNA quality was determined with a Qubit (1.0) fluorometer (Life Technologies) and a Bioanalyzer 2100 (Agilent). Only samples with a 260 nm/280 nm ratio between 1.8–2.1 and a 28S/18S ratio between 1.5–2 were further processed. The TruSeq RNA Sample Prep Kit v2 (Illumina) was used in the subsequent steps. Briefly, total RNA samples (1 μg) were poly A-enriched and reverse-transcribed into double-stranded cDNA. TruSeq adapters were ligated to double-stranded cDNA. Fragments containing TruSeq adapters on both ends were selectively enriched with PCR. The quality and quantity of the enriched libraries were validated using Qubit (1.0) Fluorometer and Caliper GX LabChip GX (Caliper Life Sciences). The product is a smear with an average fragment size of approximately 260 bp. Libraries were normalized to 10 nM in Tris-Cl 10 mM, pH 8.5 with 0.1% (v/v) Tween-20.

Cluster generation and sequencing

The TruSeq PE Cluster Kit v3-cBot-HS (Illumina) was used for cluster generation using 2 pM of pooled normalized libraries on the cBOT. Sequencing was performed on the Illumina HiSeq 2000 paired end at 2 X101 bp using TruSeq PE Cluster Kit v3-cBot-HS (Illumina).

Data analysis

Reads were quality-checked with fastqc. Low quality ends were clipped (3 bases from the start, 10 bases from the end). Trimmed reads were aligned to the reference genome

and transcriptome (fasta and gff files, respectively, UCSC mm10 database) with tophat v 2.0.6. Tophat was run with the following options: mate inner distance set to 30, the corresponding standard deviation to 100, maximum 10 multi-hits were allowed in the alignment. Reads that did not align at the first attempt were split into 25-bases long sections on which a second attempt of alignment was performed. In B6.129-*Prnp*$^{Zrchl/Zrchl}$ pMΦ, all reads mapping to *Prnp* between BstEII and EcoRI restriction sites in exon 3 and in the 3'UTR, respectively, were excluded from the analysis because they might have represented fused mRNA containing *neo* and residual *Prnp*, as reported in the brain of these mice (Büeler et al., 1992). Polymorphisms were detected using GATK v 2.1.8 using following options: baq Gap open penalty (whole-genome analysis) set to 30; minimum consensus coverage to genotype indels set to 8 (default: 5); minimum base quality score and minimum variants phred score set to 15. Variants were annotated using snpEFF v 3.0 and distribution of the reads across genomic isoform expression was quantified using http://www.biomedcentral.com/1471-2105/12/323 cufflinks v 2.0.2 and differentially expressed genes listed with its utility Cuffdiff using default options. All remaining data and statistical analyses, formatting and pictures-generating was produced via in-house R-scripts (R v 2.15.2).

4.4.3 RFLP and sequencing analysis of candidate genes

To distinguish *Sirpa*^{129} vs *Sirpa*^{B6} or *Sirpa*^{C}, *Tyro3*^{129} vs *Tyro3*^{B6}, or *Thbs1*^{129} vs *Thbs1*^{B6} or *Thbs1*^{C} alleles, gDNA was PCR-amplified using the primers listed below and amplicons were digested with the restriction enzymes listed below. Digestion products were separated by electrophoresis on an agarose gel. To distinguish *Mertk*^{129} vs *Mertk*^{B6}, gDNA was was PCR-amplified using the primers listed below and amplicons were sequenced. In the candidate recombinant mice identified in the screening for meiotic recombination between *Prnp* and *Sirpa*, recombinant haplotypes were confirmed by sequencing of *Sirpa* ORF and genotyping the resulting offspring.

For RFLP analysis of *Sirpa* (5'→3'):			
Gene	Forward primer	Reverse primer	Restriction enzyme
RFLP *Sirpa* B6vs129	CCGTTCTGAACTGCACTTTG	GGGGTGACATTACTGATACGG	AvaI
RFLP *Sirpa* Cvs129	ACAGAGGAGTAGGGCAAAGC	TAGGTACCGGCATCTTCTGG	XmnI

For RFLP analysis of *Tyro3* (5'→3'):			
Gene	Forward primer	Reverse primer	Restriction enzyme
RFLP *Tyro3* B6vs129	GGGATTAAAGGATCCGGCCC	CACCTTCGACAGTGAGCCAT	HpyCH4III

For RFLP analysis of *Thbs1* (5'→3'):			
Gene	Forward primer	Reverse primer	Restriction enzyme
RFLP *Thbs1* B6vs129	GGATAGCCAAGCGTCTGGAG	TCGCATCTGTTGTTGAGGCT	Cac8I

For *Mertk* sequencing (5'→3'):		
Gene	Forward primer	Reverse primer
Mertk	TGGTCTGCAGTAAGCCCTTG	AAGGTAAGCTCGATGGCTCG

For *Sirpa* ORF sequencing (5'→3'):		
Gene	Forward primer	Reverse primer
***Sirpa* -1**	AGTCCACCTTAAGAGGACCAAGTAGC	TGTACAGAAACAGGACGCGGA
***Sirpa* -2**	TCTCCCTCCTTGCTCTGCAG	TACCTCGCAGATGACCTTAGAATTAA
***Sirpa* -3**	CCTAGTGGAAAGAATGTCTCCTACAACA	CATATTCTGTGTGGTTGTTAGGCTCA
***Sirpa* -4**	CCAGGTACAGTCTTTGATCCAGGA	CCAGGGAGTCTCTGCTGGTCTA
***Sirpa* -5**	ACCCCAGGTTGCGTCCTTGA	GTGGGTGGTTTGCCCTGGCT
***Sirpa* -6**	CCAATGCTGACCTAATGTTGGC	CATCTATACACCCGTGTGTGTATACACA
***Sirpa* -7**	AACTTGTCTTTGTCCGGGCC	GGCACAGTTCATCCTCACCC

4.4.4 Genome-wide and Chr2 STR analysis

Genome-wide STR analysis was performed as previously described (Bremer et al., 2010). Briefly, purified gDNA was amplified using multiplex PCR with fluorescently labelled primers (FAM, NED, VIC; Applied Biosystem), diluted, denatured and subjected to capillary electrophoresis on a 3130*xl* Genetic Analyzer (Applied Biosystems). Various mouse strains were used for calibration. Peak detection, binning and allele calling were performed using the GeneMapper software in combination with an in-house–developed software.

4.4.5 High-resolution microsatellite genotyping on Chr2

This analysis was performed in collaboration with Jayne Danska and Steven Martin-Toth (Hospital for Sick Children, University of Toronto). Novel microsatellite markers were generated as previously described (Ivakine et al., 2006). DNA was amplified for 35 cycles: 30s at 94°C, 30s at 55°C, 1min at 72°C using Multiplex Master Mix (Qiagen #206143) using the following microsatellite markers:

For high resolution microsatellite genotyping on chromosome 2 (5'→3'):		
Marker_ID	primer1	primer2
D2Jyh582	ACTAAGCCCAACACAGCCTT	GCCTACCATATGCAAGACCC
D2Jyh1192	TCTCTTTGACTTTCACACATGC	CCCTGTGAGTGACAGAGGTATC
D2Gul161	GTGGCTCTTTCTCCTGTTCC	GTATGCATGTATGTTTATGTGTGGT
D2Gul169	TGCCTGAAGCTAACTACAGTGTAC	CATCATCATTATCAGAAGCATGTT
D2Ngul1543	GATGTACAGAGGGCACTGCA	AGTCACCTATGTTGGATGTACCAC
D2Ngul1586	ATGGGCTGATGATGTCACA	AGGTCCACATCCATACAGCA
D2Gul289	GGGAACTGACTTAGATCCTAAAAGT	CTGGCACACAACCCCC
D2Ngul1677	ACCTCCAAAGCAGAATCCTC	TCCACACTCTAAAGGGATCAAG
D2Ngul1686	CTCGAGAGTACATACGCATGC	AGCAAGACACCTGATAGTACGTG
D2Ngul1761	TGTGGAGCAGGTGACGTC	AGCCTCACCTCATGAAAGCT
D2Ngul1797	TTTCCCCAAAACCAGCAT	GATTTCTTTCCATTCCCCAA
D2Ngul181	ACTGTTGTGGCCAAAATGG	CCTGCACAGTCTTTGTTGTTG

6		
D2Ngul1849	AGGTGAAGGGTTATTTCTGGAC	CCAGGACAGCTTCTAGTAGTGTCT
D2Ngul1865	TTAAACAGGAATTCTTTCAACATTT	ATAAGCTGTGCTCTGGCCTT
D2Ngul1888	ACCACTTCGATATCATTGGGA	GCCCTGCAAACACTAAATCA
D2Ngul1937	GCTCATGTCCTTCCAAGAATG	GGGAAGAAGAGGAAGGAATTG
D2Jyh2400	GCAATACCTCCAGCAATTTGT	CCATCCTACCAAAAGTAATCCA
D2Jyh2407	CAGTGAGACCCTGTCTCAAAA	CTGCCTTCCTAGAGCTGTCTT
D2Gul374	ATGACTTAAGCATTTTAAGCCAAA	CCCCCCAACTTTAAACACA
D2Gul399	CAGCAGGTAAGAGCCCTTG	TGAAATTATTTTTGTCCTTTTTTGT
D2Gul498	GACCCTGCAGATCTCAGCA	CATTTTTCTAATCATTTATGTCTTATGTG

The PCR product was diluted 1/20, and 1 μl mixed with a 10 μl mixture containing formamide and a 500LIZ size standard. Samples were resolved on the 3730XL DNA Analyzer (Applied Biosystems). Alleles were sized, in comparison to standards, by viewing electropherograms in GeneMapper (Applied Biosystems)

4.4.6 Phagocytosis assay with pMΦ

On day 0, peritoneal cells were collected from age- and gender-matched adult mice according to standard methods (Fortier and Falk, 2001), resuspended to 2.2 x 10^6 in 5 ml of DMEM (GIBCO) with 10% foetal bovine serum (FBS, GIBCO), 1% Glutamax (GIBCO) and antibiotics, plated in one-well slide chambers (BD Falcon) and incubated at 37°C. After 2 hours, non-adhering cells were removed and the remaining cells (referred to as cultured pMΦ) were kept overnight in culture. On day 1, thymocytes were harvested from 3 to 8 week-old mice of the same background as the genotypes under investigation, incubated for 3 hours at 37°C in the presence of dexamethasone 1 μM to induce apoptosis, washed and added to the cultured pMΦ at different ratios for 1 hour. For each experimental group, technical replicates (at least duplicates) were performed. Cells were washed, fixed with formalin and stained with May-Grünwald-Giemsa. Slides were randomized, scanned with Nanozoomer (Hamamatsu), random fields (50 fields/slide) were generated and phagocytosis rate was assessed using in-house developed

software. The same operator blinded to experimental groups validated all software-analysed slides. For each technical replicate, >800 cells were evaluated (indicated as a dot in the graphs). Phagocytosis rate was defined as the percentage of macrophages having at least one apoptotic body.

4.4.7 Phagocytosis assay with BMDM

On day 0 femurs were collected from age and gender-matched adult mice and flushed with RPMI1640 medium (GIBCO) containing 10% FBS (GIBCO) 1% Glutamax (GIBCO) and antibiotics. Bone marrow cells were plated into 6 well plates at 2 x 10^6/well in 3 ml culture medium containing 10 ng/ml of M-CSF (Invitrogen) and cultured overnight at 37°C. On day 1, cells were transferred to new 6 well plates to remove loosely adherent stroma-like cells. On day 6, cells were harvested, adjusted to 5 x 10^5 cells in 500 µl and plated into 24 well plates. Apoptotic thymocytes (see above) were suspended at 1 x 10^6/ml in PBS and labeled with 20 ng/ml of the pH-sensitive dye pHrodo Red, SE (Invitrogen) for 30 minutes at room temperature, washed, and 500 µl of cell suspension were added to BMDM culture for 1 hour at 37°C. After washing, BMDM were harvested with Accutase (Invitrogen) and gentle scraping, stained with FITC-labeled anti-CD11b or isotype control antibody (BD Bioscience) and rate of phagocytosis was analyzed by flow cytometry as the percentage of pHrodo positivity among $CD11b^+$ cells. At least 10000 events were acquired in the living gate.

4.4.8 Flow cytometric analysis

Freshly isolated peritoneal cells were incubated with FITC-labelled anti-F4/80 or isotype control antibody (BD Pharmingen). Thymocyte apoptosis was assessed using the FITC Annexin V Apoptosis Detection Kit II (BD Pharmingen). Flow cytometry was performed

using a FACSCalibur or a FACSCanto (BD Bioscience), data were acquired with CellQuestPro or FACS Diva software, respectively, and analysed with FlowJo software.

4.4.9 Immunofluorescence

After interaction with pHrodo-labeled apoptotic thymocytes, BMDM were washed, fixed with 4% paraformaldehyde for 10 min, and stained with FITC anti-mouse F4/80 (Biolegend) and DAPI (Sigma). Images were acquired using FluoView FVi confocal microscope (Olympus) and analyzed using Imaris software (Bitplane).

4.4.10 Induction of EAE and clinical evaluation

On day 0, mice were immunized s.c. with 200 μg MOG_{35-55} peptide in CFA in the lateral abdomen. 200 ng pertussis toxin in PBS was administered i.p. on day 0 and day 2. Mice were scored daily as follows: 0, no detectable signs of EAE; 0.5, distal limp tail; 1.0, complete limp tail; 1.5, limp tail and hind-limb weakness; 2, unilateral partial hind-limb paralysis; 2.5, bilateral partial hind-limb paralysis; 3, complete bilateral hind-limb paralysis; 3.5, complete hind-limb paralysis and partial forelimb paralysis; 4, moribund (total paralysis of forelimb and hind limb); and 5, death. Statistical analysis was performed using an unpaired Student's t test, and *P* values less than 0.05 were considered significant.

4.4.11 Histology and immunohistochemistry

Whole mouse brains and spinal cords were fixed in 4% paraformaldehyde in phosphate-buffered saline, decalcified in (10%) ethylenediaminetetraacetic acid and paraffin-embedded. Slides were stained with HE, LN, Iba-1 (Wako, #019-19741), CD3 (SP7, Dako), neurofilament (NE14, Sigma) and GFAP (Dako, #Z0334).

4.4.12 Statistical analysis

Comparisons of phagocytic activity of macrophages of different genotypes were performed using One-way ANOVA and Bonferroni's multiple comparison post-test (alpha level 0.05), or two-tailed unpaired t-test, using GraphPad Prism software. The statistical test, p-values and *n* for each statistical analysis are indicated in the corresponding figure legends. For EAE experiments, data are presented as mean EAE clinical score ± standard error of the mean (SEM). Groups were compared at single timepoints using 2-sided unpaired Student's t-test using an alpha of 0.05. All analyses were performed using GraphPad Prism software.

4.5 SUPPLEMENTARY TABLES

4.5.1 Supplementary Table 1. List of differentially expressed genes in pMΦ of B6.129-*Prnp*$^{Zrchl/Zrchl}$ vs. B6.129-*Prnp*$^{wt/wt}$ identified by RNA-Seq.

The table below lists 304 differentially expressed identified by RNA-Seq ($p<0.05$), sorted by Log_2–fold change (Fig. 12). Chr2 contains significantly more differentially expressed genes (genes on Chr2 in yellow). This clustering is even more pronounced when considering the highly differentially expressed genes (absolute Log_2-fold change > 1) and correcting for chromosome size.

Gene	Locus	FPKM WT	FPKM KO	Log_2-fold change	p-value	q-value	Phag. *	SNPs §
Spint1	chr2:119237359-119249513	55.71	0.56	-6.63	0.00E+00	0.00E+00	-	-
Jmjd7	chr2:120027482-120032604	1.15	0.03	-5.31	4.13E-06	4.37E-04	-	-
Bub1b	chr2:118598210-118641592	2.15	0.1	-4.47	0.00E+00	0.00E+00	-	-
Gpr176	chr2:118277097-118373419	0.9	0.05	-4.31	2.55E-13	1.35E-10	-	-
Prnp	chr2:131909927-131938431	7.96	0.42	-4.24	0.00E+00	0.00E+00	+	-
Slc15a2	chr16:36750163-36784962	1.11	0.22	-2.33	6.35E-07	8.25E-05	-	-
Hpgds	chr6:65117292-65144730	0.78	0.18	-2.13	1.17E-06	1.39E-04	-	-
Mamdc2	chr19:23302608-23448322	0.7	0.17	-2.06	5.10E-06	5.25E-04	-	-
Cdo1	chr18:46713204-46728342	4.44	1.2	-1.89	1.34E-08	3.01E-06	-	-
Rhov	chr2:119269200-119271226	11.06	3.01	-1.88	3.11E-15	2.78E-12	-	-
Hpgd	chr8:56294551-56321046	4.1	1.27	-1.69	7.18E-08	1.19E-05	-	-
AA467197,Mir147	chr2:122637886-122641076	7.7	2.4	-1.68	8.17E-06	7.66E-04	-	-
Gcnt1	chr19:17326140-17372844	10.23	3.57	-1.52	1.78E-15	1.72E-12	-	-
Arhgap22	chr14:33216822-33369936	1.81	0.64	-1.5	1.25E-05	1.11E-03	-	-
8430406I07Rik	chr2:144271034-144281229	6.07	2.23	-1.45	1.95E-10	6.29E-08	-	+
Arhgap19	chr19:41766587-41802084	4.69	1.75	-1.42	1.02E-11	3.85E-09	-	-
Dkk2	chr3:132085291-132180304	3.76	1.44	-1.38	4.51E-09	1.12E-06	-	-
C1qc	chr4:136889801-136892914	286.23	114.96	-1.32	0.00E+00	0.00E+00	+	-
LOC100038947	chr3:15795146-15848487	8.92	3.65	-1.29	1.19E-07	1.89E-05	-	+
Gas6	chr8:13465373-13494535	2.37	0.98	-1.27	3.01E-05	2.27E-03	+	-
E2f2	chr4:136172393-	0.74	0.31	-1.26	5.50E-04	2.61E-02	-	-

	136196056							
Rab3il1	chr19:10018227-10035586	4.85	2.05	-1.25	5.25E-07	7.11E-05	-	-
Cadm1	chr9:47530351-47853385	6.32	2.67	-1.24	2.05E-10	6.43E-08	-	-
Sirpb1b	chr3:15495753-15575065	3.26	1.4	-1.22	2.37E-04	1.29E-02	-	-
Ophn1	chrX:98557514-98890985	3.2	1.37	-1.22	2.14E-07	3.23E-05	-	-
Slc46a3	chr5:147878440-147894802	7.81	3.46	-1.17	3.12E-08	6.38E-06	-	-
Slc27a6	chr18:58556239-58612869	1.62	0.72	-1.17	5.82E-04	2.74E-02	-	-
C1qb	chr4:136880144-136886177	405.41	181.39	-1.16	1.53E-14	1.19E-11	+	-
Olfml3	chr3:103735393-103738001	14	6.3	-1.15	8.99E-09	2.14E-06	-	-
Apoc1	chr7:19689480-19692658	30.41	14.03	-1.12	4.29E-05	3.10E-03	-	-
Man2a2	chr7:80349096-80371375	14.1	6.5	-1.12	4.22E-14	3.07E-11	-	-
Spg11	chr2:122028582-122118386	8.82	4.1	-1.1	2.39E-08	4.97E-06	-	+
Stard13	chr5:151037514-151190193	1.52	0.71	-1.1	4.01E-04	1.99E-02	-	-
Gm11710	chr11:115031485-115037769	23.93	11.13	-1.1	8.57E-07	1.07E-04	-	-
C1qa	chr4:136895915-136898844	324.73	152.9	-1.09	2.27E-13	1.26E-10	+	-
Sepp1	chr15:3270766-3280508	139.37	66.18	-1.07	1.47E-12	6.60E-10	-	-
Aif1	chr17:35170991-35176001	20.99	10.02	-1.07	9.23E-07	1.13E-04	+	-
Enpp1	chr10:24641410-24712102	5.7	2.74	-1.06	3.17E-07	4.67E-05	-	-
Fcgr4	chr1:171018925-171029761	4.7	2.26	-1.05	8.21E-04	3.53E-02	+	-
Apcdd1	chr18:62922326-62953195	4.55	2.2	-1.05	7.79E-06	7.60E-04	-	-
Rnf150	chr8:82863355-83091271	2.58	1.27	-1.03	4.74E-08	8.36E-06	-	-
Gm11710	chr11:115020727-115027012	7.8	3.82	-1.03	6.09E-04	2.85E-02	-	-
Tmem37	chr1:120067376-120073780	54.21	27.01	-1.01	1.04E-09	2.95E-07	-	-
Apoc2	chr7:19671578-19676864	76.59	38.56	-0.99	1.20E-08	2.73E-06	-	-
Cd300lh	chr11:115042130-115048295	24.25	12.33	-0.98	7.95E-06	7.64E-04	-	-
Ms4a7	chr19:11321405-11336116	60.5	30.74	-0.98	5.87E-08	9.91E-06	-	-
Siglec1	chr2:131069219-131086765	7.72	3.95	-0.97	2.03E-09	5.24E-07	-	-
Ccr5	chr9:124121542-124127183	31.57	16.11	-0.97	5.44E-11	1.86E-08	+	-
Arhgap15	chr2:43748823-44387623	4.98	2.57	-0.95	2.39E-05	1.92E-03	+	-
Lgals1	chr15:78926724-78930465	52.22	27.08	-0.95	3.51E-08	6.81E-06	+	-
Zfyve19	chr2:119172499-119217050	10.5	5.47	-0.94	8.84E-06	8.04E-04	-	+
Lgmn	chr12:102394097-102439697	325.24	170.66	-0.93	8.13E-09	1.97E-06	-	-
Egr1	chr18:34861206-34864956	3.5	1.83	-0.93	1.28E-04	7.78E-03	+	-
Fos	chr12:85473900-85477270	9.36	4.99	-0.91	6.93E-06	7.02E-04	+	-
Eif2ak4	chr2:118388616-118475234	7.03	3.86	-0.86	6.65E-07	8.50E-05	-	+
BC055004	chr5:138225903-138251875	5.34	2.96	-0.85	2.13E-04	1.19E-02	-	-

C530028O21Rik	chr6:124996719-125003097	9.76	5.46	-0.84	1.45E-04	8.60E-03	-	-
Sorl1	chr9:41968488-42124289	2.01	1.13	-0.83	1.24E-04	7.65E-03	-	-
Enc1	chr13:97241104-97253040	10.23	5.76	-0.83	1.82E-07	2.82E-05	-	-
Thbd	chr2:148404470-148408188	12.48	7.05	-0.82	3.16E-07	4.67E-05	-	-
Fam125b	chr2:33729955-33887946	10.54	6.07	-0.79	3.56E-07	5.05E-05	-	-
Igfbp4	chr11:99041259-99052643	9.82	5.7	-0.79	7.61E-05	4.97E-03	-	-
Fam105a	chr15:27655070-27681542	11.69	6.77	-0.79	1.32E-05	1.14E-03	-	-
Fabp4	chr3:10204342-10208576	380.32	221.92	-0.78	4.69E-08	8.36E-06	-	-
Dock4	chr12:40446052-40846488	5.59	3.25	-0.78	9.36E-07	1.13E-04	-	-
Stab1	chr14:31134852-31168641	25.8	15.06	-0.78	1.10E-07	1.77E-05	+	-
Fcgr1	chr3:96282908-96293969	17.19	10.12	-0.76	2.15E-06	2.48E-04	+	-
Klra2	chr6:131219234-131247362	15.11	8.9	-0.76	3.31E-05	2.46E-03	-	-
Daglb	chr5:143464492-143504442	23.16	13.85	-0.74	5.73E-07	7.66E-05	-	-
Rasgrp3	chr17:75435904-75529053	10.9	6.51	-0.74	2.65E-05	2.07E-03	+	-
Pld4	chr12:112760654-112768986	51.58	31.02	-0.73	3.41E-07	4.89E-05	+	-
Ms4a6c	chr19:11469367-11482196	80.23	49.42	-0.7	2.63E-05	2.07E-03	-	-
Sh3bgrl2	chr9:83548337-83600291	9.41	5.81	-0.69	4.81E-05	3.40E-03	-	-
Malat1	chr19:5795689-5802671	124.79	77.55	-0.69	9.25E-04	3.85E-02	-	-
Zfp395	chr14:65358675-65398930	6.12	3.82	-0.68	1.69E-04	9.85E-03	-	-
Mafb	chr2:160363676-160367065	107.2	67.27	-0.67	6.93E-06	7.02E-04	+	-
Hgf	chr5:16553549-16619439	7.8	4.88	-0.67	3.83E-04	1.92E-02	+	-
Mtus1	chr8:40990911-41133726	36.97	23.21	-0.67	3.81E-06	4.14E-04	-	-
Abcc3	chr11:94343294-94392976	13.59	8.55	-0.67	7.05E-06	7.08E-04	-	-
Gpcpd1	chr2:132529082-132578248	20.04	12.71	-0.66	3.63E-05	2.67E-03	-	-
Fabp5	chr3:10012605-10016610	329.2	207.78	-0.66	4.30E-06	4.47E-04	-	-
Engase	chr11:118476959-118489198	23.36	14.74	-0.66	3.66E-06	4.01E-04	-	-
Arg1	chr10:24915206-24927470	321.13	204.41	-0.65	1.17E-04	7.34E-03	+	-
Zdhhc14	chr17:5492599-5753891	6.52	4.16	-0.65	8.07E-04	3.50E-02	-	-
Zranb3	chr1:127954185-128102408	5.04	3.24	-0.63	6.94E-04	3.13E-02	-	-
Fry	chr5:150259929-150497753	4.46	2.88	-0.63	5.10E-05	3.57E-03	-	-
Iqgap2	chr13:95627176-95891922	28.48	18.37	-0.63	1.35E-05	1.16E-03	-	-
Cd244	chr1:171559192-171585316	5.69	3.7	-0.62	1.04E-03	4.17E-02	-	-
Frmd4b	chr6:97286866-97617657	12.44	8.11	-0.62	3.18E-05	2.39E-03	-	-
Lair1	chr7:4007072-4063204	9.79	6.37	-0.62	3.00E-04	1.57E-02	-	-
Maf	chr8:115703252-115706894	6.89	4.48	-0.62	6.60E-04	3.02E-02	+	-
Sgsh	chr11:119314786-119355510	7.99	5.2	-0.62	2.03E-04	1.14E-02	-	-

Rassf2	chr2:131992849-132029988	38.85	25.54	-0.61	1.84E-05	1.53E-03	-	-
Clec12a	chr6:129350243-129365303	16.78	10.96	-0.61	2.03E-04	1.14E-02	-	-
Mr1	chr1:155127877-155146780	9.38	6.18	-0.6	1.04E-03	4.17E-02	-	-
Usp35	chr7:97309379-97325964	6.56	4.31	-0.6	7.55E-04	3.35E-02	-	-
Ssh2	chr11:77216424-77460219	20.58	13.61	-0.6	2.51E-05	2.00E-03	-	-
Epas1	chr17:86753863-86833410	10.55	6.95	-0.6	6.78E-05	4.49E-03	-	-
Kif13b	chr14:64652530-64806296	11.4	7.58	-0.59	6.46E-05	4.32E-03	-	-
Dhrs3	chr4:144892826-144927645	90.01	60.34	-0.58	5.25E-05	3.66E-03	-	-
Per3	chr4:151003654-151044622	5.15	3.47	-0.57	8.23E-04	3.53E-02	-	-
Tmem176b	chr6:48833811-48841374	104.29	70.41	-0.57	2.63E-04	1.40E-02	-	-
Ccl6	chr11:83582060-83623693	193.94	130.83	-0.57	1.15E-04	7.27E-03	-	-
Bcl6	chr16:23965051-23988612	9.79	6.6	-0.57	8.01E-04	3.49E-02	-	-
Dock10	chr1:80501072-80758553	10.38	7.08	-0.55	1.22E-04	7.63E-03	-	-
C3ar1	chr6:122847139-122856157	134.63	91.83	-0.55	6.86E-04	3.11E-02	-	-
Abca9	chr11:110100821-110168153	22.04	15.03	-0.55	8.29E-05	5.39E-03	-	-
Gpr65	chr12:98268656-98276632	24.49	16.72	-0.55	3.98E-04	1.99E-02	-	-
Abhd12	chr2:150832514-150904731	146.07	100.78	-0.54	2.21E-04	1.22E-02	-	-
Plxnc1	chr10:94790865-94944578	10.01	6.86	-0.54	1.84E-04	1.05E-02	-	-
Nav1	chr1:135434579-135585355	8.4	5.82	-0.53	1.72E-04	9.87E-03	+	-
Adam8	chr7:139978940-139992488	88.42	61.22	-0.53	2.67E-04	1.42E-02	-	-
Sesn1	chr10:41810573-41908436	30.62	21.26	-0.53	6.15E-04	2.86E-02	-	-
Mctp1	chr13:76384960-77031810	9.16	6.35	-0.53	1.04E-03	4.17E-02	-	-
Ldlrad3	chr2:101950200-102186377	15.15	10.6	-0.52	6.08E-04	2.85E-02	-	-
Ptplad2	chr4:88412929-88438926	23.24	16.17	-0.52	7.98E-04	3.49E-02	-	-
Tef	chr15:81802672-81826863	32.45	22.67	-0.52	2.90E-04	1.53E-02	-	-
Slc37a2	chr9:37229148-37255738	16.55	11.59	-0.51	4.45E-04	2.18E-02	-	-
Fasn	chr11:120805957-120824547	14.35	10.05	-0.51	2.59E-04	1.39E-02	-	-
Itgb5	chr16:33829664-33949338	76.42	53.67	-0.51	4.20E-04	2.06E-02	+	-
Nceh1	chr3:27183003-27244911	36.08	25.44	-0.5	3.35E-04	1.72E-02	-	-
Atp8a1	chr5:67618140-67847431	7.14	5.03	-0.5	8.69E-04	3.68E-02	-	-
Trpm2	chr10:77907721-77969872	6.93	4.9	-0.5	1.08E-03	4.27E-02	-	-
Chd3	chr11:69344350-69369391	15.37	10.84	-0.5	3.65E-04	1.85E-02	-	-
Vps13c	chr9:67840395-67995634	18.84	13.42	-0.49	6.47E-04	3.00E-02	-	-
Nuak1	chr10:84371318-84440471	11.18	7.97	-0.49	1.14E-03	4.45E-02	-	-
Ttyh3	chr5:140620577-140649031	37.81	27.35	-0.47	9.03E-04	3.78E-02	-	-
Slc36a1	chr11:55204339-55236330	25.92	18.69	-0.47	7.67E-04	3.38E-02	-	-

Abcd2	chr15:91145870-91191807	21.2	15.26	-0.47	7.23E-04	3.22E-02	-	-
Rftn1	chr17:49993306-50190497	44.91	32.69	-0.46	1.09E-03	4.30E-02	-	-
Zdhhc18	chr4:133606991-133633429	23.83	32.75	0.46	1.16E-03	4.52E-02	-	-
Zyx	chr6:42349827-42358395	63.95	88.08	0.46	1.12E-03	4.41E-02	-	-
Met	chr6:17463956-17573980	8.41	11.62	0.47	1.29E-03	4.96E-02	-	-
Slfn4	chr11:83175185-83190216	14.27	19.84	0.47	9.49E-04	3.91E-02	-	-
Gpr84	chr15:103308234-103310438	58.68	81.13	0.47	8.53E-04	3.64E-02	-	-
B430306N03Rik	chr17:48316161-48326511	22.73	31.38	0.47	8.85E-04	3.72E-02	-	-
Slc2a6	chr2:27021364-27027998	32.1	44.68	0.48	8.51E-04	3.64E-02	-	-
Golim4	chr3:75876383-75956831	16.1	22.38	0.48	7.01E-04	3.15E-02	-	-
Oasl2	chr5:114896933-114912245	14.23	19.91	0.48	1.04E-03	4.17E-02	-	-
H2-Aa	chr17:34282750-34287771	59.85	83.2	0.48	9.30E-04	3.85E-02	+	-
Filip1l	chr16:57301999-57606867	13.4	18.78	0.49	1.05E-03	4.17E-02	-	-
Nfkb2	chr19:46304736-46327156	41.11	57.81	0.49	1.02E-03	4.14E-02	-	-
Sod2	chr17:13007838-13018119	100.16	143.55	0.52	8.78E-04	3.70E-02	+	-
Cd274	chr19:29367437-29388094	53.76	76.83	0.52	3.16E-04	1.64E-02	-	-
Vsig4	chrX:96247202-96293438	41.88	59.95	0.52	3.55E-04	1.80E-02	-	-
Smpdl3b	chr4:132732965-132757171	33.27	48.05	0.53	1.88E-04	1.06E-02	-	-
Ampd3	chr7:110772603-110812395	66.32	95.89	0.53	3.54E-04	1.80E-02	-	-
Panx1	chr9:15005784-15045478	12.36	17.82	0.53	1.28E-03	4.95E-02	-	-
Prkar2b	chr12:31958478-32061279	25.5	36.91	0.53	1.33E-04	7.98E-03	-	-
Ephx1	chr1:180989555-181017495	106.75	155.25	0.54	1.68E-04	9.83E-03	-	-
Spp1	chr5:104435110-104441053	154.37	224.33	0.54	6.76E-04	3.07E-02	+	-
Rpl23	chr11:97777525-97782439	36.59	53.03	0.54	5.67E-04	2.68E-02	-	-
Id2	chr12:25093798-25096092	61.57	89.63	0.54	1.11E-04	7.03E-03	-	-
H2-Q4	chr17:35379616-35384674	65.04	94.87	0.54	9.06E-05	5.82E-03	+	-
Fpr1	chr17:17876470-17883939	38.8	56.46	0.54	2.23E-04	1.22E-02	+	-
Ptgr1	chr4:58965589-58987078	51.38	75.38	0.55	8.56E-05	5.54E-03	-	-
Ppfibp2	chr7:107595050-107758032	16.67	24.39	0.55	5.15E-04	2.46E-02	-	-
Egr2	chr10:67537868-67542188	62.34	91.31	0.55	1.27E-04	7.77E-03	+	-
Gbp6	chr5:105270701-105293699	6.33	9.31	0.56	4.73E-04	2.28E-02	+	-
Tln2	chr9:67217084-67559703	2.63	3.88	0.56	2.60E-04	1.39E-02	-	-
Rai14	chr15:10568977-10714631	23.72	35.28	0.57	3.95E-05	2.89E-03	-	-
Rpl7a	chr2:26910806-26913311	50.23	74.88	0.58	2.39E-04	1.29E-02	-	-
Dnajc10	chr2:80315465-80354055	74.19	110.68	0.58	1.42E-04	8.45E-03	-	-
Efnb2	chr8:8617438-8660773	15.15	22.58	0.58	4.48E-05	3.22E-03	-	-

Phldb1	chr9:44686307-44735198	9.39	14.03	0.58	5.46E-05	3.76E-03	-	-
Serpinb9	chr13:33004540-33017955	16.73	25.02	0.58	4.66E-05	3.33E-03	-	-
Pfkp	chr13:6548156-6648724	22.54	33.61	0.58	6.59E-04	3.02E-02	-	-
Slc23a2	chr2:132052495-132145108	23.19	34.9	0.59	2.71E-05	2.10E-03	-	-
5730494N06Rik	chr2:132239491-132247788	19.39	29.1	0.59	9.23E-04	3.85E-02	-	-
Icam1	chr9:21015959-21028796	38.47	57.88	0.59	2.29E-05	1.87E-03	+	-
Procr	chr2:155751216-155755478	127.52	192.71	0.6	2.99E-05	2.27E-03	-	-
Bcam	chr7:19756137-19770532	6.68	10.15	0.6	1.01E-03	4.11E-02	-	-
Src	chr2:157424292-157471838	6.92	10.58	0.61	1.23E-04	7.63E-03	+	-
Tnfaip3	chr10:19000909-19015410	21.69	33.39	0.62	1.68E-05	1.41E-03	-	-
Tpm4	chr8:72135291-72153129	171.12	264.81	0.63	5.57E-05	3.79E-03	-	-
Abcc4	chr14:118482691-118706219	14.28	22.09	0.63	7.83E-06	7.60E-04	-	-
Pcx	chr19:4510471-4621752	7.35	11.37	0.63	6.41E-05	4.31E-03	-	-
Rpl36a	chrX:134585653-134588062	43.1	66.61	0.63	1.08E-03	4.27E-02	-	-
Gpr35	chr1:92973118-92986391	17	26.56	0.64	4.82E-05	3.40E-03	-	-
1500003O03Rik	chr2:119547706-119587022	51.69	80.75	0.64	4.05E-06	4.36E-04	-	-
Gss	chr2:155563182-155592706	21.04	32.89	0.64	1.63E-05	1.38E-03	-	-
Car6	chr4:150187015-150201135	16.12	25.05	0.64	1.80E-04	1.03E-02	-	-
Rps12	chr10:23785182-23787209	60.69	94.26	0.64	2.42E-04	1.31E-02	-	-
Angptl2	chr2:33136972-33371478	11.27	17.67	0.65	2.63E-05	2.07E-03	-	-
Niacr1	chr5:123863569-123865516	6.17	9.7	0.65	1.02E-03	4.14E-02	-	-
Bcl2a1d	chr9:88723287-88731850	23.6	37.06	0.65	3.32E-04	1.71E-02	-	-
Dcbld2	chr16:58408534-58469745	3.71	5.82	0.65	6.08E-05	4.12E-03	-	-
Vmn2r26	chr6:124024757-124062035	9.25	14.57	0.66	6.90E-05	4.54E-03	-	-
Adora2a	chr10:75316942-75334788	9.36	14.79	0.66	6.65E-05	4.42E-03	+	-
Fpr2	chr17:17887823-17893952	31.46	49.64	0.66	1.24E-05	1.11E-03	+	-
Psma5	chr3:108256925-108279952	8.56	13.75	0.68	1.30E-03	4.96E-02	-	-
Rassf4	chr6:116633007-116673836	83.89	134.06	0.68	1.23E-04	7.63E-03	-	-
Dusp16	chr6:134715472-134792628	5.56	8.89	0.68	5.47E-05	3.76E-03	-	-
Chn2	chr6:54039931-54430221	7.18	11.69	0.7	4.97E-04	2.38E-02	-	-
Olr1	chr6:129485246-129507165	85.3	138.84	0.7	4.10E-06	4.37E-04	+	-
Slc7a2	chr8:40862366-40922070	86.04	140.17	0.7	1.46E-04	8.61E-03	-	-
Ahrr	chr13:74211117-74292309	5.68	9.2	0.7	1.31E-05	1.14E-03	+	-
Alas1	chr9:106233454-106247954	194.52	317.73	0.71	4.12E-05	3.00E-03	-	-
Dnmt3l	chr10:78030030-78063615	5.47	8.97	0.71	8.59E-04	3.65E-02	-	-
Slc22a23	chr13:34179157-34345182	1.53	2.49	0.71	6.62E-04	3.02E-02	-	-

Ets2	chr16:95702406-95721049	15.25	24.99	0.71	6.11E-07	8.08E-05	-	-
H2-Ab1	chr17:34263226-34269418	69.92	114.49	0.71	4.33E-07	6.07E-05	+	-
Gstm2	chr3:107981701-107986436	10.48	17.3	0.72	4.56E-04	2.21E-02	-	-
Slc28a2	chr2:122426476-122461130	2.33	3.88	0.73	4.63E-04	2.24E-02	-	+
Srxn1	chr2:152105729-152111353	226.13	374.61	0.73	2.93E-05	2.24E-03	-	-
Akr1b8	chr6:34354163-34368454	18.03	29.95	0.73	8.60E-06	7.94E-04	-	-
Ppip5k1	chr2:121289601-121351013	3.88	6.49	0.74	2.35E-05	1.90E-03	-	+
F3	chr3:121723536-121735052	6.42	10.69	0.74	1.71E-04	9.86E-03	-	-
A530064D06Rik	chr17:48151895-48167257	18.11	30.27	0.74	3.23E-06	3.58E-04	-	-
Cyp1b1	chr17:79706952-79715041	10.5	17.5	0.74	6.38E-07	8.25E-05	+	-
Nfkbie	chr17:45555715-45563168	17.82	29.92	0.75	3.28E-07	4.77E-05	-	-
Ralgds	chr2:28513166-28553082	8.69	14.72	0.76	8.47E-06	7.88E-04	+	-
Cxcl14	chr13:56288642-56296551	63.47	107.74	0.76	5.62E-08	9.62E-06	-	-
Rpl12	chr2:32961711-32964045	16.87	28.82	0.77	3.67E-04	1.85E-02	-	-
Ppap2b	chr4:105157346-105232767	5.04	8.58	0.77	1.85E-05	1.53E-03	-	-
Ripk3	chr14:55784994-55788857	9.73	16.68	0.78	1.24E-05	1.11E-03	-	-
Rpl24	chr16:55966274-55971437	36.44	62.4	0.78	7.56E-06	7.46E-04	-	-
Plcb2	chr2:118707516-118728438	4.17	7.21	0.79	1.48E-06	1.74E-04	-	+
Cd53	chr3:106758860-106790149	233.15	402.03	0.79	1.48E-05	1.26E-03	-	-
Nqo1	chr8:107388224-107403205	71.95	124.92	0.8	1.48E-08	3.25E-06	-	-
Epha4	chr1:77367184-77515088	2.91	5.1	0.81	2.38E-06	2.69E-04	-	-
Dnm1	chr2:32308470-32353304	1.52	2.67	0.81	9.55E-04	3.93E-02	-	+
Vcan	chr13:89655309-89742512	2.54	4.45	0.81	5.55E-05	3.79E-03	-	-
Slc6a9	chr4:117835257-117872470	13.95	24.71	0.82	1.51E-08	3.25E-06	-	-
Socs2	chr10:95411489-95416857	6.58	11.66	0.82	1.26E-05	1.11E-03	-	-
Ltc4s	chr11:50236471-50238471	19.16	33.78	0.82	2.25E-04	1.23E-02	-	-
Pdgfb	chr15:79995875-80014808	14.97	26.5	0.82	2.08E-08	4.40E-06	-	-
Rcan1	chr16:92391952-92466146	28.14	49.59	0.82	4.14E-08	7.77E-06	-	-
Ifi205	chr1:174011997-174031755	3.27	5.82	0.83	8.10E-04	3.51E-02	-	-
Ly6i	chr15:74979811-74983430	11.27	20.06	0.83	1.30E-04	7.86E-03	-	-
Ass1	chr2:31470269-31520670	33.97	60.68	0.84	5.05E-07	6.91E-05	-	-
Rps27	chr3:90212666-90213648	54.11	96.93	0.84	2.19E-04	1.21E-02	-	-
1810029B16Rik	chr8:66476345-66486507	33.27	59.54	0.84	3.21E-08	6.44E-06	-	-
H2-Q8	chr17:35394098-35395632	8.01	14.31	0.84	1.05E-04	6.68E-03	+	-
Ptges	chr2:30889470-30903297	34.17	61.47	0.85	1.79E-09	4.74E-07	-	-
Bcl2a1a	chr9:88956919-88962416	25.95	46.93	0.85	9.16E-07	1.13E-04	-	-

Chst11	chr10:82985496-83195891	6.36	11.52	0.86	1.02E-08	2.36E-06	-	-
Gpr132	chr12:112850875-112860916	5.05	9.19	0.86	7.23E-06	7.19E-04	-	-
Susd2	chr10:75636618-75644008	1.43	2.61	0.87	1.15E-03	4.49E-02	-	-
Unc5b	chr10:60762594-60831581	4.08	7.52	0.88	3.42E-08	6.75E-06	-	-
Maff	chr15:79347677-79359076	2.77	5.11	0.88	7.08E-04	3.17E-02	-	-
Tmem119	chr5:113793728-113800352	6.4	11.84	0.89	2.34E-06	2.67E-04	-	-
Treml4	chr17:48264294-48275358	4.28	7.91	0.89	6.55E-04	3.02E-02	-	-
Malt1	chr18:65430996-65478792	13.06	24.17	0.89	5.32E-10	1.59E-07	+	-
Cxcl2	chr5:90903898-90905938	23.05	42.88	0.9	4.65E-08	8.36E-06	+	-
Igf2bp1,Mir3063	chr11:95957163-96005944	0.76	1.41	0.9	1.28E-04	7.78E-03	-	-
Tnfsf4	chr1:161395437-161418206	11.53	21.78	0.92	1.24E-07	1.94E-05	-	-
Cish	chr9:107296688-107301961	4.15	7.87	0.92	1.30E-05	1.14E-03	-	-
Nckap1	chr2:80501294-80580965	1.31	2.49	0.93	4.03E-04	2.00E-02	-	-
Clec5a	chr6:40529090-40910666	31.79	60.8	0.94	3.82E-11	1.35E-08	-	-
Hspa1a	chr17:34969358-34972156	1.93	3.69	0.94	1.67E-04	9.81E-03	-	-
Pf4	chr5:90772434-90773383	600.2	1159.14	0.95	1.55E-09	4.18E-07	+	-
Gbp2	chr3:142620662-142638008	22.24	43.92	0.98	4.25E-12	1.70E-09	-	-
Dcstamp	chr15:39745931-39760934	4.93	9.74	0.98	2.00E-06	2.33E-04	-	-
Chac1	chr2:119351241-119354327	4.96	9.88	0.99	8.08E-06	7.66E-04	-	+
H2-Q7	chr17:35439154-35443773	58.39	116.36	0.99	7.50E-10	2.18E-07	+	-
Gpr68	chr12:100876681-100908198	7.64	15.24	1	4.35E-08	8.03E-06	-	-
Il1a	chr2:129297369-129309972	19.27	39.18	1.02	6.01E-12	2.33E-09	+	-
Layn	chr9:51056779-51077094	10.93	22.12	1.02	1.37E-09	3.79E-07	-	-
Rasgrp1	chr2:117279992-117342877	0.46	0.94	1.04	1.23E-03	4.76E-02	-	-
Irg1	chr14:103047011-103056573	43.81	92.61	1.08	1.24E-14	1.03E-11	-	-
Il1b	chr2:129364579-129375733	25.65	54.76	1.09	5.89E-13	2.86E-10	+	-
Nnt	chr13:119334316-119409138	8.59	18.32	1.09	6.66E-13	3.10E-10	+	-
H2-Q6	chr17:35424876-35428361	32.54	69.21	1.09	2.29E-12	9.86E-10	+	-
A130040M12Rik	chr13:68233964-68450346	0.85	1.82	1.1	3.28E-04	1.69E-02	-	-
Heph	chrX:96455435-96574484	6.08	13.13	1.11	3.44E-11	1.25E-08	-	-
Csf1	chr3:107741047-107760469	21.98	48.32	1.14	1.75E-13	1.07E-10	+	-
Il20rb	chr9:100457718-100486473	4.52	9.97	1.14	3.12E-09	7.89E-07	-	-
Clec4e	chr6:123281788-123289871	224.77	506.54	1.17	9.20E-11	3.06E-08	-	-
Hspa1b	chr17:34956428-34959238	1.85	4.15	1.17	2.55E-06	2.85E-04	-	-
Adora2b	chr11:62248983-62266452	1.99	4.53	1.18	2.82E-05	2.17E-03	-	-
Serpinb1a	chr13:32842091-32851185	10.6	24.52	1.21	3.18E-13	1.61E-10	-	-

Plcb1	chr2:134786163-135475258	0.92	2.15	1.22	9.88E-08	1.62E-05	-	-
Traf1	chr2:34943257-34961772	2.41	5.65	1.23	1.99E-07	3.05E-05	-	+
Il1rn	chr2:24336859-24351491	23.96	56.97	1.25	0.00E+00	0.00E+00	+	-
Amotl1	chr9:14541966-14615000	0.49	1.17	1.26	8.58E-07	1.07E-04	-	-
Cdc42ep2	chr19:5917555-5924816	2.45	5.86	1.26	8.14E-06	7.66E-04	-	-
Flrt3	chr2:140395429-142390050	4.36	10.49	1.27	2.38E-12	9.89E-10	-	-
Abcb4	chr5:8893720-8959226	0.84	2.05	1.28	4.30E-06	4.47E-04	-	-
Dynlt1a	chr17:6310544-6317474	2.49	6.06	1.29	4.49E-04	2.19E-02	-	-
Nfatc4	chr14:55824794-55833943	0.91	2.31	1.34	3.31E-05	2.46E-03	-	-
Cxcl3	chr5:90786102-90788090	66.88	174.46	1.38	0.00E+00	0.00E+00	-	-
Mtap1a	chr2:121289601-121351013	0.32	0.88	1.44	1.70E-04	9.86E-03	-	+
Six1	chr12:73041826-73046712	1.2	3.47	1.53	3.81E-08	7.27E-06	-	-
Col18a1	chr10:77052178-77166530	8.82	26.31	1.58	0.00E+00	0.00E+00	-	-
Gatm	chr2:122594472-122611277	27.46	85.13	1.63	0.00E+00	0.00E+00	-	-
Ccl24	chr5:135569936-135573043	100.51	318.64	1.66	0.00E+00	0.00E+00	-	-
Tmc3	chr7:83584930-83623709	0.23	0.74	1.67	2.30E-05	1.87E-03	-	-
Osmr	chr15:6813576-6874313	0.08	0.24	1.69	1.22E-03	4.72E-02	-	-
Artn	chr4:117926161-117929763	1.51	5.18	1.78	2.28E-10	6.99E-08	-	-
Six4	chr12:73100258-73113245	0.08	0.28	1.78	3.07E-04	1.60E-02	-	-
Ccl22	chr8:94745683-94751388	0.57	2.17	1.94	1.10E-06	1.32E-04	+	-
Thy1	chr9:44043383-44048579	0.14	0.58	2.06	7.58E-04	3.35E-02	-	-
Atp8b1	chr18:64528978-64661000	0.09	0.41	2.27	4.60E-07	6.38E-05	-	-
Dynlt1b	chr17:6430111-6436295	2.89	14.91	2.36	2.08E-13	1.21E-10	-	-
Clu	chr14:65968482-65981545	0.05	0.42	3.14	4.10E-04	2.02E-02	-	-
Exd1	chr2:119519403-119547627	0.06	0.57	3.25	4.83E-08	8.38E-06	-	+
Gchfr	chr2:119167787-119172389	0.13	1.33	3.37	7.97E-04	3.49E-02	-	-
Cd163l1	chr7:140218266-140231145	0.03	0.34	3.58	8.76E-06	8.03E-04	-	-
Tmem181b-ps	chr17:6439001-6450994	0.39	5.6	3.84	0.00E+00	0.00E+00	-	-
Gm14085	chr2:122484940-122528040	0.05	1.04	4.48	1.63E-13	1.06E-10	-	-
Sfrp2	chr3:83766320-83774314	0	1.11	7.79	9.95E-04	4.08E-02	-	-
Erdr1	chrY:90785441-90816465	0.07	21.69	8.32	1.57E-13	1.06E-10	-	-
Rpl31-ps12	chr16:16753015-16829363	0.37	146.86	8.64	0.00E+00	0.00E+00	-	-

Supplementary Table 1. List of 304 differentially expressed genes in pMΦ of B6.129-*Prnp*$^{ZrchI/ZrchI}$ vs. B6.129-*Prnp*$^{wt/wt}$ identified by RNA-Seq.

4.5.2 Supplementary Table 2. Genes containing non-synonymous SNPs between B6.129-*Prnp*$^{Zrchl/Zrchl}$ vs. B6.129-*Prnp*$^{wt/wt}$

The table below lists 132 genes containing non-synonymous SNPs between B6.129-*Prnp*$^{wt/wt}$ and B6.129-*Prnp*$^{Zrchl/Zrchl}$ pMΦ identified by RNA-Seq. The genes are sorted by chromosome location. 62 of these genes (47%) are located on Chr2 and 4 thereof have been implicated in phagocytosis (Fig. 15).

Gene	Locus	FPKM WT	FPKM KO	Log_2-fold change	p-value	q-value	Diff. expr.[§]	Phag.*
Ppfia4	chr1:134296782-134332928	4.27	3.46	-0.30	0.08	0.83	no	no
Cacna1s	chr1:136052900-136119822	0.01	0.01	0.03	0.99	1.00	no	no
Atp1a4	chr1:172223507-172258424	0.00	0.00	0.00	1.00	1.00	no	no
Mgat4a	chr1:37439339-37536259	43.39	42.94	-0.01	0.92	1.00	no	no
A530032D15Rik	chr1:85088138-85109853	0.49	0.45	-0.10	0.83	1.00	no	no
Heatr7b1	chr1:88227019-88277579	0.11	0.08	-0.51	0.67	1.00	no	no
Traf1	chr2:34943257-34961772	2.41	5.65	1.23	1.99E-07	3.05E-05	yes	no
B230118H07Rik	chr2:101560780-101632528	3.39	3.73	0.14	0.57	1.00	no	no
Hipk3, Mir1902	chr2:104426481-104494489	26.64	26.82	0.01	0.94	1.00	no	no
Qser1	chr2:104754796-104816696	4.17	3.73	-0.16	0.30	1.00	no	no
Thbs1	chr2:118111921-118127133	707.41	365.26	-0.95	0.00	0.10	no	yes
Eif2ak4	chr2:118388616-118475234	7.03	3.86	-0.86	6.65E-07	8.50E-05	yes	no
Plcb2	chr2:118707516-118728438	4.17	7.21	0.79	1.48E-06	1.74E-04	yes	no
Bahd1	chr2:118901614-118924524	10.46	10.71	0.03	0.82	1.00	no	no
Chst14	chr2:118926496-118928583	7.12	7.03	-0.02	0.93	1.00	no	no
Rpusd2	chr2:119034789-119042197	1.15	1.09	-0.07	0.78	1.00	no	no
Fam82a2	chr2:119136997-119157034	10.50	12.22	0.22	0.20	1.00	no	no
Zfyve19	chr2:119172499-119217050	10.50	5.47	-0.94	8.84E-06	8.04E-04	yes	no
Chac1	chr2:119351241-119354327	4.96	9.88	0.99	8.08E-06	7.66E-04	yes	no
Exd1	chr2:119519403-119547627	0.06	0.57	3.25	4.83E-08	8.38E-06	yes	no
Ndufaf1	chr2:119655450-119662798	5.66	5.75	0.02	0.93	1.00	no	no
Rtf1	chr2:119675067-119735407	9.52	10.03	0.08	0.61	1.00	no	no
Rpap1	chr2:119763958-119787537	4.26	3.87	-0.14	0.51	1.00	no	no
Tyro3	chr2:119799513-119818103	0.26	0.36	0.46	0.28	1.00	no	yes
Mga	chr2:119897227-	7.33	7.19	-0.03	0.85	1.00	no	no

	119969581							
Mapkbp1	chr2:119972698-120027403	2.70	2.28	-0.24	0.19	1.00	no	no
Ganc	chr2:120355308-120504919	2.61	3.00	0.20	0.50	1.00	no	no
Tmem87a	chr2:120355309-120404116	12.40	17.40	0.49	0.00	0.09	no	no
Zfp106	chr2:120506829-120563831	30.17	29.02	-0.06	0.70	1.00	no	no
Cdan1	chr2:120716153-120731517	3.37	2.83	-0.25	0.16	1.00	no	no
Ttbk2	chr2:120732816-120850584	1.95	2.07	0.09	0.63	1.00	no	no
Ubr1	chr2:120850655-120970715	7.22	6.91	-0.06	0.66	1.00	no	no
Tmem62	chr2:120977061-121007842	9.92	9.71	-0.03	0.85	1.00	no	no
Lcmt2	chr2:121137291-121140698	4.63	3.57	-0.37	0.06	0.72	no	no
Adal	chr2:121142140-121156678	4.12	5.20	0.34	0.12	1.00	no	no
Zscan29	chr2:121157426-121171149	7.73	8.38	0.12	0.42	1.00	no	no
Trp53bp1	chr2:121196727-121271386	6.43	6.16	-0.06	0.76	1.00	no	no
Mtap1a	chr2:121289601-121351013	0.32	0.88	1.44	0.00	0.01	yes	no
Ppip5k1	chr2:121310561-121351013	3.88	6.49	0.74	2.35E-05	1.90E-03	yes	no
Wdr76	chr2:121506722-121544859	1.23	1.56	0.35	0.19	1.00	no	no
Spg11	chr2:122053526-122118386	8.82	4.10	-1.10	2.39E-08	4.97E-06	yes	no
B2m	chr2:122120107-122186189	3019.43	2916.05	-0.05	0.84	1.00	no	no
Slc28a2	chr2:122426476-122461130	2.33	3.88	0.73	0.00	0.02	yes	no
Slc30a4	chr2:122681238-122702663	4.89	4.35	-0.17	0.32	1.00	no	no
Pldn	chr2:122738504-122749487	9.33	11.75	0.33	0.03	0.49	no	no
Sqrdl	chr2:122765358-122809551	94.96	122.34	0.37	0.01	0.24	no	no
Usp8	chr2:126707327-126759314	38.70	36.02	-0.10	0.47	1.00	no	no
2010106G01Rik	chr2:126890394-126933235	60.17	68.69	0.19	0.21	1.00	no	no
Stard7	chr2:127270228-127298934	15.21	14.40	-0.08	0.60	1.00	no	no
Mertk	chr2:128698996-128802188	45.87	44.28	-0.05	0.72	1.00	no	yes
Polr1b	chr2:129100995-129126595	4.97	4.75	-0.06	0.72	1.00	no	no
Ckap2l	chr2:129268209-129297212	0.35	0.37	0.06	0.88	1.00	no	no
Sirpa	chr2:129592838-129632228	356.34	375.60	0.08	0.73	1.00	no	yes
Vps16	chr2:130417683-130444269	14.78	13.95	-0.08	0.63	1.00	no	no
Fam113a	chr2:130417684-130424641	5.37	7.02	0.39	0.14	1.00	no	no
1110034G24Rik	chr2:132690282-132751055	7.69	6.97	-0.14	0.52	1.00	no	no
Trmt6	chr2:132804214-132816054	9.42	8.63	-0.13	0.45	1.00	no	no
Mkks	chr2:136873781-136891406	8.87	8.21	-0.11	0.55	1.00	no	no
Rrbp1	chr2:143947394-144011263	68.09	60.61	-0.17	0.29	1.00	no	no
8430406I07Rik	chr2:144271034-144281229	6.07	2.23	-1.45	1.95E-10	6.29E-08	yes	no
Rin2	chr2:145786115-145887616	62.96	49.07	-0.36	0.01	0.29	no	no

Fam110a	chr2:151969397-151980219	6.05	5.31	-0.19	0.41	1.00	no	no
Slc52a3	chr2:151996510-152009258	0.60	0.87	0.54	0.17	1.00	no	no
Zcchc3	chr2:152411955-152415044	1.78	1.65	-0.11	0.70	1.00	no	no
Rem1	chr2:152627007-152635191	0.69	0.99	0.52	0.23	1.00	no	no
H13	chr2:152669460-152708668	20.03	19.08	-0.07	0.72	1.00	no	no
Prex1	chr2:166566344-166713832	32.51	31.06	-0.07	0.64	1.00	no	no
Gm14393	chr2:175061548-175067763	0.30	0.56	0.89	0.25	1.00	no	no
LOC100038947	chr3:15795146-15848487	8.92	3.65	-1.29	1.19E-07	1.89E-05	yes	no
Srsf11	chr3:158010492-158036639	24.25	24.62	0.02	0.88	1.00	no	no
Pip5k1a	chr3:95059595-95106858	12.33	13.67	0.15	0.35	1.00	no	no
2010305A19Rik	chr4:108328151-108340718	4.13	4.13	0.00	1.00	1.00	no	no
Aldoart1	chr4:72850582-72852634	13.44	14.33	0.09	0.58	1.00	no	no
Gbp11	chr5:105323025-105346472	0.14	0.15	0.10	0.87	1.00	no	no
Fam20c	chr5:138755080-138810063	171.49	194.08	0.18	0.28	1.00	no	no
Smurf1	chr5:144876494-144965830	17.12	18.87	0.14	0.33	1.00	no	no
Fam193a	chr5:34369932-34486458	7.19	7.21	0.00	0.98	1.00	no	no
Igbp1b	chr6:138657091-138658444	0.00	0.00	0.00	1.00	1.00	no	no
4930544G11Rik	chr6:65952570-65954014	0.00	0.00	0.00	1.00	1.00	no	no
4931417E11Rik	chr6:73468572-73469667	0.00	0.00	0.00	1.00	1.00	no	no
Plxna1	chr6:89316313-89362613	38.42	36.78	-0.06	0.68	1.00	no	no
Iqsec1	chr6:90659597-90810123	18.34	16.96	-0.11	0.42	1.00	no	yes
Atp2a1	chr7:126428766-126463073	0.03	0.05	0.88	0.69	1.00	no	no
Btbd1	chr7:81792073-81829431	11.13	12.06	0.12	0.46	1.00	no	no
Fut10	chr8:31187331-31261483	5.00	4.68	-0.10	0.68	1.00	no	no
Sugp1	chr8:70042812-70071953	12.57	11.95	-0.07	0.66	1.00	no	no
Pde4c	chr8:70724063-70751176	0.00	0.01	1.80e+308	0.16	1.00	no	no
Mast1	chr8:84911852-84937353	1.75	1.55	-0.18	0.45	1.00	no	no
Gnat1	chr9:107674473-107679592	0.02	0.02	0.11	0.95	1.00	no	no
Mre11a	chr9:14784706-14834417	4.67	4.49	-0.06	0.77	1.00	no	no
Zfp26	chr9:20428317-20460160	2.42	2.68	0.15	0.36	1.00	no	no
Abcg4	chr9:44273189-44288244	0.03	0.05	0.96	0.30	1.00	no	no
Dmxl2	chr9:54365157-54501626	22.39	23.62	0.08	0.59	1.00	no	no
Gm5136	chr10:108497649-109010975	0.00	0.00	0.00	1.00	1.00	no	no
Ikzf4	chr10:128632414-128645993	0.00	0.00	-0.14	0.95	1.00	no	no
Tcf3	chr10:80409164-80433653	14.79	14.93	0.01	0.93	1.00	no	no
Map2k2	chr10:81105946-81124697	28.87	29.66	0.04	0.79	1.00	no	no
Tubg2	chr11:101155883-101161787	0.03	0.03	0.15	0.92	1.00	no	no

Unk	chr11:116030321-116061194	6.87	6.71	-0.03	0.84	1.00	no	no
Pycr1	chr11:120635711-120643670	0.11	0.08	-0.45	0.49	1.00	no	no
Zrsr1	chr11:22899727-22982284	3.76	3.76	0.00	1.00	1.00	no	no
Cyfip2	chr11:46193848-46312859	1.65	1.69	0.03	0.88	1.00	no	no
Pmp22	chr11:63131509-63159546	104.67	120.81	0.21	0.14	1.00	no	no
Myo1g	chr11:6506547-6520958	28.34	28.85	0.03	0.85	1.00	no	yes
Zkscan6	chr11:65807243-65829239	6.13	6.10	-0.01	0.98	1.00	no	no
Myh13	chr11:67327102-67371502	0.00	0.00	-1.8e+308	0.49	1.00	no	no
Tnfaip1	chr11:78522849-78536260	14.98	14.79	-0.02	0.91	1.00	no	no
Aatf	chr11:84422855-84513501	8.33	8.91	0.10	0.62	1.00	no	no
Prps1l3	chr12:57230411-57457241	9.47	9.91	0.07	0.69	1.00	no	no
Rhob	chr12:8497758-8499985	81.65	79.56	-0.04	0.79	1.00	no	yes
Naip2	chr13:100144062-100202092	80.63	87.08	0.11	0.48	1.00	no	no
Ctsm	chr13:61536443-61541839	0.00	0.00	0.00	1.00	1.00	no	no
Slc12a7	chr13:73763696-73816742	5.93	4.32	-0.46	0.01	0.18	no	no
Nr2f1	chr13:78188972-78236564	0.00	0.00	0.00	1.00	1.00	no	no
Mapk8	chr14:33377898-33447158	2.63	2.92	0.15	0.42	1.00	no	no
Ctsb	chr14:63122461-63177793	1245.17	1117.34	-0.16	0.71	1.00	no	no
Akap11	chr14:78492245-78536860	5.72	5.33	-0.10	0.49	1.00	no	no
Fbxo32	chr15:58175878-58214892	5.90	5.97	0.02	0.91	1.00	no	no
Dnm1l	chr16:16312232-16359030	10.24	10.92	0.09	0.54	1.00	no	no
Senp5	chr16:31959669-32003287	10.18	9.99	-0.03	0.85	1.00	no	no
Tiam1	chr16:89787110-89974699	4.99	6.60	0.40	0.01	0.27	no	yes
Cbr1	chr16:93607836-93610349	22.49	20.07	-0.16	0.36	1.00	no	no
Itpr3	chr17:27057303-27122223	1.51	1.45	-0.06	0.77	1.00	no	yes
H2-T23	chr17:36029977-36032701	123.29	137.29	0.16	0.29	1.00	no	no
H2-Bl	chr17:36080188-36084249	0.12	0.16	0.46	0.60	1.00	no	no
Pabpc6	chr17:9666496-9669704	0.00	0.00	0.00	1.00	1.00	no	no
Gnal	chr18:67088335-67245830	1.09	1.07	-0.03	0.96	1.00	no	no
Cetn1	chr18:9618418-9619469	0.00	0.00	0.00	1.00	1.00	no	no
Tle4	chr19:14448071-14597983	8.14	7.82	-0.06	0.72	1.00	no	no
Pank1	chr19:34810893-34879455	1.47	1.43	-0.04	0.92	1.00	no	no
1700055N04Rik	chr19:3958807-3970438	0.01	0.00	-5.55	0.71	1.00	no	no
Ddx3y	chrY:1260714-1286613	0.00	0.00	0.00	1.00	1.00	no	no

Supplementary Table 2. Genes containing non-synonymous SNPs between B6.129-*Prnp*$^{Zrchl/Zrchl}$ vs. B6.129-*Prnp*$^{wt/wt}$. FPKM, Fragments Per Kilobase of exon per Million fragments

mapped; [§]differentially expressed as in Supplementary Table 1; * involved in phagocytosis, if retrievable records on pubmed.gov using the search terms: “gene xy phagocytosis”, and/or associated terms on geneontology.org, using unfiltered search parameters and considering all recorded species.

5 TRANSPLANTED STROMAL-VASCULAR PDGFRβ+ CELLS DEVELOP INTO FUNCTIONAL FOLLICULAR DENDRITIC CELLS

Parts of this chapter of my thesis are reproduced or adapted from the following manuscript published in *Cell* on July 6th, 2012, issue 150, pages 194-206, with the permission of Elsevier, Rightslink license number 3127281025467:

Follicular dendritic cells emerge from ubiquitous perivascular precursors

Nike Julia Krautler[1,2,*], Veronika Kana[1,*], Jan Kranich[1], Yinghua Tian[3], Dushan Perera[1], Doreen Lemm[1], Petra Schwarz[1], Annika Armulik[1], Jeffrey L. Browning[4], Michelle Tallquist[5], Thorsten Buch[6], José B. Oliveira-Martins[1], Caihong Zhu[1], Mario Hermann[1,7], Ulrich Wagner[8], Robert Brink[2], Mathias Heikenwalder[1], Adriano Aguzzi[1,#]

[1] Institute of Neuropathology, University Hospital of Zurich, 8091 Zurich, Switzerland
[2] Garvan Institute of Medical Research, Darlinghurst, New South Wales, Sydney, 2010 Australia
[3] Division of Visceral and Transplant Surgery, University Hospital Zürich, Zürich, Switzerland
[4] Biogen Idec, Immunobiology, 124 Cambridge Center, Cambridge MA 02142, United States of America
[5] UT Southwestern Medical Center at Dallas, 5323 Harry Hines Blvd, Dallas, Texas 75390-9148, United States of America
[6] Institute of Experimental Immunology, University Hospital of Zurich, 8091 Zurich, Switzerland
[7] Institute of Laboratory Animal Science, University of Zurich, 8091 Zurich, Switzerland
[8] Ludwig Institute for Cancer Research, University of California San Diego, 9500 Gilman Drive, 92093 La Jolla, United States of America
* Equal contribution

[#] Correspondence: Adriano Aguzzi; Institute of Neuropathology, University Hospital of Zurich, Schmelzbergstrasse 12; CH-8091 Zurich, Switzerland, Phone: +41 (44) 255-2107, FAX: +41 (44) 255-4402; email: adriano.aguzzi@usz.ch
http://dx.doi.org/10.1016/j.cell.2012.05.032

5.1 INTRODUCTION

5.1.1 The stromal compartment of lymphoid tissues

The immune system defends the organism against external and internal damage and is traditionally divided into innate and adaptive components. The innate system comprises all cells and molecules that act as a first line defense system. In contrast, the adaptive system counteracts invaders with sophisticated and targeted weapons, which are then stored as immunological memory. In fact, the individual components of these two systems are tightly intertwined and cells with dual characteristics fulfill crucial functions in host defense and lymphoid development (Lanier, 2013; Spits et al., 2013).

A functional immune system is essential in all parts of the organism and therefore, wherever we look, we will find immune cells on duty. To develop an optimal adaptive immune response, the immune system contains specialized compartments known as lymphoid organs. Primary lymphoid organs consist of bone marrow and the thymus, where B cells and T cells, mature from their respective precursors. This maturation process involves complex genetic rearrangements by the recombinase activating gene (RAG) encoded enzymes that lead to the acquisition of functional T and B cell receptors, and negative selection of auto-reactive cells (Kindt et al., 2007; Nishana and Raghavan, 2012). Once B and T cells have reached immunocompetence in the primary lymphoid organs, they migrate to SLO, where they encounter ideal conditions to meet antigen-presenting cells, interact with antigens and mount an adaptive immune response. The heterogeneous SLO form a network throughout the whole body, which filters and monitors body fluids for the presence of pathogens. The main SLO are LNs, spleen, and the MALT. LN occupy strategic positions in the body where they filter lymph, interstitial fluid derived from blood plasma, from the tissue (Girard et al., 2012). The spleen, located intraperitoneally, is the main blood filter of the organism (Mebius and Kraal, 2005),

whereas the mucosal surfaces in respiratory and the digestive tract undergo surveillance by MALT (Kindt et al., 2007). The highly organized microarchitecture of SLO contains distinct areas where B and T cells are concentrated. Resting naïve B cells accumulate in primary follicles, which, upon antigen challenge, become secondary follicles containing germinal centers, where B cells proliferate and undergo affinity maturation (Kindt et al., 2007).

The non-hematopoietic stromal cells contribute to the elaborate choreography of mobile hematopoietic cells in SLO. They not only provide the physical scaffold for the morphology of SLO by creating a meshwork through the whole organ, but also play an active role by secreting a variety of chemokines and adhesion molecules that facilitate communication within SLO, thereby ensuring antigen-delivery to control the entrance and exit of lymphocytes and antigen-presenting cell and to regulate their paths and positioning (Girard et al., 2012; Malhotra et al., 2013; Mueller and Germain, 2009). Recent work has advanced our understanding of the heterogeneity of stromal cells within lymphoid organs and has permitted characterization of single subsets with the use of markers, their specific locations and functions (Katakai, 2012; Katakai et al., 2008; Link et al., 2007; Malhotra et al., 2012; Malhotra et al., 2013). The main characteristics of the different stromal subsets are summarized in Table 10, and Fig. 39 and Fig. 40 show their location within the LN and spleen, respectively.

During embryogenesis, all stromal subsets are thought to derive from a common mesenchymal progenitor, which – upon retinoic acid-mediated activation from neuronal cells – becomes an LTo expressing CXCL13 and subsequently LTβR. Interaction with $LT\alpha\beta_2$-expressing $CD45^+CD4^+CD3^-$ LTi cells leads to upregulation of chemokines and expression and adhesion molecules, which then permit more hematopoietic cells to accumulate (Fig. 41) (Cupedo et al., 2004b; van de Pavert and Mebius, 2010). Similar events can take place in the adult organism upon prolonged inflammatory stimulation in a process called lymphoid neogenesis leading to the development of ectopic TLO, and

the de novo formed lymphoid organs can acquire highly organized architecture and functions as seen in SLO (Aloisi and Pujol-Borrell, 2006; Drayton et al., 2006; Mueller and Germain, 2009; Neyt et al., 2012). TLO are found in various infectious and autoimmune diseases in almost any parts of the body, suggesting that these organs contain LTo-like cells (Cupedo et al., 2004a; Katakai, 2012), but the precise initiating steps are not known so far (Neyt et al., 2012). Treatment regiments used in autoimmune diseases with ectopic lymphoid neogenesis, such as rheumatoid arthritis, include immunomodulatory medicaments that block pathways involved in TLO formation (Manzo et al., 2010). A detailed understanding of TLO development will foster the development of strategies to prevent further de novo TLO formation.

Stromal cell subset	Selected markers	Functions
LEC	gp38^{+}CD31^{+} LYVE1, ICAM1, ICAM2, VCAM1, ER-TR7 antigen, laminin, VE-cadherin, claudin 5, TLRs, CCL21, S1P	Transport of lymph, antigens and cells; facilitation of entry of leukocytes into lymphatics; chemokine production and presentation
FRC	gp38^{+}CD31^{-} ER-TR7 antigen, laminin, desmin, fibrillin, fibronectin, α-SMA, LTβR, TNFR1, TNFR2, ICAM1, VCAM1, collagen I, collagen II, collagen IV, integrin α1, integrin α4, integrin β1, MHC class I, VEGF, PDGFRαβ, CCL21, CCL19, CXCL16 and IL-7	Structural support; production of reticular fibers; formation of conduit network; chemokine production and presentation; substrate for lymphocyte migration; antigen-presenting cell adhesion; T cell homeostasis; antigen presentation
MRC	gp38^{+}CD31^{-} Madcam1, CXCL13, LTβR, ER-TR7 antigen, ICAM1, VCAM1, RANKL, laminin, desmin, 1BL-11 antigen	Structural support; chemokine production; conduit function; possibly adult stromal organizer
FDC	gp38$^{+/-}$CD31^{-} CD16, CD21, CD23, CD32, CD35, C4, ICAM1, VCAM1, Madcam1, laminin, desmin, CXCL12, CXCL13, BAFF, Mfge8	Antigen capture; presentation of immune complexes; chemokine production and presentation; B cell homeostasis
BEC	gp38^{-}CD31^{+} PNAd (in lymph nodes), CD34, VE-cadherin, laminin, JAM-A, JAM-B, JAM-C, ZO1, ZO2, ESAM1, claudin 5, CCL21 (in mice)	Transport of blood; entry of cells from the blood into tissues
IAP	gp38^{-}CD31^{-} integrin α7, calponin1, PDGFRαβ	Contractile pericytes around vessels

Table 10. Stromal cell subsets found in SLO. Location and surface expression of gp38 and CD31, as well as the expression of additional markers is used to divide stromal cells into subclasses. BAFF, B cell activating factor; C4, complement component 4; CCL, CC-chemokine ligand; ESAM1, endothelial cell-specific adhesion molecule 1; IL, interleukin; JAM, junctional adhesion molecule; LYVE1, lymphatic vessel endothelial hyaluronan receptor 1; PNAd, peripheral

node addressin; RANKL, receptor activator of NF-κB ligand; S1P, sphingosine 1-phosphate; TLR, Toll-like receptor; VEGF, vascular endothelial growth factor; ZO, zonula occludens protein. The table is reused from (Mueller and Germain, 2009) with permission from Nature Publishing Group (Rightslink license number: 3125970196683) and adapted using information found in (Katakai, 2012; Katakai et al., 2008; Link et al., 2007; Malhotra et al., 2012; Malhotra et al., 2013).

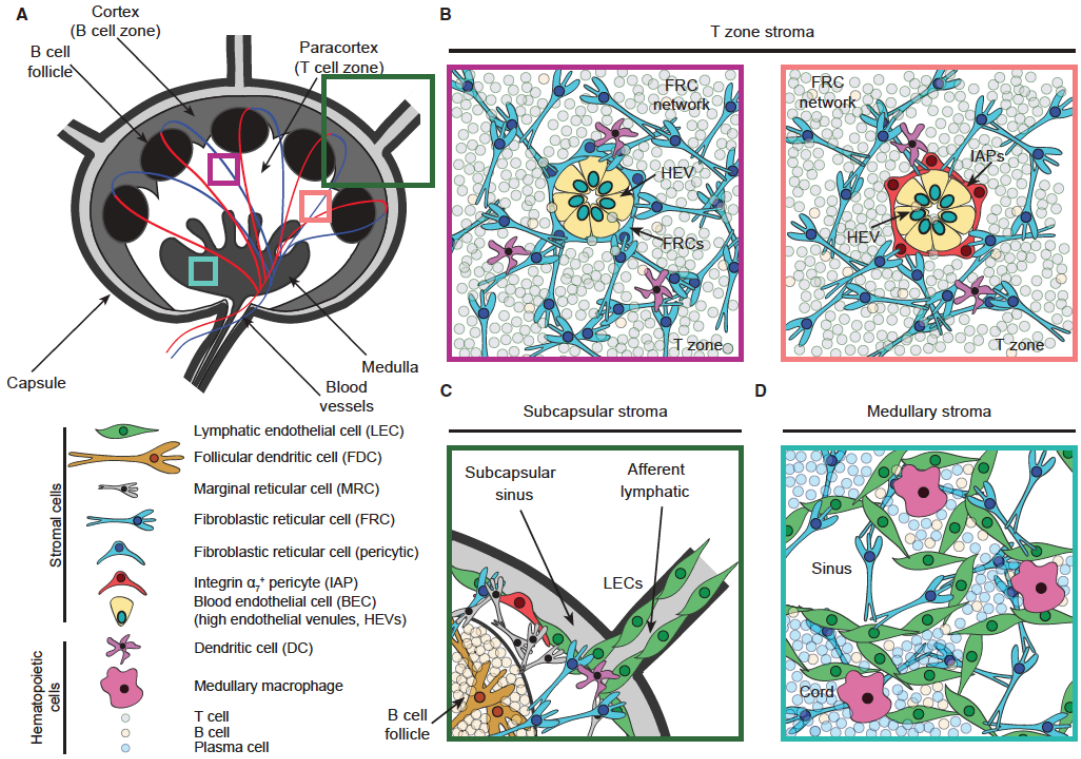

Figure 39. Anatomy of the LN and its stromal cellular subsets. (a) The LN is surrounded by a fibrous capsule and is compartmentalized into cortex (B cell zone with B cell follicles), paracortex (T cell zone) and medulla (plasma cells). (b) Blood vessels enter the LN at the hilus and end in the paracortex and cortex as specialized HEV composed of BEC, which express molecules permitting lymphocytes to enter the LN. Most HEV are surrounded by FRC, few also by contractile IAP. FRC form dense networks, on which lymphocytes and dendritic cells can crawl through the LN and interact. (c) Lymph enters the LN via afferent lymphatic vessels (3 upper endings) into the subscapular sinus that is lined by LEC and contains IAP and MRC, and is filled with macrophages and dendritic cells that capture antigens. Small antigens are also transported via special tubes in FRC conduits inside the LN. In the neighboring cortex, FDC networks embrace B cells in follicles and display antigens. (d) Many antibody secreting plasma cells and macrophages populate the LN medulla and LEC form a dense network, where they control the exit to efferent lymphatic vessels. Figure reprinted from (Malhotra et al., 2013) with permission from John Wiley & Sons A/S. Published by Blackwell Publishing Ltd; Rightslink license number: 3125500373268.

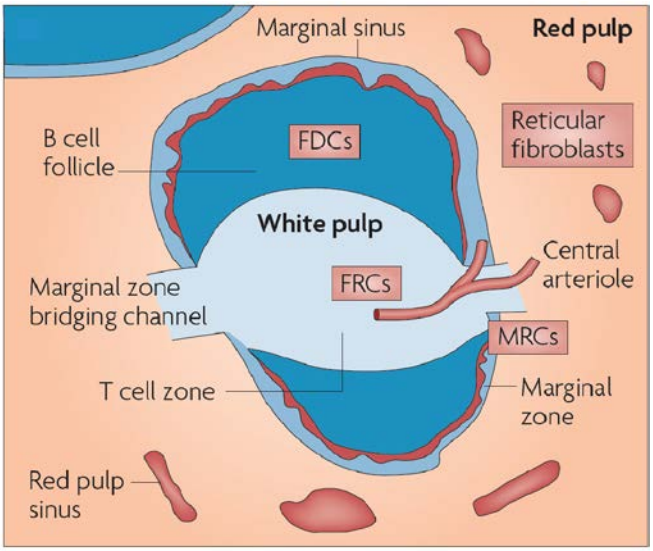

Figure 40. Stromal cell subsets in the spleen. The largest secondary lymphoid organ is specialized in filtering blood-borne antigens. Splenic arteries end in sinusoids in the red pulp, where macrophages phagocytose old erythrocytes. Reticular fibroblasts form the splenic cords within the red pulp and direct blood flow. The splenic white pulp surrounds the arterioles and contains a T cell zone held together by a FRC network (periarteriolar lymphoid sheath) and B cell follicles, which are enmeshed by FDC. The arterioles end in the marginal sinus, which surrounds the white pulp and contains a MRC network, where macrophages and dendritic cells receive blood-borne antigens. Figure adapted and reprinted from (Mueller and Germain, 2009) with permission from Nature Publishing Group, Rightslink license number: 3125950277378.

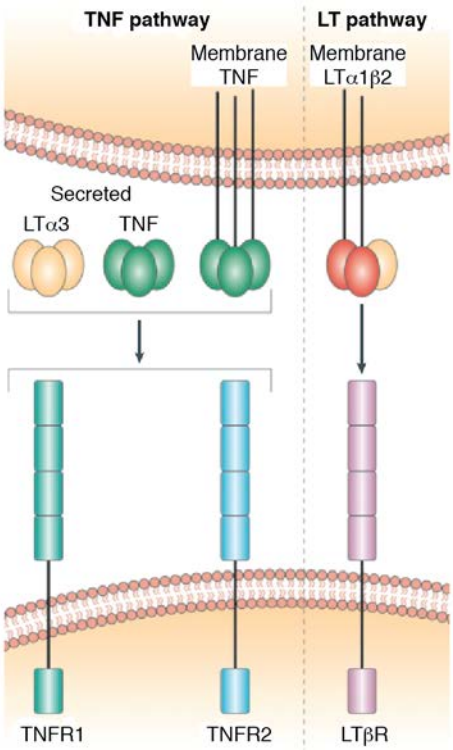

Figure 41. The TNF family: ligands and receptors of the TNF and LT pathways. Secreted $LT\alpha_3$ and TNF or membrane bound bind TNFR1 and TNFR2 and activate the canonical NFκB pathway. Membrane bound $LT\alpha\beta_2$ binds LTβR and activates both canonical and non-canonical NF-κB signaling (Wolf et al., 2010). LTβR and TNFR signaling is essential for lymphoid organ development. Figure reused and adapted from (Gommerman and Browning, 2003) with permission from Nature Publishing Group; Rightslink license number: 3126480151360.

5.1.2 FDC in physiological and pathological conditions

Almost 50 years ago, several researchers published electron microscopic studies of lymphoid follicles, which revealed the presence of highly arborizing cells, whose dendrites were coated with trapped antigens (Mitchell and Abbot, 1965; Szakal and Hanna, 1968). Later, these cells were termed FDC (Klaus et al., 1980; Mandel et al., 1980; Tew et al., 1982), and many subsequent studies have characterized the morphological and functional nature of these elegant cells (Fig. 42) (Aguzzi and Krautler, 2010; Allen and Cyster, 2008; El Shikh and Pitzalis, 2012).

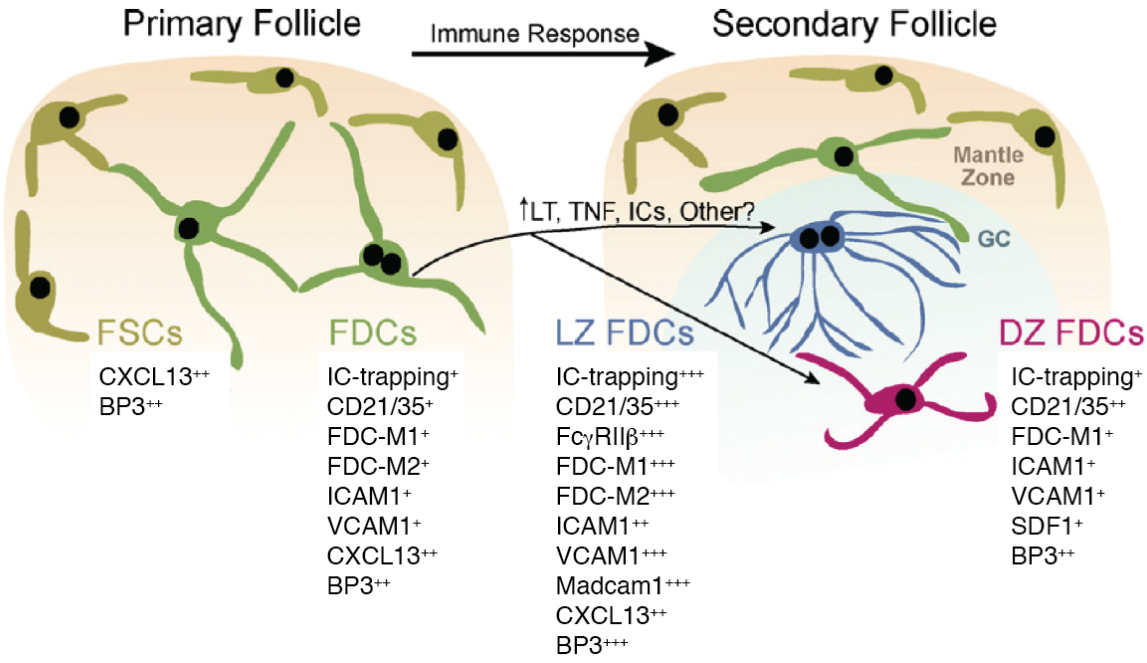

Figure 42. FDC heterogeneity in primary and secondary lymphoid follicles. FDC and follicular stromal cells (FSC, presumably consisting of MRC and IAP, see **Table 10**) are the stromal cells found in B cell follicles. In primary follicles, FDC stain for FDC-M1 antigen (Mfge8 (Kranich et al., 2008)), FDC-M2, CXCL13, BP3, ICAM1, VCAM1; FDC express CD21/35 and show moderate IC trapping. Upon immune activation, FDC in the light zone (LZ) of secondary B cell follicles change morphology and marker profile, and express high amounts of CD21/35 and in addition FcgR2b, which permits them to efficiently trap IC. Dark zone (DZ) FDC show only moderate IC trapping via CD21/35, express SDF1, but not CXCL13, FDC-M2 and Madcam1. Figure reused and adapted from (Allen and Cyster, 2008) with permission from Elsevier Limited, Oxford; Rightslink license number: 3126410594701.

What sets FDC apart from other stromal cells in SLO (Table 10) is their capability to capture and retain antigen-antibody complexes (IC) for prolonged periods of time (Donaldson et al., 1986). The native antigens are presented to naïve B cells in primary follicles, and to B cells in secondary follicles undergoing affinity maturation in GC (Allen and Cyster, 2008). In a process of negative selection, only B cells with high affinity receptors for the displayed antigens are thought to receive survival signals, whereas most B cells undergo apoptosis (McHeyzer-Williams et al., 2012). The apoptotic B cells in GC are then labeled with Mfge8 secreted by FDC, which serves as a bridging molecule for phagocytic TBM (Kranich et al., 2008). The role of the long-lasting IC retention and importance of antigen presentation by FDC in the GC reaction are under debate (Haberman and Shlomchik, 2003; Kosco-Vilbois, 2003). Affinity maturation has been shown to occur also in mice that lack FDC, yet high amounts of antigens or antigen supplied in depots are needed to obtain still suboptimal responses (Allen and Cyster, 2008; Matsumoto et al., 1996; Wu et al., 2000).

FDC capture IC via CR1 (CD35) and CR2 (CD21), and in a complement-independent mechanism via FcγRIIβ (Fig. 42). FDC do not consist of a homogeneous population, since during the transition from a primary to a secondary follicle, they dramatically change morphology, expression profile and IC trapping capability (Fig. 42) (Allen and Cyster, 2008; Yoshida et al., 1993). Two-photon live microscopy has facilitated the detailed investigation of how FDC acquire IC. In LN, IC are formed in the subcapsular sinus and bind to CR3 on subcapsular sinus macrophages, which then pass the IC into naïve B cells. The naïve B cells transport their prey to FDC and transfer the IC onto the CR2 on FDC dendrites (Gonzalez et al., 2011; Phan et al., 2007). A similar relay race takes place in the spleen, where IC-laden marginal zone B cells inexorably shuttle from marginal zone to the follicle, then pass their baton to FDC (Arnon et al., 2013).

As mentioned above, FDC can be found in TLO in various chronic infectious and autoimmune diseases (Stranford and Ruddle, 2012). Besides contributing to the

anatomical scaffold of ectopic follicles, FDC can act as deleterious enhancer of the pathology (El Shikh and Pitzalis, 2012; Neyt et al., 2012). In autoimmune diseases such as rheumatoid arthritis, FDC continuously present auto-antigen to B cells and thereby sustain autoantibody formation. Hence the presence of FDC in ectopic TLO can lead to disease progression and is associated with bad outcome (El Shikh and Pitzalis, 2012; Manzo et al., 2010).

Several pathogens have chosen FDC as their hiding place. In HIV infection, FDC retain virus particles on their surface and thereby act as the major reservoir for the virus (Smith et al., 2001). FDC mediate up-regulation of the HIV co-receptor CXCR4 on $CD4^+$ cells and their continuous presentation of virus IC to $CD4^+$ T cells leads to their infection and to an increase of the viral load (El Shikh and Pitzalis, 2012; Estes et al., 2002; Thacker et al., 2009). Also in the course of prion infection, FDC play a fatal role. Upon peripheral infection with prions, prions accumulate in SLO, long before they continue their journey to the central nervous system (Aguzzi and Zhu, 2012; Fraser and Dickinson, 1970; Glatzel et al., 2003). FDC express high levels of PrP, a prerequisite for disease propagation (Brown et al., 1999; Büeler et al., 1993; Klein et al., 1998). A recent study demonstrated that FDC-specific expression of PrP is sufficient to sustain prion propagation, suggesting that FDC not only serve as prion accumulating cells, but can also actively replicate prions (McCulloch et al., 2011).

5.1.3 Scientific aims

During embryonic lymphoid organ development, all stromal cells of future SLO derive from a mesenchymal precursor (van de Pavert and Mebius, 2010). In adulthood, ectopic lymphoid follicles containing mature FDC can occur almost anywhere in organism (Aloisi and Pujol-Borrell, 2006), suggesting the presence of a ubiquitous precursor. It is well

established that FDC are radiation-resistant stromal cells (Endres et al., 1999); however, the nature of the FDC precursor and the precise steps leading to FDC development in the adult organism remained incompletely understood.

In her PhD thesis, Nike Kräutler substantially expanded our knowledge about the characteristics of putative FDC precursors. In a series of meticulous experiments around the FDC marker Mfge8 (Kranich et al., 2008), she was able to nail down the expression patterns of FDC precursor cells and added a crucial missing piece to the puzzle to clarify the origin of FDC. Specifically, she found the perivascular location of FDC precursors and their expression of PDGFRβ (Kräutler, 2010). In a subsequent Master thesis, Dushan Pereira established the isolation protocol for stromal-vascular derived PDGFRβ$^+$ cells from adipose tissue. He showed that these cells possess FDC-precursor-like properties and that they respond to FDC differentiation factors *in vitro* (Perera, 2010).

Several questions about the perivascular origin of FDC remained unanswered. Experiments using lineage tracing mouse strains could not unequivocally show that mature FDC expressed PDGFRβ$^+$ during development. It was not clear whether the isolation of stromal-vascular derived PDGFRβ$^+$ cells from adipose tissue yield pure cell populations. And most importantly, if PDGFRβ$^+$ cells are transplanted into an environment without mature FDC, but with the presence of differentiation factors, would these cells indeed develop into mature FDC?

Here, I will describe the experiments that led to the proof that mature FDC derive from stromal, perivascular PDGFRβ$^+$ precursors.

5.2 RESULTS

5.2.1 FDC are derived from PDGFRβ$^+$ precursors

Previous experiments have shown that FDC precursors are located perivascularly and that they express the mural cell marker PDGFRβ, a marker undetectable on mature FDC (Kräutler, 2010). Lineage tracing experiments using *Pdgfrb*-Cre mice, crossed to *lacZ* (R26R) Cre-reporter mice expressing beta galactosidase (β-Gal) as a result of Cre-activity ((Foo et al., 2006), showed that indeed β-Gal activity was found in germinal centers containing mature FDC networks (Kräutler, 2010), suggesting that mature FDC express PDGFRβ during their development.

However, the technical process to detect β-Gal activity does not permit additional immunhistochemical stainings and therefore the co-localisation of β-Gal staining with mature FDC markers on consecutive sections was unable to provide sufficient proof. In order to permit immunofluorescent costainings and high-resolution imaging, we crossed *Pdgfrb*-Cre mice with a Cre-inducible fluorescent reporter line (CAG-tdTomato [Ai14]) (Madisen et al., 2010). Using confocal microscopy, we observed strong expression of tdTomato in spleen sections from Cre$^+$ animals (Fig. 43a), but not in spleens from their Cre$^-$ littermates (Fig. 43b). In fact, tdTomato was mainly localized in the vascularized parts of the spleen (red pulp, marginal sinus and central arteriole) (Fig. 43a). Importantly, we found tdTomato positive cells also in the white pulp, especially in areas of Mfge8-positive mature FDC-networks (Fig. 43c).

Ai14 mice show homogeneous cytoplasmatic tdTomato expression (Madisen et al., 2010). In contrast, Mfge8 is a secreted molecule that is detected on the surface of Mfge8-expressing cells and on opsonized apoptotic cells, such as apoptotic B cells in the germinal center of lymphoid follicles. The two signals differ in their localization within

cellular compartments, hence we did not expect to find a precise co-localisation using high-resolution imaging. Accordingly, we found that the cell bodies of Mfge8+ cells show a strong signal surrounded by weak Mfge8-staining. In contrast, the long filiform processes of these cells were strongly Mfge8^{+} and – due to their sparse cytoplasm – less tdTomato^{+} (Fig. 43). Also, we expected dissociation of the Mfge8 and tdTomato signals in areas with densely Mfge8-labeled apoptotic B cells, which would be taken up by TBM, suggesting that a small proportion of Mfge8^{+} cells would be tdTomato^{-}.

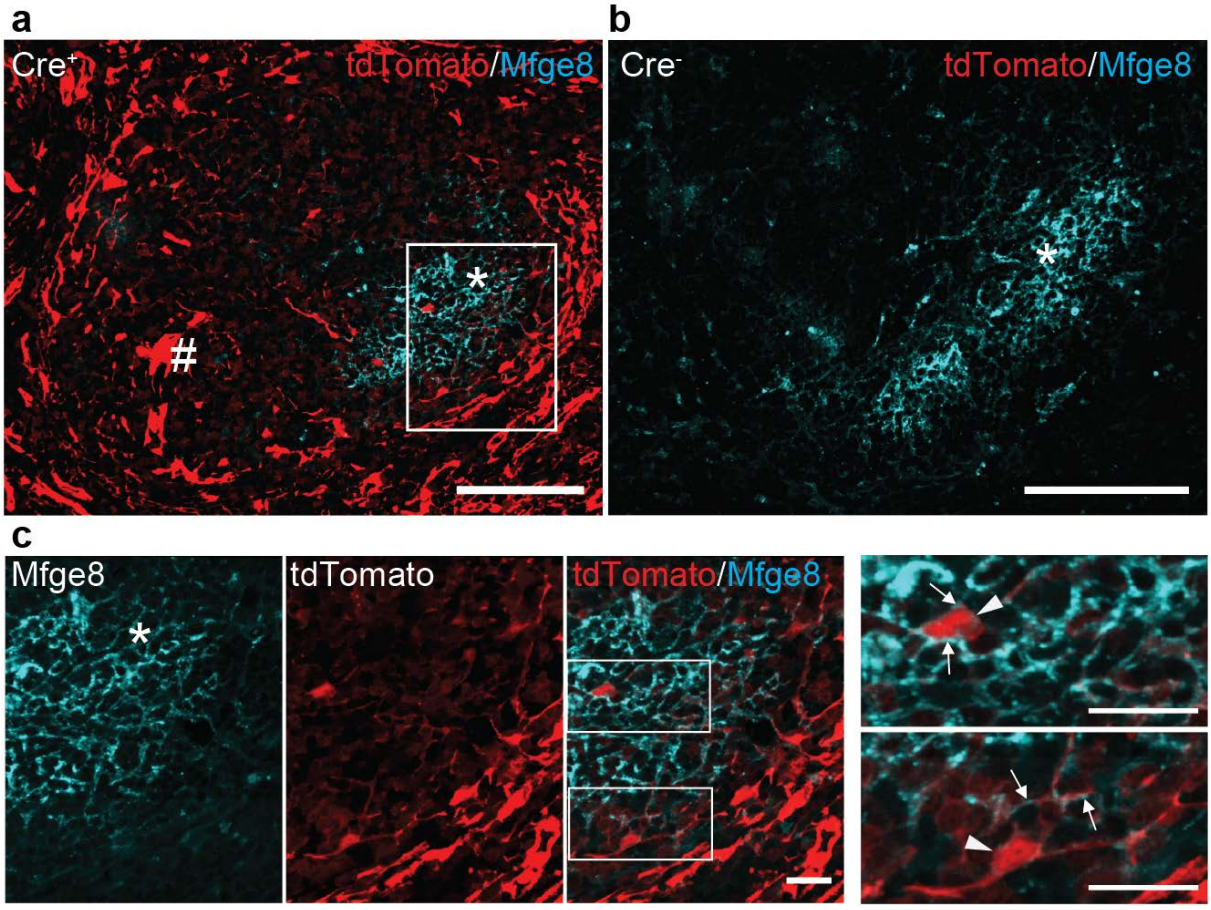

Figure 43. Immunofluorescent staining for Mfge8 on sections of *Pdgfrb*-Cre^{+} Ai14^{+} spleens. (a) Bright expression of the fluorescent reporter tdTomato in the vascular compartment of a lymphoid follicle containing Mfge8-positive FDC network. (b) No tdTomato signal was detected in Pdgfrb-Cre – Ai14+ mice. (c) Higher magnifications of box in panel a shows bright cytoplasmatic tdTomato in Mfge8+ cell bodies (arrowheads) and dendrites (arrows). # central artery. Asterisks designate FDC networks in B cell follicles. Scale bar 20 μm.

To verify that the majority of Mfge8$^+$ cells were tdTomato$^+$, we performed a quantification of the confocal images using the Surpass-spots function of Imaris software (Fig. 44 and Table 11). We found that 86.6 ± 8.2% of the Mfge8$^+$ areas in the spleen were also tdTomato$^+$. Hence we concluded that (most) Mfge8$^+$ cells (appeared to) have expressed PDGFRβ during their ontogeny.

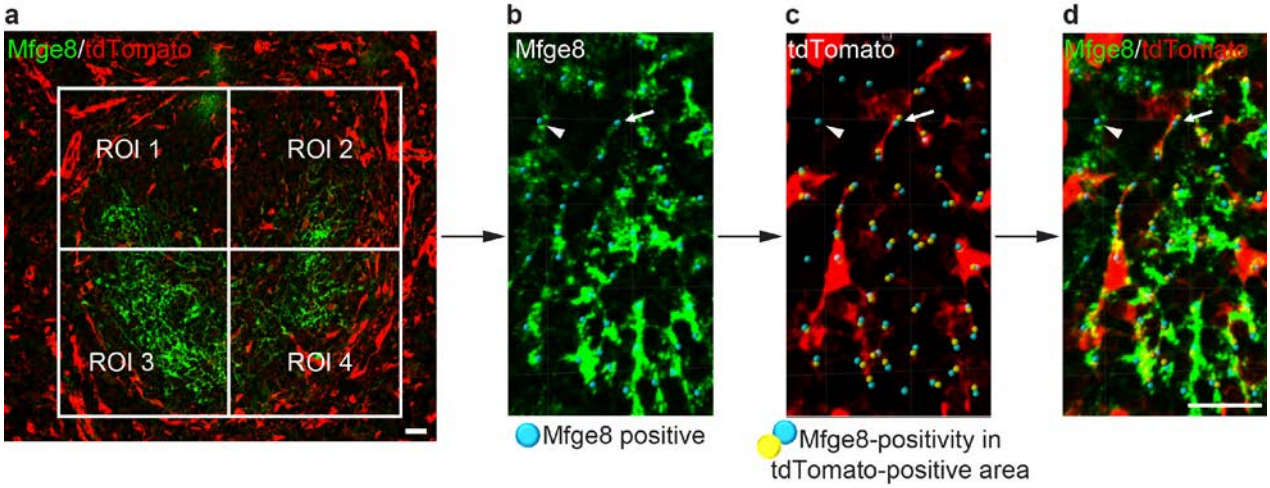

Figure 44. Morphometric analysis of splenic sections of *Pdgfrb*-Cre$^+$ Ai14$^+$ spleens stained with Mfge8. Four ROI in three confocal images were used for quantification using Imaris software. A ROI constituted of the right or left, upper or lower quadrant of a follicle (a). We first marked Mfge8$^+$ areas by blue spots in the far-red channel (b). We then assessed in the red channel, whether the blue spots were localized on or next to a tdTomato$^+$ area and marked this by a yellow dot (c). As shown in the overlay (d) most of the blue spots (Mfge8+) are associated with a yellow spot (tdTomato+) (small arrow). Arrowheads point to Mfge8+ spots not associated with tdTomato. 86.6 ± 8.2% of spots marking tdTdomato-positivity co-localized with spots marking Mfge8-positivity. Detailed numbers are listed in Table 11. Scale bar 20 μm.

Image	ROI	Number of spots in far red channel (Mfge8)	Number of spots in red channel (tdTomato)	% tdTomato$^+$ spots co-localizing with Mfge8$^+$ spots
1	1	56	52	92.86
	2	67	63	94.03
	3	46	45	97.83
	4	85	80	94.12
2	1	32	27	84.38
	2	48	42	87.50
	3	23	16	69.57
	4	51	38	74.51
3	1	161	144	89.44
	2	285	222	86.05
	3	90	77	85.56
	4	36	30	83.33
Sum		**953**	**836**	
Average±SD				**86.60±8.2**

Table 11. Details of quantification of proportion of tdTomato$^+$ in Mfge8$^+$ areas in confocal images of *Pdgfrb*-Cre$^+$ Ai14$^+$ spleens stained for Mfge8 as shown in Fig. 44**.** Four ROI in 3 confocal images were quantified using the Surpass-spot function in Imaris software. A total of 953 spots were analyzed in the far-red channel. Thereof, 836 co-localized with tdTomato signal (86.6 ± 8.2%).

5.2.2 Characterization of isolated stromal-vascular PDGFRβ$^+$ cells

To analyze if PDGFRβ$^+$ mural cells represent FDC-precursors, previous experiments were performed in our lab to establish the successful isolation of PDGFRβ$^+$ cells from the stromal-vascular fraction of perigonadal WAT (Perera, 2010; Tang et al., 2008). Intraperitoneal white adipose fat deposits in mice are composed of mesenteric fat, the omental depot surrounding the stomach and spleen and bilateral perigonadal fat pads located around ovaries and testes (Cinti, 2005). Of those, the perigonadal fat constitutes the largest and most easily accessible intraabdominal fat mass in mice and is therefore commonly used to isolate the stromal-vascular fraction of adipose tissue. Mesenteric fat is known to contain mesenteric fat-associated lymphocytic clusters (FALC) (Moro et al., 2010). FALC contain B cells required for the differentiation of FDC in secondary lymphoid organs and tertiary lymphoid tissues.

We wanted to ensure that the perigonadal fat pads, which we used for PDGFRβ$^+$ cell isolation, did not contain lymphocytic structures, which might contaminate our isolation and possibly skew our interpretations. We therefore performed serial sections through perigonadal fat pads of wild type animals and searched for the presence of lymphocytic clusters, in particular B cells. We did not detect lymphocytic infiltrates in the perigonadal fat by systematic histological analysis of perigonadal fat depots of two different mice. The fat contained abundant vasculature structures (Fig. 45a) and only scattered CD45$^+$ cells, most of which were CD68$^+$ macrophages (Fig. 45b). These results were confirmed by FACS analysis of perigonadal fat pads. Consistent with the histological analysis, CD45$^+$ cells in fat consisted mainly of CD68$^+$ macrophages (89%). Importantly, less than 0.05% of cells were B-cells and we did not find any follicular (CD23^{high}CD21/35^{low}) or marginal zone (CD23^{low}CD21/35^{high}) B cells, which are cells essential for FDC maturation (Krautler et al., 2012). We concluded that the perigonadal white adipose fat used for isolation of

the stromal-vascular fraction does not contain lymphocytic structures, in particular no follicular or marginal zone B cells.

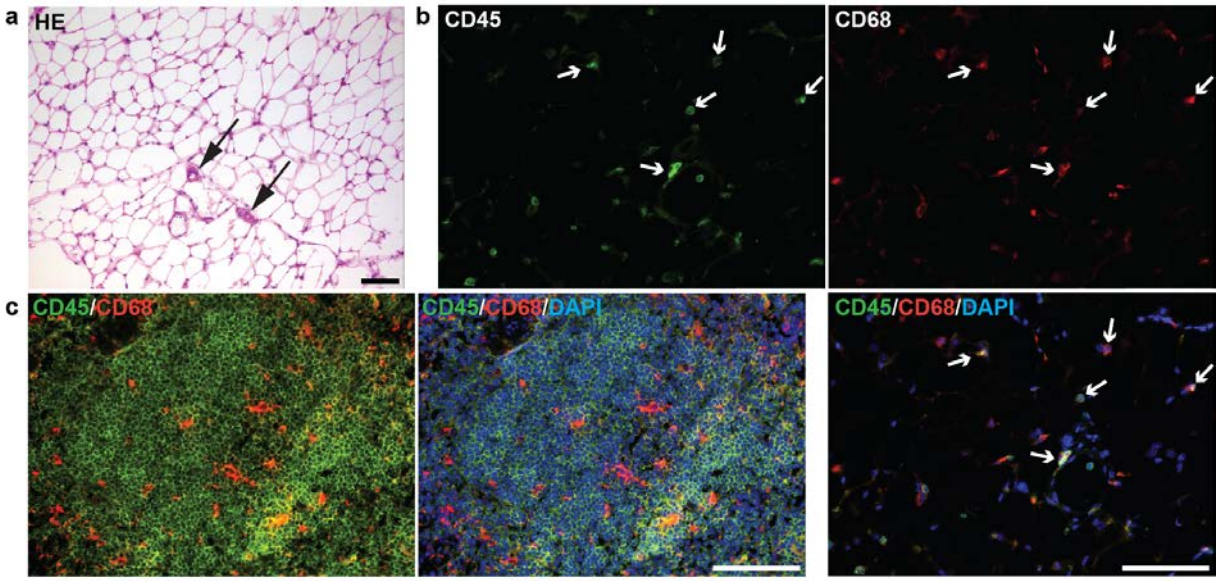

Figure 45. Histological analysis of white adipose perigonadal fat and spleen sections from B6 mice. Serial sections taken every 100 μm were analyzed by HE (a) and immunofluorescent staining of CD45, CD68 (b) and B220 (not shown). The perigonadal fat contained many blood vessels (black arrows), but no lymphocytic. In comparison to spleen (c), the fat tissue contained only few scattered hematopoietic cells, the majority being macrophages (white arrows). Scale bar 100 μm.

Next, we wanted to further analyze the purity and characteristics of the cell fraction obtained by sorting stromal-vascular cells for PDGFRβ$^+$ CD45$^-$ (Fig. 46). We extracted RNA from freshly sorted stromal-vascular PDGFRβ$^+$ cells and total fat tissue and determined the expression of *Perilipin-1* (*Plin1*) as a marker for adipocytes (Fig. 47a) and *Cd45* for hematopoietic cells by RT-PCR (Fig. 47b). Compared to the serially diluted fat cDNA (10^2 to 10^8 dilutions), the sorted PDGFRβ$^+$ cells showed 100-1000x less *Plin* and *Cd45* expression. We concluded that sorted stromal-vascular PDGFRβ$^+$ cells did not have relevant contamination by fat (*Plin*) or hematopoietic cells (*Cd45*).

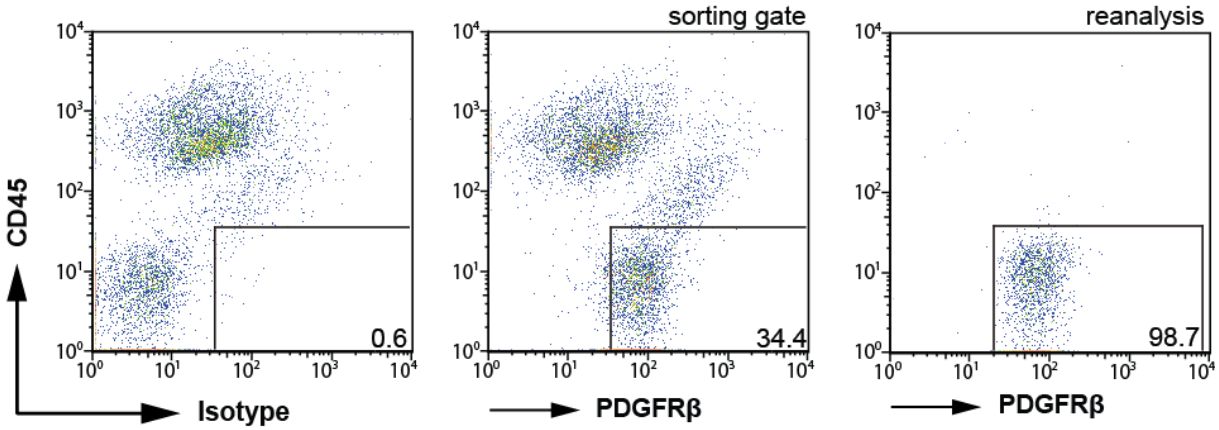

Figure 46. Gating strategy for obtaining the PDGFRβ$^+$CD45$^-$ cell fraction from collagenase-digested stromal-vascular component of perigonadal WAT from a representative experiment (middle panel). Isotype staining confirmed the specificity of the staining (left panel) and the reanalysis determined the purity of the yielded cell population (right panel): 98.7% PDGFRβ$^+$CD45$^-$ compared to 0.6% in isotype-stained sample (left panel).

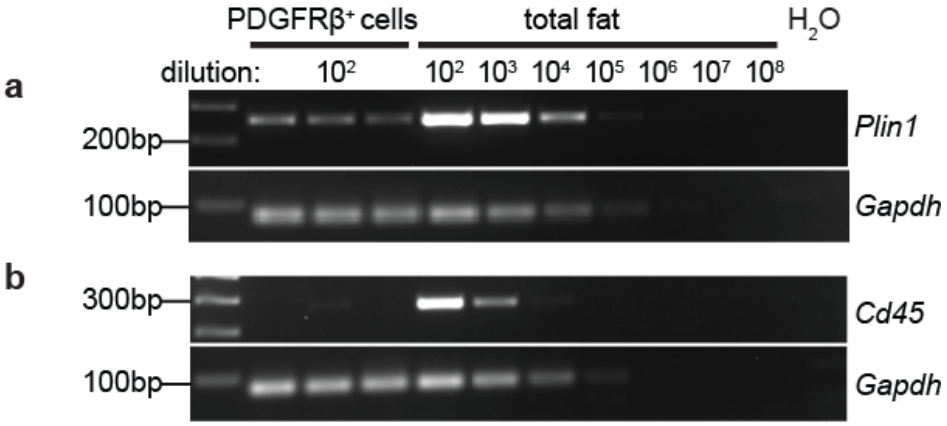

Figure 47. Purity of freshly sorted stromal-vascular PDGFRβ$^+$ cells analyzed by RT-PCR. (a) *Plin1* was used as adipose marker and (b) *Cd45* as hematopoietic marker. Total fat cDNA was serially diluted from 10^2-10^8, of PDGFRβ$^+$ stromal-vascular cell cDNA was used in 10^2 dilutions, H_2O served as negative and *Gapdh* amplification as endogenous control. 35 PCR cycles were performed. In PDGFRβ$^+$ stromal-vascular cells, both *Plin1* and *Cd45* expressions were 100-1000 times reduced.

To further characterize the expression profile of freshly sorted stromal-vascular PDGFRβ$^+$ cells, we assessed PDGFRβ$^+$ cell expression of markers for mural cells (*Pdgfrb*, *Ng2*), FDC-receptors (*Ltbr* and *Tnfr1*) and FDC-associated markers (*Bp3*, *Cd21*,

Fcgr2b, *Madcam1*, *Clusterin*, *Cxcl13*, *Vcam1*, *Icam1, Periostin* (*Postn*)), *Sdf1*) by qPCR and compared it to the expression of spleens (Fig. 48). Compared to spleen (set as 100% expression level), mural cells markers were highly upregulated (*Ng2* (1210%), *Pdgfrb* (737%)), confirming the identity of the isolated cells. Transcripts enconding LTβR and TNFR1, which are required for FDC differentiation, were both highly abundant (*Ltbr* (508%) and *Tnfr1* (1639%)), as well as *Periostin* (*Postn* (12,055%*)*, *Icam1* (235%), *Enpp2* (240%), *Sdf1* (254%), and *Prnp* (576%, not included in Fig. 48). Some transcripts were reduced (*Mfge8* (37%), *Cxcl13* (21%), *Vcam1* (64%), *Igfbp3* (96%)), and others were strongly downregulated (*Clusterin* (4%), *Madcam1* (2%), *Bp3* (0.3%)), importantly also the transcripts characteristic of mature FDC, *Cd21* (0.6%), and *Fcgr2b* (0.6%). Thus, isolated stromal-vascular PDGFRβ$^+$ cells exhibited similar characteristics of putative immature FDC located in the marginal zone of splenic follicles ("preFDC", (Kräutler, 2010)).

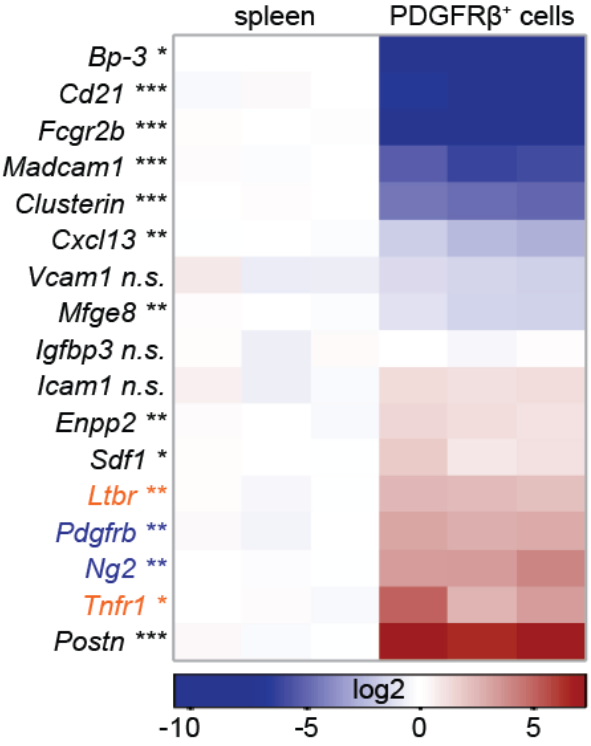

Figure 48. Characterization of PDGFRβ$^+$ cells isolated from the adipose stromal-vascular compartment. FDC-associated markers (in black), receptors essential for FDC differentiation (in orange) and mural cell markers (in blue) were analyzed by qPCR from stromal-vascular PDGFRβ$^+$ cells after sorting from perigonadal WAT and compared to their expression in spleens with *Gapdh* as endogenous control. Values are presented in a $\log_2$ scale (blue: downregulated, red: upregulated, white: no change in expression). Columns indicate individual spleens and each square represents the median expression of a particular gene (3 technical replicates) normalized to its mean expression in WT spleens (n=3). The heatmap was produced by Ulrich Wagner, Ludwig Institute for Cancer Research, University of California, San Diego.

The above measurements confirmed the purity and mural phenotype of the sorted PDGFRβ$^+$ cells. The strong upregulation of transcripts coding for the FDC differentiation receptors LTβR and TNFR1 suggested that these cells might respond to their ligands and possibly differentiate into FDC. Previous experiments already showed that PDGFRβ$^+$ cells, when cultured for 24 hours in the presence of agonistic anti-LTβR antibody and TNF (Katakai et al., 2008), responded by inducing FDC-associated markers *Vcam1*, *Icam1* and *Igfbp3*, and downregulating the mural marker *Pdgfrb*, as assessed by qPCR (Perera, 2010). These experiments suggested that treated PDGFRβ$^+$ cells indeed developed into FDC-like cells and at the same time lost their mural cell characteristics.

In order to confirm these findings and to include additional markers, we repeated this analysis (Fig. 49). We compared mRNA levels of stromal-vascular PDGFRβ$^+$ cells isolated from perigonadal WAT, which were treated with agonistic anti-LTβR antibody or its isotype control, both in the presence of TNF. Again, we found upregulation of *Vcam1* and *Icam1*, together with an increased expression of the additional FDC-associated markers *Madcam1*, *Enpp2*, and *Sdf1*, while *Igfbp3* was not changed. The mural marker *Pdgfrb* was again downregulated, whereas *Ng2* was not significantly changed. We found *Mfge8* to be slightly downregulated, which is in contrast to previous experiments, where Mfge8 was not significantly changed, but showed variable expression between the replicates (Perera, 2010). Interestingly, *Postn*, which was highly expressed in freshly isolated and sorted stromal-vascular PDGFRβ$^+$ cells, was not found in marginal zone preFDC (Kräutler 2012), whereas mature FDC again express *Postn*, possibly pointing to a transient downregulation of this marker during FDC maturation. To conclude, PDGFRβ$^+$ cells tended to respond by expressing FDC-associated markers and to lose their mural cell phenotype when stimulated with FDC maturation factors *in vitro.* Hence, the *in vitro* conditions permitted the cells to make first steps towards FDC differentiation. However, the lack of detection of *Bp3*, *Cd21* and *Fcgr2b* suggests that *in vitro* conditions

do not suffice to provide all requirements and signals needed for the differentiation of stromal-vascular PDGFRβ$^+$ cells to mature FDC.

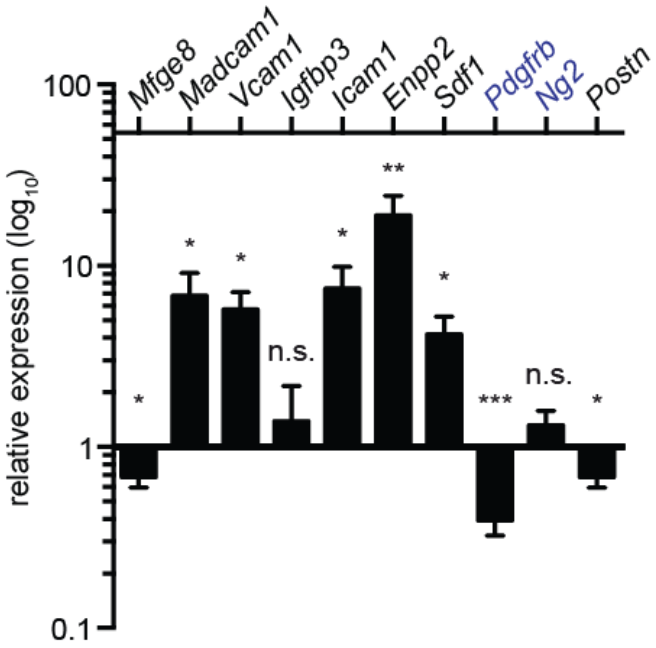

Figure 49. Analysis of mural cell (in blue) and FDC-associated (in black) markers of stromal-vascular PDGFRβ$^+$ cells. After FACS-sorting, cells were cultured for 24h, subsequently stimulated for 24h with agonistic anti-LTβR antibody and TNF or isotype control antibody. Expression of the following transcripts in agonist-, and isotype treated samples were assessed by qPCR and compared by unpaired t-test: *Mfge8* (p=0.0136), *Madcam1* (p=0.0324), *Vcam1* (p=0.0123), *Igfbp3* (p=0.3328), *Icam1* (p=0.026), *Enpp2* (p=0.0088), *Sdf1* (p=0.0195), *Pdgfrb* (p=0.0005), *Ng2* (p=0.1604), and *Periostin* (p=0.0195). The graph shows relative expression compared to isotype-treated PDGFRβ$^+$ cells and normalized over *Gapdh* mRNA levels (n=3 x 3). Error bars: SEM.

5.2.3 Transplanted PDGFRβ$^+$ stromal-vascular cells develop into mature FDC

We confirmed that mature FDC express PDGFRβ during their development, reinforcing the hypothesis that FDC stem from perivascular mural PDGFRβ$^+$ precursors. We also confirmed that PDGFRβ$^+$ cells can readily be isolated from the stromal-vascular fraction of perigonadal WAT into pure cells populations, and found that they expressed mural cell markers, receptors required for FDC differentiation, but lacked markers found on mature FDC. These cells also responded to FDC maturation factors *in vitro* by acquiring FDC-like properties. However so far, we could not show that PDGFRβ$^+$ cells can truly develop into mature FDC.

To prove their *bona fide* identity as FDC precursors and to provide all requirements for differentiation, we decided to transplant stromal-vascular PDGFRβ$^+$ cells under the renal capsule of recipient mice without FDC (*Ltbr*$^{-/-}$) or lacking a mature FDC marker (*CD21/35*$^{-/-}$). *Ltbr*$^{-/-}$ mice cannot develop mature FDC (Fütterer et al., 1998), and they show dense perivascular lymphocytic infiltrates in lung, kidney, pancreas and liver due to aberrant homing of B and T cells to non-lymphoid organs (Chin et al., 2003). *CD21/35*$^{-/-}$ mice do have FDC, however they show an impaired humoral immune response due to an impaired IC trapping capability of FDC (Ahearn et al., 1996; Fang et al., 1998). Renal capsule grafting is a method broadly used in various research fields, such as cancer research (Wang et al., 2005), developmental research (Kurita et al., 2005; Ohazama et al., 2004), diabetes research (Zmuda et al., 2011) or immunology (Suematsu and Watanabe, 2004). The highly vascularized kidney not only ensures favorable outcomes of graft survival, but also permits to study the interaction of the graft with the host tissue in an *in vivo* setting.

We again isolated the stromal-vascular fraction of perigonadal WAT from B6 donors and FACS-sorted PDGFRβ$^+$ cells (Fig. 46). We then soaked those cells into collagen

sponges (Suematsu and Watanabe, 2004) and immediately transplanted them under the renal capsule of *Ltbr*$^{-/-}$ hosts in a first transplantation round, and of *CD21/35*$^{-/-}$ hosts in a second round of experiments. At day 7 and 15 post transplantation, we immunized and boosted, the animals i.v with sRBC to stimulate the development of lymphocytic tissues. After four weeks, we found clearly visible subcapsular renal transplants (Fig. 50). In two *Ltbr*$^{-/-}$ mice, the kidneys showed signs of acute inflammation (Fig. 50b). We then performed serial cryosections through the whole transplants. Each transplant yielded 20-30 slides containing collagen sponge material and when stained by HE, lymphocytic aggregates were seen. Per transplant, we typically detected ≥10 distinct lymphocytic aggregates. When analyzed by immunohistochemistry, the transplants exhibited lymphocytic foci (Fig. 51a) containing B220^{+}CD21/35^{+} B and CD3^{+} T lymphocytes, as well as putative CD21/35^{+} and FDC-M1^{+} FDC (Fig. 51b). We further analyzed the transplants by immunofluorescence and found Mfge8^{+} cells that co-expressed the mature FDC marker CD35 and formed a network among B220^{+} B cell lymphoid aggregates (Fig. 52a). These Mfge8^{+} cell networks also co-expressed other FDC-associated markers, such as FcγRIIβ and PrP (Fig. 52b, c) In some lymphocytic foci, we found Mfge8^{+}CD68^{+} macrophages that had engulfed apoptotic cells, reminiscent of TBM found in germinal centers close to FDC (Fig. 52c) (Kranich et al., 2008). Since the *Ltbr*$^{-/-}$ hosts cannot generate FDC, we concluded that mature FDC in the collagen sponges must have developed from the transplanted donor-derived stromal-vascular PDGFRβ^{+} cells.

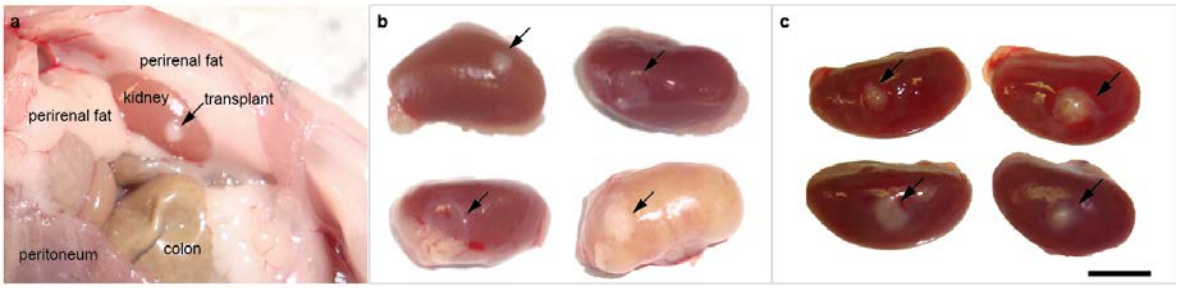

Figure 50. Macroscopic aspect of kidneys containing PDGFRβ^{+}-transplants four weeks after surgery. (a) Kidney containing subcapsular renal graft *in situ*. (b) Examples of macroscopic

aspect of *Ltbr*$^{-/-}$ kidneys containing sponges. Arrows point to subcapsular renal graft containing sorted stromal vascular PDGFRβ^{+} cells in collagen sponges. Some kidneys showed a distinct roundish graft, some large flat grafts. The lower right kidney shows signs of inflammation. (c) Macroscopic aspects of *CD21/35*$^{-/-}$ kidneys containing subcapsular renal grafts (arrows). Scale bar 5 mm.

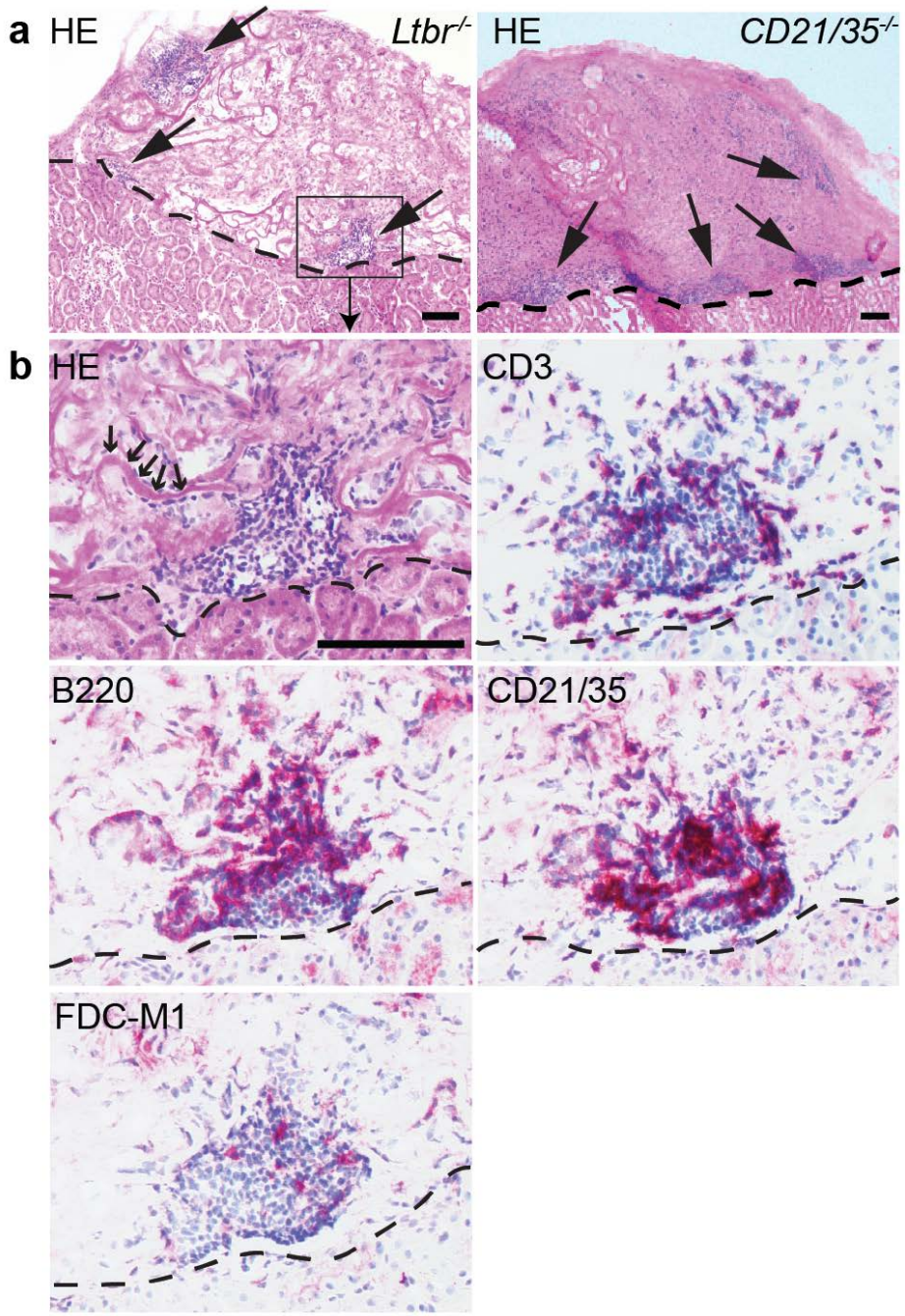

Figure 51. Analysis of subcapsular renal transplant of *Ltbr*$^{-/-}$ and *CD21/35*$^{-/-}$ recipients four weeks after transplantation of collagen sponges containing PDGFRβ^{+} cells. (a) HE sections through the transplanted collagen sponge and kidney of *Ltbr*$^{-/-}$ (left panel) and *C21/35*$^{-/-}$ (right

panel) hosts stained with HE. Sponges contained dense lymphocytic aggregates (arrows). Dashed line indicates the border of collagen sponge and renal cortex. **(b)** Consecutive sections of lymphocytic aggregate of *Ltbr*$^{-/-}$ transplant showing CD3^{+} T cells, B220^{+}/CD21/35^{+} B cells and putative CD21/35^{+} and FDC-M1^{+} FDC. Small arrows in upper middle panel designate collagen fiber. Scale bars: 100 μm.

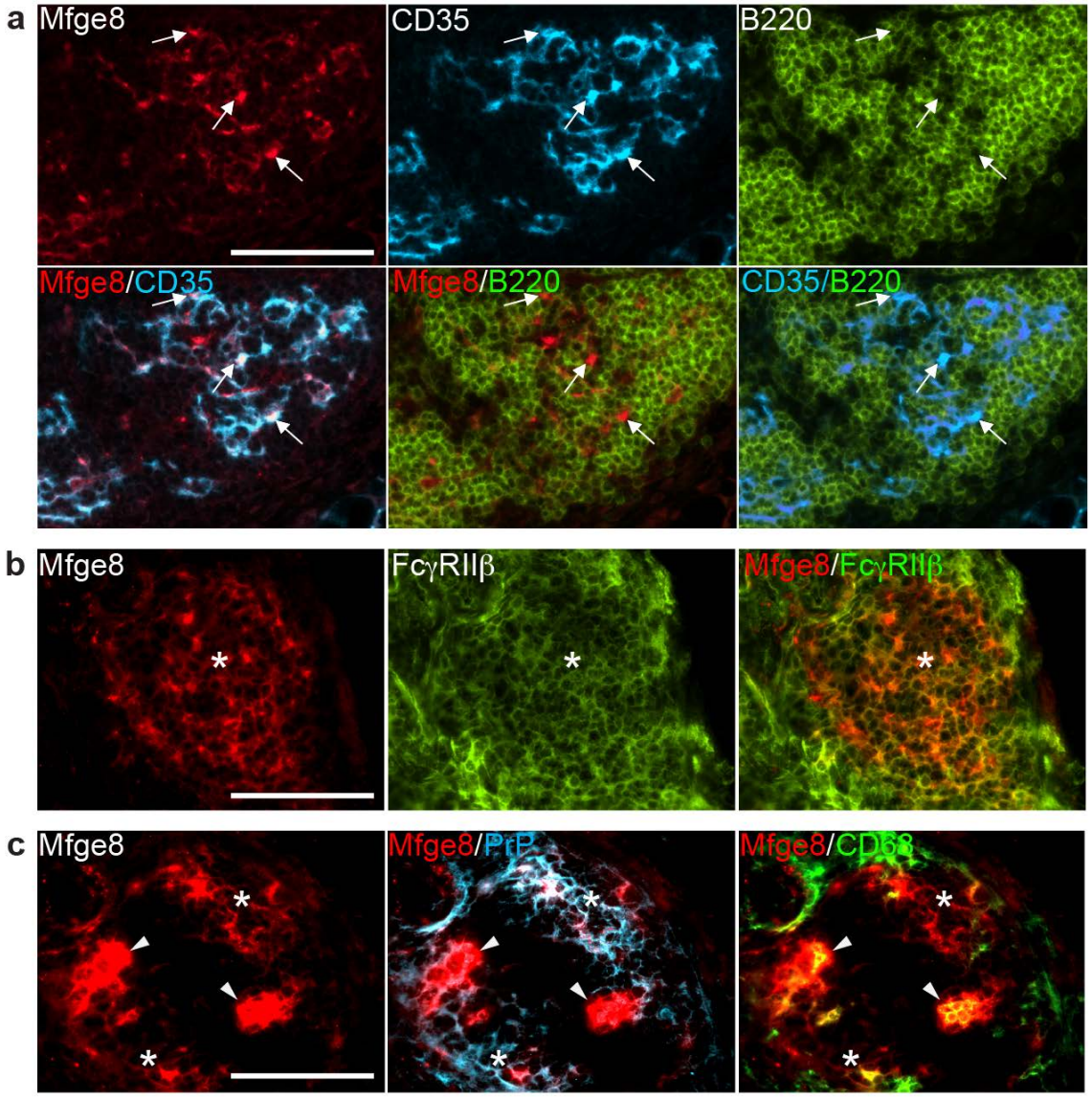

Figure 52. Immunofluorescent staining on collagen sponges containing PDGFRβ^{+} cells transplanted into *Ltbr*$^{-/-}$ host. (a) Mfge8^{+} CD35^{+} FDC enmesh B220^{+} B cell aggregate. Mfge8^{+} cells co-express FcγRIIβ (b) and PrP (c). Arrowheads point to Mfge8^{+} CD68^{+} TBM. Asterisks designate FDC-like network. Scale bars: 100 μm.

To ensure that the observed effect was dependent on the presence of PDGFRβ$^+$ cells, we performed control transplantations with collagen sponges without stromal-vascular PDGFRβ$^+$ cells into *Ltbr*$^{-/-}$ recipients (Fig. 53). These transplants contained scattered CD3$^+$ T cells, few scattered B220$^+$CD21/35$^+$ B cells and many macrophages (not shown). Apart from Mfge8$^+$ mesangial cells in the glomeruli of the renal cortex (Brunskill and Potter, 2012; Kräutler, 2010), we were unable to detect Mfge8$^+$ cells within densely packed lymphocytic aggregates in the collagen transplants, as seen in sponges containing PDGFRβ$^+$ cells (Fig. 53). Also extensive immunofluorescent studies failed to locate cells within the collagen sponges with network-like morphology and co-expressing Mfge8 with other FDC-associated markers (CD21/35, CD35, FcγRIIβ and PrP). We therefore concluded that the successful development of mature FDC in *Ltbr*$^{-/-}$ recipients depended on the addition of wild type adipose-derived stromal-vascular PDGFRβ$^+$ cells.

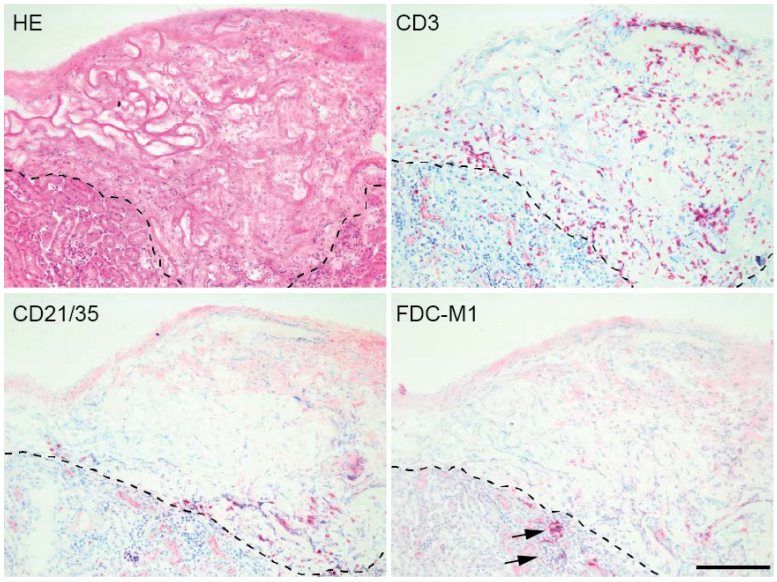

Figure 53. Analysis of subcapsular renal transplant of *Ltbr*$^{-/-}$ recipient without transplanted PDGFRβ$^+$ cells. Four weeks after surgery, HE shows transplant containing collagen fibres, dense extra cellular matrix and scattered cells, but no dense lymphocytic infiltrates. Instead, the collagen sponge contains scattered CD3-positive T cells, few scattered CD21/35 cells, and no FDC-M1 positive cells associated to lymphocytic infiltrates. Dashed line indicates the border of collagen sponge and renal cortex. Arrows point to glomeruli with FDC-M1 expressing mesangial cells. Scale bar 200 μm.

5.2.4 FDC derived from transplanted PDGFRβ$^+$ stromal-vascular cells trap IC

So far we have found that four weeks after renal subcapsular transplantation of collagen sponges containing stromal-vascular PDGFRβ$^+$ cells, these transplants showed inflammatory foci containing cells that expressed markers found on mature FDC (Mfge8$^+$ CD35$^+$ FcγRIIβ$^+$) and had the network-like morphology of FDC. Moreover, these FDC networks enmeshed B cell aggregates and some lymphoid foci contained TBM, features that can be found in germinal centers of lymphoid follicles. These findings suggest that stromal-vascular PDGFRβ$^+$ cells may give rise to mature – and possibly functional - FDC. A defining feature of FDC is their capability to trap and retain IC for a long time, presenting them to developing B cells in germinal centers. FDC trap IC using the CR1 (CD21) and CR2 (CD35) or FcγRIIβ (CD32), and their IC trapping capacity is highest in the light zone of GC in secondary follicles (Allen and Cyster, 2008; Yoshida et al., 1993). If the newly developed cells in the transplanted collagen sponges were indeed mature and functional FDC, they must be able to trap IC. We therefore wanted to test the IC trapping capability of the Mfge8$^+$ networks in the sponges.

IC trapping can be visualized *in vitro*, originally described by using anti-HRP-HRP complexes (Dijkstra et al., 1983). We used mouse PAP-IC and visualized peroxidase activity with a fluorescent dye in combination with Mfge8 or CD35 staining either in the presence of mouse serum (CR-mediated IC trapping requiring complement) or in absence of mouse serum (FcγRIIβ-mediated IC trapping) (Yoshida et al., 1993). We analyzed sections of subcapsular renal transplants of *Ltbr*$^{-/-}$ recipients four weeks after transplantation of collagen sponges containing PDGFRβ$^+$ cells (Fig. 54). Both in presence and absence of mouse serum, we failed to detect PAP-IC in collagen sponges, despite the presence of Mfge8$^+$ or CD35$^+$ cell networks (Fig. 54). PAP-IC were largely bound on the abundant CD68$^+$ macrophages in the collagen sponges (not shown). In

contrast, we found both CD35$^+$ IC-PAP$^+$ and Mfge8$^+$ IC-PAP$^+$ cells in B6 spleens (Fig. 54). Interestingly, we detected many small primary follicles with CD35$^+$ IC-PAP$^-$ and Mfge8$^+$ IC-PAP$^-$ cell networks, alike in the transplants. This suggests that the lymphocytic aggregates found in transplanted collagen sponges resemble primary splenic follicles, which show a limited IC trapping capability, although their FDC already express the necessary receptors (Allen and Cyster, 2008; Yoshida et al., 1993) .

IC trapping can also be visualized *in vivo*, for instance using fluorescent PE-anti-PE-IC (IC-PE) (Phan et al., 2007). To test this approach, we first injected B6 animals i.p. with anti-PE antibodies and 12h later with PE and analyzed spleen and lymph nodes (Fig. 55). After 24h, we detected IC-PE bound to FDC networks in splenic lymphoid follicles and large amounts of non-FDC bound IC-PE both in the red and white pulp, documenting that cells other than FDC capture large amounts of IC and deliver them to FDC (Arnon et al., 2013; Mebius and Kraal, 2005). After 72h, most of the IC-PE signal was confined to FDC networks in the white pulp and co-stained with Mfge8 and CD35 (Fig. 55).

Next, we tested the IC trapping capability of newly developed FDC in collagen sponges containing PDGFRβ^+ cells transplanted into *CD21/35*$^{-/-}$ hosts (Fig. 50, Fig. 51), which had been immunized and boosted with sRBC at day 7 and 14 after surgery, respectively. At day 28, we injected the mice i.p. with anti-PE, 12h later with PE, and sacrificed the mice three days later. The use of *CD21/35*$^{-/-}$ hosts permitted us to track potential newly developed mature FDC by the expression of CD21/35 as a genetic marker. In one of four operated animals, we detected IC-trapping cell clusters expressing CD21/35 displaying a network-like appearance (Fig. 56). Since any CD21/35 expressing cell must have been derived from the transplanted donor cells, we concluded that stromal-vascular PDGFRβ^+ cells were indeed able to develop into mature and functional FDC.

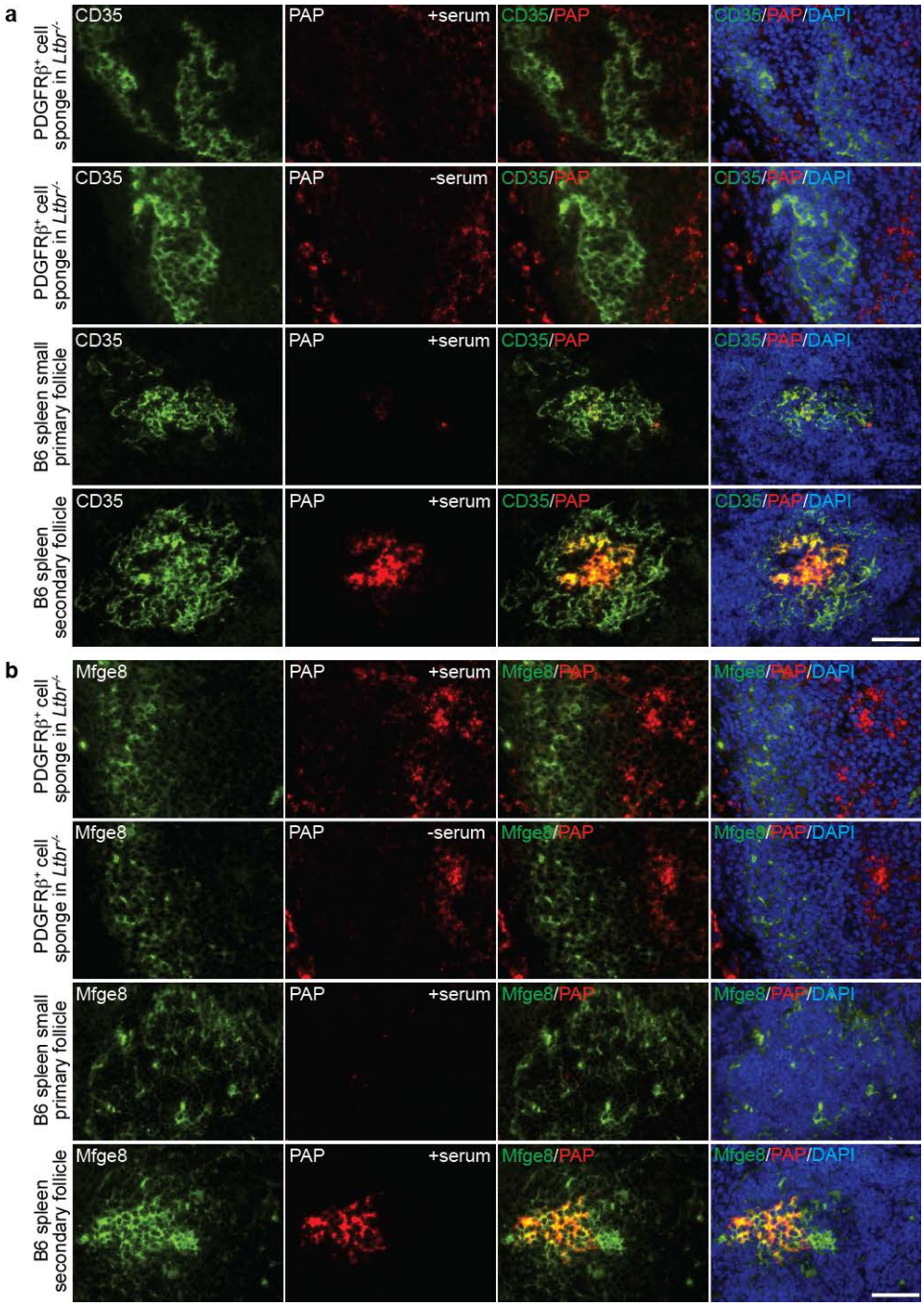

Figure 54. *In vitro* PAP IC trapping in B6 spleen and subcapsular kindey transplants containing PDGFRβ$^+$ cells four weeks after surgery. Cryosections of *Ltbr*$^{-/-}$ kidneys with collagen sponges or B6 spleens were incubated with PAP in the presence or absence of normal mouse serum, and co-stained with CD35 (a) or Mfge8 (b). No detection of CD35$^+$PAP$^+$ or Mfge8$^+$PAP$^+$ cells in transplants containing networks of CD35$^+$ or Mfge8$^+$. PAP trapping cells consisted largely of macrophages (not shown). CD35$^+$PAP$^-$ or Mfge8$^+$PAP$^-$ cell networks were also seen in small primary follicles in spleens, whereas secondary follicles exhibited high amounts of PAP trapping CD35$^+$ or Mfge8$^+$ co-expressing cells. Scale bar 50 μm

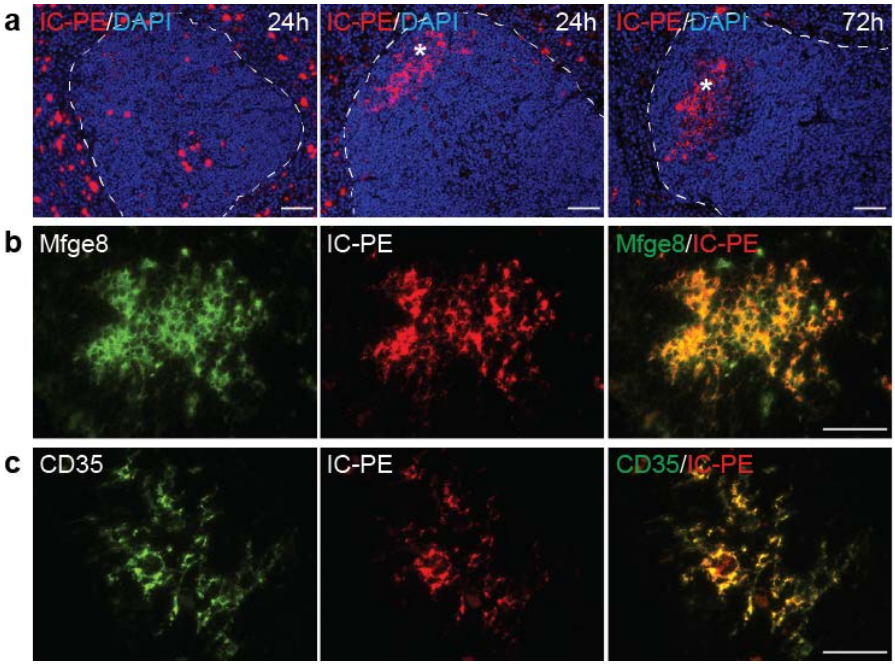

Figure 55. In vivo PE anti-PE IC trapping in B6 spleen (a) and inguinal lymph nodes (b,c). Mice were injected i.p. with anti-PE antibody and after 12h i.p. with PE to target the spleen or s.c. to target inguinal lymph nodes. 24h later, IC-PE could be detected both on FDC and on scattered cells in the red and white pulp (a, left and middle panel). After 72h, IC-PE retention was largely confined to FDC (a, right panel), and co-stained with Mfge8 and CD35, as shown in inguinal LN (b,c). Dashed line indicates border of lymphoid follicle. Asterisk marks FDC-network. Scale bar 50 μm.

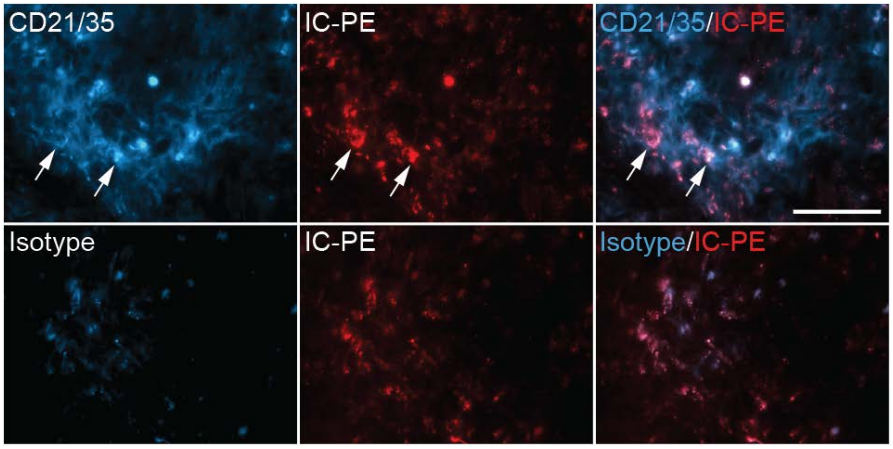

Figure 56. In vivo PE anti-PE IC trapping in *CD21/35*$^{-/-}$ mice four weeks after renal subcapsular grafting of collagen sponge containing stromal-vascular PDGFRβ^{+} cells. Mice were injected i.p. with anti-PE antibody and with PE 12h later. After 72h, mice were sacrificed. Sponges contained donor-derived CD21/35^{+} with network-like morphology, capable of trapping IC (upper panels). Isotype control staining (lower panels) was performed on a consecutive section and confirmed specificity of the CD21/35 staining. Arrows point to CD21/35^{+} IC-PE^{+} cells. Scale bar: 50 μm.

5.2.5 Factors influencing outcome of stromal-derived PDGFRβ$^+$ cells transplantations

Not all transplantations of stromal-derived PDGFRβ$^+$ cells showed a successful outcome. Of total 20 transplantations into *Ltbr*$^{-/-}$ or *CD21/35*$^{-/-}$ recipients, seven proved to be successful, as determined by the presence of lymphocytic infiltrates containing CD3$^+$, B220$^+$, CD21/35$^+$, and FDC-M1$^+$ cells (35%, Table 12). We wondered which factors might influence the successful development of a transplanted stromal-derived PDGFRβ$^+$ cell into a mature and IC-trapping FDC.

To support and stimulate the development of FDC networks, we immunized animals with sRBC i.v. Of 18 sRBC-immunized animals, six showed a successful outcome (33.3%). However, one non-immunized animal showed development of lymphocytic aggregates containing FDC (one of two non-immunized mice), hence immunization did not seem to be the main factor influencing outcome of the transplantations.

Since we treated some of the animals post-operatively with antibiotics, we also assessed the effect of antibiotic treatment on transplantation outcome (Table 12). Of eight *Ltbr*$^{-/-}$, which were kept under SPF conditions, none developed inflammatory foci with FDC, when treated with antibiotics right after surgery (0%). In contrast, six out of eight mice (75%), which did not receive post-operative antibiotic treatment, developed lymphoid aggregates in the transplants. Of four *CD21/35*$^{-/-}$ mice, which were housed under non-SPF conditions, one animal showed a successful outcome, when treated with antibiotics post-operatively. This suggested that post-operative treatment with antibiotics acted as a negative factor affecting outcome of the transplantations and that an inflammatory environment might be favorable. We concluded that the successful formation of lymphocytic aggregates and differentiation of stromal-derived PDGFRβ$^+$ cells to FDC in the transplanted collagen sponges appears to be mainly modulated by the immune status of the recipient mice.

	Recipient	(n)	Successful (n)	Successful (%)
All transplantations	*Ltbr*$^{-/-}$	16	6	
	Cd21/35$^{-/-}$	4	1	
	total	**20**	**7**	**35.0**
Effect of immunization				
Immunized	*Ltbr*$^{-/-}$	14	5	
	Cd21/35$^{-/-}$	4	1	
	total	**18**	**6**	**33.3**
Non-immunized	*Ltbr*$^{-/-}$	2	1	
	Cd21/35$^{-/-}$	0	0	
	total	**2**	**1**	**50.0**
Effect of antibiotic treatment				
Treated day 0-14	*Ltbr*$^{-/-}$	8	0	
	Cd21/35$^{-/-}$	4	1	
	total	**12**	**1**	**8.3**
Non-treated day 0-14	*Ltbr*$^{-/-}$	8	6	
	Cd21/35$^{-/-}$	0	0	
	total	**8**	**6**	**75.0**

Table 12. Overview of animals transplanted with adipose-derived stromal-vascular PDGFRβ^{+} cells and determination of the successful formation of lymphocytic aggregates containing CD3^{+}, B220^{+}, CD21/35^{+}, FDC-M1^{+} cells. Assessment of the effect of sRBC immunization and post-operative antibiotic treatment on the successful outcome of the transplantations.

5.3 DISCUSSION

5.3.1 PDGFRβ as a marker for FDC precursors

A vast amount of experimental evidence pointed to a mesenchymal origin of FDC, but the identity of the direct precursor cells is not known. Using Mfge8 as a guiding molecule, previous work of our lab identified earliest Mfge8$^+$ cells in the perivascular space, which co-expressed PDGFRβ. Here, using lineage tracing with *Pdgfrb*-Cre crossed to fluorescent reporter mice, we identified cells that co-expressed the fluorescent reporter and Mfge8 within FDC networks in B cell follicles, hence proving that these mature FDC expressed PDGFRβ$^+$ during their development. To unambiguously show that perivascular PDGFRβ$^+$ can develop to FDC, we isolated PDGFRβ$^+$ cells from the stromal-vascular fraction of adipose tissue. After previously having made sure that our isolation protocol permitted us to obtain pure cell population not contaminated with mature FDC, we transplanted collagen sponges containing PDGFRβ$^+$ cells under the renal capsule of mice, which cannot develop FDC. After four weeks, we identified lymphocytic aggregates containing mature and functional FDC within the sponges, thereby proving that FDC arise from PDGFRβ$^+$ stromal-vascular cells.

We transplanted 300,000-500,000 PDGFRβ$^+$ cells, but detected only about 10-20 conspicuous inflammatory foci in sponges of successful transplantations (Table 12). One possible reason for this apparently low yield might be a substantial loss of viable cells due to the stressful sorting and transplantation procedure. Another possibility might be that only a small fraction of the transplanted PDGFRβ$^+$ cell population contained true FDC precursors. What are the reasons to believe that?

In the adult stromal-vascular compartment, PDGFRβ$^+$ is expressed by the two mural cell populations, vSMC and pericytes, which share also the expression of NG2, CD13 and under certain circumstances, α-SMA (Armulik et al., 2011; Gaengel et al., 2009). Both

vSMC and pericytes themselves do not represent a homogeneous population in terms of origin and their characteristics vary substantially depending on vessel type and size, and activation status (Adams and Alitalo, 2007; Armulik et al., 2011; Etchevers et al., 2001; Owens et al., 2004). Moreover, the lack of specific pericytes markers has often hampered the distinction of the two populations, which both ensheath the inner endothelial vessel wall. The difference is largely based on their morphology with pericytes sharing the basement membrane directly with endothelial cells and forming a single and discontinuous layer around them, while vSMC form continuous concentric layers around vessels (Armulik et al., 2011).

Which of the cell types could represent or contain the putative FDC precursors? Both cell types have been reported to upregulate Mfge8 expression in states of stress and inflammation. In vSMC, Mfge8 has been linked to arterial wall inflammatory remodeling in hypertension, arteriosclerosis and diabetes mellitus, since Mfge8 expression is increased in activated and proliferating vSMC in an age-dependent manner (Fu et al., 2009; Wang et al., 2012a; Wang et al., 2012b). Mfge8 is also expressed in retinal pericytes and in pericytes within melanomas, where it appeared to regulate pathologic angiogenesis partly via increased PDGFRβ signaling (Motegi et al., 2011a; Motegi et al., 2011b). Hence, both vSMC and pericytes have a latent immunological potential (Olson and Soriano, 2011). In aortic arteriosclerotic lesions with TLO formation, activated vSMC expressed CXCL13 (Gräbner et al., 2009) and $NG2^+$ pericytes were even shown to be able to sense inflammatory mediators and to actively allure innate leucocytes (Stark et al., 2013).

Mural cells have also attracted attention in the stem cell field. While the existence of a vascular stem cell niche seems to be widely accepted (Bautch, 2011), the true stem cell potential and direct contribution to cell renewal of pericytes and vSMC is strongly debated (Armulik et al., 2011; Lin and Lue, 2013; Péault, 2012). Even so, mural cells seemed to gain stem cell properties when removed from their local vessel environment,

which led to the concept that pericytes might represent a stem cell reservoir (Bianco et al., 2008). Moreover, isolated mural cells carrying pericyte markers were reported to generate among others, adipocytes (Tang et al., 2008), osteoblasts and muscle fibres (Crisan et al., 2008; Dellavalle et al., 2011). Our finding that isolated mural cells can differentiate into FDC might therefore extend this list.

Independent of the question of whether PDGFRβ$^+$ cells that differentiated into mature FDC in our model should be called vSMC or pericytes or whether they represent cells in a continuum of differentiated mesenchymal stem cells within the vasculature, additional experiments are needed to better define their characteristics. Apart from PDGFRβ, additional markers such as Mfge8 might help to identify the immediate precursor cell likely to develop into FDC from the stromal-vascular compartment. In the more specialized environment of LN and spleen, gp38$^-$CD31$^-$ IAPs and gp38$^+$CD31$^-$CXCL13$^+$ MRC are the most promising cell populations for further investigation of immediate FDC precursors (Table 10) (Link et al., 2007; Malhotra et al., 2012; Malhotra et al., 2013; van de Pavert and Mebius, 2010).

5.3.2 Recapitulation of FDC development in a collagen sponge

Of 20 subcapsular kidney transplantations of PDGFRβ$^+$ cells into 16 *Ltbr*$^{-/-}$ and four *CD21/35*$^{-/-}$ recipients, seven proved to be successful (35%; six *Ltbr*$^{-/-}$ recipients and one *CD21/35*$^{-/-}$ recipient), as determined by the presence of dense lymphocytic aggregates with CD3$^+$, B220$^+$, CD21/35$^+$ and FDC-M1$^+$ cells within the collagen sponges. We analyzed sRBC immunization and postoperative antibiotic treatment as factors that might influence the outcomes of the transplantations, and found that antibiotic treatment in the first 14 days after surgery seems to correlate with a negative outcome.

What are the ideal circumstances that could enhance survival and lead to successful FDC maturation of transplanted PDGFRβ$^+$ cells in the subcapsular renal space? A

prerequisite for cell survival is a sufficient supply of oxygen and nutrients. Before transfer to the recipient, the collagen sponge containing the sorted cells was soaked in cell culture medium and the procedure of placing the collagen sponge under the renal capsule inevitably led to a small damage of the highly vascularized renal cortex causing leakage of blood into the postoperative wound. Hence, it can be assumed that the transplanted cells have received all factors needed for survival.

Transplanted PDGFRβ^+ cells not only need to survive, but crucially depend on signals to differentiate into FDCs, the most important being LT$\alpha\beta_2$ and TNF from LTi and B cells. As a consequence, and in parallel to “successful” TLO development, any factor that attracts LTi and B cells to the collagen sponge and triggers LT$\alpha\beta_2$ and TNF secretion for a prolonged time would support maturation of PDGFRβ^+ cell into FDC. Such initial trigger could be damage-associated molecular patterns (DAMPs) produced through mechanical damage introduced through the operation and placement of foreign biomaterial (Chen and Nuñez, 2010). In addition, the bacterial load introduced peri-operationally might have led to a chronic inflammatory stimulus needed for a sufficient and prolonged LT$\alpha\beta_2$ and TNF supply for the PDGFRβ^+ cell. Similar to helicobacter pylori eradication, where antibiotic treatment leads to the disappearance of lymphoid follicles located in the gastric mucosa and prevents the new formation thereof, our postoperative use of a broad-spectrum antibiotic might have prevented chronic inflammatory stimuli and subsequent differentiation of PDGFRβ^+ cells into mature FDC. Therefore, besides omitting antibiotic treatment, the addition of immunostimulatory molecules, such as CpG oligonucleotides or treatment with agonistic anti-CD40 antibody to stimulate B cells, might promote successful FDC development. On the side of the recipient, the presence of inflammatory cells at the site of operation might also be favorable. In this regard, *Ltbr*$^{-/-}$ mice represent a good model, since they show large perivascular lymphocytic infiltrates in peripheral organs including kidneys (Chin et al., 2003). Therefore, transplantations into *Ltbr*$^{-/-}$ hosts,

crossed to RIP-LTα mice (Sacca et al., 1997), which show chronic inflammation in kidneys, might even improve transplantation outcomes.

Besides searching for cells exhibiting the typical FDC network morphology and expressing typical FDC markers, we looked for evidence that our de novo FDC were functional. The ability to trap and retain IC for a long time is a functional hallmark of FDC, and we indeed identified *CD21/35*$^{+}$ cells in *CD21/35*$^{-/-}$ recipients that had trapped PE-anti PE IC *in vivo*. Yet the development of IC trapping FDC seemed to represent a rare event, since only one of four treated *CD21/35*$^{-/-}$ mice exhibited such cells. Also, previous attempts to detect IC trapping FDC *in vitro* in *Ltbr*$^{-/-}$ transplants were not successful, despite the presence of Mfge8^{+}CD21/35^{+}FcγRII^{+} networks. These findings are in contrast to the notion that the appearance of CD21/35 on developing FDC coincides with IC trapping competence (Balogh et al., 2001; Horie et al., 1999). These results were obtained in developing murine spleens or in immunized LN, hence in SLO. However, to my knowledge, the dynamics of IC trapping in TLO has not been studied so far. In order to receive an IC, FDC depend on the well-organized delivery of B cells that have received the charge from subcapsular sinus macrophages in the LN (Phan et al., 2007), or marginal zone macrophages in the spleen (Arnon et al., 2013; Batista and Harwood, 2009). Thus, in a rather disorganized environment as TLO or the transplanted collagen sponge, this process might not be as efficient as in SLO. In our transplantation setting, additional postoperative time and further stimulation of FDC development and TLO formation might have increased *in vitro* IC trapping ability of de novo generated FDC and the amount of IC trapped on their surface *in vivo*.

5.3.3 A role for FDC precursors in prion diseases?

Within lymphoid organs, PrP^{C}-expressing FDC are thought to be the main cells of extraneuronal prion accumulation and the genetic or pharmacological ablation of LT and

TNF-signaling pathways required for FDC development abrogate or delay splenic prion accumulation (Klein et al., 1997; Mabbott et al., 2003; Montrasio et al., 2000). In LN, however, prion accumulation is TNFR-signaling independent, yet requires LTβR-signaling, suggesting that cells other than mature FDC can accumulate prions (Prinz et al., 2002). These candidate prion accumulating cells have recently been more precisely characterized: in *TNFR*$^{-/-}$ LN, PrP^{Sc} was present in and around Madcam1^{+} HEV, and the prion deposition on these Madcam1^{+} cells was dependent on LT (O'Connor and Aguzzi, 2013; O'Connor et al., 2012), in agreement with the LTβR-signaling dependence of HEV development and maintenance (Browning et al., 2005). Furthermore, FDC-independent accumulation was also observed in granulomas (Heikenwalder et al., 2008), which are small nodules consisting of epitheloid macrophages surrounded by a rim of fibroblasts and lymphocytes that can develop as a reaction to chronic inflammatory stimuli or foreign bodies. In granulomas, the putative prion-accumulating cell was characterized as a CD45^{-}gp38^{-}CD31^{-}FDC-M1^{-}VCAM^{-}PrP^{+}PDGFRαβ^{+}LTβR^{+} stromal cell with mesenchymal stem cell characteristics (Heikenwalder et al., 2008; Nuvolone et al., 2009).

Our finding that FDC arise from stromal perivascular PDGFRβ^{+} cells raises the interesting question whether cells that have been found to accumulate prions in the absence of mature FDC are in fact FDC precursors. Similar to the prion-accumulating cells in granulomas, FDC precursors express high levels of LTβR, PrP and PDGFRβ, and share markers and properties with FRC and IAP, which surround HEV (Link et al., 2007; Malhotra et al., 2013; von Andrian and Mempel, 2003). Upon LTβR and TNFR stimulation, they upregulate Madcam1 expression and lose their mesenchymal stem cell like characteristics, in accordance with the concept that all stromal subsets of the secondary follicle derive from a common mesenchymal origin (Cupedo et al., 2004a; van de Pavert and Mebius, 2010), and that the stromal cells involved in ectopic lymphoneogenesis derive from perivascular pericytes-like mesenchymal cells.

In contrast to our findings that FDC precursors express Mfge8, granulomas did not contain FDC-M1^{+} staining, nor detectable *Mfge8* transcripts as assessed by RT-PCR compared to *Mfge8*$^{-/-}$ and *Ltbr*$^{-/-}$ spleens (Heikenwalder et al., 2008). However, careful examination of *Ltbr*$^{-/-}$ organs reveals a distinct perivascular Mfge8 staining, indicating that very low levels of *Mfge8* mRNA expressed by single putative FDC precursor cells could have been missed.

Interestingly, vessel-associated PrP^{Sc} depositions have been found in patients suffering from sporadic and variant Creutzfeldt-Jakob disease, both within intracranial and peripheral vessel walls (Armstrong, 2010; Koperek et al., 2002). Whereas some of these deposits co-localized with CD68 staining indicating uptake by macrophages, other deposits were found on unidentified perivascular cells. Again, the presence of perivascular prion deposits poses the question whether these cells could be vessel-associated FDC progenitors. Future experiments will assess whether FDC precursors are already capable of accumulating and/or replicating prions, or whether this capability is an exclusive feature peculiar to mature FDC.

5.4 MICE, MATERIAL AND METHODS

5.4.1 Mice

The following mice were used: *Ltbr*$^{-/-}$ (Fütterer et al., 1998), *CD21/35*$^{-/-}$ (*Cr2*$^{-/-}$) (Ahearn et al., 1996) (obtained from Manfred Kopf), and C57BL/6 purchased from Harlan. *Pdgfrb*-Cre mice (obtained from Ralf Adams) were crossed with Cre-inducible (CAG-tdTomato) Ai14 fluorescent reporter mice (Madisen et al., 2010). All animals were kept under SPF conditions, with the exception of *CD21/35*$^{-/-}$ (*Cr2*$^{-/-}$) mice. All animal experiments were performed in compliance with the Swiss Animal Protection Law, under the approval of the Veterinary office of the Canton Zurich.

5.4.2 Isolation of perigonadal white adipose stromal-vascular cell fraction

Perivascular stromal cells were isolated as previously described (Perera, 2010; Tang et al., 2008). In brief, perigonadal white adipose depots were dissected, cut into little pieces and digested in stromal cell isolation buffer (DMEM with 2% fetal calf serum) containing 1mg/mL collagenase D (Roche) at 37 ºC with constant shaking at 70 rpm for 2h. After approximately 1h, clumps were gently triturated using a blunt glass pipette to further dissociate the clumps. After digestion, the suspension was again gently triturated until all cells were dissociated and passed through a 210 µm nylon filter. The floating adipocyte layer was removed by aspiration. After red blood cells lysis in 5 ml of RBC lysis buffer (eBioscience), cells were filtered through a 50µm cell strainer and then subjected to sorting (FACS Aria, BD biosciences) to obtain a pure population of PDGFRβ^+ stromal-vascular cells.

5.4.3 Quantitative RT PCR

Total RNA from fat, freshly sorted or treated (24h with 100ng/mL agonistic LTβR (AC.H6, Biogen) or hamster IgG (Ha4/8-3.1, Biogen) in the presence of 5ng/mL mTNF (R&D Systems)) PDGFRβ$^+$ stromal-vascular cells was isolated using Trizol (Invitrogen) and subsequent chloroform extraction. cDNA synthesis was performed with QuantiTect, Reverse Transcription kit (Qiagen) using the manufacturer's instructions. Samples were analyzed by quantitative real-time PCR using QuantiFast SYBR Green Master Mix (Qiagen) on a 7900HT (Fast Real-Time PCR systems; Applied Biosystems) using default cycling conditions. Expression levels were normalized to *Gapdh* expression levels. The following primers were used:

Gene	**Forward primer**	**Reverse primer**
Bp3	CTCCTCACCTCCAGAGCATC	AATCGCCAACTTTGCCATAC
Cxcl13	TCGTGCCAAATGGTTACAAA	ACAAGGATGTGGGTTGGGTA
Cd21	CCCATAGTACCAGGGGGATT	AGACTGGCAGAGCTGTGGGT
Cd45	AAACGATCGGTGACTTTTGG	AGCTCTTCCCCTTTCCATGT
Clusterin	CCAGTTCCCAGACGTTGATT	AGCAGGGATGAGGTGTGGAG
Enpp2	TGGCTTACGTGACATTGAGG	AAATCCAAACCGGTGAGATG
Fcgr2b	AATTGTGGCTGCTGTCACTG	CAGTTTTGGCAGCTTCTTCC
Gapdh	CCACCCCAGCAAGGAGACT	GAAATTGTGAGGGAGATGCT
Icam1	ACTGCTTGGGGAACTGGAC	AGGCATGGCACACGTATGTA
Igfbp3	CGAGTCTAAGCGGGAGACAG	TTGTTGGCAGTCTTTTGTGC
Ltbr	GCCGAGGTCACAGATGAAAT	CAGGACACTGGTGAAGAGCA
Madcam1	CCTCTGCTGAGCCCTACATC	CTTGTGGTAGGTTGCCAGGT
Mfge8	ATATGGGTTTCATGGGCTTG	GAGGCTGTAAGCCACCTTGA
Ng2	GATCCACCTCGCATCATCTT	GTTCCCGACAGGAAAACTCA
Pdgfrb	CCGGAACAAACACACCTTCT	TAGCTGGGGGACTCAATGTC
Plin1	ACACTCTCCGGAACACCATC	CCTCTGCTGAAGGGTTATCG
Postn	AGTGCTCTGAGGCCATCACT	AGGTCGGTGAAAGTGGTTTG
Prnp*	GCTGGCCCTCTTTGTGACTA	CTGGGCTTGTTCCACTGATT
Sdf1	GCTCTGCATCAGTGACGGTA	GGGCAGCCTTTCTCTTCTTC
Tnfr1	ACCAAGTGCCACAAAGGAAC	CACGCACTGGAAGTGTGTC
Vcam1	GGCATCCTCACCTTAATTGC	ACAGGTCTCCCATGCACAA

* *Prnp* primers from (Huber et al., 2005)

5.4.4 Subcapsular renal transplantation of PDGFRβ^{++} stromal-vascular cells

An isoflurane-anaesthetized *Ltbr*$^{-/-}$ or *Cd21/35*$^{-/-}$ mouse was laid on its side, shaved around the renal protrusion and the skin was sterilized. A skin incision of approximately 2 cm was made, followed by a slightly shorter incision of the peritoneum. The kidney was externalized from the abdomen by gentle pressure and kept humid with sterile saline solution. Using a fine forceps, the kidney capsule was pinched, a small incision was made using the tip of a 21 gauge needle and a small pouch was gently formed with a fine straight iris spatula by blunt dissection. A collagen sponge (CS-35; KOKEN) of approximately 1mm^3 size (Suematsu and Watanabe, 2004) soaked with 300-500'000 FACS-sorted PDGFRβ$^+$ cells was transferred to the kidney surface and gently pushed into the prepared subcapsular pouch using the spatula. The kidney was gently released into the abdomen, the peritoneum and skin were sutured and disinfected with Bethadine solution (Mundipharma). The animal was injected s.c. with 60 μl of 0.05 mg/ml Temgesic (Schering-Plough), transferred into recovery and monitored daily. Some mice were immunized 1 week after surgery with 2x10^8 sRBC (ACILA AG) and boosted after 15 days with with 1x10^8 sRBC. Some mice were treated with 1:500 dilution 24% Borgal in drinking water (see Table 12 for details).

5.4.5 *In vitro* IC trapping

Protocol adapted from (Dijkstra et al., 1983). Cryosections were fixed with acetone and 0.2% H_2O_2, air-dried, blocked with PBS with 1% goat serum and 0.5% BSA. Sections were incubated with 1:10 mouse PAP (Jackson Immuno) diluted 1:10 in PBS with 1% goat serum and 0.5% BSA and with or without 10% normal mouse serum (DAKO) for 1h at room temperature. Sections were washed and PAP-IC were detected using Alexa

647-Tyramide Signal Amplification (Molecular Probes, Invitrogen) according to manufacturer's instructions.

5.4.6 In vivo IC trapping

Protocol adapted from (Balogh et al., 2001; Phan et al., 2007). On day one, mice were injected i.p. with 2mg/200µl polyclonal rabbit IgG anti-PE antibodies (Rocklands), and after 12h with 20µg/100 µl PE (Invitrogen) in PBS i.p. to target subcapsular kidney transplant or with 10µg/50µl PE in PBS s.c. into the flank to target inguinal lymph nodes. Mice were sacrificed after 24-72 hours.

5.4.7 Immunohistochemistry and immunofluorescence

Cryosections were stained with HE or with antibodies against CD3 (500A2), CD21/35 (7G6), and FDC-M1 (BD biosciences) and detected using respective AP-coupled secondary and tertiary antibodies in combination with Fast Red staining kit (Sigma) or on the Leica Bond-III IHC stainer using the Leica Bond Polymer Refine Red detection kit. For immunofluorescent analysis, cryosections were stained using the following primary and secondary antibodies: anti-Mfge8 (2422, Alexis Corporation, sometimes used in biotinylated form), FDC-M1 (4C11, BD Biosciences), anti-CD68 (MAC1957, Serotec), anti-CD16/32 (FcgRIIb, 2.4G2, BD biosciences), anti-PrP (XN, made in our laboratory (Montrasio et al., 2000)), anti-CD21/35 FITC (7G6, BD biosciences), anti-CD35 (8C12, BD biosciences) and the secondary antibodies anti-rat Alexa488, anti-rabbit Alexa546, anti-rat Alexa594, anti-hamster Alexa647, streptavidin Alexa 647 (all Invitrogen). Tissues of Ai14 fluorescent protein reporter mice were pretreated as described (Madisen et al., 2010). In short, animals were perfused with 4% PFA in PBS, organs were fixed overnight and subsequently cryoprotected in 20% (wt/vol) sucrose in PBS overnight. Sections were analyzed by fluorescence microscopy on a BX61 microscope (Olympus) or on a CLSM

Leica SP5, and images were processed using Imaris-Multicolor and 4D Image Processing and Analysis (Bitplane).

5.4.8 Quantification of Mfge8 staining on *Pdgfrb*-Cre^{+} x CAG-tdTomato (Ai14) spleen sections

Images of splenic follicles were acquired using a CLSM Leica SP5 and were processed using Imaris software. With the Surpass-spots function of Imaris software, the two channels containing Mfge8 signals (far-red channel) and tdTomato signals (red channel) were subsequently analyzed. First, Mfge8 signals were marked with spots. Then, tdTomato co-localization in the red channel was tested in relation to the previously set Mfge8^{+} spots. The cut-off for co-localization was set at the width of one spot. A co-localizing tdTomato^{+} area was then marked with a second spot. No tdTomato^{+} area within the one spot range was scored as absence of co-localization. Three confocal images from four ROI containing Mfge8 signals from were quantified.

6 ACKNOWLEDGMENTS

None of this work would have been possible without the valuable contributions of the following people to whom I want to express my gratitude:

Adriano Aguzzi for his enormously inspiring, enthusiastic and clear-sighted guidance during my MDPhD studies, for all his generosity and constant support, for many fascinating discussions, his brilliant ideas and for the opportunity to combine my MDPhD education with a residency in neuropathology.

Mario Nuvolone for being an excellent scientist and colleague, for sharing the "*Sirpa*-projects" with me, for many hours of intense discussions, for his cogent scientific insights, his critical acumen and for reading and correcting this thesis.

Gregor Hutter for formulating the *Sirpa*-hypothesis in his thesis, for his database search of polymorphic genes and for establishing the STR analysis in our institute; Daiji Sakata for performing the phagocytosis experiments using BMDM; Giancarlo Russo from FGCZ for performing the RNA-Seq data analysis and for his patience with all our requests.

Jayne Danska for her valuable collaboration, for her insights into *Sirpa* genetics, and her coworkers Steven Mortin-Toth, Sujeetha Rajakumar, Andrei Malko for all their work.

Sabine Spath for teaching me the secrets of EAE, for performing long EAE and many additional experiments and for a very enjoyable collaboration; Burkhard Becher for support and constructive discussions.

Nike Kräutler for her brilliant work on the origin of FDC, for an enormously intense and successful collaboration – and for the good times.

Mathias Heikenwälder for having noted potential FDC precursors in granulomas, for excellent inputs, many interesting discussions and for collaboration on the myositis-project; Jan Kranich for his work on Mfge8 that set the basis for our study; Dushan Perera for having established the isolation of FDC precursors; Doreen Lemm for her great work before leaving the institute and for coming back in times of need; Annika Keller for teaching us about pericytes, for her excellent inputs and her art at the

microscope; Caihong Zhu and Mario Hermann for all their FDC work and many discussions.

Elisabeth Rushing for introducing me to the field of myopathology, for her constant inputs, support and her generosity, for being a great mentor, for all the trips to myopathology meetings, the daily chocolate and for reading and correcting this thesis.

Petra Schwarz for her tremendous help in analyzing the kidney transplants and her support in other projects, for taking care of the mice and animal permits, for keeping the lab running and for ensuring that we do not suffer from hypoglycemia.

Monika Bieri and Norbert Wey for development of the phagocytosis assay software and for many excellent suggestions and a lot of help.

Yvonne Fuhrer, Rita Moos and the genotyping team for providing excellent technical support; Mirzet Delic for all his help and support with mice and for many discussions; Brigitte Piccapietra and Marianne König for excellent work in the histolab; José María Mateos Melero from the Center for Microscopy and Image Analysis at the University of Zürich for help with image analysis and quantification.

The members of my PhD committee, Cornelia Halin Winter, Christian Grimm and Christian Münz, for discussions, suggestions and their support.

Hans-Hilmer Goebel for sharing his amazing knowledge in myopathology; Herbert Budka for his valuable teaching; Karl Frontzek, Christian Kempf, Henning Leske, Regina Reimann for enjoyable times at and next to the microscope.

Jana Sponarova for many discussions about AA amyloidosis and other important topics; Tiziana Sonati for many discussions and her friendship; Alzbeta Trancikova and Anna Maria Calella for their support during my first year of PhD; Paolo Dametto, Badma Segarane, Silvia Sorce, Uli Herrmann, Tracy O'Connor, Boris Ballmer, Bei Li, Simone Hornemann, Cinzia Tiberi, Monika Wolf, Gitta Seleznik, Juliane Bremer, Dino Saban, Pawel Pelczar, Hitoshi Takizawa, Yasuyuki Saito and Thorsten Buch for help, suggestions, discussions and a lot of fun.

The Swiss National Foundation and the Swiss Academy of Medical Sciences for generous funding and the Molecular Life Sciences Graduate School for guidance during my PhD.

I am very grateful to my friends Annina Sievi, Barbara Eckle, Angelika Strobel, to Marianne Stampf and Alex Anderfuhren and my brother, Martin Kana, for believing in me and always supporting me.

Finally, I want to express my deepest gratitude to Erik Wallerstein for standing by me and filling me with joy and happiness.

7 CURRICULUM VITAE AND PUBLICATIONS

Veronika Kana

Born September 21, 1980

Swiss (Chur, GR) and Czech citizen

CURRENT POSITION

MDPhD student, Institute of Neuropathology, University Hospital of Zurich, Prof. Adriano Aguzzi, Title: "The Role of the Prion Protein in the Immune System".
Resident physician, Institute of Neuropathology, University Hospital of Zurich, Prof. Adriano Aguzzi

EDUCATION

Since 2011	Resident physician, Institute of Neuropathology, University Hospital of Zurich
Since 2009	MDPhD-Program, Molecular Life Science Graduate School, ETH and University of Zürich
2009	Medical dissertation, University of Basel, Laboratory of Molecular Neurooncology, Prof. A. Merlo. Title: „Hemizygous Deletion of *NOTCH2* is a Diagnostic Marker for Oligodendrogliomas."
2008	State exam, Medical School, University of Basel
2002	Eidgenössische Maturität, Typus B (Latin)
1998-2001	Violin studies, Academy of Music, Lausanne and Zürich (SMPV)

PRACTICAL TRAINING/INTERNSHIPS

2006/07	Neurology, Dept. of Neurology, FN Motol, Charles University, Prague, CZ Gynaecology and Obstetrics, Stadtspital Triemli, Zürich Neurosurgery, University Hospital Basel Visceral surgery, University Hospital Basel Internal medicine, St. Clara Hospital, Basel Neurology, Dept. of Neurology, University Hospital Zürich Neuropathology, Institute of Neuropathology, University Hospital Zürich
2004-2006	Internal Medicine, Dr. med. R. Wenger, Basel

RESEARCH ACTIVITIES

Since 2009	MDPhD-Program, Institute of Neuropathology, University Hospital of Zurich, Prof. A. Aguzzi
2005-2007	Laboratory of Molecular Neurooncology, University Hospital of Basel, Prof. A. Merlo
2006	Internship, Institute of Neuropathology, University Hospital of Zurich, Prof. A. Aguzzi
2004	3rd International Summer School, University of Basel Laboratory of Molecular Neurooncology, University Hospital of Basel, Prof. A. Merlo

FELLOWSHIPS AND HONOURS

2008-2011	MD/PhD- Fellowship of the Swiss National Science Foundation (donated by the Swiss Academy of Medical Sciences (SAMW))
2009	Award from the Mary & Ewald E. Bertschmann Foundation for the best dissertations 2008/09 at the Medical Faculty of the University of Basel
2008	Scholarship from the Anna Carolina Stiftung, ETH Zürich Foundation
2005-2007	Scholarship from the Dr. Max Husmann Foundation

ORIGINAL PUBLICATIONS

Krautler NJ*, **Kana V***, Kranich J, Tian Y, Perera D, Lemm D, Schwarz P, Armulik A, Browning JL, Tallquist M, Buch T, Oliveira-Martins JB, Zhu C, Hermann M, Wagner U, Brink R, Heikenwalder M, Aguzzi A (2012). „Follicular dendritic cells emerge from ubiquitous perivascular precursors.“ Cell 150(1): 194 – 206.
* equal contribution

Julius C, Hutter G, Wagner U, Seeger H, **Kana V**, Kranich J, Klöhn P, Weissmann C, Miele G and Aguzzi A (2008). "Transcriptional stability of cultured cells upon prion infection." J Mol Biol 375(5): 1222-33.

Boulay J, Miserez AR, Zweifel C, Sivasankaran B, **Kana V**, Ghaffari A, Luyken C, Sabel M, Zerrouqi A, Wasner M, Van Meir E, Tolnay M, Reifenberger G, Merlo A (2007). “Loss of NOTCH2 Positively Predicts Survival in Subgroups of Human Glial Brain Tumors.” PLoS ONE 2(6): e576.

BOOK CHAPTERS, REVIEWS

Petersen JA, **Kana V**, Jung HH (2012). „Differentialdiagnose entzündlicher Myopathien“ rheuma Schweiz 6: 10-16

Aguzzi A, **Kana V** (2011). Neurodegeneration: The Molecular Pathology of Dementia and Movement Disorders.
Chapter 1.4 “Protein Aggregation in Neurodegeneration.”
Chapter 6.1 “Introduction to Prion Diseases.”

8 BIBLIOGRAPHY

Adams, J.C., and Lawler, J. (2004). The thrombospondins. Int J Biochem Cell Biol *36*, 961-968.

Adams, R.H., and Alitalo, K. (2007). Molecular regulation of angiogenesis and lymphangiogenesis. Nat Rev Mol Cell Biol *8*, 464-478.

Aguzzi, A., Barres, B.A., and Bennett, M.L. (2013). Microglia: scapegoat, saboteur, or something else? Science *339*, 156-161.

Aguzzi, A., Baumann, F., and Bremer, J. (2008). The prion's elusive reason for being. Annu Rev Neurosci *31*, 439-477.

Aguzzi, A., and Calella, A.M. (2009). Prions: protein aggregation and infectious diseases. Physiol Rev *89*, 1105-1152.

Aguzzi, A., and Heikenwalder, M. (2006). Pathogenesis of prion diseases: current status and future outlook. Nat Rev Microbiol *4*, 765-775.

Aguzzi, A., Heikenwalder, M., and Polymenidou, M. (2007). Insights into prion strains and neurotoxicity. Nat Rev Mol Cell Biol *8*, 552-561.

Aguzzi, A., and Krautler, N.J. (2010). Characterizing follicular dendritic cells: A progress report. Eur J Immunol *40*, 2134-2138.

Aguzzi, A., and O'Connor, T. (2010). Protein aggregation diseases: pathogenicity and therapeutic perspectives. Nat Rev Drug Discov *9*, 237-248.

Aguzzi, A., and Polymenidou, M. (2004). Mammalian prion biology: one century of evolving concepts. Cell *116*, 313-327.

Aguzzi, A., and Zhu, C. (2012). Five questions on prion diseases. PLoS Pathog *8*, e1002651.

Ahearn, J.M., Fischer, M.B., Croix, D., Goerg, S., Ma, M., Xia, J., Zhou, X., Howard, R.G., Rothstein, T.L., and Carroll, M.C. (1996). Disruption of the Cr2 locus results in a reduction in B-1a cells and in an impaired B cell response to T-dependent antigen. Immunity *4*, 251-262.

Ajami, B., Bennett, J.L., Krieger, C., McNagny, K.M., and Rossi, F.M. (2011). Infiltrating monocytes trigger EAE progression, but do not contribute to the resident microglia pool. Nat Neurosci *14*, 1142-1149.

Albert, P.R. (2011). What is a functional genetic polymorphism? Defining classes of functionality. J Psychiatry Neurosci *36*, 363-365.

Allen, C.D., and Cyster, J.G. (2008). Follicular dendritic cell networks of primary follicles and germinal centers: phenotype and function. Semin Immunol *20*, 14-25.

Aloisi, F., and Pujol-Borrell, R. (2006). Lymphoid neogenesis in chronic inflammatory diseases. Nat Rev Immunol *6*, 205-217.

Armstrong, R.A. (2010). Dispersion of prion protein deposits around blood vessels in variant Creutzfeldt-Jakob disease. Folia Neuropathol *48*, 150-158.

Armulik, A., Genové, G., and Betsholtz, C. (2011). Pericytes: developmental, physiological, and pathological perspectives, problems, and promises. Dev Cell *21*, 193-215.

Arnon, T.I., Horton, R.M., Grigorova, I.L., and Cyster, J.G. (2013). Visualization of splenic marginal zone B-cell shuttling and follicular B-cell egress. Nature *493*, 684-688.

Ballerini, C., Gourdain, P., Bachy, V., Blanchard, N., Levavasseur, E., Gregoire, S., Fontes, P., Aucouturier, P., Hivroz, C., and Carnaud, C. (2006). Functional implication of cellular prion protein in antigen-driven interactions between T cells and dendritic cells. J Immunol *176*, 7254-7262.

Balogh, P., Aydar, Y., Tew, J.G., and Szakal, A.K. (2001). Ontogeny of the follicular dendritic cell phenotype and function in the postnatal murine spleen. Cell Immunol *214*, 45-53.

Barclay, A.N. (2009). Signal regulatory protein alpha (SIRPalpha)/CD47 interaction and function. Curr Opin Immunol *21*, 47-52.

Barclay, A.N., and Brown, M.H. (2006). The SIRP family of receptors and immune regulation. Nat Rev Immunol *6*, 457-464.

Batista, F.D., and Harwood, N.E. (2009). The who, how and where of antigen presentation to B cells. Nat Rev Immunol *9*, 15-27.

Bautch, V.L. (2011). Stem cells and the vasculature. Nat Med *17*, 1437-1443.

Baxter, A.G. (2007). The origin and application of experimental autoimmune encephalomyelitis. Nat Rev Immunol *7*, 904-912.

Bianco, P., Robey, P.G., and Simmons, P.J. (2008). Mesenchymal stem cells: revisiting history, concepts, and assays. Cell Stem Cell *2*, 313-319.

Biasini, E., Turnbaugh, J.A., Unterberger, U., and Harris, D.A. (2012). Prion protein at the crossroads of physiology and disease. Trends Neurosci *35*, 92-103.

Bolton, D., McKinley, M., and Prusiner, S. (1982). Identification of a protein that purifies with the scrapie prion. Science *218*, 1309-1311.

Bremer, J., Baumann, F., Tiberi, C., Wessig, C., Fischer, H., Schwarz, P., Steele, A.D., Toyka, K.V., Nave, K.A., Weis, J.*, et al.* (2010). Axonal prion protein is required for peripheral myelin maintenance. Nat Neurosci *13*, 310-318.

Bremer, J., Heikenwalder, M., Haybaeck, J., Tiberi, C., Krautler, N., Kurrer, M., and Aguzzi, A. (2009). Repetitive immunization enhances the susceptibility of mice to peripherally administered prions. PLoS One *4*, e7160.

Brooke, G., Holbrook, J.D., Brown, M.H., and Barclay, A.N. (2004). Human lymphocytes interact directly with CD47 through a novel member of the signal regulatory protein (SIRP) family. J Immunol *173*, 2562-2570.

Brown, K.L., Stewart, K., Ritchie, D.L., Mabbott, N.A., Williams, A., Fraser, H., Morrison, W.I., and Bruce, M.E. (1999). Scrapie replication in lymphoid tissues depends on prion protein- expressing follicular dendritic cells. Nat Med *5*, 1308-1312.

Brown, P., Brandel, J.P., Sato, T., Nakamura, Y., MacKenzie, J., Will, R.G., Ladogana, A., Pocchiari, M., Leschek, E.W., and Schonberger, L.B. (2012). Iatrogenic Creutzfeldt-Jakob disease, final assessment. Emerg Infect Dis *18*, 901-907.

Browning, J.L., Allaire, N., Ngam-Ek, A., Notidis, E., Hunt, J., Perrin, S., and Fava, R.A. (2005). Lymphotoxin-beta receptor signaling is required for the homeostatic control of HEV differentiation and function. Immunity *23*, 539-550.

Brunskill, E.W., and Potter, S.S. (2012). Changes in the gene expression programs of renal mesangial cells during diabetic nephropathy. BMC Nephrol *13*, 70.

Burger, P., Hilarius-Stokman, P., de Korte, D., van den Berg, T.K., and van Bruggen, R. (2012). CD47 functions as a molecular switch for erythrocyte phagocytosis. Blood *119*, 5512-5521.

Büeler, H.R., Aguzzi, A., Sailer, A., Greiner, R.A., Autenried, P., Aguet, M., and Weissmann, C. (1993). Mice devoid of PrP are resistant to scrapie. Cell *73*, 1339-1347.

Büeler, H.R., Fischer, M., Lang, Y., Bluethmann, H., Lipp, H.P., DeArmond, S.J., Prusiner, S.B., Aguet, M., and Weissmann, C. (1992). Normal development and behaviour of mice lacking the neuronal cell-surface PrP protein. Nature *356*, 577-582.

Calella, A.M., Farinelli, M., Nuvolone, M., Mirante, O., Moos, R., J, F., Mansuy, I.M., and Aguzzi, A. (2010). Prion protein and Aβ-related synaptic toxicity impairment. EMBO Mol Med *in press*.

Carlson, C.B., Lawler, J., and Mosher, D.F. (2008a). Structures of thrombospondins. Cell Mol Life Sci *65*, 672-686.

Carlson, C.B., Liu, Y., Keck, J.L., and Mosher, D.F. (2008b). Influences of the N700S thrombospondin-1 polymorphism on protein structure and stability. J Biol Chem *283*, 20069-20076.

Cashman, N.R., Loertscher, R., Nalbantoglu, J., Shaw, I., Kascsak, R.J., Bolton, D.C., and Bendheim, P.E. (1990). Cellular isoform of the scrapie agent protein participates in lymphocyte activation. Cell *61*, 185-192.

Chao, M.P., Weissman, I.L., and Majeti, R. (2012). The CD47-SIRPα pathway in cancer immune evasion and potential therapeutic implications. Curr Opin Immunol *24*, 225-232.

Chen, G.Y., and Nuñez, G. (2010). Sterile inflammation: sensing and reacting to damage. Nat Rev Immunol *10*, 826-837.

Chepelev, I., Wei, G., Tang, Q., and Zhao, K. (2009). Detection of single nucleotide variations in expressed exons of the human genome using RNA-Seq. Nucleic Acids Res *37*, e106.

Chesebro, B., Race, R., Wehrly, K., Nishio, J., Bloom, M., Lechner, D., Bergstrom, S., Robbins, K., Mayer, L., and Keith, J. (1985). Identification of scrapie prion protein-specific mRNA in scrapie-infected and uninfected brain. Nature *315*, 331-333.

Chin, R.K., Lo, J.C., Kim, O., Blink, S.E., Christiansen, P.A., Peterson, P., Wang, Y., Ware, C., and Fu, Y.X. (2003). Lymphotoxin pathway directs thymic Aire expression. Nat Immunol *4*, 1121-1127.

Chong, H.C., Tan, C.K., Huang, R.L., and Tan, N.S. (2012). Matricellular proteins: a sticky affair with cancers. J Oncol *2012*, 351089.

Cinti, S. (2005). The adipose organ. Prostaglandins Leukot Essent Fatty Acids *73*, 9-15.

Colby, D.W., and Prusiner, S.B. (2011). De novo generation of prion strains. Nat Rev Microbiol *9*, 771-777.

Constantinescu, C.S., Farooqi, N., O'Brien, K., and Gran, B. (2011). Experimental autoimmune encephalomyelitis (EAE) as a model for multiple sclerosis (MS). Br J Pharmacol *164*, 1079-1106.

Cowles, C.R., Hirschhorn, J.N., Altshuler, D., and Lander, E.S. (2002). Detection of regulatory variation in mouse genes. Nat Genet *32*, 432-437.

Crisan, M., Yap, S., Casteilla, L., Chen, C.W., Corselli, M., Park, T.S., Andriolo, G., Sun, B., Zheng, B., Zhang, L.*, et al.* (2008). A perivascular origin for mesenchymal stem cells in multiple human organs. Cell Stem Cell *3*, 301-313.

Crusio, W.E., Goldowitz, D., Holmes, A., and Wolfer, D. (2009). Standards for the publication of mouse mutant studies. Genes Brain Behav *8*, 1-4.

Cupedo, T., Jansen, W., Kraal, G., and Mebius, R.E. (2004a). Induction of secondary and tertiary lymphoid structures in the skin. Immunity *21*, 655-667.

Cupedo, T., Lund, F.E., Ngo, V.N., Randall, T.D., Jansen, W., Greuter, M.J., de Waal-Malefyt, R., Kraal, G., Cyster, J.G., and Mebius, R.E. (2004b). Initiation of cellular organization in lymph nodes is regulated by non-B cell-derived signals and is not dependent on CXC chemokine ligand 13. J Immunol *173*, 4889-4896.

de Almeida, C.J., Chiarini, L.B., da Silva, J.P., PM, E.S., Martins, M.A., and Linden, R. (2005). The cellular prion protein modulates phagocytosis and inflammatory response. J Leukoc Biol *77*, 238-246.

de Almeida, C.J., and Linden, R. (2005). Phagocytosis of apoptotic cells: a matter of balance. Cell Mol Life Sci *62*, 1532-1546.

de Ledesma, A.M., Desai, A.N., Bolivar, V.J., Symula, D.J., and Flaherty, L. (2006). Two new behavioral QTLs, Emo4 and Reb1, map to mouse Chromosome 1: Congenic strains and candidate gene identification studies. Mamm Genome *17*, 111-118.

Deleault, N., Harris, B., Rees, J., and Supattapone, S. (2007). Formation of native prions from minimal components in vitro. Proc Natl Acad Sci U S A *104*, 9741-9746.

Dellavalle, A., Maroli, G., Covarello, D., Azzoni, E., Innocenzi, A., Perani, L., Antonini, S., Sambasivan, R., Brunelli, S., Tajbakhsh, S*., et al.* (2011). Pericytes resident in postnatal skeletal muscle differentiate into muscle fibres and generate satellite cells. Nat Commun *2*, 499.

Dijkstra, C.D., te Velde, A.A., and Van Rooijen, N. (1983). Localization of horseradish peroxidase (HRP)-anti-HRP complexes in cryostat sections: influence of endotoxin on trapping of immune complexes in the spleen of the rat. Cell Tissue Res *232*, 1-7.

Donaldson, D.S., Kobayashi, A., Ohno, H., Yagita, H., Williams, I.R., and Mabbott, N.A. (2012). M cell-depletion blocks oral prion disease pathogenesis. Mucosal Immunol *5*, 216-225.

Donaldson, S.L., Kosco, M.H., Szakal, A.K., and Tew, J.G. (1986). Localization of antibody-forming cells in draining lymphoid organs during long-term maintenance of the antibody response. J Leukoc Biol *40*, 147-157.

Dowds, C.A., Burks, D.J., and Saling, P.M. (1996). A cDNA encoding part of a novel putative receptor tyrosine kinase. In NUCLEOTIDE SEQUENCE [MRNA] OF 472-994 (Submitted (JAN-1996) to the EMBL/GenBank/DDBJ databases).

Drayton, D.L., Liao, S., Mounzer, R.H., and Ruddle, N.H. (2006). Lymphoid organ development: from ontogeny to neogenesis. Nat Immunol *7*, 344-353.

Eisener-Dorman, A.F., Lawrence, D.A., and Bolivar, V.J. (2009). Cautionary insights on knockout mouse studies: the gene or not the gene? Brain Behav Immun *23*, 318-324.

Eisener-Dorman, A.F., Lawrence, D.A., and Bolivar, V.J. (2010). Behavioral and genetic investigations of low exploratory behavior in Il18r1(-/-) mice: we can't always blame it on the targeted gene. Brain Behav Immun *24*, 1116-1125.

El Shikh, M.E., and Pitzalis, C. (2012). Follicular dendritic cells in health and disease. Front Immunol *3*, 292.

Endres, R., Alimzhanov, M.B., Plitz, T., Futterer, A., Kosco-Vilbois, M.H., Nedospasov, S.A., Rajewsky, K., and Pfeffer, K. (1999). Mature follicular dendritic cell networks depend on

expression of lymphotoxin beta receptor by radioresistant stromal cells and of lymphotoxin beta and tumor necrosis factor by B cells. J Exp Med *189*, 159-168.

Estes, J.D., Keele, B.F., Tenner-Racz, K., Racz, P., Redd, M.A., Thacker, T.C., Jiang, Y., Lloyd, M.J., Gartner, S., and Burton, G.F. (2002). Follicular dendritic cell-mediated up-regulation of CXCR4 expression on CD4 T cells and HIV pathogenesis. J Immunol *169*, 2313-2322.

Etchevers, H.C., Vincent, C., Le Douarin, N.M., and Couly, G.F. (2001). The cephalic neural crest provides pericytes and smooth muscle cells to all blood vessels of the face and forebrain. Development *128*, 1059-1068.

Falsig, J., and Aguzzi, A. (2008). The prion organotypic slice culture assay--POSCA. Nat Protoc *3*, 555-562.

Fang, Y., Xu, C., Fu, Y.X., Holers, V.M., and Molina, H. (1998). Expression of complement receptors 1 and 2 on follicular dendritic cells is necessary for the generation of a strong antigen-specific IgG response. J Immunol *160*, 5273-5279.

Fischer, M., Rülicke, T., Raeber, A., Sailer, A., Moser, M., Oesch, B., Brandner, S., Aguzzi, A., and Weissmann, C. (1996). Prion protein (PrP) with amino-proximal deletions restoring susceptibility of PrP knockout mice to scrapie. EMBO J *15*, 1255-1264.

Foo, S.S., Turner, C.J., Adams, S., Compagni, A., Aubyn, D., Kogata, N., Lindblom, P., Shani, M., Zicha, D., and Adams, R.H. (2006). Ephrin-B2 controls cell motility and adhesion during blood-vessel-wall assembly. Cell *124*, 161-173.

Ford, M.J., Burton, L.J., Morris, R.J., and Hall, S.M. (2002). Selective expression of prion protein in peripheral tissues of the adult mouse. Neuroscience *113*, 177-192.

Fortier, A.H., and Falk, L.A. (2001). Isolation of murine macrophages. Curr Protoc Immunol *Chapter 14*, Unit 14 11.

Fraser, H., and Dickinson, A.G. (1970). Pathogenesis of scrapie in the mouse: the role of the spleen. Nature *226*, 462-463.

Fu, Z., Wang, M., Gucek, M., Zhang, J., Wu, J., Jiang, L., Monticone, R.E., Khazan, B., Telljohann, R., Mattison, J.*, et al.* (2009). Milk fat globule protein epidermal growth factor-8: a pivotal relay element within the angiotensin II and monocyte chemoattractant protein-1 signaling cascade mediating vascular smooth muscle cells invasion. Circ Res *104*, 1337-1346.

Fütterer, A., Mink, K., Luz, A., Kosco-Vilbois, M.H., and Pfeffer, K. (1998). The lymphotoxin beta receptor controls organogenesis and affinity maturation in peripheral lymphoid tissues. Immunity *9*, 59-70.

Gadotti, V.M., Bonfield, S.P., and Zamponi, G.W. (2012). Depressive-like behaviour of mice lacking cellular prion protein. Behav Brain Res *227*, 319-323.

Gaengel, K., Genove, G., Armulik, A., and Betsholtz, C. (2009). Endothelial-mural cell signaling in vascular development and angiogenesis. Arterioscler Thromb Vasc Biol *29*, 630-638.

Gal, A., Li, Y., Thompson, D.A., Weir, J., Orth, U., Jacobson, S.G., Apfelstedt-Sylla, E., and Vollrath, D. (2000). Mutations in MERTK, the human orthologue of the RCS rat retinal dystrophy gene, cause retinitis pigmentosa. Nat Genet *26*, 270-271.

Gao, A.G., Lindberg, F.P., Finn, M.B., Blystone, S.D., Brown, E.J., and Frazier, W.A. (1996). Integrin-associated protein is a receptor for the C-terminal domain of thrombospondin. J Biol Chem *271*, 21-24.

Gerlai, R. (1996). Gene-targeting studies of mammalian behavior: is it the mutation or the background genotype? Trends Neurosci *19*, 177-181.

Girard, J.P., Moussion, C., and Förster, R. (2012). HEVs, lymphatics and homeostatic immune cell trafficking in lymph nodes. Nat Rev Immunol *12*, 762-773.

Glatzel, M., Abela, E., Maissen, M., and Aguzzi, A. (2003). Extraneural pathologic prion protein in sporadic Creutzfeldt-Jakob disease. N Engl J Med *349*, 1812-1820.

Glatzel, M., Heppner, F., Albers, K., and Aguzzi, A. (2001). Sympathetic innervation of lymphoreticular organs is rate limiting for prion neuroinvasion. Neuron *31*, 25-34.

Glatzel, M., Stoeck, K., Seeger, H., Lührs, T., and Aguzzi, A. (2005). Human prion diseases: molecular and clinical aspects. Arch Neurol *62*, 545-552.

Gold, R., Linington, C., and Lassmann, H. (2006). Understanding pathogenesis and therapy of multiple sclerosis via animal models: 70 years of merits and culprits in experimental autoimmune encephalomyelitis research. Brain *129*, 1953-1971.

Goldschmidt, L., Teng, P., Riek, R., and Eisenberg, D. (2010). Identifying the amylome, proteins capable of forming amyloid-like fibrils. Proc Natl Acad Sci U S A.

Gommerman, J.L., and Browning, J.L. (2003). Lymphotoxin/light, lymphoid microenvironments and autoimmune disease. Nat Rev Immunol *3*, 642-655.

Gonzalez, S.F., Degn, S.E., Pitcher, L.A., Woodruff, M., Heesters, B.A., and Carroll, M.C. (2011). Trafficking of B cell antigen in lymph nodes. Annu Rev Immunol *29*, 215-233.

Gourdain, P., Ballerini, C., Nicot, A.B., and Carnaud, C. (2012). Exacerbation of experimental autoimmune encephalomyelitis in prion protein (PrPc)-null mice: evidence for a critical role of the central nervous system. J Neuroinflammation *9*, 25.

Greenman, C., Stephens, P., Smith, R., Dalgliesh, G.L., Hunter, C., Bignell, G., Davies, H., Teague, J., Butler, A., Stevens, C.*, et al.* (2007). Patterns of somatic mutation in human cancer genomes. Nature *446*, 153-158.

Gregory, C.D., and Devitt, A. (2004). The macrophage and the apoptotic cell: an innate immune interaction viewed simplistically? Immunology *113*, 1-14.

Greter, M., Heppner, F.L., Lemos, M.P., Odermatt, B.M., Goebels, N., Laufer, T., Noelle, R.J., and Becher, B. (2005). Dendritic cells permit immune invasion of the CNS in an animal model of multiple sclerosis. Nat Med *11*, 328-334.

Griffith, J. (1967). Self-replication and scrapie. Nature *215*, 1043-1044.

Gräbner, R., Lötzer, K., Döpping, S., Hildner, M., Radke, D., Beer, M., Spanbroek, R., Lippert, B., Reardon, C.A., Getz, G.S.*, et al.* (2009). Lymphotoxin beta receptor signaling promotes tertiary lymphoid organogenesis in the aorta adventitia of aged ApoE-/- mice. J Exp Med *206*, 233-248.

Haberman, A.M., and Shlomchik, M.J. (2003). Reassessing the function of immune-complex retention by follicular dendritic cells. Nat Rev Immunol *3*, 757-764.

Halliday, H.L. (1997). Synthetic or natural surfactants. Acta Paediatr *86*, 233-237.

Hatherley, D., Harlos, K., Dunlop, D.C., Stuart, D.I., and Barclay, A.N. (2007). The structure of the macrophage signal regulatory protein alpha (SIRPalpha) inhibitory receptor reveals a binding face reminiscent of that used by T cell receptors. J Biol Chem *282*, 14567-14575.

Heikenwalder, M., Julius, C., and Aguzzi, A. (2007). Prions and peripheral nerves: a deadly rendezvous. J Neurosci Res *85*, 2714-2725.

Heikenwalder, M., Kurrer, M., Margalith, I., Kranich, J., Zeller, N., Haybaeck, J., Polymenidou, M., Matter, M., Bremer, J., Jackson, W.*, et al.* (2008). Lymphotoxin-dependent prion replication in inflammatory stromal cells of granulomas. Immunity *29*, 998-1008.

Heikenwalder, M., Zeller, N., Seeger, H., Prinz, M., Klöhn, P., Schwarz, P., Ruddle, N., Weissmann, C., and Aguzzi, A. (2005). Chronic lymphocytic inflammation specifies the organ tropism of prions. Science *307*, 1107-1110.

Heppner, F., Greter, M., Marino, D., Falsig, J., Raivich, G., Hövelmeyer, N., Waisman, A., Rülicke, T., Prinz, M., Priller, J.*, et al.* (2005). Experimental autoimmune encephalomyelitis repressed by microglial paralysis. Nat Med *11*, 146-152.

Holmdahl, R., and Malissen, B. (2012). The need for littermate controls. Eur J Immunol *42*, 45-47.

Horie, K., Chen, D., and Hoshi, H. (1999). Development of immune complex trapping: experimental study of lymphoid follicles and germinal centers newly induced by exogenous stimulants in mouse popliteal lymph nodes. Histol Histopathol *14*, 11-21.

Hornemann, S., Korth, C., Oesch, B., Riek, R., Wider, G., Wuthrich, K., and Glockshuber, R. (1997). Recombinant full-length murine prion protein, mPrP(23-231): purification and spectroscopic characterization. FEBS Lett *413*, 277-281.

Horvath, P., and Barrangou, R. (2013). RNA-guided genome editing à la carte. Cell Res.

Hsiao, K., and Prusiner, S. (1990). Inherited human prion diseases. Neurology *40*, 1820-1827.

Hu, W., Nessler, S., Hemmer, B., Eagar, T.N., Kane, L.P., Leliveld, S.R., Müller-Schiffmann, A., Gocke, A.R., Lovett-Racke, A., Ben, L.H.*, et al.* (2010). Pharmacological prion protein silencing accelerates central nervous system autoimmune disease via T cell receptor signalling. Brain *133*, 375-388.

Huber, C., Thielen, C., Seeger, H., Schwarz, P., Montrasio, F., Wilson, M.R., Heinen, E., Fu, Y.X., Miele, G., and Aguzzi, A. (2005). Lymphotoxin-beta receptor-dependent genes in lymph node and follicular dendritic cell transcriptomes. J Immunol *174*, 5526-5536.

Inagaki, K., Yamao, T., Noguchi, T., Matozaki, T., Fukunaga, K., Takada, T., Hosooka, T., Akira, S., and Kasuga, M. (2000). SHPS-1 regulates integrin-mediated cytoskeletal reorganization and cell motility. EMBO J *19*, 6721-6731.

Ingram, R.J., Isaacs, J.D., Kaur, G., Lowther, D.E., Reynolds, C.J., Boyton, R.J., Collinge, J., Jackson, G.S., and Altmann, D.M. (2009). A role of cellular prion protein in programming T-cell cytokine responses in disease. Faseb J.

Ironside, J.W. (2012). Variant Creutzfeldt-Jakob disease: an update. Folia Neuropathol *50*, 50-56.

Isaacs, J.D., Jackson, G.S., and Altmann, D.M. (2006). The role of the cellular prion protein in the immune system. Clin Exp Immunol *146*, 1-8.

Ivakine, E.A., Gulban, O.M., Mortin-Toth, S.M., Wankiewicz, E., Scott, C., Spurrell, D., Canty, A., and Danska, J.S. (2006). Molecular genetic analysis of the Idd4 locus implicates the IFN response in type 1 diabetes susceptibility in nonobese diabetic mice. J Immunol *176*, 2976-2990.

Jaiswal, S., Jamieson, C.H., Pang, W.W., Park, C.Y., Chao, M.P., Majeti, R., Traver, D., van Rooijen, N., and Weissman, I.L. (2009). CD47 is upregulated on circulating hematopoietic stem cells and leukemia cells to avoid phagocytosis. Cell *138*, 271-285.

Joung, J.K., and Sander, J.D. (2013). TALENs: a widely applicable technology for targeted genome editing. Nat Rev Mol Cell Biol *14*, 49-55.

Kanagawa, O., Xu, G., Tevaarwerk, A., and Vaupel, B.A. (2000). Protection of nonobese diabetic mice from diabetes by gene(s) closely linked to IFN-gamma receptor loci. J Immunol *164*, 3919-3923.

Katakai, T. (2012). Marginal reticular cells: a stromal subset directly descended from the lymphoid tissue organizer. Front Immunol *3*, 200.

Katakai, T., Suto, H., Sugai, M., Gonda, H., Togawa, A., Suematsu, S., Ebisuno, Y., Katagiri, K., Kinashi, T., and Shimizu, A. (2008). Organizer-like reticular stromal cell layer common to adult secondary lymphoid organs. J Immunol *181*, 6189-6200.

Kim, J., Cali, I., Surewicz, K., Kong, Q., Raymond, G., Atarashi, R., Race, B., Qing, L., Gambetti, P., Caughey, B.*, et al.* (2010). Mammalian prions generated from bacterially expressed prion protein in the absence of any mammalian cofactors. J Biol Chem *285*, 14083-14087.

Kindt, T.J., Osborne, B.A., and Goldsby, R.A. (2007). Kuby Immunology, Sixth Edition edn (New York: W. H. Freeman and Company).

Klaus, G.G., Humphrey, J.H., Kunkl, A., and Dongworth, D.W. (1980). The follicular dendritic cell: its role in antigen presentation in the generation of immunological memory. Immunol Rev *53*, 3-28.

Klein, M., Frigg, R., Flechsig, E., Raeber, A., Kalinke, U., Bluethmann, H., Bootz, F., Suter, M., Zinkernagel, R., and Aguzzi, A. (1997). A crucial role for B cells in neuroinvasive scrapie. Nature *390*, 687-690.

Klein, M., Kaeser, P., Schwarz, P., Weyd, H., Xenarios, I., Zinkernagel, R., Carroll, M., Verbeek, J., Botto, M., Walport, M.*, et al.* (2001). Complement facilitates early prion pathogenesis. Nat Med *7*, 488-492.

Klein, M.A., Frigg, R., Raeber, A.J., Flechsig, E., Hegyi, I., Zinkernagel, R.M., Weissmann, C., and Aguzzi, A. (1998). PrP expression in B lymphocytes is not required for prion neuroinvasion. Nat Med *4*, 1429-1433.

Kobayashi, M., Ohnishi, H., Okazawa, H., Murata, Y., Hayashi, Y., Kobayashi, H., Kitamura, T., and Matozaki, T. (2008). Expression of Src homology 2 domain-containing protein tyrosine phosphatase substrate-1 in pancreatic beta-Cells and its role in promotion of insulin secretion and protection against diabetes. Endocrinology *149*, 5662-5669.

Koperek, O., Kovács, G.G., Ritchie, D., Ironside, J.W., Budka, H., and Wick, G. (2002). Disease-associated prion protein in vessel walls. Am J Pathol *161*, 1979-1984.

Kosco-Vilbois, M.H. (2003). Are follicular dendritic cells really good for nothing? Nat Rev Immunol *3*, 764-769.

Kranich, J., Krautler, N.J., Heinen, E., Polymenidou, M., Bridel, C., Schildknecht, A., Huber, C., Kosco-Vilbois, M.H., Zinkernagel, R., Miele, G.*, et al.* (2008). Follicular dendritic cells control engulfment of apoptotic bodies by secreting Mfge8. J Exp Med *205*, 1293-1302.

Krautler, N.J., Kana, V., Kranich, J., Tian, Y., Perera, D., Lemm, D., Schwarz, P., Armulik, A., Browning, J.L., Tallquist, M.*, et al.* (2012). Follicular dendritic cells emerge from ubiquitous perivascular precursors. Cell *150*, 194-206.

Kräutler, N. (2010). The origin of follicular dendritic cells. In Faculty of Science (Zurich: University of Zurich).

Ksantini, M., Lafont, E., Bocquet, B., Meunier, I., and Hamel, C.P. (2012). Homozygous mutation in MERTK causes severe autosomal recessive retinitis pigmentosa. Eur J Ophthalmol *22*, 647-653.

Kumar, P., Henikoff, S., and Ng, P.C. (2009). Predicting the effects of coding non-synonymous variants on protein function using the SIFT algorithm. Nat Protoc *4*, 1073-1081.

Kurita, T., Medina, R., Schabel, A.B., Young, P., Gama, P., Parekh, T.V., Brody, J., Cunha, G.R., Osteen, K.G., Bruner-Tran, K.L.*, et al.* (2005). The activation function-1 domain of estrogen receptor alpha in uterine stromal cells is required for mouse but not human uterine epithelial response to estrogen. Differentiation *73*, 313-322.

Lanier, L.L. (2013). Shades of grey--the blurring view of innate and adaptive immunity. Nat Rev Immunol *13*, 73-74.

Lauber, K., Ernst, A., Orth, M., Herrmann, M., and Belka, C. (2012). Dying cell clearance and its impact on the outcome of tumor radiotherapy. Front Oncol *2*, 116.

Laurén, J., Gimbel, D.A., Nygaard, H.B., Gilbert, J.W., and Strittmatter, S.M. (2009). Cellular prion protein mediates impairment of synaptic plasticity by amyloid-beta oligomers. Nature *457*, 1128-1132.

Legname, G., Baskakov, I., Nguyen, H., Riesner, D., Cohen, F., DeArmond, S., and Prusiner, S. (2004). Synthetic mammalian prions. Science *305*, 673-676.

Legrand, N., Huntington, N.D., Nagasawa, M., Bakker, A.Q., Schotte, R., Strick-Marchand, H., de Geus, S.J., Pouw, S.M., Bohne, M., Voordouw, A.*, et al.* (2011a). Functional CD47/signal regulatory protein alpha (SIRP(alpha)) interaction is required for optimal human T- and natural killer- (NK) cell homeostasis in vivo. Proc Natl Acad Sci U S A *108*, 13224-13229.

Legrand, N., Huntington, N.D., Nagasawa, M., Bakker, A.Q., Schotte, R., Strick-Marchand, H., de Geus, S.J., Pouw, S.M., Böhne, M., Voordouw, A.*, et al.* (2011b). Functional CD47/signal regulatory protein alpha (SIRP(alpha)) interaction is required for optimal human T- and natural killer- (NK) cell homeostasis in vivo. Proc Natl Acad Sci U S A *108*, 13224-13229.

Lemke, G., and Rothlin, C.V. (2008). Immunobiology of the TAM receptors. Nat Rev Immunol *8*, 327-336.

Li, E., and Hristova, K. (2010). Receptor tyrosine kinase transmembrane domains: Function, dimer structure and dimerization energetics. Cell Adh Migr *4*, 249-254.

Li, J., Browning, S., Mahal, S., Oelschlegel, A., and Weissmann, C. (2010). Darwinian evolution of prions in cell culture. Science *327*, 869-872.

Li, L., Xiao, X., Li, S., Jia, X., Wang, P., Guo, X., Jiao, X., Zhang, Q., and Hejtmancik, J.F. (2011). Detection of variants in 15 genes in 87 unrelated Chinese patients with Leber congenital amaurosis. PLoS One *6*, e19458.

Ligios, C., Sigurdson, C., Santucciu, C., Carcassola, G., Manco, G., Basagni, M., Maestrale, C., Cancedda, M., Madau, L., and Aguzzi, A. (2005). PrPSc in mammary glands of sheep affected by scrapie and mastitis. Nat Med *11*, 1137-1138.

Lin, C.S., and Lue, T.F. (2013). Defining vascular stem cells. Stem Cells Dev *22*, 1018-1026.

Linden, R., Martins, V., Prado, M., Cammarota, M., Izquierdo, I., and Brentani, R. (2008). Physiology of the prion protein. Physiol Rev *88*, 673-728.

Linger, R.M., Keating, A.K., Earp, H.S., and Graham, D.K. (2008). TAM receptor tyrosine kinases: biologic functions, signaling, and potential therapeutic targeting in human cancer. Adv Cancer Res *100*, 35-83.

Link, A., Vogt, T.K., Favre, S., Britschgi, M.R., Acha-Orbea, H., Hinz, B., Cyster, J.G., and Luther, S.A. (2007). Fibroblastic reticular cells in lymph nodes regulate the homeostasis of naive T cells. Nat Immunol *8*, 1255-1265.

Liu, T., Li, R., Wong, B.S., Liu, D., Pan, T., Petersen, R.B., Gambetti, P., and Sy, M.S. (2001). Normal cellular prion protein is preferentially expressed on subpopulations of murine hemopoietic cells. J Immunol *166*, 3733-3742.

Mabbott, N., Young, J., McConnell, I., and Bruce, M. (2003). Follicular dendritic cell dedifferentiation by treatment with an inhibitor of the lymphotoxin pathway dramatically reduces scrapie susceptibility. J Virol *77*, 6845-6854.

Mabbott, N.A., Mackay, F., Minns, F., and Bruce, M.E. (2000). Temporary inactivation of follicular dendritic cells delays neuroinvasion of scrapie. Nat Med *6*, 719-720.

Madisen, L., Zwingman, T.A., Sunkin, S.M., Oh, S.W., Zariwala, H.A., Gu, H., Ng, L.L., Palmiter, R.D., Hawrylycz, M.J., Jones, A.R.*, et al.* (2010). A robust and high-throughput Cre reporting and characterization system for the whole mouse brain. Nat Neurosci *13*, 133-140.

Majewski, J., and Pastinen, T. (2011). The study of eQTL variations by RNA-seq: from SNPs to phenotypes. Trends Genet *27*, 72-79.

Makarava, N., Kovacs, G., Bocharova, O., Savtchenko, R., Alexeeva, I., Budka, H., Rohwer, R., and Baskakov, I. (2010). Recombinant prion protein induces a new transmissible prion disease in wild-type animals. Acta Neuropathol *119*, 177-187.

Malhotra, D., Fletcher, A.L., Astarita, J., Lukacs-Kornek, V., Tayalia, P., Gonzalez, S.F., Elpek, K.G., Chang, S.K., Knoblich, K., Hemler, M.E.*, et al.* (2012). Transcriptional profiling of stroma from inflamed and resting lymph nodes defines immunological hallmarks. Nat Immunol *13*, 499-510.

Malhotra, D., Fletcher, A.L., and Turley, S.J. (2013). Stromal and hematopoietic cells in secondary lymphoid organs: partners in immunity. Immunol Rev *251*, 160-176.

Mandel, T.E., Phipps, R.P., Abbot, A., and Tew, J.G. (1980). The follicular dendritic cell: long term antigen retention during immunity. Immunol Rev *53*, 29-59.

Manson, J., Clarke, A., Hooper, M., Aitchison, L., McConnell, I., and Hope, J. (1994). 129/Ola mice carrying a null mutation in PrP that abolishes mRNA production are developmentally normal. Mol Neurobiol *8*, 121-127.

Manzo, A., Bombardieri, M., Humby, F., and Pitzalis, C. (2010). Secondary and ectopic lymphoid tissue responses in rheumatoid arthritis: from inflammation to autoimmunity and tissue damage/remodeling. Immunol Rev *233*, 267-285.

Matozaki, T., Murata, Y., Okazawa, H., and Ohnishi, H. (2009). Functions and molecular mechanisms of the CD47-SIRPalpha signalling pathway. Trends Cell Biol *19*, 72-80.

Matsumoto, M., Lo, S.F., Carruthers, C.J., Min, J., Mariathasan, S., Huang, G., Plas, D.R., Martin, S.M., Geha, R.S., Nahm, M.H.*, et al.* (1996). Affinity maturation without germinal centres in lymphotoxin-alpha-deficient mice. Nature *382*, 462-466.

Mattei, V., Garofalo, T., Misasi, R., Circella, A., Manganelli, V., Lucania, G., Pavan, A., and Sorice, M. (2004). Prion protein is a component of the multimolecular signaling complex involved in T cell activation. FEBS Lett *560*, 14-18.

McCulloch, L., Brown, K.L., Bradford, B.M., Hopkins, J., Bailey, M., Rajewsky, K., Manson, J.C., and Mabbott, N.A. (2011). Follicular dendritic cell-specific prion protein (PrP) expression alone is sufficient to sustain prion infection in the spleen. PLoS Pathog *7*, e1002402.

McHenry, C.L., Liu, Y., Feng, W., Nair, A.R., Feathers, K.L., Ding, X., Gal, A., Vollrath, D., Sieving, P.A., and Thompson, D.A. (2004). MERTK arginine-844-cysteine in a patient with severe rod-cone dystrophy: loss of mutant protein function in transfected cells. Invest Ophthalmol Vis Sci *45*, 1456-1463.

McHeyzer-Williams, M., Okitsu, S., Wang, N., and McHeyzer-Williams, L. (2012). Molecular programming of B cell memory. Nat Rev Immunol *12*, 24-34.

Mebius, R.E., and Kraal, G. (2005). Structure and function of the spleen. Nat Rev Immunol *5*, 606-616.

Miller, S., Karpus, W., and Davidson, T. (2010). Experimental autoimmune encephalomyelitis in the mouse. Curr Protoc Immunol *Chapter 15*, Unit 15.11.

Mitchell, J., and Abbot, A. (1965). Ultrastructure of the antigen-retaining reticulum of lymph node follicles as shown by high-resolution autoradiography. Nature *208*, 500-502.

Montrasio, F., Frigg, R., Glatzel, M., Klein, M.A., Mackay, F., Aguzzi, A., and Weissmann, C. (2000). Impaired prion replication in spleens of mice lacking functional follicular dendritic cells. Science *288*, 1257-1259.

Moore, R.C., Lee, I.Y., Silverman, G.L., Harrison, P.M., Strome, R., Heinrich, C., Karunaratne, A., Pasternak, S.H., Chishti, M.A., Liang, Y.*, et al.* (1999). Ataxia in prion protein (PrP)-deficient mice is associated with upregulation of the novel PrP-like protein doppel. J Mol Biol *292*, 797-817.

Moore, R.C., Redhead, N.J., Selfridge, J., Hope, J., Manson, J.C., and Melton, D.W. (1995). Double replacement gene targeting for the production of a series of mouse strains with different prion protein gene alterations. Biotechnology (N Y) *13*, 999-1004.

Moro, K., Yamada, T., Tanabe, M., Takeuchi, T., Ikawa, T., Kawamoto, H., Furusawa, J., Ohtani, M., Fujii, H., and Koyasu, S. (2010). Innate production of T(H)2 cytokines by adipose tissue-associated c-Kit(+)Sca-1(+) lymphoid cells. Nature *463*, 540-544.

Motegi, S., Garfield, S., Feng, X., Sárdy, M., and Udey, M.C. (2011a). Potentiation of platelet-derived growth factor receptor-β signaling mediated by integrin-associated MFG-E8. Arterioscler Thromb Vasc Biol *31*, 2653-2664.

Motegi, S., Leitner, W.W., Lu, M., Tada, Y., Sárdy, M., Wu, C., Chavakis, T., and Udey, M.C. (2011b). Pericyte-derived MFG-E8 regulates pathologic angiogenesis. Arterioscler Thromb Vasc Biol *31*, 2024-2034.

Mueller, S.N., and Germain, R.N. (2009). Stromal cell contributions to the homeostasis and functionality of the immune system. Nat Rev Immunol *9*, 618-629.

Nagata, S., Hanayama, R., and Kawane, K. (2010). Autoimmunity and the clearance of dead cells. Cell *140*, 619-630.

Nakaishi, A., Hirose, M., Yoshimura, M., Oneyama, C., Saito, K., Kuki, N., Matsuda, M., Honma, N., Ohnishi, H., Matozaki, T.*, et al.* (2008). Structural insight into the specific interaction between murine SHPS-1/SIRP alpha and its ligand CD47. J Mol Biol *375*, 650-660.

Napoli, I., and Neumann, H. (2010). Protective effects of microglia in multiple sclerosis. Exp Neurol *225*, 24-28.

Neyt, K., Perros, F., GeurtsvanKessel, C.H., Hammad, H., and Lambrecht, B.N. (2012). Tertiary lymphoid organs in infection and autoimmunity. Trends Immunol *33*, 297-305.

Ng, P.C., and Henikoff, S. (2001). Predicting deleterious amino acid substitutions. Genome Res *11*, 863-874.

Nico, P.B., de-Paris, F., Vinade, E.R., Amaral, O.B., Rockenbach, I., Soares, B.L., Guarnieri, R., Wichert-Ana, L., Calvo, F., Walz, R.*, et al.* (2005). Altered behavioural response to acute stress in mice lacking cellular prion protein. Behav Brain Res *162*, 173-181.

Nishana, M., and Raghavan, S.C. (2012). Role of recombination activating genes in the generation of antigen receptor diversity and beyond. Immunology *137*, 271-281.

Nishida, N., Tremblay, P., Sugimoto, T., Shigematsu, K., Shirabe, S., Petromilli, C., Erpel, S.P., Nakaoke, R., Atarashi, R., Houtani, T.*, et al.* (1999). A mouse prion protein transgene rescues mice deficient for the prion protein gene from purkinje cell degeneration and demyelination. Lab Invest *79*, 689-697.

Nuvolone, M., Aguzzi, A., and Heikenwalder, M. (2009). Cells and prions: a license to replicate. FEBS Lett *583*, 2674-2684.

O'Connor, T., and Aguzzi, A. (2013). Prions and lymphoid organs: Solved and remaining mysteries. Prion *7*, 157-163.

O'Connor, T., Frei, N., Sponarova, J., Schwarz, P., Heikenwalder, M., and Aguzzi, A. (2012). Lymphotoxin, but not TNF, is required for prion invasion of lymph nodes. PLoS Pathog *8*, e1002867.

Oesch, B., Westaway, D., Wälchli, M., McKinley, M., Kent, S., Aebersold, R., Barry, R., Tempst, P., Teplow, D., and Hood, L. (1985). A cellular gene encodes scrapie PrP 27-30 protein. Cell *40*, 735-746.

Ohazama, A., Modino, S.A., Miletich, I., and Sharpe, P.T. (2004). Stem-cell-based tissue engineering of murine teeth. J Dent Res *83*, 518-522.

Ohnishi, H., Murata, T., Kusakari, S., Hayashi, Y., Takao, K., Maruyama, T., Ago, Y., Koda, K., Jin, F.J., Okawa, K.*, et al.* (2010). Stress-evoked tyrosine phosphorylation of signal regulatory protein alpha regulates behavioral immobility in the forced swim test. J Neurosci *30*, 10472-10483.

Okazawa, H., Motegi, S., Ohyama, N., Ohnishi, H., Tomizawa, T., Kaneko, Y., Oldenborg, P.A., Ishikawa, O., and Matozaki, T. (2005). Negative regulation of phagocytosis in macrophages by the CD47-SHPS-1 system. J Immunol *174*, 2004-2011.

Oldenborg, P.A., Zheleznyak, A., Fang, Y.F., Lagenaur, C.F., Gresham, H.D., and Lindberg, F.P. (2000). Role of CD47 as a marker of self on red blood cells. Science *288*, 2051-2054.

Oldstone, M.B., Race, R., Thomas, D., Lewicki, H., Homann, D., Smelt, S., Holz, A., Koni, P., Lo, D., Chesebro, B.*, et al.* (2002). Lymphotoxin-alpha- and lymphotoxin-beta-deficient mice differ in susceptibility to scrapie: evidence against dendritic cell involvement in neuroinvasion. J Virol *76*, 4357-4363.

Olson, L.E., and Soriano, P. (2011). PDGFRβ signaling regulates mural cell plasticity and inhibits fat development. Dev Cell *20*, 815-826.

Owens, G.K., Kumar, M.S., and Wamhoff, B.R. (2004). Molecular regulation of vascular smooth muscle cell differentiation in development and disease. Physiol Rev *84*, 767-801.

Paar, C., Wurm, S., Pfarr, W., Sonnleitner, A., and Wechselberger, C. (2007). Prion protein resides in membrane microclusters of the immunological synapse during lymphocyte activation. Eur J Cell Biol *86*, 253-264.

Perera, D.M.T. (2010). Perivascular origin of follicular dendritic cells. In Faculty of Sciences (Zurich: University of Zurich).

Pettitt, S.J., Liang, Q., Rairdan, X.Y., Moran, J.L., Prosser, H.M., Beier, D.R., Lloyd, K.C., Bradley, A., and Skarnes, W.C. (2009). Agouti C57BL/6N embryonic stem cells for mouse genetic resources. Nat Methods *6*, 493-495.

Peyron, P., Bordier, C., N'Diaye, E.N., and Maridonneau-Parini, I. (2000). Nonopsonic phagocytosis of Mycobacterium kansasii by human neutrophils depends on cholesterol and is mediated by CR3 associated with glycosylphosphatidylinositol-anchored proteins. J Immunol *165*, 5186-5191.

Phan, T.G., Grigorova, I., Okada, T., and Cyster, J.G. (2007). Subcapsular encounter and complement-dependent transport of immune complexes by lymph node B cells. Nat Immunol *8*, 992-1000.

Poon, I.K., Hulett, M.D., and Parish, C.R. (2010). Molecular mechanisms of late apoptotic/necrotic cell clearance. Cell Death Differ *17*, 381-397.

Prinz, M., Heikenwalder, M., Junt, T., Schwarz, P., Glatzel, M., Heppner, F., Fu, Y., Lipp, M., and Aguzzi, A. (2003). Positioning of follicular dendritic cells within the spleen controls prion neuroinvasion. Nature *425*, 957-962.

Prinz, M., Montrasio, F., Klein, M., Schwarz, P., Priller, J., Odermatt, B., Pfeffer, K., and Aguzzi, A. (2002). Lymph nodal prion replication and neuroinvasion in mice devoid of follicular dendritic cells. Proc Natl Acad Sci U S A *99*, 919-924.

Prusiner, S. (1982). Novel proteinaceous infectious particles cause scrapie. Science *216*, 136-144.

Péault, B. (2012). Are mural cells guardians of stemness?: From pluri- to multipotency via vascular pericytes. Circulation *125*, 12-13.

Ransohoff, R.M., and Engelhardt, B. (2012). The anatomical and cellular basis of immune surveillance in the central nervous system. Nat Rev Immunol *12*, 623-635.

Ravichandran, K.S., and Lorenz, U. (2007). Engulfment of apoptotic cells: signals for a good meal. Nat Rev Immunol *7*, 964-974.

Ridgway, W.M., Healy, B., Smink, L.J., Rainbow, D., and Wicker, L.S. (2007). New tools for defining the 'genetic background' of inbred mouse strains. Nat Immunol *8*, 669-673.

Riek, R., Hornemann, S., Wider, G., Billeter, M., Glockshuber, R., and Wüthrich, K. (1996). NMR structure of the mouse prion protein domain PrP(121-231). Nature *382*, 180-182.

Riek, R., Hornemann, S., Wider, G., Glockshuber, R., and Wüthrich, K. (1997). NMR characterization of the full-length recombinant murine prion protein, mPrP(23-231). FEBS Lett *413*, 282-288.

Roberts, D.D., and Lau, L.F. (2011). Matricellular proteins. In The extracellular matrix: an overview, R.P. Mecham, ed. (Berlin-Heidelberg: Springer-Verlag), pp. 369-413.

Rossi, D., Cozzio, A., Flechsig, E., Klein, M.A., Aguzzi, A., and Weissmann, C. (2001). Onset of ataxia and Purkinje cell loss in PrP null mice inversely correlated with Dpl level in brain. EMBO J *20*, 1-9.

Rothlin, C.V., and Lemke, G. (2010). TAM receptor signaling and autoimmune disease. Curr Opin Immunol *22*, 740-746.

Sacca, R., Turley, S., Soong, L., Mellman, I., and Ruddle, N.H. (1997). Transgenic expression of lymphotoxin restores lymph nodes to lymphotoxin-alpha-deficient mice. J Immunol *159*, 4252-4260.

Sakaguchi, S., Katamine, S., Shigematsu, K., Nakatani, A., Moriuchi, R., Nishida, N., Kurokawa, K., Nakaoke, R., Sato, H., and Jishage, K. (1995). Accumulation of proteinase K-resistant prion protein (PrP) is restricted by the expression level of normal PrP in mice inoculated with a mouse-adapted strain of the Creutzfeldt-Jakob disease agent. J Virol *69*, 7586-7592.

Sano, S., Ohnishi, H., and Kubota, M. (1999). Gene structure of mouse BIT/SHPS-1. Biochem J *344 Pt 3*, 667-675.

Schalkwyk, L.C., Fernandes, C., Nash, M.W., Kurrikoff, K., Vasar, E., and Kõks, S. (2007). Interpretation of knockout experiments: the congenic footprint. Genes Brain Behav *6*, 299-303.

Schreiner, B., Heppner, F.L., and Becher, B. (2009). Modeling multiple sclerosis in laboratory animals. Semin Immunopathol *31*, 479-495.

Scott, R.S., McMahon, E.J., Pop, S.M., Reap, E.A., Caricchio, R., Cohen, P.L., Earp, H.S., and Matsushima, G.K. (2001). Phagocytosis and clearance of apoptotic cells is mediated by MER. Nature *411*, 207-211.

Seeger, H., Heikenwalder, M., Zeller, N., Kranich, J., Schwarz, P., Gaspert, A., Seifert, B., Miele, G., and Aguzzi, A. (2005). Coincident scrapie infection and nephritis lead to urinary prion excretion. Science *310*, 324-326.

Seong, E., Saunders, T.L., Stewart, C.L., and Burmeister, M. (2004). To knockout in 129 or in C57BL/6: that is the question. Trends Genet *20*, 59-62.

Silver, L.M. (2008). Mouse genetics. (www.informatics.jax.org/silver: Jackson Laboratory).

Smith, B.A., Gartner, S., Liu, Y., Perelson, A.S., Stilianakis, N.I., Keele, B.F., Kerkering, T.M., Ferreira-Gonzalez, A., Szakal, A.K., Tew, J.G.*, et al.* (2001). Persistence of infectious HIV on follicular dendritic cells. J Immunol *166*, 690-696.

Smithies, O., and Maeda, N. (1995). Gene targeting approaches to complex genetic diseases: atherosclerosis and essential hypertension. Proc Natl Acad Sci U S A *92*, 5266-5272.

Sparkes, R.S., Simon, M., Cohn, V.H., Fournier, R.E., Lem, J., Klisak, I., Heinzmann, C., Blatt, C., Lucero, M., Mohandas, T.*, et al.* (1986). Assignment of the human and mouse prion protein genes to homologous chromosomes. Proc Natl Acad Sci U S A *83*, 7358-7362.

Spits, H., Artis, D., Colonna, M., Diefenbach, A., Di Santo, J.P., Eberl, G., Koyasu, S., Locksley, R.M., McKenzie, A.N., Mebius, R.E.*, et al.* (2013). Innate lymphoid cells--a proposal for uniform nomenclature. Nat Rev Immunol *13*, 145-149.

Stark, K., Eckart, A., Haidari, S., Tirniceriu, A., Lorenz, M., von Brühl, M.L., Gärtner, F., Khandoga, A.G., Legate, K.R., Pless, R.*, et al.* (2013). Capillary and arteriolar pericytes attract innate leukocytes exiting through venules and 'instruct' them with pattern-recognition and motility programs. Nat Immunol *14*, 41-51.

Steele, A., Lindquist, S., and Aguzzi, A. (2007). The prion protein knockout mouse: a phenotype under challenge. Prion *1*, 83-93.

Stranford, S., and Ruddle, N.H. (2012). Follicular dendritic cells, conduits, lymphatic vessels, and high endothelial venules in tertiary lymphoid organs: Parallels with lymph node stroma. Front Immunol *3*, 350.

Striebel, J.F., Race, B., Pathmajeyan, M., Rangel, A., and Chesebro, B. (2013). Lack of influence of prion protein gene expression on kainate-induced seizures in mice: studies using congenic, coisogenic and transgenic strains. Neuroscience.

Strom, A., Wang, G.S., and Scott, F.W. (2011). Impaired glucose tolerance in mice lacking cellular prion protein. Pancreas *40*, 229-232.

Strowig, T., Rongvaux, A., Rathinam, C., Takizawa, H., Borsotti, C., Philbrick, W., Eynon, E.E., Manz, M.G., and Flavell, R.A. (2011). Transgenic expression of human signal regulatory protein alpha in Rag2-/-gamma(c)-/- mice improves engraftment of human hematopoietic cells in humanized mice. Proc Natl Acad Sci U S A *108*, 13218-13223.

Suematsu, S., and Watanabe, T. (2004). Generation of a synthetic lymphoid tissue-like organoid in mice. Nat Biotechnol *22*, 1539-1545.

Supattapone, S. (2010). Biochemistry. What makes a prion infectious? Science *327*, 1091-1092.

Szakal, A.K., and Hanna, M.G. (1968). The ultrastructure of antigen localization and viruslike particles in mouse spleen germinal centers. Exp Mol Pathol *8*, 75-89.

Tada, K., Tanaka, M., Hanayama, R., Miwa, K., Shinohara, A., Iwamatsu, A., and Nagata, S. (2003). Tethering of apoptotic cells to phagocytes through binding of CD47 to Src homology 2 domain-bearing protein tyrosine phosphatase substrate-1. J Immunol *171*, 5718-5726.

Takenaka, K., Prasolava, T.K., Wang, J.C., Mortin-Toth, S.M., Khalouei, S., Gan, O.I., Dick, J.E., and Danska, J.S. (2007). Polymorphism in Sirpa modulates engraftment of human hematopoietic stem cells. Nat Immunol *8*, 1313-1323.

Tang, W., Zeve, D., Suh, J.M., Bosnakovski, D., Kyba, M., Hammer, R.E., Tallquist, M.D., and Graff, J.M. (2008). White fat progenitor cells reside in the adipose vasculature. Science *322*, 583-586.

Taylor, D.R., and Hooper, N.M. (2006). The prion protein and lipid rafts. Mol Membr Biol *23*, 89-99.

Tew, J.G., Thorbecke, G.J., and Steinman, R.M. (1982). Dendritic cells in the immune response: characteristics and recommended nomenclature (A report from the Reticuloendothelial Society Committee on Nomenclature). J Reticuloendothel Soc *31*, 371-380.

Thacker, T.C., Zhou, X., Estes, J.D., Jiang, Y., Keele, B.F., Elton, T.S., and Burton, G.F. (2009). Follicular dendritic cells and human immunodeficiency virus type 1 transcription in CD4+ T cells. J Virol *83*, 150-158.

Theocharides, A.P., Jin, L., Cheng, P.Y., Prasolava, T.K., Malko, A.V., Ho, J.M., Poeppl, A.G., van Rooijen, N., Minden, M.D., Danska, J.S.*, et al.* (2012). Disruption of SIRPα signaling in macrophages eliminates human acute myeloid leukemia stem cells in xenografts. J Exp Med *209*, 1883-1899.

Tomizawa, T., Kaneko, Y., Saito, Y., Ohnishi, H., Okajo, J., Okuzawa, C., Ishikawa-Sekigami, T., Murata, Y., Okazawa, H., Okamoto, K.*, et al.* (2007). Resistance to experimental autoimmune encephalomyelitis and impaired T cell priming by dendritic cells in Src homology 2 domain-containing protein tyrosine phosphatase substrate-1 mutant mice. J Immunol *179*, 869-877.

Tsutsui, S., Hahn, J., Johnson, T., Ali, Z., and Jirik, F. (2008). Absence of the cellular prion protein exacerbates and prolongs neuroinflammation in experimental autoimmune encephalomyelitis. Am J Pathol *173*, 1029-1041.

van de Pavert, S.A., and Mebius, R.E. (2010). New insights into the development of lymphoid tissues. Nat Rev Immunol *10*, 664-674.

Verma, A., Warner, S.L., Vankayalapati, H., Bearss, D.J., and Sharma, S. (2011). Targeting Axl and Mer kinases in cancer. Mol Cancer Ther *10*, 1763-1773.

von Andrian, U.H., and Mempel, T.R. (2003). Homing and cellular traffic in lymph nodes. Nat Rev Immunol *3*, 867-878.

Wade, C.M., and Daly, M.J. (2005). Genetic variation in laboratory mice. Nat Genet *37*, 1175-1180.

Wang, F., Wang, X., Yuan, C., and Ma, J. (2010). Generating a prion with bacterially expressed recombinant prion protein. Science *327*, 1132-1135.

Wang, M., Fu, Z., Wu, J., Zhang, J., Jiang, L., Khazan, B., Telljohann, R., Zhao, M., Krug, A.W., Pikilidou, M.*, et al.* (2012a). MFG-E8 activates proliferation of vascular smooth muscle cells via integrin signaling. Aging Cell *11*, 500-508.

Wang, M., Wang, H.H., and Lakatta, E.G. (2012b). Milk Fat Globule Epidermal Growth Factor VIII Signaling in Arterial Wall Remodeling. Curr Vasc Pharmacol.

Wang, Y., Xue, H., Cutz, J.C., Bayani, J., Mawji, N.R., Chen, W.G., Goetz, L.J., Hayward, S.W., Sadar, M.D., Gilks, C.B.*, et al.* (2005). An orthotopic metastatic prostate cancer model in SCID mice via grafting of a transplantable human prostate tumor line. Lab Invest *85*, 1392-1404.

Wang, Z., Gerstein, M., and Snyder, M. (2009). RNA-Seq: a revolutionary tool for transcriptomics. Nat Rev Genet *10*, 57-63.

Weissmann, C., and Aguzzi, A. (1999). Perspectives: neurobiology. PrP's double causes trouble. Science *286*, 914-915.

Weissmann, C., and Flechsig, E. (2003). PrP knock-out and PrP transgenic mice in prion research. Br Med Bull *66*, 43-60.

Williams, S.K., Fairless, R., Weise, J., Kalinke, U., Schulz-Schaeffer, W., and Diem, R. (2011). Neuroprotective effects of the cellular prion protein in autoimmune optic neuritis. Am J Pathol *178*, 2823-2831.

Wilson, D.A., and Nixon, R.A. (2009). Sniffing out a function for prion proteins. Nat Neurosci *12*, 7-8.

Wolf, M.J., Seleznik, G.M., Zeller, N., and Heikenwalder, M. (2010). The unexpected role of lymphotoxin beta receptor signaling in carcinogenesis: from lymphoid tissue formation to liver and prostate cancer development. Oncogene *29*, 5006-5018.

Wolfer, D.P., Crusio, W.E., and Lipp, H.P. (2002). Knockout mice: simple solutions to the problems of genetic background and flanking genes. Trends Neurosci *25*, 336-340.

Wu, X., Jiang, N., Fang, Y.F., Xu, C., Mao, D., Singh, J., Fu, Y.X., and Molina, H. (2000). Impaired affinity maturation in Cr2-/- mice is rescued by adjuvants without improvement in germinal center development. J Immunol *165*, 3119-3127.

Yamauchi, T., Takenaka, K., Urata, S., Shima, T., Kikushige, Y., Tokuyama, T., Iwamoto, C., Nishihara, M., Iwasaki, H., Miyamoto, T.*, et al.* (2013). Polymorphic Sirpa is the genetic

determinant for NOD-based mouse lines to achieve efficient human cell engraftment. Blood *121*, 1316-1325.

Yokoyama, T., Kimura, K.M., Ushiki, Y., Yamada, S., Morooka, A., Nakashiba, T., Sassa, T., and Itohara, S. (2001). In vivo conversion of cellular prion protein to pathogenic isoforms, as monitored by conformation-specific antibodies. J Biol Chem *276*, 11265-11271.

Yoshida, K., van den Berg, T.K., and Dijkstra, C.D. (1993). Two functionally different follicular dendritic cells in secondary lymphoid follicles of mouse spleen, as revealed by CR1/2 and FcR gamma II-mediated immune-complex trapping. Immunology *80*, 34-39.

Zabel, M., Greenwood, C., Thackray, A., Pulford, B., Rens, W., and Bujdoso, R. (2008). Perturbation of T-cell development by insertional mutation of a PrP transgene. Immunology.

Zmuda, E.J., Powell, C.A., and Hai, T. (2011). A method for murine islet isolation and subcapsular kidney transplantation. J Vis Exp.